Assessment of Mission Design Including Utilization of Libration Points and Weak Stability Boundaries

Authors: E.Canalias, G.Gomez, M.Marcote, J.J.Masdemont.
Academic Institution: Department de Matematica Aplicada, Universitat Politecnica de Catalunya and Department de Matematica Aplicada, Universitat de Barcellona.
Approved by: Dario Izzo, Advanced Concepts Team (ESTEC)

Contacts:

Josep Masdemont
e-mail: josep@barquins.upc.es

Dario Izzo
Tel: ++31 (0)71565 – 3511
Fax: ++31 (0)71565 – 8018
e-mail: act@esa.int

Ariadna id: 03/4103
Study length: 2 months.
Contract Number: 18142/04/NL/MV

Available on the ACT net (www.esa.int/act)

Contents

Chapter 1

Introduction

The last 25 years have produced an explosion in the capabilities of designing and managing libration point missions. The starting point was the ground-breaking mission of the third International Sun-Earth Explorer spacecraft (ISEE–3). The ISEE-3 was launched August 12, 1978 to pursue studies of the Earth–Sun interactions, in a first step of what now is known as Space Weather. After a direct transfer of the ISEE-3 to the vicinity of the Sun-Earth L_1 Lagrange point, it was inserted into a nearly-periodic halo orbit, in order to monitor the solar wind about one hour before it reached the Earth's magneto-sphere as well as the ISEE–1 and 2 spacecraft (which where in an elliptical orbit around the Earth). After completing some revolutions around the halo orbit, the spacecraft visited the vicinity of the L_2 libration point to explore the magneto-tail of the Earth. Finally, and after making use of a double lunar swing-by the spacecraft was renamed as the International Cometary Explorer (ICE) and had a close encounter with the comet Giacobini-Zinner.

Interest in the scientific advantages of the Lagrange libration points for space missions has continued to increase and to inspire even more challenging objectives that are reflected, in part, in some of the current missions such as SOHO, MAP and Genesis. Also, increasing understanding of the available mission options has emerged due to the theoretical, analytical, and numerical advances in many aspects of libration point mission design.

The Lagrange libration points are the equilibrium solutions of the Restricted Three Body Problem (RTBP) which describes the motion of a particle, of very small mass, under the gravitational attraction of two massive bodies (usually called primaries, or primary and secondary). It is assumed that the particles are in a circular (Keplerian) motion around their centre of masses. For space missions, the particle is the spacecraft and the two primaries can be taken, for example, as the Sun and the Earth-Moon barycentre, or the Earth and the Moon.

Since Euler and Lagrange, some relevant solutions of both the General Three Body Problem and the RTBP are known. For one of these solutions, the three bodies are in the edges of an equilateral triangle, with the centre of masses at the origin, that can rotate with an angular velocity that depends on the masses of the bodies and the size of the side of the triangle. Aside from these triangular configurations, the bodies can also rotate aligned, if the ratio of the relative distances of one body to the other two verifies some algebraic quintic equation. For the RTBP, suitable rotating coordinates can be introduced to keep both primaries fixed. In this reference system, the solutions found by Euler and Lagrange become equilibrium solutions. They are the

so-called Lagrange libration points.

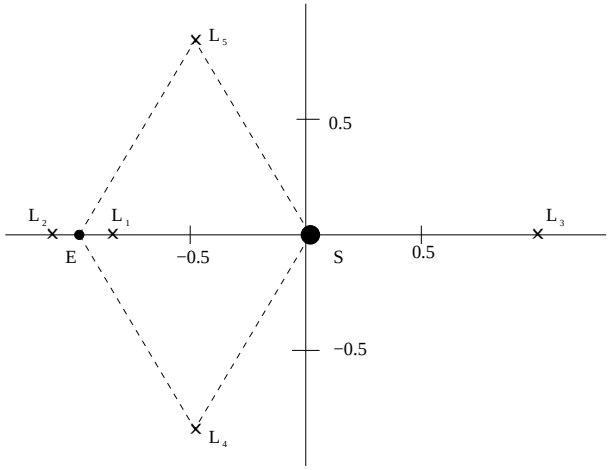

Figure 1.1: The Lagrange libration points in the usual RTBP synodic reference system and units.

Three of the five libration points lie on the line joining both primaries: one, that is usually denoted by L_1, is between the primaries, and the other two at both sides of the two primaries, the one closest to the smaller primary is called L_2 and the third one L_3. The two remaining equilibrium points, L_4 and L_5, are in the plane of motion of the primaries and they form an equilateral triangle with the two primaries (see Figure 1.1).

The Lagrange points offer many new orbits and applications. Around the triangular equilibrium points, L_4 and L_5, there are large regions with good stability properties that could be used as parking regions at which no station keeping is needed. The collinear points, L_1, L_2 and L_3, generate and control many trajectories with interesting applications to space missions and planetary science due to several reasons:

- They are easy and inexpensive to reach from Earth.
- They provide good observation sites of the Sun.
- For missions with heat sensitive instruments, orbits around the L_2 point of the Sun–Earth system provide a constant geometry for observation with half of the entire celestial sphere available at all times, since the Sun, Earth and Moon are always behind the spacecraft.
- The communications system design is simple and cheap, since the libration orbits around the L_1 and L_2 points of the Sun–Earth system always remain close to the Earth, at a distance of roughly 1.5 million km with a near-constant communications geometry.
- The L_2 environment of the Sun–Earth system is highly favourable for non-cryogenic missions requiring great thermal stability, suitable for highly precise visible light telescopes.
- The libration orbits around the L_2 point of the Earth–Moon system, can be used to establish a permanent communications link between the Earth and the hidden part of the Moon, as was suggested by A.C. Clark in 1950 and proposed by R. Farquhar in 1966.

- The libration point orbits can provide ballistic planetary captures, such as for the one used by the Hiten mission.

- The libration point orbits provide Earth transfer and return trajectories, such as the one used for the Genesis mission.

- The libration point orbits provide interplanetary transport which can be exploited in the Jovian and Saturn systems to design a low energy cost mission to tour several of their moons (Petit Grand Tour mission).

- Recent work has shown that even formation flight with a rigid shape is possible using libration point orbits.

The fundamental breakthrough that has given the theoretical and numerical framework for most of the mission concepts of the list above is the use of Dynamical Systems tools. Classical methods can be used only for ordinary halo orbit missions, but all the new concepts require the more powerful Dynamical Systems methods, in order to get qualitative and quantitative insight into the problem.

Dynamical Systems Theory, founded by Poincaré by the end of the XIX century, has used the RTBP as one of the paradigmatic models for its application. Following Poincaré's idea, that it is better to study the full set of orbits rather than individual ones, the Dynamical Systems approach looks at these models from a global point of view. Its procedures are both qualitative and quantitative and have as their final goal to get a picture, as accurate as possible, of the evolution of all the states of the system. This full set of states constitutes the phase space. So, Dynamical Systems tries to get the dynamic picture of the phase space of a given model.

Although the application of Dynamical Systems Theory to space mission design is very recent, it has already been used in various missions, starting with SOHO and followed by Genesis, MAP and Triana. In the case of Genesis this approach not only provided a Δv saving of almost 100 m/s but also a systematic and fast way to perform the mission analysis, with which it was possible to easily redefine the nominal trajectory when the launch date was delayed.

Another relevant example of these advantages are the transfers to libration point orbits, for which previous efforts in its design relied on a manual trial-and-error search followed by and optimisation procedure. The process can now be addressed in a more meaningful and insightful manner by introducing the concept, as well as the explicit calculations, of invariant manifolds as a means to describe the phase space. The result is not only the efficient determination of the desired transfers, but also the emergence of other trajectory and mission options. By understanding the geometry of the phase space and the solution arcs that populate it, the mission designer is free to creatively explore concepts and ideas that previously may have been considered intractable, or even better, had not yet been envisioned. This has been evidenced recently as studies, ranging from flying formations of spacecraft near libration points to sending humans further into space, have been initiated and in fact show great promise.

Beyond baseline trajectory design, of course, other analyses required for any mission can also benefit from studies of motion in this regime, for example, station-keeping strategies for various mission scenarios. The techniques, developed using a variety of approaches, have helped establishing many options that provide robust control scenarios for many or all of the current

mission scenarios. Some station-keeping methods have also been shown to be applicable for a more general class of trajectories, i.e., not just libration point trajectories. The availability of these methods has played an important part in establishing more confidence in mission designers and managers alike regarding potential real world problems that may arise and the ability to effectively handle them.

The final goal of this report is to present a study on the implementation of the tools derived from the Dynamical Systems Theory, taking into account the performance of nowadays computers. It has been framed in the context of present and future missions, as well as in the current state of supporting mathematical tools.

The report is structured as follows. In the second chapter we present a gallery of missions related to libration point orbits including their main paticularities. In the third chapter we summarise the state of the art in the basic but most important topics related with these type of missions. Finally, in chapter four we present the ideas we think might be useful and necessary in the future. These ideas focus on systematising the computation of any type of mission involving libration points and low energy transfers. The report ends with an exhaustive summary of papers and other works involving libration point orbits.

Chapter 2

Missions Using the Dynamics of Lagrange Points

Several spacecraft have previously reached the vicinity of L_1 and L_2 and, thus, design and analysis capabilities are clearly available for such missions. In fact, the design strategies used for some spacecraft launched in the last few years have been very successful, but much more challenging trajectory goals are already being suggested for the next few decades. Within the last ten years, new analytical tools have been developed that provide approximations for many different solutions around the libration points, in a number of dynamical models, and that include various types of periodic and quasi-periodic motions in their vicinity. The structure of the phase space in the vicinity of the collinear points has been examined and the fundamental motions (both planar and three-dimensional) are under investigation. Families of periodic and quasi-periodic orbits have been determined. These include the periodic halo orbits, as well as Lissajous trajectories and quasi-halos. The capability to numerically produce these types of motion is an ongoing development. The local behaviour near these orbits is also of critical importance in any effort to develop general methodologies for mission analysis and has been the focus of the efforts of a number of researchers. These studies have been directly responsible for the application of invariant manifolds to ultimately produce viable transfer trajectories for several missions currently being planned.

Only a few missions have already used the Sun-Earth libration points. But as we see in Table 2.1, in the near future several missions are planned to both the L_1 and L_2 collinear libration points. While similar in their orbital dynamical properties, the diversity of the orbits is characterised by their transfers and final orientations and size (amplitudes in each coordinate) in a Sun-Earth rotating coordinate frame cantered at the libration point. For the International Sun-Earth Explorer (ISEE-3), the first libration point mission, the complexity of mission design was handled through a combination of analytical methods that predetermined the required libration orbit, along with proven operational numerical techniques for targeting and optimisation and orbit evolution prediction. While the SOHO transfer and mission orbit was similar to ISEE-3, the station-keeping control method did not follow the same scheme of following a predetermined analytical path, but the scheme of meeting operational constraints and flying with respect to a quasi-periodic orbit. ACE, the most recently launched libration orbiter, was again different because the transfer orbit was optimised for a capture into a small L_1 Lissajous orbit which is

ISEE–3 (NASA)	L_1 Earth-Sun	1978	Solar wind, cosmic rays
WIND (NASA)	L_1 Earth-Sun	1994	Solar wind, Earth magneto-sphere
SOHO (ESA–NASA)	L_1 Earth-Sun	1996	Solar observatory
ACE (NASA)	L_1 Earth-Sun	1997	Solar wind, particles
MAP (NASA)	L_2 Earth-Sun	2001	Background cosmic radiation
GENESIS (NASA)	L_1, L_2 Earth-Sun	2001	Solar wind composition
WSO	L_2 Earth-Sun	2006	Ultraviolet astronomy
FIRST/HERSCHEL (ESA)	L_2 Earth-Sun	2007	Infrared astronomy
PLANK (ESA)	L_2 Earth-Sun	2007	Cosmic microwave background
TRIANA (NASA)	L_1 Earth-Sun	2008	Earth observation
GAIA (ESA)	L_2 Earth-Sun	2010-2012	Astrometry
NGST/JWST (NASA)	L_2 Earth-Sun	2011	Space telescope
Constellation X (NASA)	L_2 Earth-Sun	2013	X–ray astronomy
DARWIN (ESA)	L_2 Earth-Sun	2014	Planetary systems
TPF (NASA)	L_2 Earth-Sun	2015	Planetary systems
SAFIR (NASA)	L_2 Earth-Sun	2015	Infrared telescope

Table 2.1: Missions to the libration points.

fuel intensive. The WIND mission used multiple lunar gravity assists to minimise fuel cost to meet scientific requirements.

Unique to upcoming missions are the designs of constrained transfer trajectories and mission orbits. They are designed to meet both linear and non-linear orbit goals for smaller Lissajous orbits, to minimise fuel and operational requirements, and to provide formation or constellation options. Traditionally, libration orbit design has been analysed with a baseline trajectory concept set in place by project requirements or analytical boundary methods. That is, a trajectory had been base-lined so that science requirements are met. Future mission design requires a more generalised approach as operational considerations require the launch window, gravity assist, transfer trajectories, final orbits, and the number of spacecraft to be as flexible as possible to optimise science return while minimising operational and launch requirements.

2.1 Gallery of Missions to the Libration Points

2.1.1 ISEE-3: The International Sun-Earth Explorer 3

Mission overview

- **Orbit** Halo orbit around the Earth-Sun libration point L_1.

  $A_x = 175000$ km, $A_y = 666670$ km, $A_z = 1200$ km.

- **Transfer** Direct Transfer, 100 days.
- **Launch** September 12, 1978
- **Launcher** Delta rocket #144.
- **Mission** Investigate Solar-Terrestrial relationships, solar wind, magneto-sphere, and cosmic rays.
- **Operational Lifetime** Planned for 4 years, extended in 1981 and renamed ICE. It will return to the vicinity of the Earth-Moon system in August 2014.
- **Manoeuvres**
  1. 3 trajectory manoeuvres at the transfer (57 m/s).
  2. 15 station keeping manoeuvres (30 m/s).
  3. Attitude and spin control and an anomalous jet firing (32 m/s).
- **Agency** NASA
- **Web page** `http://stardust.jpl.nasa.gov/comets/ice.html`

Spacecraft

- **Mass** 479 kg (includes 89 kg fuel at launch.)
- **Dimensions** cylinder-shaped spacecraft measuring 1.77 m diameter and 1.58 m height. Twelve thrusters made up of four radial, four spin-change, two upper-axial and two lower axial jets.
- **Structure**
- **Propulsion** Hidrazyne fuel for orbit and attitude control
- **Power** 173 W
- **Attitude Subsystem** Spinning spacecraft (20 rpm). Spin axis perpendicular to the ecliptic plane (allowed deviation $\pm$ 1 deg). Redundant pair of high resolution Sun-sensors (accuracy $\sim$ 0.1 deg).

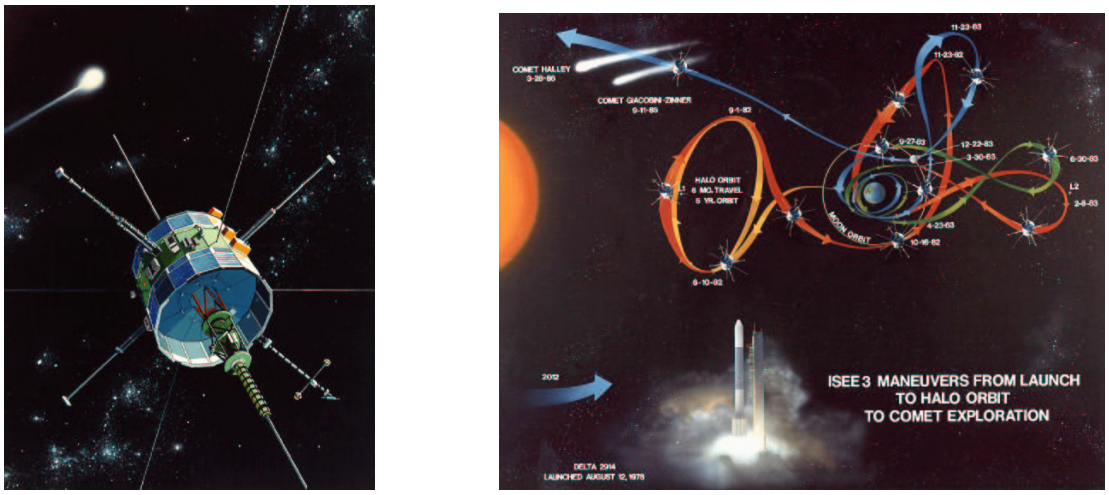

Figure 2.1: The ISEE–3: spacecraft and extended mission trajectory. (`http://heasarc.gsfc.nasa.gov`)

- **Communication Subsystem** The tower structure supports the medium-gain S-band antenna. This antenna has a flat, disk-like ("pancake") pattern that is perpendicular to the spin axis and has an effective beam-width of 12 deg. Its gain is roughly 7 dB over an isotropic antenna.
- **Instrumentation** X-ray spectrometer (University of California) to study both solar flares and cosmic gamma-ray bursts. Goddard Gamma-Ray Burst Spectrometer (high purity germanium detector).

Notable remarks

1. First spacecraft stationed in a libration point orbit.
2. First continuous monitor of solar-wind conditions upstream the Earth.
3. First real-time warning system for geomagnetic storms.
4. First use of multiple lunar swingbys for orbital control in the Earth-Moon System.
5. First exploration of Earth's magneto-tail between 80 and 240 Earth radii.
6. First use of lunar gravity-assist manoeuvre to "launch" spacecraft towards a body outside the Earth-Moon System.
7. First encounter with a comet

More about the mission

The International Sun Earth Explorer 3 (ISEE-3) spacecraft was part of a three spacecraft mission (ISEE 1,2 & 3) whose purpose was to study the solar wind and the solar terrestrial

relationship at the boundaries of the Earth's magneto-sphere. After a series manoeuvre and lunar flybys, ISEE-3 (renamed to ICE) encountered Comet Giacobini-Zinner in 1985 and provided distance observations of Comet Halley in 1986.

Launched on August 12, 1978, ISEE-3 was placed into a large amplitude class-I halo orbit around the Sun-Earth L_1 libration point. This orbit was selected by two reasons:

1. The orbit passes slightly above and below the ecliptic plane, and easily clears the zone of solar interference.

2. For a large amplitude halo orbit the Δv requirements for orbit insertion is significantly lower (the Δv cost decreases linearly as the amplitude increases).

ISEE-3 used a tight-control technique to maintain its trajectory close to the nominal halo orbit. All of the station-keeping manoeuvres were performed with ISEE-3's radial jets, which could be controlled more accurately and were better calibrated from the transfer trajectory correction manoeuvres than were the axial jets. Since ISEE-3's spin axis was maintained perpendicular to the ecliptic, all of the station-keeping manoeuvres were in, or parallel to, the ecliptic plane.

In 1981, it was proposed that ISEE-3 be manoeuvred into Earth's magneto-tail, and then later towards a comet. On June 10, 1982 the first of these manoeuvre was started which moved the spacecraft out of its halo orbit were it has orbited for nearly 4 years. Fifteen manoeuvres were required through the magneto-tail, along with the five lunar flybys to get the spacecraft out of the Earth-Moon system and on it way towards comet Giacobini-Zinner. The fifth an final lunar flyby on December 22, 1983, passed only 119,4 km above the Moon's surface near the Apollo 11 landing site. At this point, the spacecraft was renamed International Cometary Explorer (ICE).

On June 5, 1985, the spacecraft was manoeuvred 26,550 km behind comet Giacobini-Zinner so that its fields and particles instruments could sample the comet's tail. ICE approached the comet at a distance of 7,862 km at its closest approach on September 11, 1985, with a flyby velocity of 20.7 km/s. Because the spacecraft did not carry any dust protection equipment, it was expected to suffer some damage during the encounter. However, the spacecraft survived relatively unscathed.

In 1986, ICE made distant observations of comet Halley on the sun-ward side of the comet. It flew by a distance of 31 millions km from the comet on March 28, 1986, and provided upstream solar wind data.

In 2014, ICE will return to the vicinity of Earth were it could possibly be captured for analysis of its exterior dust impacts.

2.1.2 WIND

Mission overview

- **Orbit** Lissajous orbit around Sun-Earth libration point L_1.
  $A_x = 10000$ km, $A_y = 350000$ km, $A_z = 25000$ km.
- **Transfer** Multiple Lunar Gravity Assist.
- **Launch** November 1, 1994.
- **Launcher** Delta II.
- **Mission** Study the solar wind and its interaction with the Earth's magneto-sphere.
- **Operational Lifetime** 3 years. Extended mission since 1997 continues to evolve. WIND will return to the Earths on November 2008.
- **Manoeuvres** 685 m/s (allocation cost). During WIND's nominal mission phase, sixty-two manoeuvres were executed with a total Δv of 307 m/s.
- **Agency** NASA
- **Web page** `http://www-istp.gsfc.nasa.gov/istp/wind/`
  `http://pwg.gsfc.nasa.gov/wind.shtml`

Spacecraft

- **Mass** 1195 kg (includes 300 kg fuel at launch).
- **Dimensions** cylinder-shaped spacecraft measuring 2.4 m in diameter and 1.8 m in height.
- **Structure**
- **Propulsion** Hydrazine propellant for orbit and attitude control.
- **Power**
- **Attitude Subsystem** Spinning spacecraft (20 rpm). Spin axis within 1 degree of normal to the ecliptic. Four 2.2-N thrusters for spin control.
- **Communication Subsystem**
- **Instrumentation** Two gamma ray detectors (TGRS, KONUS), radio wave receivers (WAVES, MFI), and five instruments to measure solar wind properties (EPACT, SWE, SMS, 3-D PLASMA, SWIM).

Notable remarks

1. Eclipse duration lower to 90 minutes.

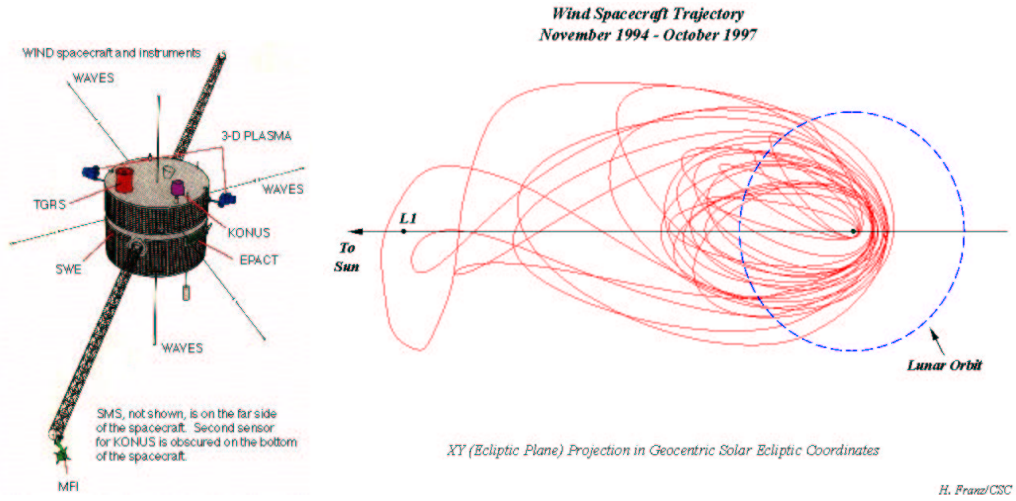

Figure 2.2: WIND spacecraft and nominal orbit (`http://www-istp.gsfc.nasa.gov/istp/wind/`).

2. Sun-Earth-Vehicle angle $> 3^o$ in DLS and $> 5^o$ in halo orbit loop

3. Geocentric Ecliptic Latitude $< 10^o$ for range $< 50^o$ Earth radii.

More about the mission

The Interplanetary Physics Laboratory spacecraft, better known as Wind, was launched on November 1, 1994, on a mission to study the solar wind and its interactions with the Earth's magneto-sphere. Wind is a component of NASA's Global Geospace Science initiative, an element of the International Solar Terrestrial Physics (ISTP) Program. Wind's nominal mission comprised 3 years in a Double Lunar Swingby trajectory, in which pairs of lunar flybys alternately raise and lower apogee and maintain orbital alignment near the Sun-Earth line. The DLS trajectory allowed Wind to study different regions of the magneto-sphere and the upstream solar wind with a minimum of propellant.

Upon completion of its 3-year nominal mission, Wind embarked on an ambitious extended mission in October 1997. To date, the extended mission has comprised 13 separate phases including a variety of orbit types. Wind has made space history on several occasions, holding the current record for lunar gravity assist flybys -38 so far. In addition, Wind was the first spacecraft to complete the treacherous Lunar Back-flip Trajectory in April 1999, as well as the first to fly a distant prograde orbit in August 2000. Wind also utilised high Earth orbits (or "petal orbits", as are they known within the Wind Project) at varying ecliptic inclinations. These different orbit configurations have allowed the project scientists to expand Wind's original charter and obtain measurements in previously unexplored regions of the Sun-Earth environment. Future plans for Wind include visit L_2 and spending considerable time in a Lissajous orbit at the Sun-Earth L_1 point.

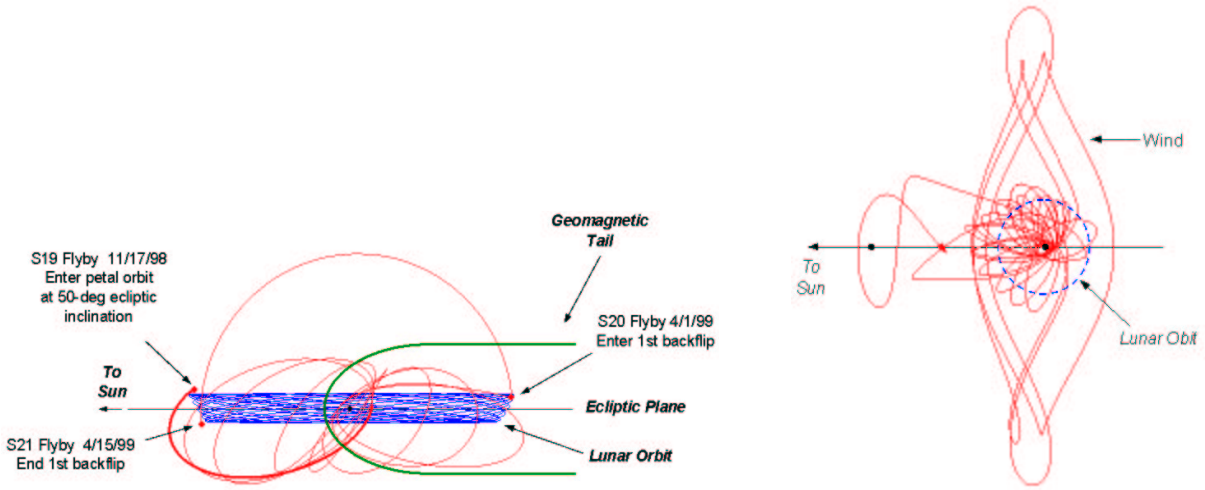

Figure 2.3: XY projection in geocentric solar ecliptic coordinates of WIND extended mission trajectory 1st time back-flip (November 1998-April 1999) and XY projection in L_1 rotating libration point coordinates of WIND extended mission trajectory (January 2000-July 2003).(`http://fdf.gsfc.nasa.gov/plots.htm`).

2.1.3 SOHO: Solar Heliospheric Observatory

Mission overview

- **Orbit** L_1 Halo orbit,
  $A_x = 206448$ km, $A_y = 666672$ km, $A_z = 120000$ km.
- **Transfer** Direct
- **Launch** December, 2nd 1995
- **Launcher** Atlas II-AS rocket (AC-121)
- **Mission** Study the Sun, from its deep core to the outer corona, the solar wind and cosmic rays
- **Operational Lifetime** Planned for 2 years, extended in 1997 to 2003, and in 2002 for 4 more years
- **Manoeuvres** 275 m/s (allocation cost). Total capability 318 m/s
- **Agency** ESA–NASA
- **Web page** `http://sohowww.nascom.nasa.gov, http://solar-center.stanford.edu/`

Spacecraft

- **Mass** 1853 kg (launch weight), including 610 kg of payload and 251 kg of fuel
- **Dimensions** $4.3 \times 2.7 \times 3.65$ m
  9.5 m width with deployed solar array
  21.9 m^2 deployed cross sectional area
- **Structure** Modular, with two main elements: payload module (scientific instruments) and the services module (thrusters, power, communications, thermal control)
- **Propulsion** first stage: Atlas sustainer and 2 booster and 4 Thiokol Castor IVA solid rocket booster (SRB)
  second stage: Centaur (2 LO2/LH2 engines)
  In-orbit: On board hydrazine thrusters
- **Power** 1150 W, solar cell array panels
- **Attitude Subsystem** 3-axis stabilised, one axis always facing the Sun with one arc-second precision. Attitude stabilisation and pointing control via a closed loop system employing an inertial reference frame consisting of 3 roll gyroscopes, 4-wheel reaction wheel assembly for momentum management, a fixed-head star tracker and 2 sun sensors

- **Communication Subsystem** S-band, Earth-pointing high gain antenna, 200 kbps during real time operation, 40 kbps during on-board storage mode transmitting continuously to the DSN ground stations

- **Instrumentation** 12 instruments which observe and study the solar corona, solar oscillations, ultraviolet emissions and solar wind

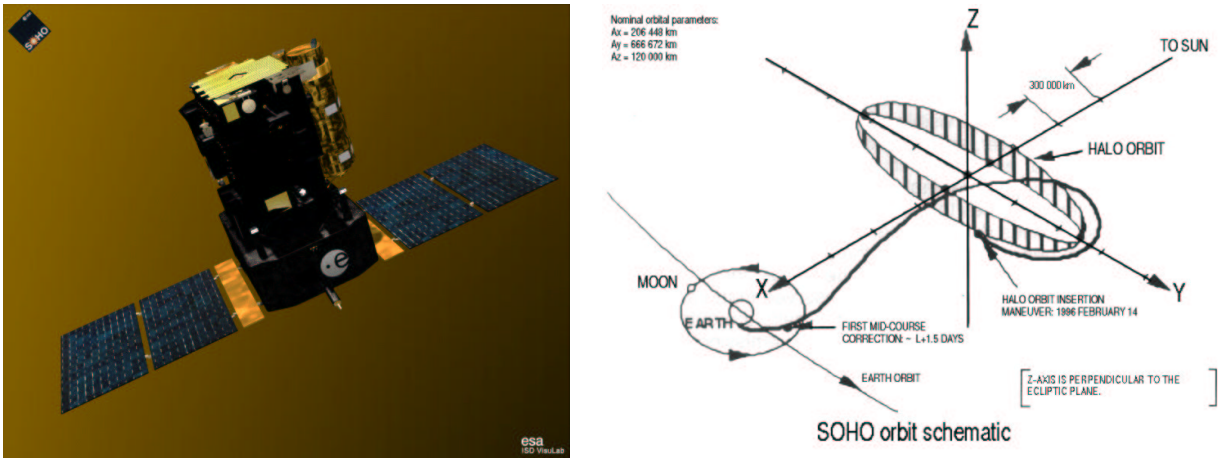

Figure 2.4: SOHO spacecraft and orbit around L_1.

Notable remarks

1. Second mission orbiting L_1 to observe the Sun (after ISEE-3)

2. Enlargement of the mission due to perfect orbit insertion with low fuel consumption

3. When in a certain control mode, SOHO is capable of autonomously stabilising its Sun-pointing attitude using thrusters

More about the mission

SOHO Halo orbit has a period of 178 days (it cycles L_1 twice a year approximately). It has several particular advantages as compared to low Earth orbits (LEO):

1. It provides a smooth Sun-spacecraft velocity change throughout the orbit, appropriate for helioseismology.

2. It is permanently outside of the magneto-sphere, appropriate for the *in situ* sampling of the solar wind and particles.

3. It allows uninterrupted observation of the Sun, appropriate for all the investigations.

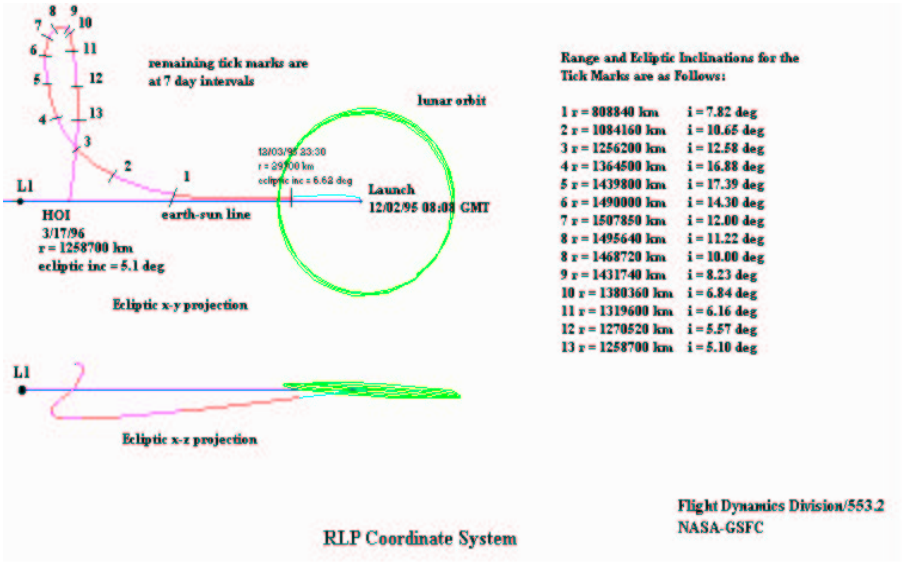

Figure 2.5: SOHO orbit insertion.

The primary mission constraints for the halo orbit were: 1) That the minimum Sun-Earth-Vehicle (SEV) angle never be less than 4.5 degrees (solar exclusion zone, where strong solar interference would make communication impossible), 2) That he maximum SEV angle never be greater than 32 degrees (limit for the High gain antenna). The selected halo orbit fulfils both of these requirements, with a SEV angle never greater than 25.5 degrees.

This joint ESA and NASA mission has been very successful. Its almost perfect orbit transfer and insertion have led to a low fuel consumption, which will allow SOHO to complete a 11 year solar cycle around L_1. In addition to all solar data gathered by the Observatory, since the beginning of the observations around L_1 SOHO has found more than 620 comets.

However, SOHO has had to face some important problems in his operating life up to now. In June, 24th-25th 1998 it suffered a loss of communication with the Earth. SOHO's roll rate began increasing, and the attitude control failed as it rolled into a tumble while still thrusting. Fortunately at the time of the loss there was still 206 kg of fuel remaining in SOHO's tanks, representing a Δv capability of 225 m/s to perform correcting manoeuvres. If re-contact and recovery could not be achieved, SOHO would be flying an uncontrolled, decaying trajectory that would either escape to heliocentric orbit or fall back to Earth. All that could be done at that time was to study possibilities for the SOHO mistaken trajectory, and the necessary recovery manoeuvres for each case. After some weak radio contacts from SOHO and gradually longer contacts during early August, its position was guessed and attitude control reestablished. Two recovery manoeuvres were performed on September the 1st and 25th, with a total moderate cost of 7 m/s. Nevertheless, two of the three roll control gyros were now useless.

Another correcting manoeuvre was necessary in October, and by the last half of November the situation for SOHO was rapidly improving. A small orbit correcting manoeuvre (10 cm/s) was planned for December the 21st 1998, when the only remaining gyroscope failed irretrievable.

The orbital energy was continually increasing, which threatened SOHO to escape into solar orbit. The mission was again in great danger. Doppler data and *Swingby* simulations were used to plan a new 'recovery strategy', successfully carried out on January the 31st 1999.

Despite all the problems, which account for SOHO's being one of the most spectacular mission in the history of space flight, it was estimated to have as much as 145 kg of fuel remaining after the crisis, representing a Δv capability of 170 m/s (more than enough to complete the three years of extended nominal mission). The gyro-less operation has proven to be successful, after all, and the science achievements of the Solar observatory are immense.

2.1.4 ACE: Advanced Composition Explorer

Mission overview

- **Orbit** Lissajous orbit around the Earth-Sun libration point L_1.

  $A_x = 81755$ km, $A_y = 264071$ km, $A_z = 157406$ km.

- **Transfer** Direct (Constrained), 109 days.
- **Launch** August 25, 1997.
- **Launcher** Delta II 7920.
- **Mission** Measure the composition of energetic particles from the Sun, the heliosphere and the Galaxy.
- **Operational Lifetime** There is sufficient hydrazine for ACE to remain in an L_1 orbit until 2019, depending of the details of the orbit.
- **Manoeuvres** Baseline for the launch/transfer trajectory

  1. Transfer trajectory insertion (TTI).
  2. Orbit Shaping Manoeuvres (OSM) - by Launch+20 days, restricts the Sun-Earth-Vehicle (SEV) angle.
  3. Lissajous Orbit Insertion Manoeuvre (LOI) - at TTI + 109 days, establishes the desired motion about L_1.

  Maintenance manoeuvres

  1. Station Keeping manoeuvres - once every 8 weeks.
  2. Orbit Shaping manoeuvres - once every 3-6 months or as necessary to maintain SEV angle requirements.
  3. Attitude reorientation manoeuvres - once every 5-7 days.
  4. Spin rate adjustment manoeuvres - as required.

- **Agency** NASA
- **Web page** `http://www.srl.caltech.edu/ACE/`

Spacecraft

- **Mass** 785 kg (includes 195 kg fuel at launch).
- **Dimensions** Two octagonal decks, 1.6 m across, 1.0 m high.

- **Structure** Six of the scientific instruments are on the sun-ward deck, two are on side-panels, and the ninth is mounted on the Y-axis booms. The earth-ward deck has the fixed high gain antenna for communication.
- **Propulsion** Hydrazine fuel for insertion and maintenance in orbit.
- **Power** 443 W, four fixed solar arrays.
- **Attitude Subsystem** Spinning spacecraft (5 rpm), spin axis aligned within 20 degrees of the Earth/Sun line. Star Sensor and Sun Sensors.
- **Communication Subsystem** S-band, 7 kbps (real time), 2 Gbit (total) solid state recorders.
- **Instrumentation** Nine instruments that measure plasma and energetic particle composition, and one to measure the interplanetary magnetic field.

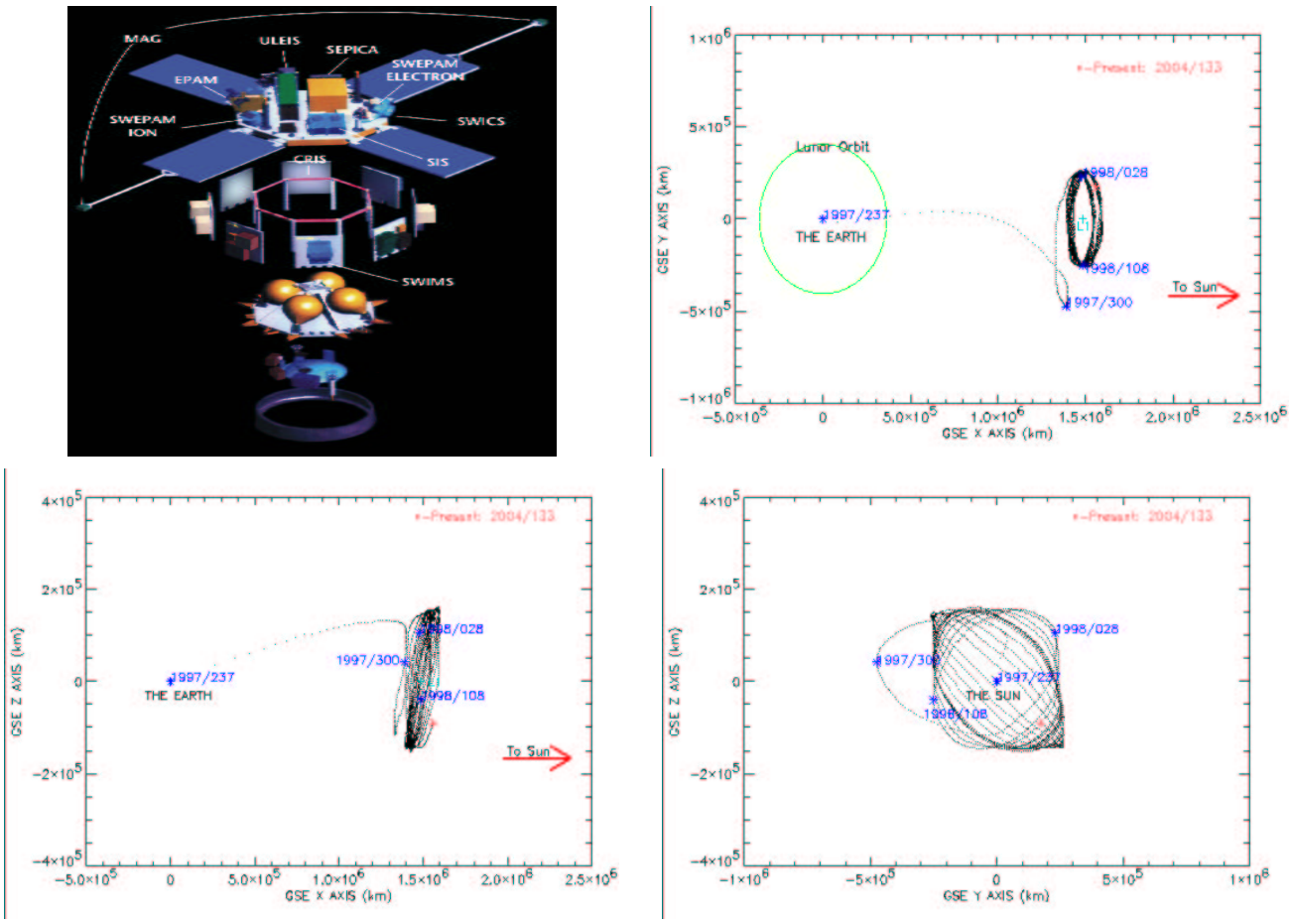

Figure 2.6: Exploded view of the ACE spacecraft structure and projections, in Geocentric Solar Ecliptic Coordinates (GSE), of the position of the ACE spacecraft (`http://www.srl.caltech.edu/ACE/`).

Notable remarks

1. First spacecraft flying in a small amplitude Lissajous orbit.

2. First mission including "z-axis control" manoeuvres to avoid the solar exclusion zone.

More about the mission

Launched on August 25, 1997, ACE was placed in a modified halo orbit around the Sun-Earth L_1 libration point. This orbits is a "broken Lissajous" approximation to a true halo orbit providing Sun-Earth-ACE angles of ten and five degrees respectively. The period of this orbit is about 178 days.

The ACE spacecraft is spin-stabilised at 5 rpm with the spin axis of the spacecraft required to point within 20 degrees (β-angle) of the Sun at all times, as a result of thermal, power, and payload considerations. In addition, the High Gain Antenna is required to point Earth-ward within 4.5 degrees. This two constrains require ACE to perform reorientation manoeuvres as frequently as every 5 days.

The ACE station-keeping strategy is a loose control virtually identical to that used for SOHO. The station-keeping technique is a one-dimensional differential correction process in order to obtain an RLP VX = 0 km/sec at a future Sun-Earth line crossing. The lone independent targeting variable is the Δv along the spin-axis. Given the ACE β-angle constraint, 94 % of this manoeuvres are parallel to the ACE-Sun line.

Due to range ambiguity problems in the tracking systems in 1998 ACE seemed to indicate that a small, continuous extraneous force of unknown origin was acting on the spacecraft as success with SOHO.

Another particular concern of the ACE mission is the sensitivity of the science instruments to the expelled fuel during manoeuvres. It was decided in early 1998 that station keeping burns would be performed before the Δv grew to a magnitude of 0.30 m/sec.

2.1.5 MAP: Microwave Anisotropy probe

Mission overview

- **Orbit** L_2 Lissajous,

  $A_y = 264000$ km, $A_z = 264000$ km.

- **Transfer** 3 Earth-moon phasing loops, lunar gravity assist to L_2
- **Launch** June, 30th 2001
- **Launcher** Delta II-7425-10 number 286
- **Mission** Produce an accurate full-sky map of the cosmic microwave background temperature fluctuations (anisotropy), the oldest light in the universe
- **Operational Lifetime** 27 months: 3 months trajectory to orbit insertion + 2 years at L_2. Fuel limit over 3 years
- **Manoeuvres** Station keeping trim manoeuvres approximately every three months
- **Agency** NASA
- **Web page** `http://map.gsfc.nasa.gov/`

Spacecraft

- **Mass** 836 kg
- **Dimensions** 3.6 m (height), the disk in the basis has a diameter of 5.1 m
- **Structure** Upper part: high gain antennas, data gathering instruments. Middle: thermal control, thrusters, attitude control. Basis: medium gain antennas, circular solar array panels
- **Propulsion** Blow-down hydrazine with 8 thrusters
- **Power** 419 W (solar arrays + battery)
- **Attitude Subsystem** 3-axis controlled. Attitude control electronics, 3 wheels, 1 gyro, star trackers, 6 prime and 6 redundant coarse Sun sensors, 2 star trackers. It spins every two minutes and its spin axis maintains a constant 22.5 degrees angle with the Sun-Earth line
- **Communication Subsystem** Two S-band transponders (2GHz), one prime and the other redundant, with an output power ≥ 5 which receive data from the antennas at all time. Two omni-directional antennas and two medium gain antennas for high speed data transmission to Earth

- **Instrumentation** A set of passively cooled microwave radiometers with 1.4 × 1.6 m diameter primary reflectors to measure the temperature of the microwave sky to an accuracy of one millionth of a degree. (Instrument parts: 2 primary reflectors, 2 secondary reflectors, differential microwave receivers, diffraction shielding, thermally isolating cylinder and passive radiators)

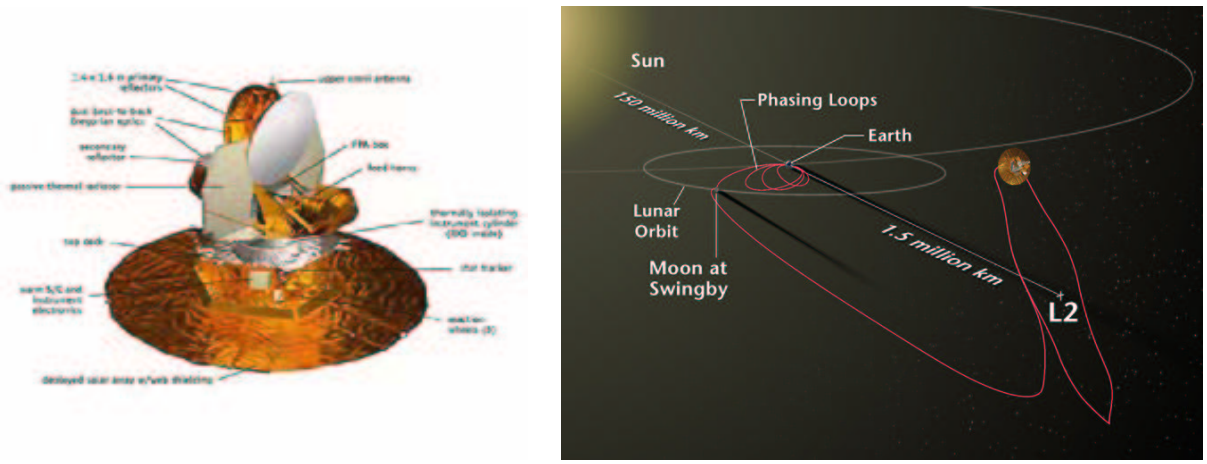

Figure 2.7: MAP spacecraft and orbit.

Notable remarks

1. First mission to use L_2 as its permanent observing station, orbits L_2 every six months and requires occasional station keeping manoeuvres (usually about every 3 months to remain in position)

2. The angle between MAP-Earth vector and Sun-Earth vector must be > 0.5 degrees to avoid eclipses, and < 10.5 degrees to maintain the antenna angles necessary for a sufficient communication link margin

3. MAP's design allows a highly interconnected and redundant set of differential observations to be made in 5 frequency bands (22 to 90 GHz) to enable a separation of galactic foreground signal and cosmic background radiation

More about the mission

An orbit about the Sun-Earth L_2 libration point provides for a very stable thermal environment and near 100% observing efficiency since the Sun, Earth, and Moon are always behind the instruments field of view.

During the phasing loops and until MAP is past the Moon, MAP communicates with Earth with the use of its transponders and two omni antennas located at the top and bottom of the spacecraft. On the way to L_2, MAP switched to use of the Medium Gain Antennas located at

the bottom of the spacecraft. Data is transmitted to Earth once per day from L_2. On orbit operations are conducted at NASA's Goddard Space Flight Center

MAP uses a scan strategy that rapidly covers the sky and allows for a comparison of many sky pixels on many time scales. To realize the full value of the MAP measurements, sources of error must be controlled to an extraordinary level. This was the most important factor driving the MAP design, and led to the following design choices:

- Differential: MAP measures temperature differences on the sky using symmetric microwave receivers coupled to back-to-back telescopes. By measuring temperature differences, rather than absolute temperatures, most spurious signals cancel. This is analogous to measuring the relative height of bumps on a high plateau rather than each bumps elevation above sea level.

- Sky scan pattern: MAP spins like a top. This observing pattern covers a large fraction of the sky (approximately 30 percent) during each one hour precession.

- Multi-frequency: Five frequency bands from 22 GHz to 90 GHz allow emission from the Galaxy and environmental disturbances to be modelled and removed based on their frequency dependence.

- Stability: The L_2 Lagrange point offers an exceptionally stable environment and an unobstructed view of deep space, with the Sun, Earth, and Moon always behind MAP's protective shield. MAP's large distance from Earth protects it from near-Earth emission and other disturbances. At L_2, MAP maintains a fixed orientation with respect to the Sun for thermal and power stability.

2.1.6 Genesis

Mission overview

- **Orbit** Lissajous Orbit around Sun-Earth libration point Point L_1.
  $A_x = 25000$ km, $A_y = 800000$ km, $A_z = 250000$ km.
- **Transfer** Direct, 83 days.
- **Launch** August 28, 2001.
- **Launcher** Delta 7326.
- **Mission** Collect and return solar wind samples to Earth.
- **Operational Lifetime** On 8 September 2004 the sample return capsule will re-enter the Earth's atmosphere.
- **Manoeuvres** Genesis Δv budget estimated

Launch Error Corrections	93 m/s
LOI	6–36 m/s
Station Keeping	24 m/s
Return Station Keeping	45 m/s
Primary Entry Target	4 m/s
Deboost Spacecraft	20 m/s
ACS	71 m/s
Backup Entry	87 m/s
Margin	70 m/s

- **Agency** NASA
- **Web page** `http://genesismission.jpl.nasa.gov/`,
  `http://www.gps.caltech.edu/genesis/IP.html`

Spacecraft

- **Mass** 636 kg (includes 142 kg fuel at launch).
- **Dimensions** 2.3 meters long, 2 meters wide spacecraft deck with two fixed solar panels wings with a total span of 7.9 meters and a sample return capsule mounted on top of the deck.
- **Structure** Equipment deck that supports engineering components and the science instruments. The medium-gain antenna is on the underside, and the low-gain antennas are mounted on the solar winds.

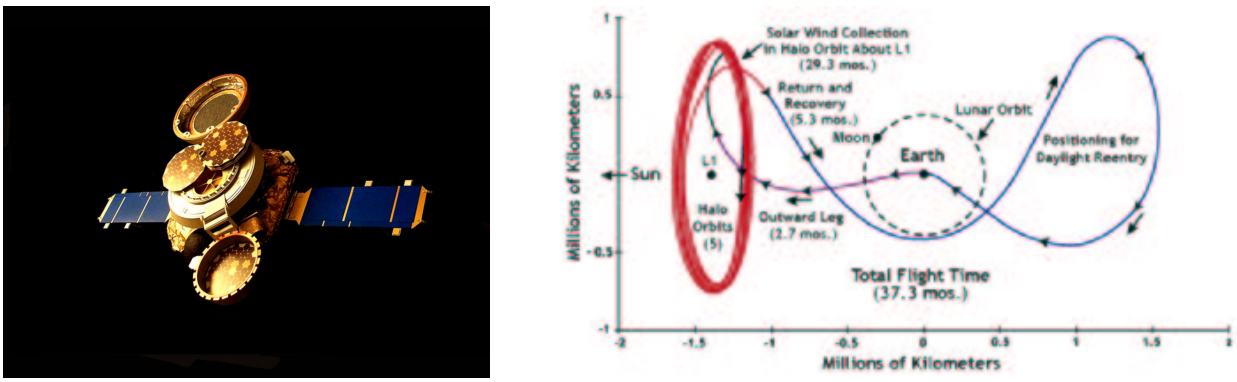

Figure 2.8: Genesis spacecraft and mission trajectory (`http://genesismission.jpl.nasa.gov/`).

- **Propulsion** Hydrazine mono-propellant thruster using a helium pressurant.
- **Power** 254 W
- **Attitude Subsystem** Spinning spacecraft (1.6 rpm during solar wind collection, during manoeuvres, the spin rate will be increased). Spin axis pointing 4.5^o ahead of the Sun. Three axis stabilisation with only a star tracker and two types of Sun sensors.
- **Communication Subsystem** S-band telemetry reception at 15 kilobits per second during the halo orbit phase, and 120 bits per second during the cruise and return phases.
- **Instrumentation** The science payload includes three primary components: the solar wind monitors (an ion monitor and an electron monitor), five collector arrays, and a concentrator.

Notable remarks

1. First mission designed using modern Dynamical Systems Theory.
2. After launch, only one deterministic Δv of 6-36 m/s is required for the entire trajectory (for the insertion in the target orbit).
3. As many as four TCM's were planned to correct the launch error.
4. About 13 station keeping manoeuvres were anticipated to maintain the L_1 libration point orbit (approximately one station keeping manoeuvre every three months)
5. To avoid battery depletion, a time limit of about 85 minutes is imposed during which the spacecraft can be more than 30 degrees off Sun.
6. A manoeuvre may be required every day to compensate the approximate one degree precession angle drift between the spin-axis and the Sun-spacecraft line.
7. Thermal requirements prevent the spacecraft from pointing more than 60 degrees away from the Sun.

More about the mission

Genesis has three operations phases: launch segment, acquisition and return leg. The techniques used to design the pieces represent an innovative approach to trajectory design so Genesis is the first mission designed using modern Dynamical Systems Theory. The near optimal Genesis trajectory launch segment was obtained using the stable manifold of the nominal Lissajous orbit and the return leg by using the unstable manifold, in fact, exploiting the homoclinic behaviour of the L_1 and L_2 regions (homoclinic and heteroclinic chains).

Launched on August 28, 2001, from Delta 7326 launch vehicle using a Thiakol Star37 motor as the final upper state. The most important error introduced by the inaccuracies of the launch vehicle were the velocity magnitude error. In this case the expected error was 7 m/s (1 σ value) relative to a boost of approximately 3200 m/s from a 200 km circular parking orbit. Due to the sensitivity to launch errors of the halo orbit missions, this error must be corrected within the first days after launch. This critical Trajectory Correction Manoeuvre is called TCM1, being the first TCM of any mission. Since TCM1 was executed so well TCM3 was cancelled (TCM2 and TCM4 were contingency manoeuvres).

Genesis was placed in a Lissajous orbit around the Sun-Earth libration point L_1 on November16, 2001, with solar-wind collection starting shortly thereafter, on December 3. The spacecraft completed five orbits by April, 2004, making approximately two orbits per year. To maintain its sun pointing, the spacecraft executes an autonomous 1-degree precession manoeuvres each day. It has three station keeping manoeuvres each orbit. In April, 2004, it departed from the Lissajous orbit, swings past the Earths (there is no lunar flyby), and passe close to L_2 point. This trajectory puts the spacecraft in position for a daylight re-entry.

2.1.7 TRIANA

Mission overview

- **Orbit** L_1 Lissajous orbit,

  $A_x = 264000$ km, $A_y = 81000$ km, $A_z = 148000$ km.

- **Transfer** Direct transfer (depending on the launcher) from a LEO along an outgoing asymptote, that is essentially in the Earth-Sun line, to the Lissajous
- **Launch** Winter 2008
- **Launcher** Space Shuttle preferably. However, other options are being studied (Delta II, Ukrainian Tsyklon ...)
- **Mission** Send images of the nearly fully lit Earth disk in 10 different wavelengths once every 15 minutes. Educational products
- **Operational Lifetime** 2 years minimum, 5 year goal
- **Manoeuvres** 620 m/s (Allocation Δv)
- **Agency** NASA
- **Web page** `http://triana.gsfc.nasa.gov/home/`

Spacecraft

- **Mass** Observatory+instruments= 565 kg, spacecraft ejected total mass=2989 kg
- **Dimensions**
- **Structure** Two major components: Observatory (science instruments, the Spacecraft Bus, and the subsystems required to operate the mission and process the data) and the GUS = Gyroscopic Upper Stage (provides the power and thrust to transport the Observatory from Low Earth Orbit (LEO) to the Lissajous Orbit Insertion (LOI) point)
- **Propulsion** Hydrazine: Star-48B kick motor (in GUS)
- **Power** 1700 W (10 solar cell modules)
- **Attitude Subsystem** 4 wheels, gyro, star tracker, sun sensors, propulsion module
- **Communication Subsystem** 100 to 200 kbps down-link / 2 kbps up-link, 1.3 meter communication high gain antenna and two omni antennas to insure that a communication link to Triana is always available
- **Instrumentation** Earth viewing and solar wind instruments (NISTAR radiometer, EPIC telescope and Plasma Magnetometer Solar Weather Instrument)

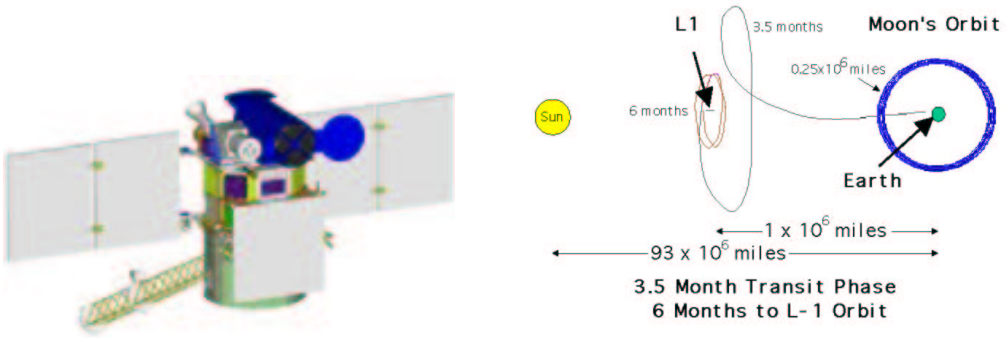

Figure 2.9: TRIANA spacecraft and orbit.

Notable remarks

1. First Earth science mission to take advantage of a Lissajous around L_1
2. The satellite is ready to fly, it just needs an adequate ride to space
3. It will use IRIS (Italian Research Interim Stage) to provide the physical supporting structure for Triana while it's in the Space Shuttle Payload bay. IRIS spins the Spacecraft up to 60 rpm and then ejects it from the Shuttle
4. In the past, scientists have had to stitch together thousands of measurements from satellites in low Earth or geostationary orbits to get a perspective comparable to Triana's

More about the mission

From L_1, Triana will have a continuous view of the Sun-lit side of the Earth at a distance of 1.5 million kilometres. In order to obtain the same coverage with current Earth-observing satellites in low Earth orbits and geostationary orbits, scientists must manipulate, calibrate, and correlate data from four or more independent satellites. The full view of the Sun-lit disk of the Earth, afforded by the L_1 location, has tremendous potential for Earth science. Triana will be the first mission to explore this potential by helping to answer difficult questions facing climate researchers. For example, scientists still do not accurately know how much of the Sun's energy the Earth absorbs, re-emits, and reflects. This common measurement, called the planetary albedo, is vital for climate research. Unfortunately, it is difficult to measure the Earth's albedo due to cloud cover, ice, snow, smoke, volcanic ash, and other factors which cause it to constantly change. Triana can provide significantly better measurements of global albedo, and can re-determine the albedo every fifteen minutes, making it a good barometer of global change.

Budget reductions resulted in cutting the number of Space Shuttle missions per year. Thus, Triana is being kept "in a box" waiting for a travel option. Meanwhile, Triana Project has explored various expendable launch vehicle options. Delta II ELVs have the capability to boost Triana directly onto its transfer trajectory, and this seems to be a viable option, as the software available allowed for a solution to be found concerning the orbit insertion. However, the lack

of funding on the Triana Project is responsible for this still haven't come to fruition. A 3-stage version of the Ukrainian Tsyklon vehicle, being proposed by United Start, would be capable of putting the Triana/GUS stack into an orbit from which a transfer to L_1 would be possible. The final possibility, and possibly the most difficult to accommodate is Ariane 5. What makes it difficult is that Ariane's standard product is a specific geostationary transfer orbit, which would imply a new transfer trajectory (triangular) to be computed. These trajectory has departing asymptotes that are much farther off the Earth-Sun line than the baseline trajectory.

To sum up, even though Triana is ready for launch, its future observations being very useful for Earth-observation educational products and investigation, it is waiting for its opportunity to fly and follow its L_1 libration orbit.

2.1.8 NGST/JWST: Next Generation Space Telescope

Mission overview

- **Orbit** Lissajous orbit around the Earth-Sun libration point L_2

  $A_x \simeq 290000$ km, $A_y \simeq 800000$ km, $A_z \simeq 131000$.

- **Transfer** Direct.
- **Launch** August 2011.
- **Launcher** Ariane 5.
- **Mission** Determine the shape of the Universe, explain galaxy evolution, understand the birth and formation of stars, determine how planetary systems form and interacts, determine how the Universe built up its present chemical/elemental composition and probe the nature and abundance of Dark Matter.
- **Operational Lifetime** 5 to 10 years.
- **Manoeuvres** 150 m/s (allocation cost)
- **Agency** CESA, ESA, NASA
- **Web page** `http://ngst.gsfc.nasa.gov/`

Spacecraft

- **Mass** Approximately 6200 kg, including observatory, on-orbit consumables and launch vehicle adaptator.
- **Dimensions** 6.5 m primary mirror, comprised of 18 hexagonal-shaped segments. Five-layer sun-shield, nearly the size of a tennis court.
- **Structure** NGST has three elements: Optical Telescope Element (deployable optical system with diffraction limited by 2 μm), Integrate Science Instrument Module Element, and Spacecraft Element (highly stable pointing platform)
- **Propulsion** Hydrazine thrusters for gyro despin.
- **Power** Solar power.
- **Attitude Subsystem** The Fine Guidance Sensor is integral to the attitude control system of NGST, and consists of two fully redundant instruments that will enable precise (3 milliarcseconds) pointing of the telescope.
- **Communication Subsystem** X-band 1.6 Mbps down-link.
- **Instrumentation** Near-Infrared Multi-Object Spectrometer, Near-Infrared Camera, Mid-Infrared Camera/Spectrometer.

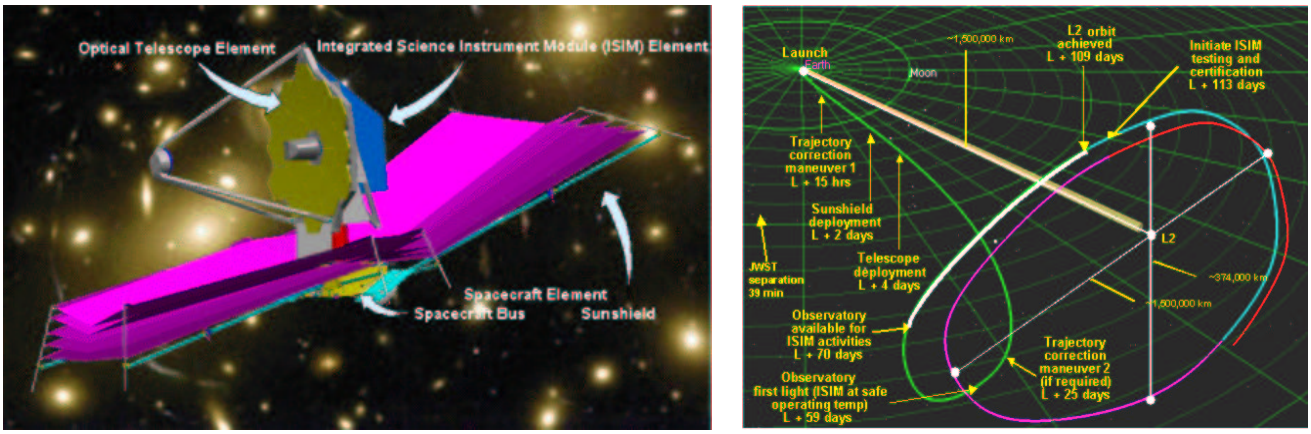

Figure 2.10: NGST artistic image and transfer orbit (`http://ngst.gsfc.nasa.gov/`).

Notable remarks

1. Basic challenges compared to the HST
   - Primary mirror ten times larger in collecting area,
   - A quarter of the mass (and cost),
   - Located far from Earth.
2. Technological Challenges At-A-Glance
   - Developing a lightweight, 6-meter-class deployable mirror that will unfold en-route to its nominal orbit.
   - Tennis court-sized deployable sun-shield, which passively cools instruments and other mechanisms to 35 Kelvin and prevents the electronics from radiating heat and interfering with the collection of extremely faint infrared photons.
   - Constructing a highly capable spacecraft that weighs about 5000 kg.
   - Building low-noise, large-area detectors.
   - Designing, launching and operating JWST at a significantly lower cost than that of its predecessors.

More about the mission

The Next Generation Space Telescope (NGST), renamed James Webb Space Telescope (JWST) on September 10, 2002 in honour of James E. Webb, NASA administrator from 1961-1968, is in many ways a successor to the highly successful Hubble Space Telescope (HST). With a planned launch in August 2011, the NGST will be bigger and much more powerful than the HST, yet also cheaper to build and operate.

The powerful observatory's design features a 6.5 meter aperture primary mirror, comprised of 18 hexagonal-shaped segments. The large-size mirror, which could fit seven HST mirrors within

its surface area, gives it the light-collecting sensitivity to see objects 400 times fainter than those currently observed by ground and space-based telescopes.

The telescope's five-layer sun-shield wild shield the telescope from sunlight and keep it a cold temperature only 30 degrees above absolute zero. The extreme cold enables NGST to see light in infrared wavelengths, allowing it to detect light through dense, dusty clouds were star and planet formation take place.

To fit inside the launch vehicle, an Ariane 5, the large NGST mirror must be folded in sections for launch, then unfolded (deployed) precisely into places after launch, making it the first segmented optical system deployed in space. Once in space, the sun-shield that was folded over the optics during launch wild unfold to its full size and keep the telescope in the cold shadow of the Sun.

2.1.9 FIRST/HERSCHEL: Far InfraRed and Submillimeter Telescope

Mission overview

- **Orbit** L_2 large amplitude Lissajous

  $A_x \simeq 800000$ km, $A_y \simeq 500000$ km, $A_z \simeq 500000$.

- **Transfer** Stable manifold transfer from ARIANE launch
- **Launch** 2007
- **Launcher** ARIANE 5
- **Mission** Far infrared astronomy. To investigate the history of how stars and galaxies formed and to study how they continue to form in our own and other galaxies.
- **Operational Lifetime** At least 3 years, 4 years extended
- **Manoeuvres** Once it is inserted in the Lissajous, not more than 1 m/s per year of station keeping Δv. A manoeuvre once per month
- **Agency** ESA
- **Web page** `http://www.rssd.esa.int/Herschel/` `http://www.space-technology.com/projects/herschel/`

Spacecraft

- **Mass** 2970 kg
- **Dimensions** 9.3 m high $\times$ 4.3 m wide, primary mirror 3.5 m diameter
- **Structure** Payload module (telescope, liquid helium cooling system, sunshade, support structures) mounted on top of the services module (power, attitude and orbit control, communications)
- **Propulsion**
- **Power** 1450 W (solar panels)
- **Attitude Subsystem** three-axis stabilised
- **Communication Subsystem**
- **Instrumentation** Infrared telescope and 3 scientific instruments: PACS and SPIRE are cameras to take pictures in six 'different colours' in the far-infrared. HIFI is a spectrometer with extremely high resolution

Notable remarks

Figure 2.11: HERSCHEL (left) and PLANCK (middle) spacecraft and their joint configuration inside the launcher (right).

1. Accurate orbit selection, according to launch constraints, as well as cheap station-keeping and eclipse avoidance criteria
2. It is the largest and most advanced infrared telescope ever built and can observe wavelengths never covered before. Its primary mirror is so large that it cannot be built in one single piece.
3. The spacecraft design takes advantage of the type of manoeuvres needed to follow the nominal orbit, which will be all nearly aligned

More about the mission

The design of FIRST/HERSCHEL orbit was constrained in several ways. It had to be an orbit which can be reached from a maximum mass ARIANE launch, taking into account the Sun aspect angle during the ARIANE powered ascent and the duration of the eclipse in the transfer. An specific feature of an ARIANE launch is due to the launch site location, near the equator. The orbits around L_2 lie near the ecliptic plane, so orbits into which ARIANE can deliver large payloads may not always be suitable for a L_2 "cheap" transfer. This led to the class of large size Lissajous orbits.

In spite of the good observing conditions and stable thermal environment around L_2, this region is dynamically unstable. The escape direction can be computed at every point by linear

Dynamical Systems Theory (obtaining a fairly good approximation) in order to use it in the manoeuvres plan. Δv performance in the non-escape direction will result in a globally cheaper strategy. All manoeuvres will be nearly aligned or opposite to a direction 28.6 degrees from the Sun to Earth axis.

The insertion in the orbit also uses Dynamical Systems Theory to minimise fuel consumption, by choosing suitable launch windows. If ARIANE is launched sometime inside these windows, the conditions it reaches touch the stable manifolds of large Lissajous orbits, so that FIRST/HERSCHEL can approach its planned orbit with near zero cost by travelling along these manifolds towards its observing location.

Eclipse avoidance when the satellite is orbiting the Lissajous can be achieved by reverting its velocity at the point with maximum $|y|$ position ($\dot{y} = 0$), previous to entering the exclusion zone (a disk of about 13000 km radius in the yz-plane). However, with a good insertion phase (which can leave the satellite in a non-eclipse trajectory for about 6 years) these kind of manoeuvres may not be necessary.

2.1.10 PLANCK

Mission overview

- **Orbit** L_2 Lissajous, maximum elongation from L_2 of 280000 km, Sun-Earth-Spacecraft angle never exceeding 10 degrees. 6 months period
- **Transfer** With Herschel. Lissajous amplitude reduction manoeuvre 3 months after launch
- **Launch** 2007
- **Launcher** ARIANE 5
- **Mission** Cosmic microwave background: image the anisotropies of the Cosmic Background Radiation Field over the whole sky, with unprecedented sensitivity and angular resolution
- **Operational Lifetime** 21 months (15 months orbiting L_2 and collecting data after 6 months transfer)
- **Manoeuvres** To maintain the spin-axis in the Sun-spacecraft line, approximately 1 manoeuvre/hour of 2.5arc-minutes along the ecliptic plane (most simple law, which may be modified to fulfil the mission)
- **Agency** ESA
- **Web page** `http://www.rssd.esa.int/index.php?project=PLANCK`, `http://www.jb.man.ac.uk/research/cmb/planck.html`

Spacecraft

- **Mass** 1430 kg
- **Dimensions** 4.1 high $\times$ 4.2 diameter (m)
- **Structure** Payload module (telescope, focal plane unit, cryogenic radiator baffle) and services module
- **Propulsion**
- **Power** 1655 W
- **Attitude Subsystem** Uses gyroscopic rigidity (spin-stabilisation) not passive but with an on-board capacity for decision and control. Low spinning system (1 rpm), the spin axis is displaced approximately 1 degree per day in the direction of Sun-Earth rotation
- **Communication Subsystem** Collects data in a solid state recorder and down-link it to ground station 3 hours/day. Spacecraft not reoriented towards the Earth, thus the telemetry antenna is designed to have and adequate gain within a 10 degrees half-cone from the spin axis to achieve full band width even in the extremes of the orbit

- **Instrumentation** A telescope for microwave observations, LFI (low frequency instrument) which collects data in 4 frequencies from 30 to 100 GHz, HFI (high frequency instrument) in 6 frequencies from 100 to 857 GHz

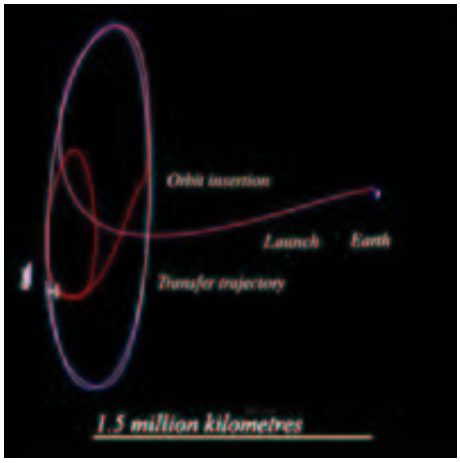

Figure 2.12: HERSCHEL and PLANCK orbit.

Notable remarks

1. Launched together with Herschel, it will need an additional manoeuvre to enter its small size Lissajous around L_2

2. Planck's observations will help to answer questions such as - how did the Universe begin, how did it evolve to the state we observe today, and how will it continue to evolve in the future.

More about the mission

Planck will be delivered by ARIANE into the stable manifold of a Lissajous orbit of large size, together with Herschel (during the launch Planck is on place of the lower passenger, inside of a launcher adapter). It will have to be manoeuvred from there to an orbit with a smaller size. The amplitude reduction manoeuvres will be in the plane spanned by the non escape direction in the xy-plane and by z. Since the motion in the xy-plane and the motion in the z-plane are decoupled, the problem of finding a cheap reduction manoeuvre can also be decoupled. The cost and availability of a combined manoeuvre obtained by vector addition can be studied afterwards, to suit the mission constraints.

Planck Surveyor will observe the whole sky at least twice at all nine frequencies over two separate six month periods, and after about 18 months in orbit the data will be combined into maps of the microwave sky at the various data processing centres situated around Europe. It is important to have redundant observations (same regions of sky observed several times and in different satellite attitudes) to remove systematic effects.

2.1.11 GAIA

Mission overview

- **Orbit** L_2 Lissajous, approx. square A_y=A_z=110000 km
- **Transfer** First inserted in a circular orbit of 51.8 degrees inclination, 190 km altitude. A second burn, with or without lunar gravity assist (which could save about 50 m/s), will insert GAIA to its orbit around L_2
- **Launch** 2010-2012
- **Launcher** Soyuz-Fregat
- **Mission** Galactic structure, astrometry: measure the positions of an extremely large number of stars with unprecedented accuracy. Clarify the origin and history of our Galaxy, by providing tests of the various formation theories, and of star formation and evolution.
- **Operational Lifetime** 5 years planned (220-240 days transfer + 4 years observations). 6 years extended
- **Manoeuvres** 180 m/s (for a 6 months launch window)
- **Agency**
- **Web page** ESA `http://www.rssd.esa.int/gaia/, http://www.esa.int`

Spacecraft

- **Mass** 3137 kg (payload = 803 kg, service module = 893 kg, system margin (20%) = 339 kg, fuel = 1010 kg, launch adaptor = 92 kg)
- **Dimensions** payload: diameter = 4.2 m, height = 2.1 m; service module: diameter = 4.2 m (stowed)/8.5 m (deployed), height = 0.8 m. 9 m width with solar array deployed
- **Structure** Hexagonal conical shape which consists of: payload module (top) and service module. In the basis, 6 deployable solar array panels and a sun-shield
- **Propulsion** Chemical bi-propellant propulsion (transfer phase). Redundant set of FEEP thrusters once in L_2
- **Power** 14 A/h lithium-ion battery launch and early operations. Once in orbit 2569 W (payload = 1528 W, service module = 641 W, harness losses = 76 W, contingency (10%) = 224 W
- **Attitude Subsystem** 3 Sun acquisition sensors + 1 gyro provide spin-axis (5 rpm) stabilisation during the transfer phase. For the 3-axis stabilised phase, it uses a large field of view star tracker plus the main instrument sky mappers and electrical (FEEP) thrusters

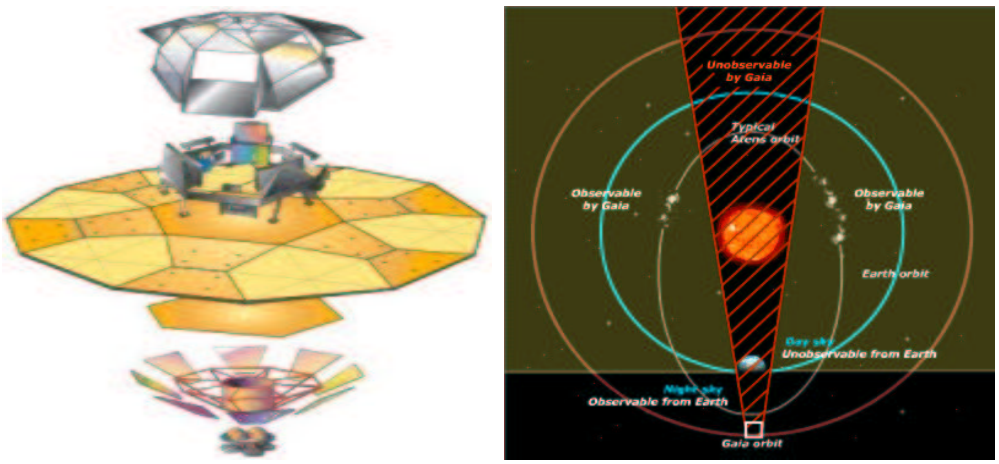

Figure 2.13: GAIA spacecraft and observable sky schematic representation.

- **Communication Subsystem** Continuous payload data rate of about 1Mbps. Down-link to Earth stations 8 hours a day, X-band 3 Mbps capacity
- **Instrumentation** Two astrometric telescopes with a common focal plane and a spectra telescope comprising a radial velocity spectrograph and a medium-band photo-meter

Notable remarks

1. Eclipse avoidance manoeuvres as planned for Herschel and Planck are not possible for GAIA, because of the extreme low thrust level of the electric propulsion system
2. GAIA will rely on the proven principles of ESA's Hipparcos mission, and take them to an enormous degree of accuracy using the technology available

More about the mission

The selection of the orbit arises from a trade-off between communication, operations, cost, thermal environment, and accessibility with current rockets.

The system fits within a dual-launch Ariane 5 configuration, without deployment of any payload elements. The telescopes are of moderate size, with no specific design or manufacturing complexity.

GAIA will be a continuously scanning spacecraft, accurately measuring one-dimensional co-ordinates along great circles, and in two simultaneous fields of view, separated by a well-defined and well-known angle (these one-dimensional coordinates are then converted into the astrometric parameters in a global data analysis). The method used by GAIA to compile its 10^9 star catalogue will be measurements of stellar parallax, that is the apparent angular movement of a star in the sky when observed from opposite sides of the Earth's orbit around the Sun. However GAIA will make these measurements with astounding accuracy, up to 10 micro-arc-seconds (about 3 billionth of a degree) due to its stable position in space and the freedom from distortions induced

by the shimmering atmosphere of Earth. Such accuracy will allow astronomers to compile the most detailed 3-D model of the distribution of stars in our Galaxy ever obtained.

Yet there is more to GAIA than just measuring the position of stars. The photometric detectors used by the spacecraft telescopes will also measure the brightness of the stars in up to 18 wave-bands. The spacecraft will also study the amount of red-shift or blue-shift of the light to assess the rate at which the star is approaching or receding from Earth. These measurements will reveal many of the essential properties (e.g. age, mass, true luminosity) of the stars allowing astronomers to refine theories of how stars evolve.

GAIA will also detect subtle changes in the brightness of stars and small wobbles in their position. Such variations may reveal the presence of extra-solar planets passing in front of the star, blocking its light, or by pulling on the star as they orbit. It is thought that up to 30000 new worlds may be detected. GAIA will also look at objects much closer to home with astronomers expecting the instruments to detect up to a million asteroids and Kupier Belt objects during their survey of the sky.

2.1.12 Constellation X

Mission overview

- **Orbit** L_2 Lissajous orbit. Constellation in loose formation
- **Transfer** Lunar gravity assist with phasing loops
- **Launch** 2013
- **Launcher** Atlas V-500 / Delta II / Delta IV
- **Mission** X-ray astronomy (black holes, Einstein's theory of general relativity, galaxy formation, evolution of the universe, recycling of matter and energy, nature of dark matter ...)
- **Operational Lifetime** 3 years minimum, 5 years goal
- **Manoeuvres** 150-250 m/s (allocation cost)
- **Agency** NASA
- **Web page** `http://constellation.gsfc.nasa.gov/`

Spacecraft

Baseline Configurations	GSFC/SAO	TRW	Ball Aerospace
spacecraft	4	3	2
mass (kg)	1450	3700	–
structure	bus+payload (EOB [1],telescopes)	bus + EOB + solar arrays	FOB, temperature separation of components
launcher	Delta II	Delta IV-Medium	EELV (US Air Force)
propulsion	–	bi-propellant (transfer) hydrazine only (once in orbit)	–
power	–	1700 W	–
communication	–	X-band,up-link at 2kbps, return data 1Mbps	–

Table 2.2: Possible configurations for each spacecraft of the constellation. See Figure 2.14.

Notable remarks

1. Multi-satellite design saves money and reduces risk
2. The constellation will collect more data in an hour than they would have collected in days or weeks with current telescopes, with a sensitivity 100 times greater

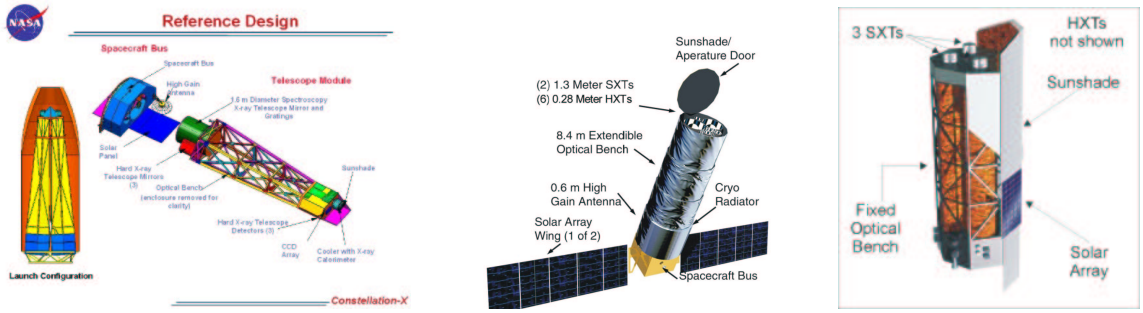

Figure 2.14: From left to right: GSFC/SAO, TRW and BALL AEROSPACE baseline configurations for Constellation X spacecraft.

More about the mission

The satellites are light enough to be launched individually or in pairs. Depending on the chosen configuration and launcher, from 2 to 4 launches will be needed to put the whole constellation in orbit. This yields a more difficult orbit and station keeping design, while reducing costs and risk, as the use of multiple telescopes allows each of them to be cheaper than a huge one, and the need for several launches reduces the probability of total failure of the mission.

The spacecraft will be inserted into the Lissajous orbit via a lunar swingby. The lunar swingby is necessary in order to reduce the amount of on-board Δv. To increase the number of launch opportunities, a number of phasing loops will be performed prior to the lunar swingby.

The mission separations between the flotilla are not determined but initial goals indicate separations of greater than 50 km but less than 50000 km.

The main scientific observation constraints to be taken into account are: 90% of the sky must be accessible at least twice a year, with viewing windows not shorter than 2 weeks in duration. 100% of the sky available at least once a year, viewing window of 1 week.

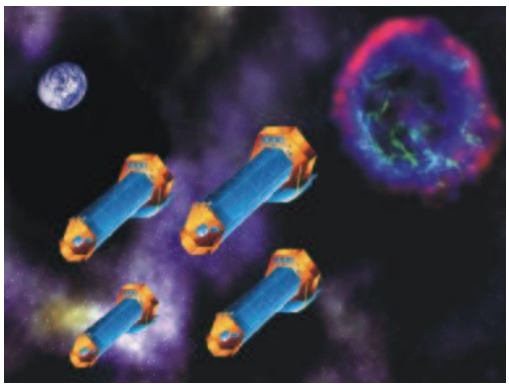

Figure 2.15: Artist impression of the whole Constellation-X fleet.

2.1.13 WSO: World Space Observatory

Mission overview

- **Orbit** L_2, halo type of max. amplitude 800000 km
- **Transfer** via a 3 months transfer from a LEO (200 km) into Earth's escape to L_2
- **Launch** mid 2006
- **Launcher** Proton-block DM (other option: Ariane 5)
- **Mission** Astronomy in the ultraviolet wavelength range to study planets (atmospheric and ionospheric conditions), stars, comets, asteroids and galaxies. Long term study of black holes. Search for planet candidates. Study of star formation.
- **Operational Lifetime** 5 years nominal mission duration (10 years design lifetime)
- **Manoeuvres** main Δv=75 m/s at the beginning of cruise (80% of propellant mass used). Enough propellant left for a 10 year mission almost without intervention
- **Agency** International endeavour
- **Web page** `http://wso.vilspa.esa.es/`

Spacecraft

- **Mass** 3456 kg
- **Dimensions** 8.5 m height, SVM 3.1 m $\times$ 2.8 m $\times$ 1.1 m, 21 m^2 of deployable and fixed solar arrays
- **Structure** Modular: Service module, telescope, optical bench
- **Propulsion** Highest instruments throughput 9.51Mbps. Data acquisition per day 32Gbits (worst scenario. On board capacity of data acquired during 2 days. Ground: Transmission: 7190-7235 MHz frequency band, and antenna gain 57 dBi. Reception: 8450-8500 MHz, 60 dBi
- **Power** Batteries (first part of the mission): power required 313 W, capacity 7 Ah (in case of an Ariane 5 launch, capacity must be enhanced to 14.2 Ah due to a longer eclipse during orbit insertion). Solar cells (6): power supplied per cell = 400 W, power required = 282.5 W (excess of power used to re-charge batteries)
- **Attitude Subsystem** Hydrazine reaction control system combined with control wheels for control actuation, star trackers and fine guidance sensors

- **Communication Subsystem** 1 X-band high gain antenna (HGA) and 3 fixed X-band LGA (low gain antenna). Down-load 32 Gbits per day, transmission time of 8 hours (constrained to 1.5 Mbps, project design uses an average of 1.1Mbps as the down-load data rate). Up-link 4 kbps

- **Instrumentation** Telescope (with primary and secondary mirror systems), UV spectrograph, UV imager

Notable remarks

1. The WSO concept is aimed at promoting an international cooperation in the field of Astronomy/solar system missions in the UV frequency range

2. In the selected orbit, the spacecraft completes the celestial sphere within one year

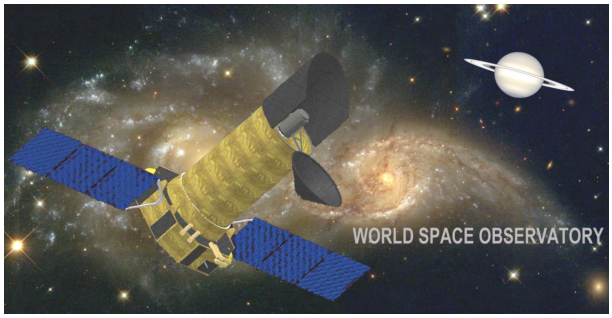

Figure 2.16: WSO spacecraft.

More about the mission

WSO capabilities will fill a hole in the collection of astronomical data, which cannot be filled by any other observatory, neither in the ground nor in space.

The World Space Observatory will create opportunities for participation of all countries of the world, even without the need for excessive investment.

The main advantages of choosing a very big orbit around L_2 were the lack of eclipses, (compared to, for example, a highly inclined eccentric orbit), and the free observing environment, contrary to the large portion of celestial sphere which is not accessible at any time for a circular orbit of 50000 km to 80000 km of altitude, due to the Sun, Earth and Moon.

2.1.14 Darwin

Mission overview

- **Orbit** L_2 halo orbit
- **Transfer** Direct
- **Launch** January 2014
- **Launcher** Ariane 5
- **Mission** To look for Earth-like planets, and signs of life on them, and to provide imaging of space in the 5 to 28 micron band
- **Operational Lifetime** Five years
- **Manoeuvres**
- **Agency** ESA
- **Web page** `http://sci.esa.int/science-e/www/area/index.cfm?fareaid=28`

Spacecraft

- **Mass** 4240 kg
- **Dimensions** Master satellite: 1 m sided cube, each telescope at least 1.5 m in diameter (possibly 2.8 m long $\times$ 1.7 m wide, constrained because the eight spacecraft must fit in the nose of Ariane 5 rocket)
- **Structure** Flotilla of six space telescopes, the hub and the master spacecraft (8 total). The hub will be six sided, so that each side of the central spacecraft will always face one of the free-flying telescopes
- **Propulsion** Ion engines (corrosive) or squirting cold gas out of the thrusters
- **Power**
- **Attitude Subsystem** Field Effect Electrical Propulsion (FEEP) for in-flight alignment manoeuvres, controlling the spacecraft to nanometric optical path differences and milliarcsecond pointing accuracies. The master satellite is expected to detect deviations of the flotilla by means of radio and laser transmitters, and emit the corresponding correction orders
- **Communication Subsystem** In the master satellite
- **Instrumentation** Under investigation (active optics control, achromatic phase shifters, detecting and cooling systems, fibre-optic wavefront filtering...)

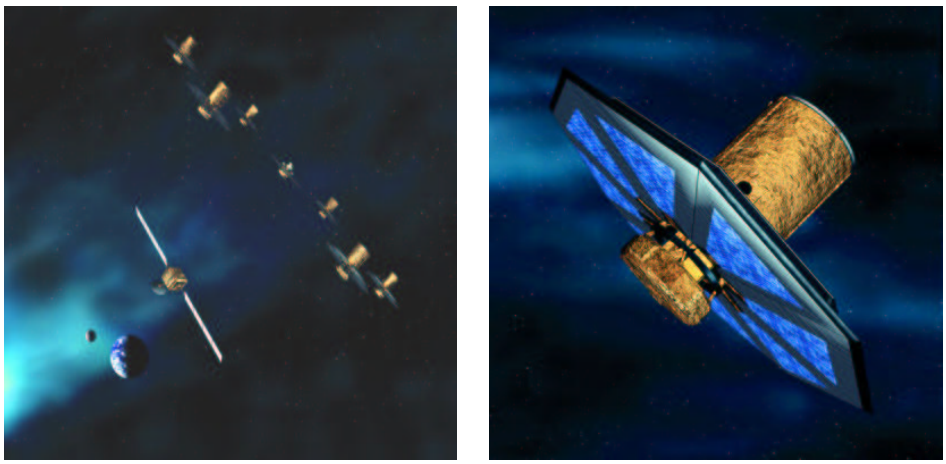

Figure 2.17: Darwin configuration and detail of a telescope.

Notable remarks

1. The six telescopes will be placed around L_2 in a hexagonal formation, with the hub in the center and the master satellite behind

2. NASA is planning a similar mission (Terrestrial Planet Finder). Maybe the final project will be a joint Darwin/TPF, with collaboration of other countries such as Russia and Japan

3. Investigations are still going on, in order to see whether there is a way to achieve the same scientific results using 4 free-flying telescopes instead of 6

More about the mission

Darwin will observe in the mid-infrared. Life on Earth leaves its mark at these wavelengths, so they are good places to look for fingerprints of Earth-like planets and life. In addition to searching for planets, it is designed to provide images with 10 - 100 times more detail than can be achieved now (similar technology as Hubble telescope). Darwin will also provide detailed images of other objects, such as galaxies. Peering into these galaxies it may even "see" black holes. Its observing window will be a cone of about 45 degrees off the anti-Sun direction.

The central spacecraft, the hub, does not observe the stars itself but collects and combines the light from the six telescopes. This is known as interferometry. In order to cancel the starlight and don't let it overwhelm the planet's weak gleaming, the light collected by some of the telescopes will be very slightly delayed before it is combined. This way, starlight is cancelled. Light from planets is not affected by the delay and can be seen. At the beginning it was supposed to carry the antenna to communicate with Earth. However, moving the antenna to keep Earth in sight would cause disturbances to the sensitive optical systems on-board. So, the master satellite had to be added to the flotilla.

During observation time, the telescopes and the hub must stay rigorously in formation. A deviation of more than just thousandths of a millimetre will ruin the observation. To achieve

this accuracy, ESA will rely on an enhanced variation of the GPS (Global Positioning System). Each of the spacecraft will be equipped with radio transmitters and a number of receivers. If any spacecraft begins to drift, this will show up immediately in the time it takes for signals from the other spacecraft to reach its various receivers. On board computers will then quickly compute the tiny thrust needed to correct for this and activate the propulsion system. The master satellite has an own propulsion system, which allows it to be placed behind the others, detect and solve possible separations.

SMART-2 (launch: 2006) will consist of two spacecraft to demonstrate the formation flying that is essential to the success of Darwin's fleet. In addition, some other technologies are still being developed for Darwin, for instance the cooling system which will maintain the telescopes within 20-30 K, to avoid their own heat radiation to obstruct the observations.

2.1.15 TPF: Terrestrial Planet Finder

Mission overview

- **Orbit** Lissajous Orbit around the Sun-Earth libration point L_2
- **Transfer**
- **Launch**
- **Launcher** 2012-2015
- **Mission** Ariane 5, EELV, or Delta IV Heavy.
- **Operational Lifetime** To search for Earth-like planets that might harbour life. TPF will take family portraits of stars and their orbiting planets and determine which planets may have the right chemistry to sustain life.
- **Manoeuvres** Five years mission duration.
- **Agency** At the data collection phase the formation drift along the slides of a regular N-gon, with manoeuvres at the corners of the polygon.
- **Web page** NASA, ESA `http://planetquest.jpl.nasa.gov/TPF/tpf_index.html`
  `www.terrestrial-planet-finder.com`

Spacecraft

- **Mass** Combiner 687 kg, outer collector 731 kg, Inner collector 713 kg.
- **Dimensions**
- **Structure** Four-element linear array of 3.5 meters free-flying telescopes equally spaced along the interferometer baseline, and one combiner located at the vertex of an isosceles triangle formed with the two inner collectors.
- **Propulsion** Electric propulsion (mini-hydrazine, hot gas, or heated hydrogen are also under consideration).
- **Power** Fixed solar arrays.
- **Attitude Subsystem** Fine guidance sensors. Reaction wheels, with vibration isolation, are used for momentum accumulation and slewing. Six degree-of-freedom attitude and translation control of each spacecraft, using bi-directional arrays of micro-thrusters and vibration free magnetic-bearing reaction wheels.
- **Communication Subsystem** Combiner 986 W, outer collector 568 W, inner collector 568 W (averaged power).

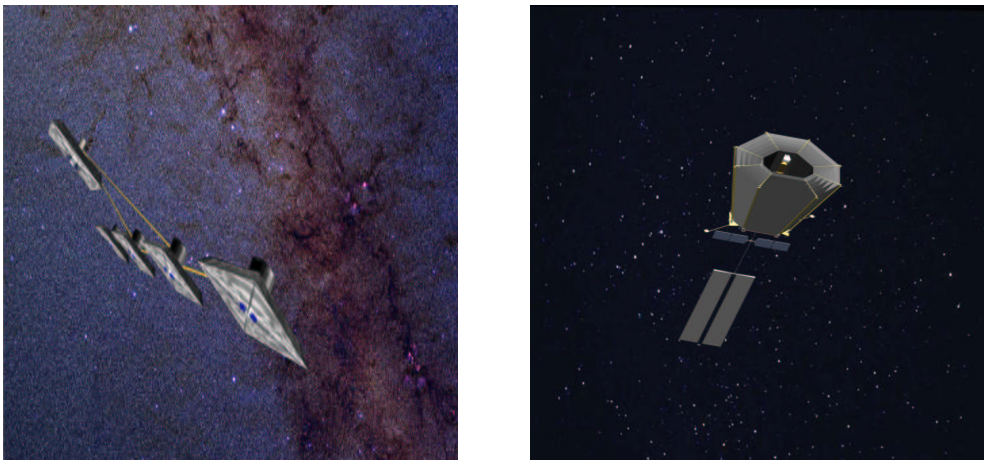

Figure 2.18: Artist's concepts of TPF-I (left) and TPF-C (right) (`http://planetquest.jpl.nasa.gov/TPF/tpf_architectures.cfm`).

- **Instrumentation** four telescopes, the beam combining apparatus and astronomical instrumentation.

Notable remarks

1. Distributed sensing-and-control autonomous formation flying approach is used
2. Determination of relative position knowledge to $\pm 1cm$, relative velocity to $\pm 0.1mm/s$, and attitude knowledge to ± 1 arcmin.
3. To minimised off-axis aberration, the telescopes keep pointed to within approximately one arcsecond of the target star.
4. Diffraction-limited at 2 μm, operating at $< 40K$.
5. Baseline from 75 to 1000 m.
6. Angular resolution of 0.75 milli-arcsec (3 μm at 1000 m baseline).

More about the mission

The Terrestrial Planet Finder (TPF) is a spacecraft based infrared interferometer that will combine high sensitivity and spatial resolution to detect and characterise approximately 150 planetary systems within 15 pc of our Sun. In a five year mission, TPF will look for the atmospheric signatures of life using the methods of planetary spectroscopy and long-baseline stellar interferometry.

The technological challenges for this mission include the need to control the separated telescopes and their delay lines to produce a stabilised interference patter, and to control the fringe pattern to suppress or "null" the light from the parent star relative to the light from the planet.

Several of the contractors involved in the architecture studies have focused their attention on the design of a single large aperture optical telescope equipped with a chronograph and a high performance adaptive optics system. Whereas this approach is unlike proposed, it would be competitive if it could be shown capable of detecting Earth-like planets and meet the other science goals of the TPF program.

Included in the nation's new vision for space is a plan for NASA to "conduct advanced telescope searches for Earth-like planets and habitable environments around other stars." To meet this challenge, NASA has chosen on May, 2004 to fly two separate missions with distinct and complementary architectures to achieve the goal of the Terrestrial Planet Finder. The two missions are:

- **Terrestrial Planet Finder-C:** a moderate-sized visible-light telescope, similar to the 4- by 6-meter (13.1- by 19.6-foot) version currently under study, to launch around 2014. On-board corona-graph instrumentation will use a central disc and other specialised techniques to block the glare of a star, allowing detection and characterisation of dimmer planets around it.

- **Terrestrial Planet Finder-I:** multiple spacecraft carrying 3 to 4 meter (9 to 13 foot) infrared telescopes flying in precise formation, to launch before 2020, and to be conducted jointly with the European Space Agency. Combining the infrared, or heat radiation gathered by the multiple telescopes, using a technique called interferometry, will simulate a much larger telescope. This will enable the mission to detect and study individual planets orbiting a parent star observed by TPF-C and also new ones beyond the reach of TPF-C.

2.1.16 SAFIR: Single Aperture Far-Infrared Observatory

Mission overview

- **Orbit** Sun-Earth L_2 point.
- **Transfer**
- **Launch** 2015-2020.
- **Launcher**
- **Mission** Probe the epoch of reionization due to the first stars when the Universe was less than 1/20 its present age, trace the formation and evolution of star-forming and active galaxies since their inception, explore the connection between black holes and their host galaxies, reveal the details of star and planet formation in nearby debris-disk systems, search for and quantify prebiotic molecules in the interstellar medium.
- **Operational Lifetime** Five years.
- **Manoeuvres**
- **Agency** NASA
- **Web page** `http://safir.jpl.nasa.gov/`

Spacecraft

- **Mass**
- **Dimensions** Primary mirror diameter 10 m with a wavelength coverage from 20 microns to 1 mm.
- **Structure** two promising architectures: conventional telescope with segmented fractionary mirrors and a new concept called the Dual Anamorphic Reflector Telescope (DART).
- **Propulsion**
- **Power**
- **Attitude Subsystem**
- **Communication Subsystem** While the communication segment baseline for SAFIR is the set of DSN antennas, a dedicated ground station would also meet SAFIR's modest down-link needs if a larger antenna and/or higher transmitting power were implemented on the Spacecraft.
- **Instrumentation** Background-limited detector arrays with thousands of pixels for broad-band imaging over the full wavelength range, moderate resolution spectrometers with back-ground-limited sensitivity and near-unit fractional bandwidth, heterodyne spectrometers tunable over the full wavelength regime with quantum-noise limited performance.

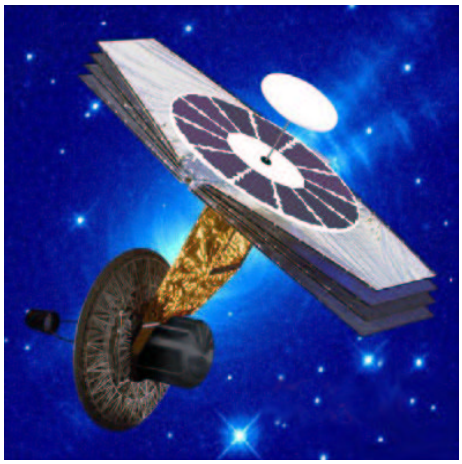

Figure 2.19: A SAFIR concept based on the segmented-mirror technology to be employed for the JWST (link). The telescope (in the lower left) would be composed of several mirror segments. Multiple layers of shielding would block the sun's heat and allow the cryocoolers to keep the telescope at a temperature of 4 K (`http://safir.jpl.nasa.gov`).

Notable remarks

1. Large, cryogenic deployable mirrors.
2. Long-life cryocoolers capable of reaching 5 K.
3. Background-limited direct detectors for both continuum and spectral observations.
4. Quantum-noise-limited heterodyne spectrometers tunable over the far-IR spectral region.

More about the mission

SAFIR is a large (10 m-class), cold (4-10 K) space telescope for wavelengths between 20 μm and 1 mm. It will provide sensitivity of a factor of a hundred or more over that of SIRTF and Herschel, leveraging their capabilities and building on their scientific legacies. Covering this scientifically critical wavelength regime, it will be complement the expected wavelength performance of the future flagship endeavours JWST and ALMA.

Must of the key technologies that will make SAFIR possible has been or is being developed for other missions:

- Lightweight telescopes with large primary mirrors that can collapse for launch and reassembled in space are under intense development for the JWST and TPF.
- Cryogenic systems with multiple stage closed-cycle coolers which provide base temperatures of a few degrees above absolute zero, are being developed and will be used by PLANCK and JWST.

- A heterodyne spectrometer is also envisioned for SAFIR, with receiver elements beyond even those of Herschel's HIFI instrument.

The SAFIR study was started on April 2004 and today is just completed the draft of science requisites. On June will be completed a draft about the reference mission design.

2.2 Other Missions

2.2.1 Hiten

Mission overview

- **Orbit** Hiten was put into a highly elliptical Earth orbit which passed by the Moon ten times during the mission, which ended when Hiten was intentionally crashed into the Moon on 10 April 1993.
- **Transfer** First Low Energy Transfer
- **Launch** January 24, 1990
- **Launcher** Mu-3SII-5 rocket
- **Mission** Hiten was meant to test technology for future missions. It included Hagoromo, a small satellite which was inserted into orbit around the moon. Objectives of the mission included testing trajectory control, inserting the small satellite, aerobraking experiments, and measuring the mass and velocity of micro-meteorite particles.
- **Operational Lifetime** 3 years
- **Manoeuvres** Orbital Information

Orbit	C. Body	Start/End Date(s)	Periapsis	Apoapsis	Period	Inc.	Ecc.
Flyby	Moon	1990.077:20:04:09 (18 Mar)	16472.4 km				
Orbiter	Moon	1992.046:13:33:00 (15 Feb)					
		1993.100:18:03:26 (10 Apr)	6.52 LR	29.42 LR	4.7 d	34.7	0.32
Lander	Moon	1993.100:18:03:26 (10 Apr)					

LR = Lunar radii = 1738 km

- **Agency** ISAS (Japanese Space Agency)
- **Web page** `http://nssdc.gsfc.nasa.gov/nmc/tmp/1990-007A.html`

Spacecraft

- **Mass** The fully fueled mass of Hiten was 197 kg, this included 42 kg of hydrazine fuel and the 12 kg Hagoromo orbiter.
- **Dimensions** Hiten was a cylindrically shaped spacecraft, 1.4 m in diameter and 0.8 m high. The small polyhedral-shaped Hagoromo lunar orbiter was mounted on top of the spacecraft.
- **Structure**
- **Propulsion** Spacecraft propulsion and attitude control was provided by eight 23-N and four 3-N hydrazine thrusters.

- **Power** 110 W supplied by solar cells on the cylindrical surface of the spacecraft backed up by a small onboard battery.
- **Attitude Subsystem** The spacecraft was spin-stabilized at 10 - 20.5 rpm.
- **Communication Subsystem** A medium gain collinear array antenna in both X-band and S-band protruding from the bottom surface of the spacecraft and two cross dipole omni-directional low gain antennas in S-band only, one mounted on the top and one on the bottom. Downlink is via onboard X-band and S-band transmitters, each with two power levels. Two receivers are used for S-band uplink, one connected to the low-gain antennas and the other to the medium gain antenna. Commands were sent from ground stations at 1 kbps. The onboard command computer consists of three independent processor cells with a total of 2 Mbits ROM and 512 Kbits RAM.
- **Instrumentation**

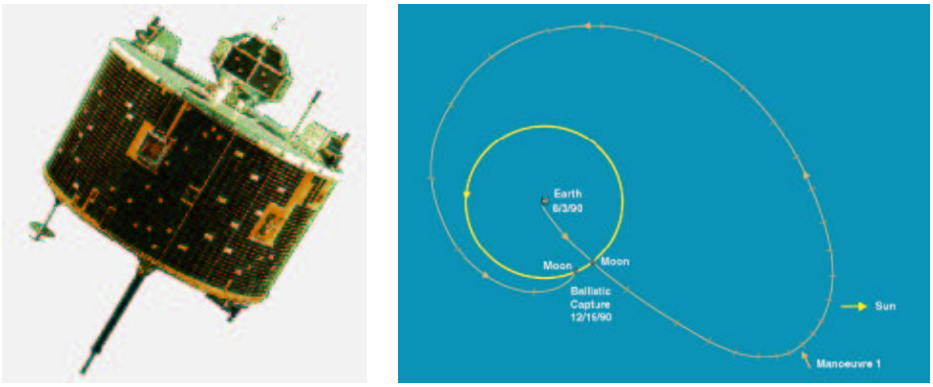

Figure 2.20: HITEN spacecraft and orbit.

Notable remarks

1. The primary objectives of the mission were to:
   (a) Test trajectory control utilizing gravity assist double lunar swingbys.
   (b) Insert a sub-satellite into lunar orbit.
   (c) Conduct optical navigation experiments on a spin-stabilized spacecraft.
   (d) Test fault tolerant onboard computer and packet telemetry.
   (e) Conduct cis-lunar aerobraking experiments.
   (f) Detect and measure mass and velocity of micro-meteorite particles.
2. Three follow-on objectives were also added: excursion to the L_4 and L_5 Lagrangian points of the Earth-Moon system, orbit of the Hiten spacecraft around the Moon, and hard landing on the lunar surface. Hiten was named after a flying, music-playing Buddhist angel. Hagoromo was named for the veil worn by Hiten. This mission included Japan's first-ever lunar flyby, lunar orbiter, and lunar surface impact.

More about the mission

Hiten was launched into highly elliptical Earth orbit on a Mu-3SII-5 rocket from Kagoshima Space Center in Japan at 11:46:00 UT (20:46:00 JST) on 24 January 1990. Injection velocity was 50 m/s less than the nominal value, resulting in an apogee of only 290000 km compared to the expected 476000 km. A number of trajectory correction maneuvers were performed and Hiten was put back in a nominal orbit. At 19:37 UT on 18 March 1990 (04:37 19 March JST) as Hiten approached its first lunar flyby, the small Hagoromo spacecraft was released into lunar orbit, making Japan the third nation to orbit the Moon. Although the S-bamd transmitter aboard Hagoromo had failed on 21 February 1990, the ignition of the Hagoromo deceleration rocket was confirmed by ground observation at 20:04:03 UT, the estimated orbit was 7400 × 20000 km with a period of 2.01 days. Six seconds later, at 20:04:09 UT (05:04:09 19 March JST) Hiten reached its closest flyby distance to the Moon of 16472.4 km.

Further manuevers were made to have Hiten simulate the planned trajectory of the future Geotail spacecraft. Hiten completed seven more lunar swingbys by 4 March 1991 and then started the aerobraking portion of its mission. On 19 March at 00:43 UT Hiten flew into the Earth's upper atmosphere at an altitude of 125.5 km over the Pacific at 11.0 km/s. Atmospheric drag lowered the velocity by 1.712 m/s and the apogee altitude by 8665 km. This was the first time aerobraking was used to modify a spacecraft orbit at close to escape velocity. Another aerobraking maneuver was done at 11:36 UT on 30 March at 120 km altitude, reducing velocity by 2.8 m/s and apogee by 14000 km. This concludied the primary mission and a follow-on mission was started. A ninth lunar swingby was used to increase the apogee to 1532000 km and a tenth on 2 October 1991 put Hiten into a looping orbit which passed through the L_4 and L_5 stable libration points to look for trapped dust particles. No obvious increase was found. On 15 February 1992 at 13:33 UT (22:33 JST) at a closest approach of 422 km most of Hiten's remaining fuel was used to put it into lunar orbit. The very last fuel was used to have the spacecraft, whose orbit was decaying after almost two months in lunar orbit, crash into the lunar surface on 10 April 1993 at 18:03:25.7 UT (11 April 03:03:25.7 JST) at 55.3 E, 34.0 S.

The Hagoromo orbiter was a 12 kg, 26-faced polyhedron, 36 cm between opposite faces. A solid propellant (KM-L) retrorocket with a mass of 4 kg was mounted inside the spacecraft for lunar orbit insertion. Sixteen of the surfaces were covered with 1000 sheets of indium-phosphorus solar cells which could generate about 10 W. Two way communications with a ground station were provided by an S-band transponder and an omni-directional cross-dipole antenna mounted on top of the orbiter. No scientific instrumentation was included, only housekeeping data such as temperature was transmitted. The transmitter malfunctioned on 21 February 1990, before lunar orbit insertion, and no data were transmitted after this time.

2.2.2 JIMO: Jupiter Icy Moons Orbiter

Mission overview

- **Orbit** Around Jupiter (capture orbit), and successively orbiting the moons Callisto, Ganymede and Europa
- **Transfer** Spiralling from high Earth orbit to Jupiter gravitational capture
- **Launch** 2012 or later
- **Launcher** heavy lift expendable launch vehicle
- **Mission** Investigate the origin of Jupiter's moons and the possibility that they sustained life
- **Operational Lifetime** Not determined. Constrained by the intensity of the radiation belts of Europa
- **Manoeuvres**
- **Agency** NASA
- **Web page** `http://www.jpl.nasa.gov/jimo/mission.cfm`

Spacecraft

- **Mass** launch mass of 20 tones
- **Dimensions** deployed length of 30 meters
- **Structure**
- **Propulsion** Ion thrusters with a nuclear fission reactor and a system for converting the reactor's heat to electricity
- **Power** 10-30 kW. Generous electrical power supply, available from the on-board nuclear system
- **Attitude Subsystem**
- **Communication Subsystem** Much higher data transmission rate than previous missions
- **Instrumentation** Radar instrument for mapping the thickness of surface ice, laser instrument for mapping surface elevations. Possibly a camera, an infrared imager, a magnetometer and instruments to study charged particles, atoms and dust found near each moon

Notable remarks

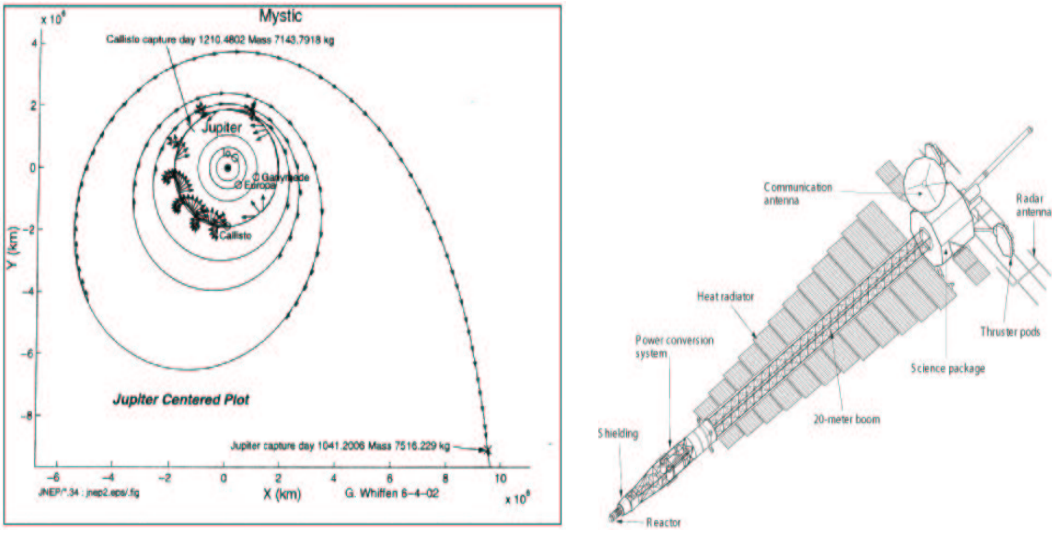

Figure 2.21: JIMO orbit and spacecraft.

1. This mission, still under investigation, will test new technologies and propulsion systems

2. JIMO is a mission to search life far from the Earth

3. It would be the biggest space probe ever flown (JIMO's design is still being considered)

More about the mission

Voyager (1979) encountered Jupiter moons and Galileo (1995) found evidence for subsurface oceans on them. JIMO will successively orbit around Europa, Ganymede and Callisto, which apparently have three ingredients essential for life: water, energy and the necessary chemical elements.

In addition to the scientific goals of JIMO mission, it is also conceived to develop a nuclear reactor and prove that it can be processed and operated safely in deep space for long-duration space exploration. The amount of power available from a nuclear reactor would make the use of more capable instruments and faster data transmission possible. A subsidiary objective is the development of nuclear fission technology and associated system technologies necessary for demonstrating their effectiveness in deep space exploration.

The severe radiation environment around the moons, particularly Europa, are important in the selection of micro-electronics technologies, and in the use of new methods for radiation risk mitigation such as better shielding.

2.2.3 Bepi Colombo

Mission overview

- **Orbit** 400 × 11800 km (MMO, magneto-spheric orbiter) and 400 × 1500 km (MPO, planetary orbiter) polar orbits around Mercury
- **Transfer** 4.2 years heliocentric transfer with Earth/Venus/Mercury gravity assists
- **Launch** 2012
- **Launcher** Soyuz-Fregat
- **Mission** Study the origin and structure of the planet, close to the Sun, and the origin of Mercury's magnetic field
- **Operational Lifetime** 1 year orbit around Mercury (+ 4 years transfer)
- **Manoeuvres**
- **Agency** ESA
- **Web page** `http://sci.esa.int/science-e/www/area/index.cfm?fareaid=30`

Spacecraft

- **Mass** 1500 kg
- **Dimensions**
- **Structure** Planetary orbiter and magneto-spheric orbiter
- **Propulsion** Ion-propulsion during cruise trajectory (0.34N), chemical engine (4000N) for capture and insertion
- **Power**
- **Attitude Subsystem** Planetary orbiter: 3-axis stabilised, Magneto-spheric orbiter: 15 rpm spin-stabilised
- **Communication Subsystem** 1.5 m X/Ka band high-gain antenna and UHF data relay package
- **Instrumentation** Planetary orbiter: Visible/near IR camera, photon spectrometer, neutron spectrometer, accelerometer. Magneto-spheric orbiter: Magnetometer, ion spectrometer, ion/electron analyser, wave analyser, cold plasma detector, energetic particle detector

Notable remarks

1. First ESA mission travelling to hot parts of the Solar System
2. It will use the combination of gravity assist with low thrust solar electric propulsion (demonstrated by SMART-1)

More about the mission

Bepi Colombo is a joint mission of ESA (MPO) with the Japanese Space Agency (MMO). It is named after Giuseppe Colombo (mathematician and engineer from the university of Padua) who was the inspirer of NASA's Marine 10 passes by Mercury in 1974/75.

It is a challenging and costly mission, because it consists of two spacecraft and will explore unknown regions of the solar system, which yield serious problem (such as high temperatures).

Data gathered by BepiColombo is expected to cast some light on the origin and formation not only of Mercury itself, but of all inner planets, including the Earth.

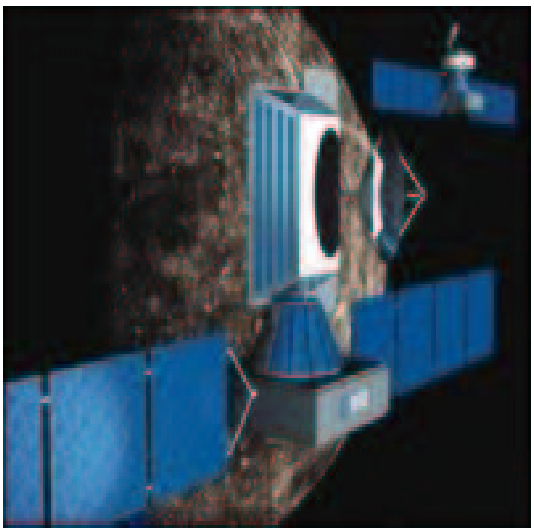

Figure 2.22: BepiColombo spacecraft.

2.2.4 Mars Express

Mission overview

- **Orbit** Orbital Inclination: 86.3 degrees, pericentre: 258 km, apocentre: 11560 km, period: 7.5 h (around Mars)
- **Transfer** Taking advantage of Mars closest approach to Earth (summer 2003)
- **Launch** 2 June 2003
- **Launcher** Soyuz-Fregat
- **Mission** Answer questions about: geology, atmosphere, surface environment, history of water and potential for life on Mars
- **Operational Lifetime** 2.5 years (until Nov. 2005)
- **Manoeuvres**
- **Agency** ESA
- **Web page** `http://www.esa.int/SPECIALS/Mars_Express/`

Spacecraft

- **Mass** 1223 kg (including propellant 427 kg, payload 116 kg)
- **Dimensions** Spacecraft bus: $1.5 \times 1.8 \times 1.4$ m
- **Structure** The spacecraft and its instruments, the lander
- **Propulsion** Mixture of two propellants which are contained in two tanks each with a capacity of 267 litres. The fuel is fed into the engine using pressurised helium from a 35-litre tank
- **Power** Observation: 410 W, Manoeuvre: 360 W, Communication: 500 W. Provided by solar arrays (11.42 m^2) or lithium batteries (3 at 22.5 Ah each) during eclipses
- **Attitude Subsystem** Two star trackers, six laser gyros, two coarse Sun sensors
- **Communication Subsystem** Rate of up to 230 kbps down-link (between 0.5 and 5 Gbits of scientific data very day). 12 Gbit solid state mass memory prior to the down-link to Earth. 1.6-metre diameter high-gain antenna for receiving and transmitting radio signals when the spacecraft is a long way from Earth. 40 centimetre-long low-gain antenna, when close to the Earth

- **Instrumentation** Seven instruments and a lander (at launch): High Resolution Stereo Camera (HRSC), Energetic Neutral Atoms Analyser (ASPERA), Planetary Fourier Spectrometer (PFS), Visible and Infra Red Mineralogical Mapping Spectrometer (OMEGA), Sub-Surface Sounding Radar Altimeter (MARSIS), Mars Radio Science Experiment (MaRS), Ultraviolet and Infrared Atmospheric Spectrometer (SPICAM)

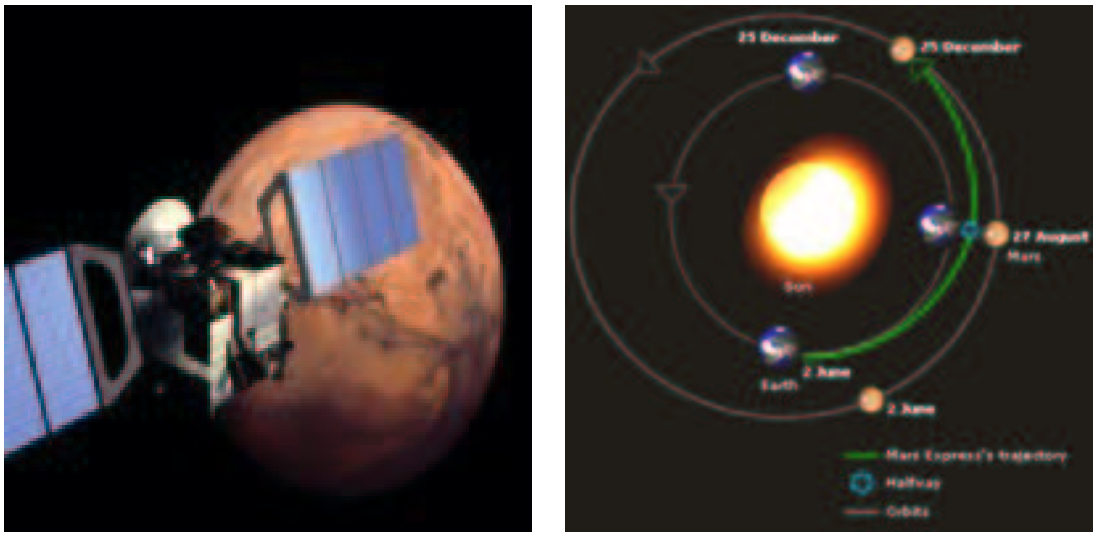

Figure 2.23: Mars Express spacecraft and insertion orbit.

Notable remarks

1. First European mission to Mars, a planet on which there is a strong possibility to find life (past or present)

2. The mission is a test case for new working methods to speed up spacecraft production and minimise mission costs

More about the mission

Mars Express project is the start of a new way of organising the building blocks for European missions. The spacecraft was built and launched in record time and at a much lower cost than previous, similar missions into outer space. It is maybe the start of low cost European missions.

The orbiters instruments are now performing remote sensing of the red planet. The lander, Beagle 2, had to carry out on-the-spot investigations of the surface. Unfortunately, it was declared lost on 6 February 2004 after no signals were received. It was also the lander which was supposed to look for signs of past or present life, by searching for water from deep under the surface to the highest layers of the Martian atmosphere.

Mars Express can also provide relay communication services between the Earth and the two NASA rovers, deployed on the surface in early 2004, so forming a centrepiece of the international effort in Mars exploration.

Chapter 3

Review on the Main Topics of Libration Point Dynamics

Many missions, such as the near-Earth missions, or even the Voyager and Galileo multiple fly-bys, are well approximated by two-body problems, which are fully integrable. This enables analysis using the well developed "patched conics" or "multi-conics" techniques. Conic segments provide excellent approximations to the final trajectories along with estimates of propulsion and power requirements. For missions in which this approximation is not valid, trajectory design requires greater sensitivity to the underlying dynamics as well as appropriate computational tools.

The use for mission design of dynamical models of motion beyond the two body problem, represents one of the most interesting challenges of the future. This is because of

1. The sophistication and realism of the more elaborated models.

2. The great amount of techniques that have been developed around these models.

The less elaborated of these dynamical models is the RTBP. The dynamics of the RTBP is simple except at the vicinities of the libration points. Indeed, close enough to the secondary, a massless particle moves like a satellite of it. Far away from the secondary, the particle is just a satellite of the primary, unless the libration points are approached in the phase space. The interesting (and most difficult) point is to know where and how the transition between these two different regimes of motion is organised. The objects which play a key role in this organisation, not only in this problem but for any dynamical system, are those which remain invariant under the action of the dynamics. Among them we have: the equilibrium points and the periodic orbits. Other invariant objects, which also have an important role, are: the invariant tori, invariant unstable and stable manifolds, centre manifolds, energy manifolds, etc. Altogether they give a key to interpret and predict the behaviour of most of the points in the phase space and constitute, in some sense, the skeleton of the system.

As an illustration of organising role of the above mentioned invariant objects, Figure 3.1 displays the orbit of the comet Oterma and the invariant stable and unstable manifolds of the libration points L_1 and L_2 for the Sun-Jupiter system. These two sets are invariant in the sense that if a particle starts its motion on one of the them it will never leave it. They are called stable and unstable manifolds of the equilibrium points, because if a particle starts moving on the stable

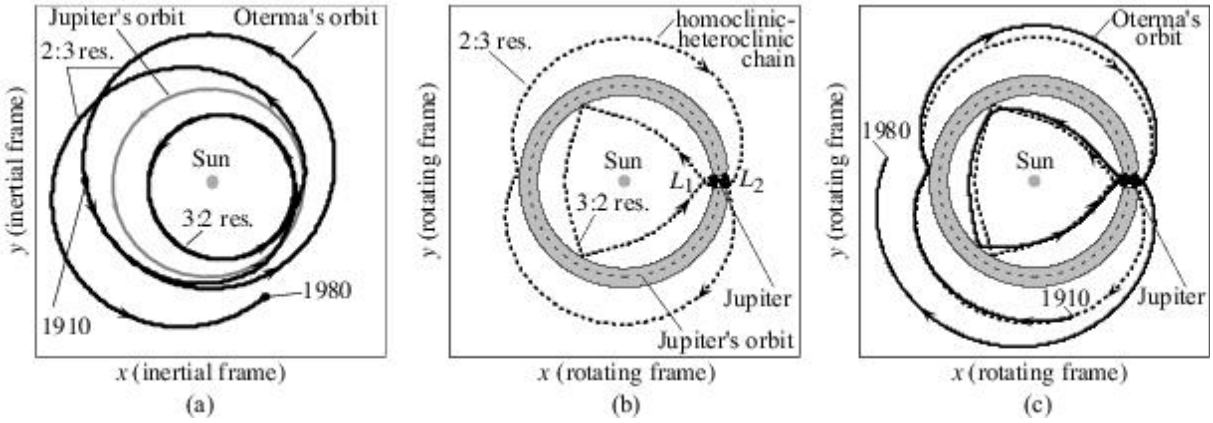

Figure 3.1: The orbit of comet Oterma in an inertial and synodical reference frames (see [20]).

(unstable) manifold, it will tend to the equilibrium point as time tends to plus (minus) infinity. From the Figure 3.1 it is clear that these manifolds act as natural guide-lines or channels for the motion of the comet Oterma in its transition between two resonant motions around the Sun.

The invariant manifolds are surfaces in the trajectory design space consisting of global families of trajectories that wind on and off periodic orbits such as halo orbits. Dynamical Systems Theory (DST) enables us to compute and visualise these surfaces so that we can obtain a map of the orbit design space and hone in on the specific trajectories useful to a particular mission. An example is the design of the trajectory for the Genesis Discovery Mission, which was the first mission designed using DST. The entire trajectory after launch requires a single deterministic manoeuvre of only 6 m/s to capture into halo orbit for two years and automatically return to Earth. Without this approach, this mission could not have been accomplished within its propellant budget.

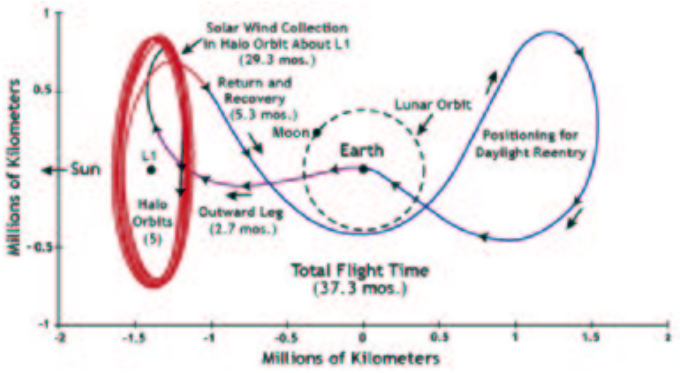

Figure 3.2: The Genesis mission trajectory. (`http://genesismission.jpl.nasa.gov`)

Based on a deeper understanding of these invariant manifolds, a network of "passageway" that are called dynamical channels, govern the material transport in the solar system. A number of new techniques for constructing spacecraft trajectories with desired characteristics have also been developed using this methodology. These techniques have been used to design a "Petit Grand

Tour" of Jovian moons (see [127]) and an Earth-to-Moon lunar ballistic capture (see [159]) mission which uses up to 20% less fuel than a Hohmann transfer. This network of dynamical channels can be a key component in designing low-fuel paths for the exploration of the solar system.

All these invariant objects can be obtained by a combination of symbolic computation and numerical continuation. It is essential to know about the dynamical properties in a neighbourhood of these objects in order to design robust algorithms for their computation.

The important role played by the libration points in the dynamics of the RTBP has produced a lot of studies. Since Poincaré published his fundamental work in 1892 ([205]), much of the attention has been focused on the search for periodic solutions around them which, aside from the considerations already done, have been seen for a long time as "the only opening through which the reputably inaccessible problem of three bodies could be penetrated". Early investigations quickly narrowed the study to solutions in the planar circular RTBP, and a number of families of periodic orbits were identified. This work was mainly done under the direction of Elis Strömgren, at the Copenhagen Observatory during the first quarter of the XX-th century (1900-1925). After this, it was possible to give a rather complete picture of how the "most relevant" families of periodic orbits were organised in the RTBP (for the case of equal masses) and the role that some of them had in the dynamics of the problem. This work was completed during the 60's and 70's, mainly by the work of Deprit and Henrard, making use of electronic computers for both the numerical computation of families of periodic orbits and the analytical study of the dynamics of the model.

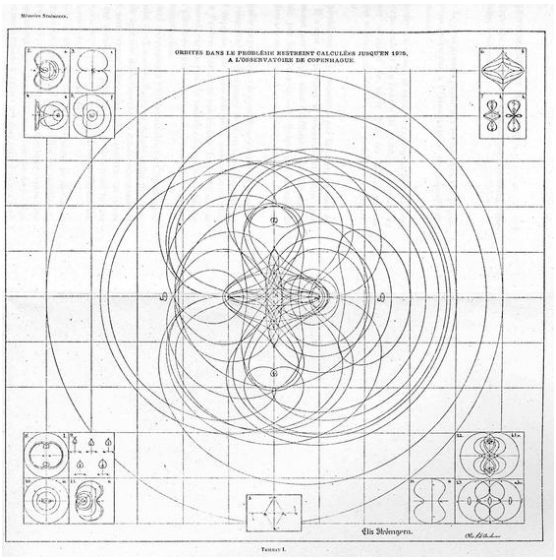

Figure 3.3: Periodic orbits computed at the Copenhague Observatory ([214]).

By 1920, Moulton ([203]) considered the three-dimensional problem and, significantly for this discussion, he was interested in oscillating satellites in the vicinity of the collinear libration points. But, definitively, the new interest in this problem came with the ISEE-3 spacecraft. This spacecraft used, for the first time, a trajectory for which both the gravitational effects of the Sun and the Earth where of the same order of magnitude and so, the motion of the spacecraft could

not be considered as the perturbation of a Sun-spacecraft or Earth-spacecraft two-body problem. In this situation, the RTBP was a suitable model for the mission analysis and the role of the libration points was displayed, since they allowed some orbital acrobatics of the spacecraft in the Sun-Earth-Moon system. It was mainly because of this mission that the use of the dynamics of the collinear libration points was considered a feasible engineering technology more than a merely scientific curiosity.

In the rest of this section we will review the state of the art in the main topics related to the dynamics of the libration points. In particular, we will consider the following topics:

- N-body models as a perturbation of the RTBP.
- Libration points and dynamical substitutes.
- The phase space around the libration points in the RTBP.
- Analytical computation of libration point orbits in the RTBP.
- Computation of nominal libration point orbits in accurate solar system models.
- Station keeping strategies.
- Transfers from the Earth to libration point orbits.
- Transfers between libration point orbits.
- Low energy transfers and weak stability boundaries.
- Formation flight using libration point orbits.

3.1 The Restricted Three Body Problem and the Libration Points

3.1.1 The Restricted Three Body Problem and its Perturbations

The RTBP is a simple model useful to gain insight and to give a fairly complete description of the phase space in the regions of interest around the libration points. For concrete applications better models are required. The more realistic models are the numerical ones, for instance the one provided by the JPL ephemeris. These numerical models, accurate for the purpose of designing missions, are not suitable if what is required is to obtain a global picture of the vicinity of a libration point. One can recur to compute many orbits, but always on the basis of one by one orbit. This is precisely what has to be done in the final step of the definition of a nominal orbit, but it is not useful when trying to choose among many nearby orbits or if one wants to understand the geometry of the phase space.

Between the RTBP and these more realistic models, there are several intermediate models of motion that have been considered in the literature and that will be described in this section. Their study provides a closer approach to the real situation than the one given by the RTBP in some cases.

In this section we will review some of the most relevant restricted models for the analysis of the motion in the vicinity of the libration points and we will write the equations of motion for these models as a perturbation of the RTBP, in order to identify and compute the dynamical substitutes of the libration points in them.

Most of the well known restricted problems take as starting point the circular RTBP, which models the motion of a massless particle under the gravitational attraction of two punctual primaries revolving in circular orbits around their centre of mass. In a suitable coordinate system and with adequate units, the Hamiltonian of the RTBP is (see [215])

$$\begin{aligned} H &= \frac{1}{2}(p_x^2+p_y^2+p_z^2)+yp_x-xp_y \\ &\quad -\frac{1-\mu}{((x-\mu)^2+y^2+z^2)^{1/2}}-\frac{\mu}{((x-\mu+1)^2+y^2+z^2)^{1/2}}, \end{aligned}$$

being $\mu = m_2/(m_1+m_2)$, where $m_1 > m_2$ are the masses of the primaries and x, y, z, p_x, p_y, p_z are the coordinates and momenta, respectively. In order to get closer to more realistic situations, or simplifications, this model is modified in different ways. For instance:

1. Hill's problem. Is useful for the analysis of the motion around m_2. Can be obtained setting the origin at m_2, rescaling coordinates by a factor $\mu^{1/3}$ and keeping only the dominant terms of the expanded Hamiltonian in powers of $\mu^{1/3}$. The Hamiltonian function is

$$H = \frac{1}{2}(p_x^2+p_y^2+p_z^2)+yp_x-xp_y-\frac{1}{(x^2+y^2+z^2)^{1/2}}-x^2+\frac{1}{2}(y^2+z^2).$$

   This Hamiltonian corresponds to a Kepler problem perturbed by the Coriolis force and the action of the Sun up to zeroth-order in $\mu^{1/3}$. Hill's model is the first approximation to the RTBP appropriate for studying the neighbourhood of m_2 and taking into account the action of the primary m_1 (see [10], [5]). This model has a remarkable set of solutions known as the *Variation Orbit Family*. This is a family of $2\pi m$–periodic solutions (m is the parameter of the family) which serves as the first approximation in the modern theory of lunar motion.

2. Restricted Hill four body problem. This is a time periodic model that contains two parameters: the mass ratio μ of the RTBP and the period parameter m of the Hill Variation Orbit. As $m \to 0$, the RTBP is recovered and the classical Hill model is recovered as $\mu \to 0$, both in the proper reference frames (see [9]).

3. The elliptic RTBP. It is a non–autonomous time–periodic perturbation of the RTBP in which the primaries move in an elliptic orbit instead of a circular one (see [215]).

4. The Bicircular Restricted Problem. It is one of the simplest restricted problem of four bodies, obtained from the RTBP by adding a third primary. It can be also considered a periodic perturbation of the the RTBP in which one primary has been splitted in two that move around their common centre of mass. This model is suitable to take into account the gravitational effect of the Sun in the Earth–Moon RTBP or the effect of the Moon in the Sun–Earth RTBP. In a coordinate system revolving with Earth and Moon, the Hamiltonian

of this problem is (see [253])

$$\begin{aligned} H &= \frac{1}{2}(p_x^2+p_y^2+p_z^2)+yp_x-xp_y \\ &\quad -\frac{1-\mu}{((x-\mu)^2+y^2+z^2)^{1/2}}-\frac{\mu}{((x-\mu+1)^2+y^2+z^2)^{1/2}} \\ &\quad -\frac{m_S}{((x-a_S\cos\theta)^2+(y+a_S\sin\theta)^2+z^2)^{1/2}}-\frac{m_S}{a_S^2}(y\sin\theta-x\cos\theta), \end{aligned}$$

with $\theta = w_S t + \theta_0$, where w_S is the mean angular velocity of the Sun, m_S its mass and a_S the distance from the Earth–Moon barycentre to the Sun.

5. The coherent models. They are restricted four body problems in which the three primaries move along a true solution of the three body problem. These models have been introduced for the study of the motions around the geometrically defined collinear and triangular equilibrium points of the Earth–Moon system (see [1], [6]) and the Sun–Jupiter system perturbed by Saturn (see [3]). The Hamiltonian of these problems can be written as

$$\begin{aligned} H &= \frac{1}{2}\alpha_1(p_x^2+p_y^2+p_z^2)+\alpha_2(yp_x-xp_y) \\ &\quad +\alpha_3(xp_x+yp_y+zp_z)+\alpha_4 x+\alpha_5 y \\ &\quad -\alpha_6\left(\frac{1-\mu}{((x-\mu)^2+y^2+z^2)^{1/2}}+\frac{\mu}{((x-\mu+1)^2+y^2+z^2)^{1/2}}\right. \\ &\quad \left.+\frac{m_S}{((x-\alpha_7)^2+(y-\alpha_8)^2+z^2)^{1/2}}\right), \end{aligned}$$

where the α_i are time periodic functions, with the same basic frequency as the Bicircular Problem.

In a different approach, instead of taking as starting equations those of the RTBP, we can consider Newton's equation for the motion of an infinitesimal body in the force field created by the bodies of the Solar System

$$\mathbf{R}'' = G\sum_i m_i\frac{\mathbf{R}_i-\mathbf{R}}{\|\mathbf{R}-\mathbf{R}_i\|^3}.$$

Performing a suitable change of coordinates (see [47], [4]), the above equations can be written in Hamiltonian form with the following Hamiltonian function

$$\begin{aligned} H &= \beta_1(p_x^2+p_y^2+p_z^2)+\beta_2(xp_x+yp_y+zp_z)+\beta_3(yp_x-xp_y)+ \\ &\quad +\beta_4(zp_y-yp_z)+\beta_5x^2+\beta_6y^2+\beta_7z^2+\beta_8xz+ \\ &\quad +\beta_9p_x+\beta_{10}p_y+\beta_{11}p_z+\beta_{12}x+\beta_{13}y+\beta_{14}z+ \\ &\quad +\beta_{15}\left(\frac{1-\mu}{[(x-\mu)^2+y^2+z^2]^{1/2}}+\frac{\mu}{[(x-\mu+1)^2+y^2+z^2]^{1/2}}+\right. \\ &\quad \left.+\sum_{i\in\mathcal{S}^*}\frac{\mu_i}{[(x-x_i)^2+(y-y_i)^2+(z-z_i)^2]^{1/2}}\right), \end{aligned}$$

where $\mathcal{S}^*$ denotes the set of bodies of the Solar System except the two selected as primaries and the β_i are time dependent functions that can be computed in terms of the positions, velocities, accelerations and over-accelerations of the two primaries. Notice that this Hamiltonian is, formally, a perturbation of the RTBP one. Most of all the intermediate models that have been mentioned are particular cases of this one. Once two primaries have been selected, a Fourier analysis of the β_i functions (see [4]) allows the explicit construction of a graded set of models with an increasing number of frequencies, that can be considered between the RTBP and the true equations.

3.1.2 Libration Points and their Dynamical Substitutes

For most of the models of the preceding section, although they close to the RTBP, the dynamical libration points do not subsist; since as they are non autonomous they do not have any critical point. However, some geometrically defined libration points can be introduced, such that a particle placed on them moves slowly, provided it is not too far from them. There is still a lot of effort to be done towards the understanding of the dynamics of these more elaborated models which can be of much help for mission design.

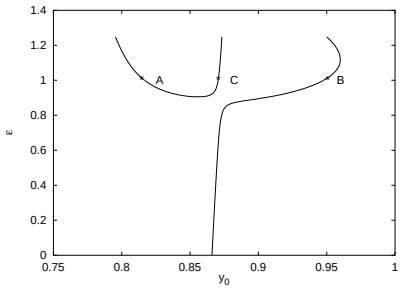

Figure 3.4: Evolution with the continuation parameter ϵ (y-axis) of the initial y_0 coordinate (x-axis) of the libration point L_4 and some periodic orbits.

If a model is time–periodic, under very general non–resonance conditions between the natural modes around the equilibrium points and the perturbing frequency, the libration points can be continued to periodic orbits of the model. In the continuation process, the periodic orbit can go through bifurcations and end up in more than a single periodic orbit or reach a turning point and disappear. This fact is displayed in Figure 3.4 in which we show the evolution, with respect to a continuation parameter ϵ, of a periodic orbit around the triangular libration point L_4. For $\epsilon = 0$ we have the RTBP and for $\epsilon = 1$ a bicircular restricted problem. The infinitesimal solution at L_4 evolves with ϵ to yield a periodic orbit at the point B. Starting at A, for $\epsilon = 1$, we get a third orbit C which is much smaller than the other two. All these periodic orbits, which have the same period as the perturbation, are the dynamical substitutes of the equilibrium points. For models with a quasi–periodic perturbation the corresponding substitutes will also be quasi–periodic solutions. In Figure 3.5 we show the dynamical substitutes for the L_1 point in the Earth–Moon system for a time–periodic and a quasi–periodic model.

Dynamical substitutes of the triangular points, for several of the models already mentioned, have been studied in Gómez et al.[235], Simó et al.[253] and Jorba et al.[196]. For the collinear points of the Sun–Earth system, the dynamical substitutes of L_2 for time–periodic models have

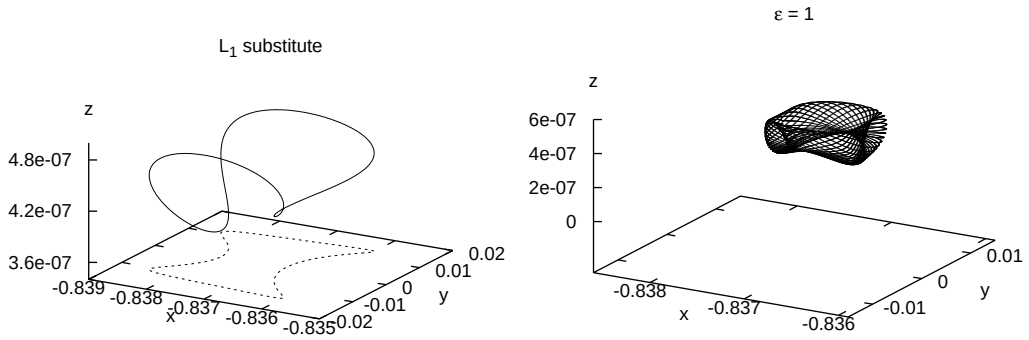

Figure 3.5: Dynamical substitutes for the L_1 point in the Earth–Moon system for a time–periodic (left) and a quasi–periodic (right) model.

been given by Farquhar [45], Howell [6]. In [1], Andreu does a complete study of the substitutes of the collinear libration points for a coherent model close to the Earth–Moon problem and compares some of the results obtained with the ones corresponding to a bicircular model. For models depending in more than one frequency, results can be found in [4].

3.2 The Phase Space around the Libration Points

Concerning the understanding the dynamics around the collinear libration points, a lot of effort has been devoted to give a global description of the different kinds of solutions that appear around them. This has enlarged the possibilities of the libration point orbits for spacecraft missions. In a first approximation, the motion in the vicinity of these equilibrium points can be seen as the composition of two oscillators and some "hyperbolic" behaviour. This means that the oscillations are not stable and that very small deviations will be amplified as time increases. One of the oscillations takes place in the plane of motion of the primaries and the other orthogonal to this plane. These two periodic motions are known as the planar and vertical Lyapunov periodic orbits. The frequencies of the oscillations vary with the amplitudes (since the problem is not linear) and for a suitable amplitude, both frequencies become equal. At this point the well known halo type periodic orbits appear. When the frequencies of the two oscillations (vertical and planar) are not commensurable, the motion is not periodic and it remembers a Lissajous orbit. Then we say that we have a quasi-periodic orbit. This kind of motion can be found both around the vertical periodic orbit and around the halo orbits. Some of these different kinds of orbits have been represented in Figure 3.6. A more synthetic way of displaying all this zoo of orbits consists in representing only their intersection with the $z = 0$ plane. This is what is usually called Poincaré map representation. A planar orbit will appear as a closed curve on the plane and a quasi-periodic orbit as a set of points lying, more or less, on a curve. Figure 3.7 shows one of these representations. Near the centre of the figure one can see a fixed point. It corresponds to a vertical periodic orbit that crosses the $z = 0$ plane just at this point. It (and so, the corresponding orbit) is surrounded by quasi-periodic motions that take place on invariant tori. The external curve of the figure is the planar Lyapunov orbit (corresponding to a given value of the Jacobi constant). Two other fixed

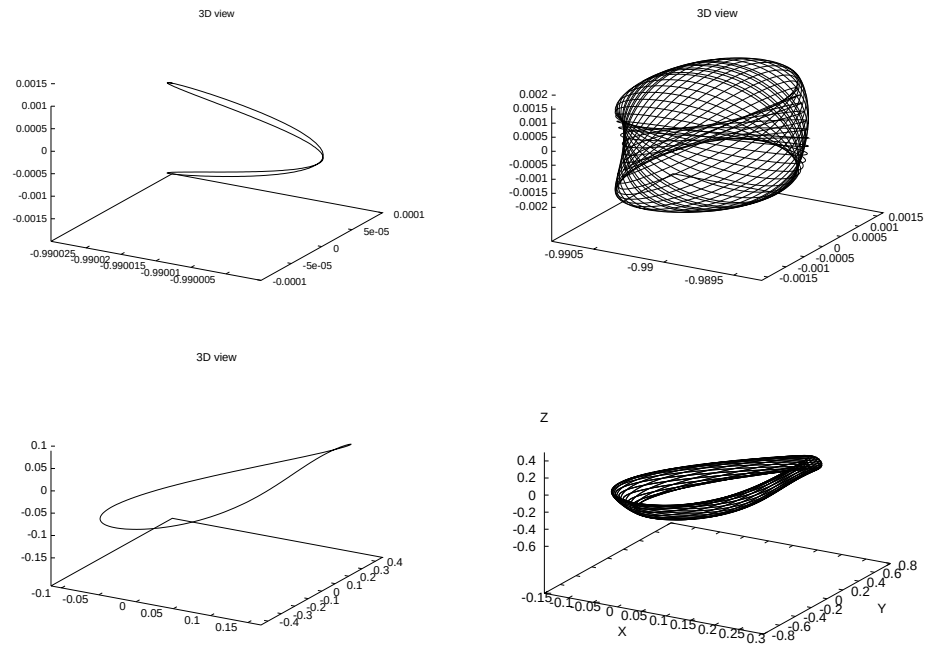

Figure 3.6: Several types of orbits around L_1. Upper left: vertical Lyapunov periodic orbit. Upper right: Quasi-periodic orbit around a vertical periodic orbit (Lissajous orbit). Lower left: halo periodic orbit. Lower right: quasi-halo orbit (quasi-periodic orbit around a halo orbit).

points correspond to the two halo orbits, which are symmetrical to one another with respect to $z = 0$. They are, in turn, surrounded by invariant 2D tori. Between the 2D tori around the vertical orbit and the ones around the halo orbit there is the trace of the stable and unstable manifolds of the planar Lyapunov orbit.

Since we are interested in the motion in the vicinity of a given libration point, following Richardson [56], we set the origin of coordinates at the libration point and scale variables in such a way that the distance from the smallest primary to the selected equilibrium point will be equal to one. Expanding $r_1 = ((x-\mu)^2+y^2+z^2)^{1/2}$ and $r_2 = ((x-\mu+1)^2+y^2+z^2)^{1/2}$ in power series, one gets

$$H = \frac{1}{2}\left(p_x^2+p_y^2+p_z^2\right) + yp_x - xp_y - \sum_{n\geq 2} c_n(\mu)\rho^n P_n\left(\frac{x}{\rho}\right), \tag{3.1}$$

where $\rho^2 = x^2+y^2+z^2$, the c_n are constants depending on the equilibrium point and the mass ratio μ and P_n is the Legendre polynomial of degree n. With a linear symplectic change of coordinates (see [46]), the second order part of the Hamiltonian is set into its real normal form,

$$H_2 = \lambda x p_x + \frac{\omega_p}{2}(y^2+p_y^2) + \frac{\omega_v}{2}(z^2+p_z^2),$$

where, for simplicity, we have kept the same notation for the variables. Here, λ, ω_p and ω_v are positive real numbers. From H_2, it is clear that the linear behaviour near the collinear equilibrium points is of the type **saddle** $\times$ **centre** $\times$ **centre**. Hence, one can expect families of periodic orbits

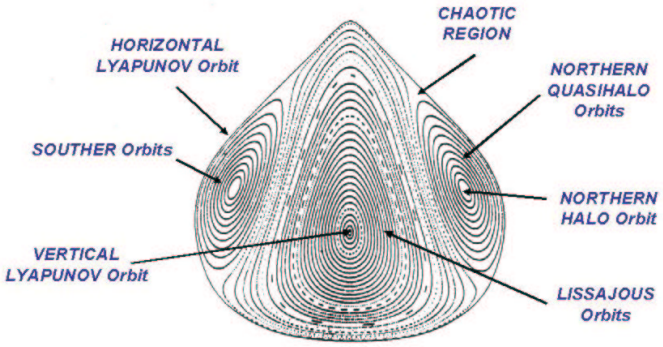

Figure 3.7: Poincaré map representation of the orbits near the libration point L_1 for the value of the Jacobi constant 3.00078515837634. The RTBP mass parameter corresponds to the Earth+Moon–Sun system.

which in the limit have frequencies related to both centres: ω_p and ω_v (called planar and vertical frequencies, respectively). This is assured by the Lyapunov centre theorem, unless one of the frequencies is an integer multiple of the other (which only happens for a countable set of values of the mass ratio (see [207])). Near the libration points we can also expect 2D tori to appear, with two basic frequencies which tend to ω_p and ω_v when the amplitudes tend to zero. The rigorous existence of these tori is more problematic. Firstly, the basic frequencies at the collinear point can be too close to resonant. Furthermore, the frequencies change with their amplitudes and so, they go across resonances when the amplitudes are changed. This leads to a Cantor set of tori. The proof of the existence of these tori follows similar lines to the proof of the KAM theorem (see [199]).

Close to the L_1 and L_2 libration points, the dynamics is that of a strong unstable equilibrium, because of the saddle component of the linear approximation. This is the reason why it is not feasible to perform a direct numerical simulation of the Poincaré map in order to get an idea of the phase space. Due to the **centre** $\times$ **centre** part, and considering all the energy levels, there are 4D centre manifolds around them (they are also called neutrally stable manifolds). On a given energy level this is just a 3D set where dynamics have a "neutral behaviour". There are periodic orbits and 2D invariant tori on it. The L_3 point has the same linear behaviour, however the instability is quite mild. Nevertheless, the long term effects associated to the unstable/stable manifolds of L_3 or to the ones of the central manifold around L_3 are extremely important (see [235], [47]). In what follows we will show results about the phase space in a large neighbourhood of the collinear libration points and will see how all the mentioned invariant sets (periodic orbits and tori) are organised. We will use two different and complementary methods: an analytical approach and a numerical procedure.

3.2.1 Analytical Approach

The analysis of the dynamics in the centre manifold for values of the energy close to the one of the equilibrium point can be done in a semi-analytical way using different strategies. One consists in performing a reduction of the Hamiltonian that decreases the number of degrees of freedom,

removes the hyperbolic directions and allows the numerical study of the Poincaré map in a vicinity of the equilibrium points (see [46] and [17]). Another possibility is to reduce Hamiltonian to its normal form around the equilibrium point (see [22]). This approach is usually known as the reduction to the centre manifold. Note that, generically, the expansions required for these computations cannot be convergent in any open set, because of the crossing of resonances. Another procedure consists in the use of Lindstedt-Poincaré methods to explicitly compute the periodic orbits the invariant tori (see [54], [46], [47], [235]) . It looks for an analytical expressions for them in terms of suitable amplitudes and phases. Both approaches are limited by the convergence of the expansions used, for the changes of coordinates and the Hamiltonian in the first case and for the periodic orbits and invariant tori in the second, which is discussed in the mentioned papers. The general ideas and main results obtained with both procedures will be discussed in the next sections.

3.2.2 Reduction to the Centre Manifold

The reduction to the centre manifold is similar to a normal form computation. The objective is not to remove all the monomial in the expansion H, up to a given order, but to remove only some, in order to have an invariant manifold tangent to the elliptic directions of H_2. This is done through a series of changes of variables which can be implemented by means of the Lie series method (see [190]).

The Hamiltonian of the RTBP, with the second order terms in normal form, can be written in a suitable set of coordinates and momenta, as

$$H(q,p) = \sqrt{-1}\omega_v q_1 p_1 + \sqrt{-1}\omega_p q_2 p_2 + \lambda q_3 p_3 + \sum_{n\geq 3} H_n(q,p), \tag{3.2}$$

where H_n denotes an homogeneous polynomial of degree n.

To remove the instability associated with the hyperbolic character of H, we first note that the second order part of the Hamiltonian, H_2, displays the instability associated with the term $\lambda q_3 p_3$. In the linear approximation of the equations of motion, the central part is obtained setting $q_3 = p_3 = 0$. If we want that the trajectory remains tangent to this space when adding the nonlinear terms, this is, with $q_3(t) = p_3(t) = 0$ for all $t > 0$, once we set $q_3(0) = p_3(0) = 0$, we need to have $\dot{q}_3(0) = \dot{p}_3(0) = 0$. Then, because of the autonomous character of the system, we will obtain $q_3(t) = p_3(t) = 0$ for all $t \geq 0$.

Recalling the form of the Hamiltonian equations of motion, $\dot{q}_i = H_{p_i}$, $\dot{p}_i = -H_{q_i}$, one can get the required condition, $\dot{q}_3(0) = \dot{p}_3(0) = 0$ when $q_3(0) = p_3(0) = 0$, if in the series expansion of the Hamiltonian, H, all the monomial, $h_{ij}q^i p^j$, with $i_3 + j_3 = 1$ have $h_{ij} = 0$ (i and j stand for (i_1, i_2, i_3) and (j_1, j_2, j_3), respectively). This happens if there are no monomial with $i_3 + j_3 = 1$ Of course, other expansions could give us the same required tangency condition, but this is the one that needs to cancel less monomial in (3.2) and, in principle, it is better behaved both in terms of convergence and from a numerical point of view.

All the computations can be implemented using specific symbolic manipulators that can carry out the full procedure up to an arbitrary order (see [17]). In this way, we end up with a Hamiltonian $H(q,p) = H_N(q,p) + R_N(q,p)$, where $H_N(q,p)$ is a polynomial of degree N in (q,p) without terms with $i_3 + j_3 = 1$ and $R_N(q,p)$ is a remainder of order $N+1$ that is skipped in the computations.

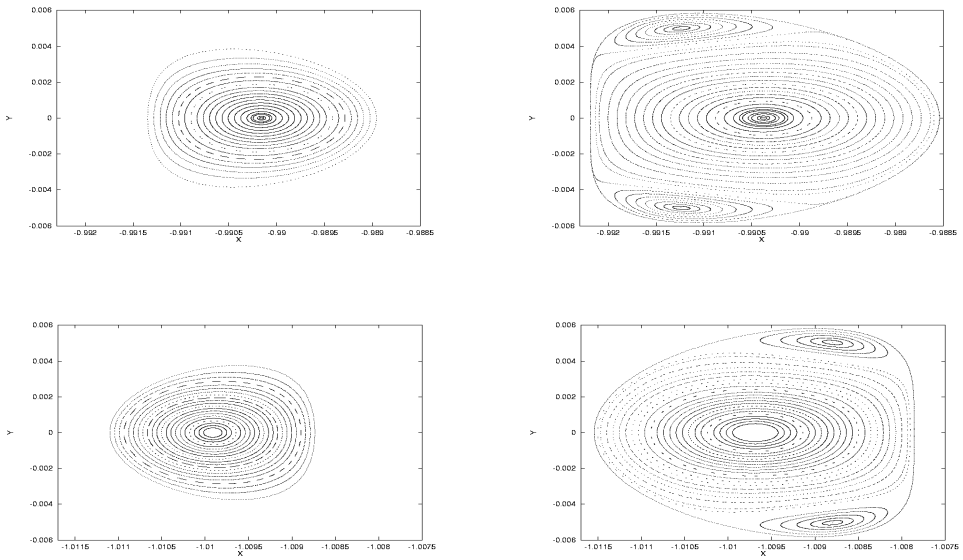

Figure 3.8: Poincaré maps of the orbits in the central manifold of L_1 (two top figures) and L_2 (two bottom figures) for the following values of the Jacobi constant: 3.00085, and 3.00078515837634. RTBP mass parameter of the Earth+Moon–Sun system, $\mu = 3.040423398444176 \times 10^{-6}$.

In order to reduce the number of degrees of freedom, after setting $q_3 = p_3 = 0$ in the initial conditions, we look only at the orbits in the same energy level; in this way only three free variables remain. A further reduction is obtained by looking at the orbits when they cross a surface of section. Now, all the libration orbits with a fixed Hamiltonian value, can be obtained just varying two variables in the initial conditions. For instance, the initial conditions can be chosen selecting arbitrary values for q_2 and p_2. Setting $q_1 = 0$ (the surface of section) and finally computing p_1 in order to be in the selected level of Hamiltonian energy. The propagation of this initial condition, looking when and where it crosses the surface of section again and again, gives what is called the images of the Poincaré map on the Poincaré section $q_1 = 0$. Alternatively, the plane $z = 0$ (in RTBP coordinates) can be used to get a more familiar picture. Note that, due to the linear part of the RTBP equations of motion around the collinear equilibrium points (3.7), $z = 0$, is a surface of section for all the libration orbits in a neighbourhood of the equilibrium point, except for the planar ones which are contained in the $z = 0$ plane.

This is the procedure used to get Figure 3.8, where the libration orbits around L_1 and L_2 are displayed for two different values of the Jacobi constant, C_J, of the RTBP. From Figure 3.8, we note that for each level of C_J there is a bounded region in the Poincaré section. The boundary of the region is the planar Lyapunov orbit of the selected energy (related to the planar frequency ω_p of H_2) and is completely contained in the surface of section. The fixed point, in the central part of the figures, corresponds to an almost vertical periodic orbit, related to the vertical frequency ω_v. Surrounding the central fixed point, we have invariant curves corresponding to Lissajous orbits. The motion in this region is essentially quasi-periodic (except for very small chaotic zones that cannot be seen in the pictures).

Depending on the value of the Jacobi constant, there appear two additional fixed points close

to the boundary. These points are associated to halo orbits of class I (north) and class II (south). Surrounding the fixed points corresponding to the halo orbits, we have again invariant curves related to quasi-periodic motions. These are Lissajous orbits around the halos that we call quasi-halo orbits (see [235]).

Finally, in the transition zone from central Lissajous to quasi-halo orbits there is an homoclinic connection of the planar Lyapunov orbit. We note that the homoclinic trajectory that goes out from the orbit and the one that goes in, do not generally coincide; they intersect with a very small angle. This phenomenon is known as splitting of separatrices. We also note in this case, that the planar Lyapunov orbit is unstable even in the central manifold.

3.2.3 Numerical Approach

In this section we will show how with a numerical approach, the analysis of the phase space using semi-analytical methods, can be extended to a wider range of energy values, including several bifurcations and also to the L_3 libration point. The approach is based in the computation of the 2D invariant tori of the centre manifolds of the three collinear libration points.

Numerical methods have been widely used to compute fixed points and periodic orbits and we will not enter into the details for their computation here. The reader can find an excellent exposition in the paper by Doedel et al. [27]. There are not many papers dealing with the numerical computation of invariant tori. For this purpose, there are mainly two different methods: one is based in looking for a torus as a fixed point of a power of the Poincaré map, P^x, with x being a real number and where P^x is obtained by interpolation. The details of the method, as well as some numerical examples, can be found in [209]. The second procedure, introduced in [228], is based in looking for the Fourier series of the parametrisation of an invariant curve on a torus, asking numerically for quasi-periodic motion. This has been the approach, combined with a multiple shooting procedure, that we have used to study the quasi–periodic motions in a neighbourhood of the collinear libration points. The details can be found in [23] and in [48].

As a first step of the numerical approach, the study of the families of periodic orbits around the libration points and their normal behaviour must be done.

3.2.4 Normal Behaviour Around a Periodic Orbit

Let $\varphi_t(\mathbf{x})$ be the flow of the RTBP. The normal behaviour of a T-periodic orbit through $\mathbf{x}_0$ is studied in terms of the time-T flow around $\mathbf{x}_0$, whose linear approximation is given by the monodromy matrix $M = D\varphi_T(\mathbf{x}_0)$ of the periodic orbit. As the monodromy matrix M is symplectic, we have that

$$\operatorname{Spec} M = \{1, 1, \lambda_1, \lambda_1^{-1}, \lambda_2, \lambda_2^{-1}\}.$$

The stability parameters of the periodic orbit, that are defined as $s_j = \lambda_j + \lambda_j^{-1}$ for $j = 1, 2$, can be of one of the following kinds:

- *Hyperbolic*: $s_j \in \mathbb{R}$, $|s_j| > 2$. It is equivalent to $\lambda_j \in \mathbb{R}\backslash\{-1, 1\}$.
- *Elliptic*: $s_j \in \mathbb{R}$, $|s_j| < 2$. It is equivalent to $\lambda_j = e^{i\rho}$ with $\rho \in \mathbb{R}$ (if $|s_j| = 2$, then it is said to be *parabolic*).

- *Complex unstable*: $s_j \in \mathbb{C}\backslash\mathbb{R}$. It is equivalent to $\lambda_j \in \mathbb{C}\backslash\mathbb{R}$, $|\lambda_j| \neq 1$.

If s_j is complex unstable, then s_{3-j} is also complex unstable and, in fact, $s_{3-j} = \overline{s_j}$. After the complex unstable bifurcation, following a Hamiltonian Hopf pattern, there appear invariant tori, as is shown in [204]. If s_j is hyperbolic, then the periodic orbit has stable and unstable manifolds, whose sections at $\mathbf{x}_0$ through the $\{\lambda_j, \lambda_j^{-1}\}$–eigenplane of M are tangent to the $\{\lambda_j, \lambda_j^{-1}\}$–eigenvectors at $\mathbf{x}_0$. If s_j is elliptic, the $\{\lambda_j, \lambda_j^{-1}\}$–eigenplane of M through $\mathbf{x}_0$ is foliated (in the linear approximation) by invariant curves of the restriction of the linearisation of φ_T (that is, the map $\mathbf{x} \to \mathbf{x}_0 + M(\mathbf{x} - \mathbf{x}_0)$), which have rotation number ρ. For the full system, some of these invariant curves subsist and give rise to 2D tori.

In what follows, we will say that a periodic orbit has central part if one of the stability parameters s_1, s_2 is elliptic and we will use them to compute the tori of the central manifolds.

3.2.5 Numerical Computation of Invariant Tori

We look for a parametrisation of a 2-dimensional torus $\psi : \mathbb{T}^2 = \mathbb{R}^2/2\pi\mathbb{Z} \to \mathbb{R}^6$, satisfying

$$\psi(\theta + \omega t) = \varphi_t\big(\psi(\theta)\big), \qquad \forall \theta \in \mathbb{T}^2,\ \forall t \in \mathbb{R}, \tag{3.3}$$

where $\omega = (\omega_1, \omega_2) \in \mathbb{R}^2$ are the frequencies of the torus and $\varphi_t(\mathbf{x})$ is the flow associated to the RTBP. Let us denote by T_i the period corresponding to the ω_i frequency, that is $T_i = 2\pi/\omega_i$, and $\theta = (\xi, \eta)$. In order to reduce the dimension of the problem, instead of looking for the parametrisation of the whole torus, we can look for the parametrisation of a curve $\{\eta = \eta_0\}$ (or $\{\xi = \xi_0\}$) on the torus, which is invariant under φ_{T_2}, namely

$$\varphi_{T_2}\big(\psi(\xi, \eta_0)\big) = \psi(\xi + \omega_1 T_2, \eta_0), \qquad \forall \xi \in \mathbb{T}^1. \tag{3.4}$$

Then, we look for a parametrisation $\varphi : \mathbb{T}^1 \to \mathbb{R}^n$ satisfying

$$\varphi(\xi + \rho) = \phi_\delta\big(\varphi(\xi)\big), \qquad \forall \xi \in \mathbb{T}^1, \tag{3.5}$$

where $\delta = T_2$ and $\rho = \delta\omega_1$. Note that ρ is the rotation number of the curve we are looking for. We assume for φ truncated Fourier series representation

$$\varphi(\xi) = A_0 + \sum_{k=1}^{N_f} \big(A_k \cos(k\xi) + B_k \sin(k\xi)\big), \tag{3.6}$$

with A_k, $B_k \in \mathbb{R}^n$. This representation of the geometrical torus $\{\psi(\theta)\}_{\theta\in\mathbb{T}^2}$ is non unique for two reasons: (1) For each choice of η_0 we have a different φ in (3.6), i.e., a different invariant curve on the torus. (2) Given the parametrisation (3.6), for each $\xi_0 \in \mathbb{T}^1$, $\varphi(\xi - \xi_0)$ is a different parametrisation with a different Fourier expansion of the same invariant curve of the torus. In order to overcome both indeterminations, some components of the Fourier coefficients A_k must be fixed.

Finally, and in order to deal with high instabilities, a multiple shooting procedure is used. It consists of looking for several invariant curves on the torus $\{\psi(\theta)\}_{\theta\in\mathbb{T}^d}$ instead of just one, in order to reduce the maximum time of integration to a fraction of δ. Concretely, we will look

for m parametrisations $\varphi_0, \varphi_1, \ldots, \varphi_{m-1}$ satisfying for all $\xi \in \mathbb{T}^1$: $\varphi_{j+1}(\xi) = \phi_{\delta/m}\big(\varphi_j(\xi)\big)$, for $j = 0 \div m-2$ and $\varphi_0(\xi+\rho) = \phi_{\delta/m}\big(\varphi_{m-1}(\xi)\big)$.

The details of the computational aspects (implementation, computing effort, parallel strategies, etc.) of this procedure are given in [48]. As a sample of the tori that can be computed with this procedure, in Fig. 3.9 we display families around bifurcated halo-type orbits of L_1 and L_2 with central part.

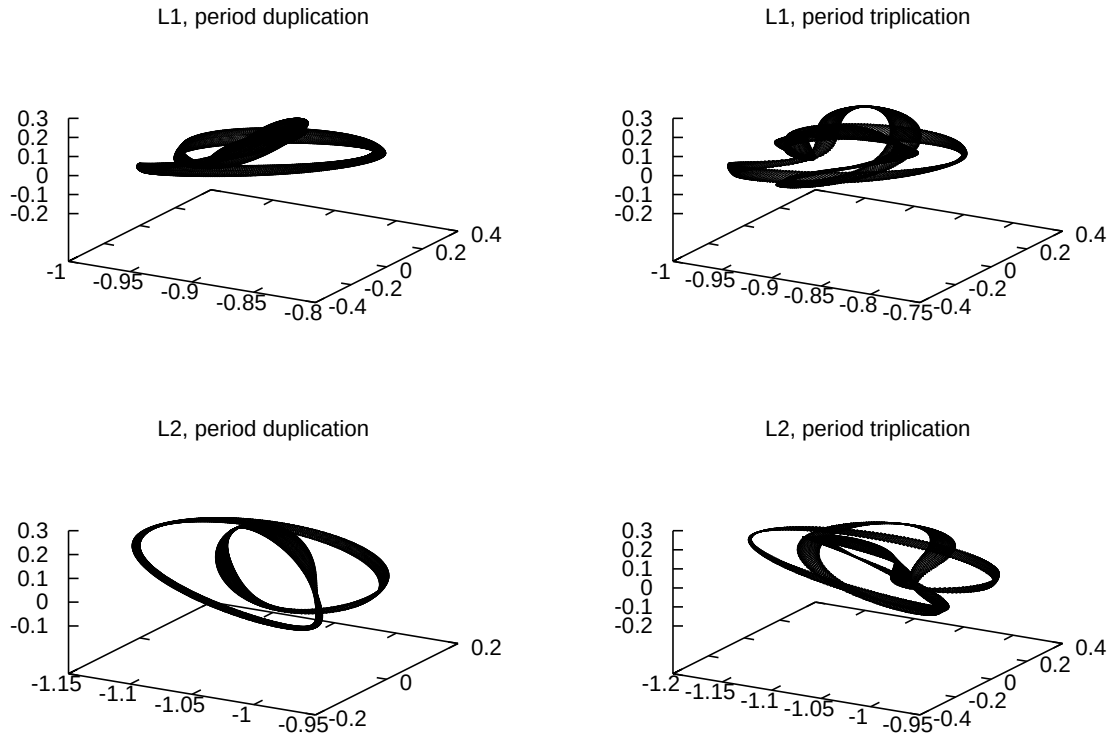

Figure 3.9: Tori around the bifurcated halo-type orbits. The two on the top are in the families around L_1 and have energy $h = -1.501$. The two on the bottom are in the families around L_2 and have energy $h = -1.507$.

3.2.6 Invariant Tori Starting Around Vertical Orbits

In Fig. 3.10 we have displayed the region (in the energy–rotation number plane) covered by the 2–parametric family of tori computed starting from the vertical L_1 Lyapunov families of periodic orbits with central part. The diagrams corresponding to L_2 and L_3 are similar (see [48]). The boundary has different pieces:

- The lower left piece α (from vertex 1 to 2) is related to the planar Lyapunov family. The orbits of this family represented in the curve are just the first piece of the family with central part. The horizontal coordinate is the energy level h of the curve and the vertical coordinate is $\rho = (2\pi)^2/(2\pi-\nu) - 2\pi$, where $2\cos\nu$ is the stability parameter of the orbit.

- The upper piece β (from vertex 2 to 3) is strictly related to the vertical Lyapunov family. The points on this curve are (h, ρ) where h is the energy of the orbit and the rotation number ρ is such that the elliptic stability parameter of this orbit is $2\cos\rho$. Note that this relation between ρ and ν is different from the previous item in order to have continuity of ρ along an isoenergetic family of tori.

- The bottom boundary γ (from vertex 3 to 1), that corresponds to $\rho = 0$, begins at the value of the energy where the halo families are born. It is related to a separatrix between the tori around the vertical Lyapunov families and the halo ones.

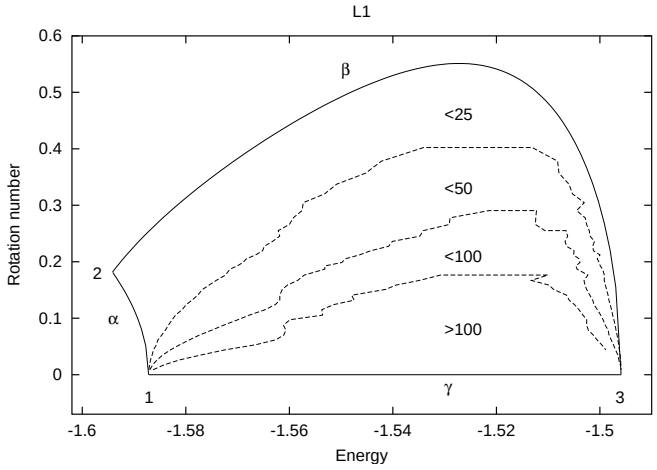

Figure 3.10: Region in the energy–rotation number plane, covered by the two-parametric family of tori computed using the vertical Lyapunov family of p.o. for L_1 as the starting point. The number of harmonics used for the computation of the tori (< 25, < 50, < 100 and > 100) is shown in the figure. Vertex 1 is at the value of the energy at which the halo family is born. Vertex 2 is at the value of the energy of the equilibrium point. Vertex 3 is at the value of the energy of the first bifurcation of the vertical Lyapunov family.

There are different ways of computing the tori within the region surrounded by the curves mentioned above. We always start from the pieces of boundary formed by periodic orbits. One possibility is then to perform the continuation procedure keeping the value of the energy h fixed. Another one is to allow the variation of the energy but keeping the rotation number ρ fixed. In this last case, and in order to be as close as possible to conditions that guarantee the existence of tori, it is convenient to set the rotation number "as irrational as possible". To this end, when we used this second strategy, we set the values of ρ such that $2\pi/\rho$ is an integer plus the golden number. In both cases, and for all L_1, L_2 and L_3 cases, we have always reached a region where the number of harmonics is larger than the maximum value allowed, which at most has been set equal to 100. Larger values of this parameter make computing time prohibitive. Just to have an idea of the computing effort, the constant rotation number family with $\rho = 0.176$ requires about 3 days of CPU time of an Intel Pentium III at 500MHz.

3.2.7 An Extended View of the Centre Manifold

Using the periodic orbits and the tori computed using the aforementioned strategies, we have been able to extend the Poincaré map representation of the central manifolds around the collinear libration points.

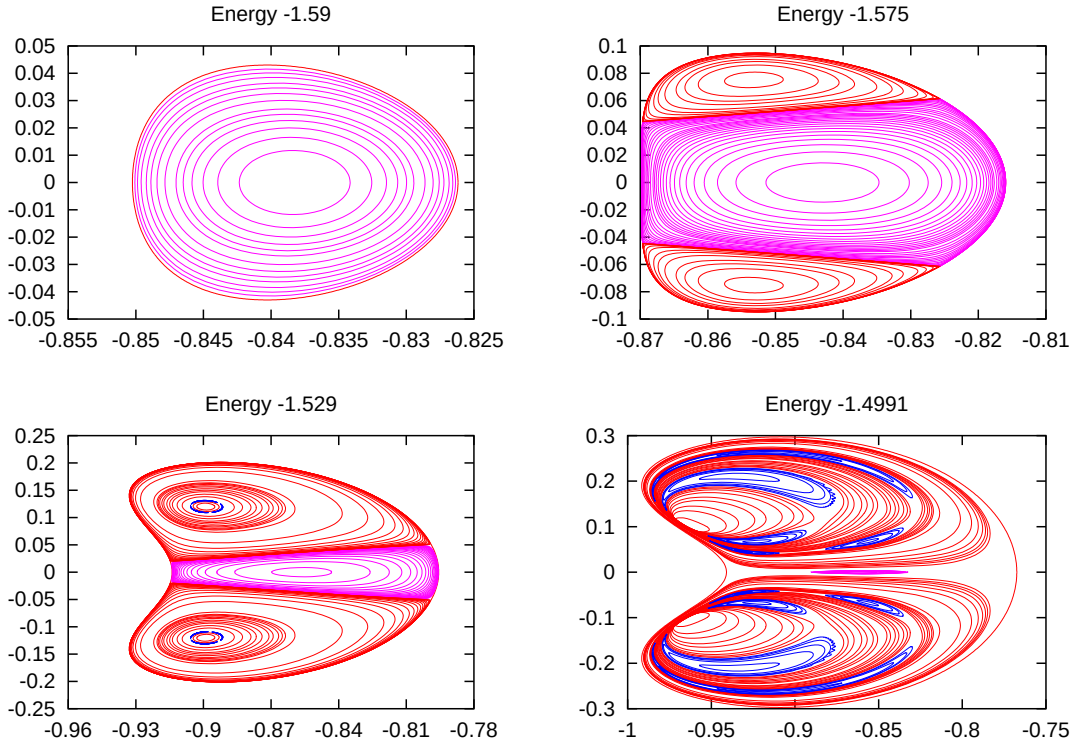

Figure 3.11: Energy slices of the section $z = 0$, $p_z > 0$ of the invariant tori around L_1

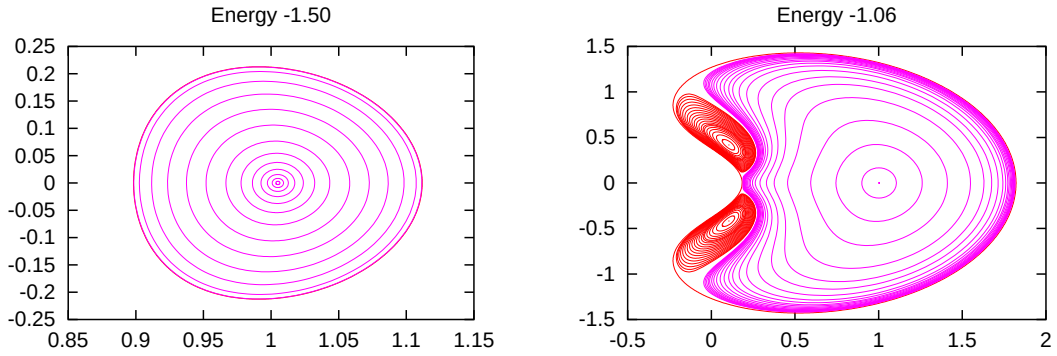

Figure 3.12: Energy slices of the section $z = 0$, $p_z > 0$ of the invariant tori around L_3.

Figures 3.11, and 3.12 show the results for L_1, and L_3, respectively (the results for L_2 are close to the ones obtained for L_1). In all these figures we have represented the x–y coordinates at the intersections with $z = 0$, $p_z > 0$. All the plots have a similar structure. The exterior curve in each plot is the Lyapunov planar orbit of the energy level corresponding to the plot.

As this orbit is planar, it is completely included in the surface of section, and it is the only orbit for which this happens. For the three equilibrium points, and for small energy values, the whole picture is formed by invariant curves surrounding the fixed point associated to the vertical orbit. They are related to the intersections of the Lissajous type trajectories around the vertical periodic orbit. The halo orbits appear at the energy levels corresponding to the first bifurcation of the Lyapunov planar family. This can be clearly seen in the Poincaré map representations, since there appear two additional fixed points surrounded by invariant curves. Increasing the values of the energy, the L_1 and L_2 families of halo orbits have two relevant bifurcations, by period triplication and duplication (see Figure 3.9). Both bifurcations can also be detected in the Poincaré representations. This additional structure has not been detected for the L_3 case. Within the bifurcated families there are some which have got a central part, which are surrounded by invariant tori. These tori give rise to the "island chain" structure typical of two–dimensional area–preserving maps. This behaviour is only clear in a magnification of the figures, as is shown in [48].

The region between the tori around the vertical Lyapunov orbit and the tori around the halo orbits is not empty, as it appears in the above figures, and should contain, at least, the traces, on the surface of section, of the invariant manifolds of the Lyapunov planar orbit. These manifolds act as separatrices between both kinds of motion. The same thing happens between the islands of the bifurcated halo–type orbits and the tori around the halo orbits. In this case, the region between both kinds of tori is filled with the traces of the invariant manifolds of the bifurcated hyperbolic halo–type orbits. In all these boundary regions, the motion should have a chaotic behaviour. With the current tools we have not been able to compute these separatrices.

3.3 Orbit Computations

3.3.1 Analytical Computation Using Lindstedt-Poincaré Procedures

The planar and vertical Lyapunov periodic orbits as well as the Lissajous, halo and quasi-halo orbits can be computed using Lindstedt-Poincaré procedures and ad hoc algebraic manipulators. In this way one obtains their expansions, in RTBP coordinates, suitable to be used in a friendly way. In this section we will give the main ideas used for their computation.

We will start with the computation of the Lissajous trajectories (2D tori) and halo orbits (1D tori or periodic orbits). The RTBP equations of motion can be written as

$$\begin{aligned} \ddot{x} - 2\dot{y} - (1+2c_2)x &= \frac{\partial}{\partial x}\sum_{n\geq 3} c_n \rho^n P_n\left(\frac{x}{\rho}\right), \\ \ddot{y} + 2\dot{x} + (c_2-1)y &= \frac{\partial}{\partial y}\sum_{n\geq 3} c_n \rho^n P_n\left(\frac{x}{\rho}\right), \\ \ddot{z} + c_2 z &= \frac{\partial}{\partial z}\sum_{n\geq 3} c_n \rho^n P_n\left(\frac{x}{\rho}\right), \end{aligned} \tag{3.7}$$

with c_n, ρ and P_n as in (3.1). The solution of the linear part of these equations is

$$\begin{aligned} x(t) &= \alpha\cos(\omega_p t+\phi_1),\\ y(t) &= \kappa\alpha\sin(\omega_p t+\phi_1),\\ z(t) &= \beta\cos(\omega_v t+\phi_2), \end{aligned} \tag{3.8}$$

where ω_p and ω_v are the planar and vertical frequencies and κ is a constant. The parameters α and β are the in-plane and out-of-plane amplitudes of the orbit and ϕ_1, ϕ_2 are the phases. These linear solutions are already Lissajous trajectories. When we consider the nonlinear terms, we look for formal series solutions in powers of the amplitudes α and β of the type

$$\left\{\begin{array}{c} x\\ y\\ z\end{array}\right\} = \sum_{i,j=1}^{\infty}\left(\sum_{|k|\le i,|m|\le j}\left\{\begin{array}{c} x\\ y\\ z\end{array}\right\}_{ijkm}\left\{\begin{array}{c} \cos\\ \sin\\ \cos\end{array}\right\}(k\theta_1+m\theta_2)\right)\alpha^i\beta^j, \tag{3.9}$$

where $\theta_1=\omega t+\phi_1$ and $\theta_2=\nu t+\phi_1$. Due to the presence of nonlinear terms, the frequencies ω and ν cannot be kept equal to ω_p and ω_v, and they must be expanded in powers of the amplitudes

$$\omega=\omega_p+\sum_{i,j=1}^{\infty}\omega_{ij}\alpha^i\beta^j,\quad \nu=\omega_v+\sum_{i,j=1}^{\infty}\nu_{ij}\alpha^i\beta^j.$$

The goal is to compute the coefficients x_{ijkm}, y_{ijkm}, z_{ijkm}, ω_{ij}, and ν_{ij} recurrently up to a finite order $N=i+j$. Identifying the coefficients of the general solution (3.9) with the ones obtained from the solution of the linear part (3.8), we see that the non zero values are $x_{1010}=1$, $y_{1010}=\kappa$, $z_{1010}=1$, $\omega_{00}=\omega_p$ and $\nu_{00}=\omega_v$. Inserting the linear solution (3.8) in the equations of motion, we get a reminder for each equation, which is a series in α and β beginning with terms of order $i+j=2$. In order to get the coefficients of order two, this known order 2 terms must be equated to the unknown order 2 terms of the left hand side of the equations. The general step is similar. It assumes that the solution has been computed up to a certain order $n-1$. Then it is substituted in the right hand side of the RTBP equations, producing terms of order n in α and β. This known order n terms must be equated with the unknown terms of order n of the left hand side.

The procedure can be implemented up to high orders. In this way we get, close to the equilibrium point, a big set of KAM tori. In fact, between these tori there are very narrow stochastic zones (because the resonances are dense). Hence we will have divergence everywhere. However, small divisors will show up only at high orders (except the one due to the 1:1 resonance), because at the origin ω_p/ω_v is close to 29/28. The high order resonances have a very small stochastic zone and the effect is only seen after a big time interval.

Halo orbits are periodic orbits which bifurcate from the planar Lyapunov periodic orbits when the in plane and out of plane frequencies are equal. This is a 1:1 resonance that appears as a consequence of the nonlinear terms of the equations and, in contrast with the Lissajous orbits, they do not appear as a solution of the linearised equations. Of course, we have to look for these 1-D invariant tori as series expansion with a single frequency. In order to apply the Lindstedt-Poincaré procedure, following [54], we modify the equations of motion (3.7) by adding to the third equation a term like $\Delta\cdot z$, where Δ is a frequency type series

$$\Delta=\sum_{i,j=0}^{\infty}d_{ij}\alpha^i\beta^j,$$

that must verify the condition $\Delta = 0$. We start looking for the (non trivial) librating solutions with frequency ω_p

$$\begin{aligned} x(t) &= \alpha \cos(\omega_p t + \phi_1), \\ y(t) &= \kappa\alpha \sin(\omega_p t + \phi_1), \\ z(t) &= \beta \cos(\omega_p t + \phi_2). \end{aligned} \tag{3.10}$$

We note that after this step, halo orbits are determined up to order 1, and $\Delta = 0$ is read as $d_{00} = 0$. Halo orbits depend only on one frequency or one amplitude since they are 1-D invariant tori, so we have not two independent amplitudes α and β. The relation between α and β is contained in the condition $\Delta = 0$ which implicitly defines $\alpha = \alpha(\beta)$.

When we consider the full equations, we look for formal expansions in powers of the amplitudes α and β of the type

$$\left\{ \begin{array}{c} x \\ y \\ z \end{array} \right\} = \sum_{i,j=1}^{\infty} \left(\sum_{|k|\leq i+j} \left\{ \begin{array}{c} x \\ y \\ z \end{array} \right\}_{ijk} \left\{ \begin{array}{c} \cos \\ \sin \\ \cos \end{array} \right\} (k\theta) \right) \alpha^i \beta^j,$$

where $\theta = \omega t + \phi$ and, as in the case of 2-D invariant tori, the frequency ω must be expanded as $\omega = \sum_{i,j=0}^{\infty} \omega_{ij} \alpha^i \beta^j$. The procedure for the computation of the unknown coefficients x_{ijk}, y_{ijk}, z_{ijk}, ω_{ij} and d_{ij} is close to the one described for the Lissajous trajectories.

Quasi-halo orbits are quasi-periodic orbits (depending on two basic frequencies) on two dimensional tori around a halo orbit. Given a halo orbit of frequency ω, the series expansions for the coordinates of the quasi-halo orbits around it will be of the form

$$\left\{ \begin{array}{c} x \\ y \\ z \end{array} \right\} = \sum_{i=1}^{\infty} \left(\sum_{|k|<i,|m|<i} \left\{ \begin{array}{c} x \\ y \\ z \end{array} \right\}_{i}^{km} \left\{ \begin{array}{c} \cos \\ \sin \\ \cos \end{array} \right\} (k(\omega t + \phi_1) + m(\nu t + \phi_2)) \right) \gamma^i.$$

These expansions depend on two frequencies (ω, ν) and one amplitude, γ (related to the size of the torus around the halo orbit). The frequency ν is the second natural frequency of the torus, and it is close to the normal frequency around the base halo orbit. The amplitude, γ, is related to the size of the torus around the "base" halo orbit which is taken as backbone.

In order to apply the Lindstedt-Poincaré method to compute the quasi-halo orbits, it is convenient to perform a change of variables transforming the halo orbit to an equilibrium point of the equations of motion. Then, orbits librating around the equilibrium point in the new coordinates correspond to orbits librating around the halo orbit in the original ones. The details of the procedure for their computation can be found in [235].

All the different kinds of orbits displayed in Figure 3.8 have been computed using the Lindsted-Poincaré procedure according to the previous explanations.

3.3.2 Numerical Refinement

The purpose of this section is to show procedures aimed getting solutions, close to the ones previously obtained for the RTBP, of more realistic equations of motion as Newton's equations using JPL ephemeris for the motion of the bodies of the solar system, or some of the intermediate

models mentioned in previous sections. For these more realistic models there is not a complete study of the phase space around the libration points (or their dynamical substitutes) like the one that exists for the RTBP.

Since the solutions will be computed numerically and the equations of motion are time dependent, an initial epoch and a fixed time span is selected and the orbit is computed for this period of time. In the next section we describe a multiple shooting procedure similar to the one used for the numerical solution of boundary-value problems (see [213]).

Multiple shooting

As in the standard multiple shooting method, the total time span is splitted into a number of shorter subintervals selecting, for instance, N equally spaced points $t_1, t_2, ..., t_N$. (t_1 is the initial epoch and $t_N - t_1$ the length of the time interval mentioned above). Different time intervals could have been used too. Let us denote by $\Delta t = t_{i+1} - t_i$ and by

$$Q_i = (t_i, x_i, y_i, z_i, \dot{x}_i, \dot{y}_i, \dot{z}_i,)^T, \quad i = 1, 2, ..., N$$

the points on a fixed orbit of the RTBP, equally spaced (Δt) in time. This orbit can be, for instance, any of the ones for which we have been able to compute their formal expansions using a Lindstedt–Poincaré method. Let $\phi(Q_i)$ be the image of the point Q_i under the flow associated to the equations of motion in the solar system after an amount of time Δt. As, in this way, the epochs t_i are fixed, we can write $Q_i = (x_i, y_i, z_i, \dot{x}_i, \dot{y}_i, \dot{z}_i,)^T$. If all the points Q_i would be on the same orbit of the new equations, then $\phi(Q_i) = Q_{i+1}$ for $i = 1, ..., N-1$. As this is not the case, a change of the starting values is needed in order to fulfil the matching conditions. Consequently, one must solve a set of $N-1$ nonlinear equations, which can be written as

$$F \begin{pmatrix} Q_1 \\ Q_2 \\ \vdots \\ Q_N \end{pmatrix} = \begin{pmatrix} \phi(Q_1) \\ \phi(Q_2) \\ \vdots \\ \phi(Q_{N-1}) \end{pmatrix} - \begin{pmatrix} Q_2 \\ Q_3 \\ \vdots \\ Q_N \end{pmatrix} = \Phi \begin{pmatrix} Q_1 \\ Q_2 \\ \vdots \\ Q_{N-1} \end{pmatrix} - \begin{pmatrix} Q_2 \\ Q_3 \\ \vdots \\ Q_N \end{pmatrix} = 0.$$

A Newton's method is used to solve the system above. If $Q^{(j)} = \left(Q_1^{(j)}, Q_2^{(j)}, ..., Q_N^{(j)}\right)^T$, denotes the j-th iterate of the procedure, Newton's equations can be written as

$$DF(Q^{(j)}) \cdot (Q^{(j+1)} - Q^{(j)}) = -F(Q^{(j)}),$$

where the differential of the function F has the following structure

$$DF = \begin{pmatrix} A_1 & -I & & & \\ & A_2 & -I & & \\ & & \ddots & \ddots & \\ & & & A_{N-1} & -I \end{pmatrix},$$

with $D\Phi = \mathrm{diag}(A_1, A_2, ..., A_{N-1})$. As each of the transition matrices, A_i, that appear in $D\Phi$ are 6×6, at each step of the method we have to solve a system of $(N-1) \times 6$ equations with $6 \times N$ unknowns, so some additional conditions must be added. This is the only difference with

the standard multiple shooting method and is due to the fact that our problem is not a real boundary-value one. As additional equations we could fix some initial and final conditions at $t = t_0$ and $t = t_N$. In this case, one has to take care with the choice because the problem can be ill conditioned from a numerical point of view. This is because the matrix $DF(Q)$ can have a very large condition number. To avoid this bad conditioning, we can choose a small value for Δt, but in this case, as the number of points Q_i increases (if we want to cover the same time span) the instability is transfered to the procedure for solving the linear system. In addition, the extra boundary conditions can force the solution in a non natural way giving convergence problems when we try to compute the orbit for a long time interval.

To avoid this, we can apply Newton's method directly. As the system has more unknowns than equations, we have (in general) an hyper-plane of solutions. From this set of solutions we try to select the one closer to the initial orbit used to start the procedure. This is done by requiring the correction to be minimum with respect to some norm (i.e. the Euclidean norm). The use of the normal equations must be avoided because they are usually ill conditioned too. More precisely, denoting by $\Delta Q^{(j)}$

$$\Delta Q^{(j)} = Q^{(j+1)} - Q^{(j)},$$

requiring $\|\Delta Q^{(j)}\|_2$ to be minimum, one gets the Lagrange function $\mathrm{L}(\Delta Q, \mu)$ with (vector) multiplier μ

$$L(\Delta Q, \mu) = \Delta Q^T \cdot \Delta Q + \mu^T \cdot (F(Q) + DF(Q) \cdot \Delta Q),$$

we get

$$\Delta Q^{(j)} = -DF(Q^{(j)})^T \cdot \left[DF(Q^{(j)}) \cdot DF(Q^{(j)})^T\right]^{-1} \cdot F(Q^{(j)}), \tag{3.11}$$

which gives the value of $\Delta Q^{(j)}$ explicitly. However since the matrix $DF(Q^{(j)})$ is usually very big, a special factorisation in blocks is suitable to get the solution 3.11 in a computationally and efficient way. See [235] for the implementation and the properties of the algorithm.

In order to illustrate the procedure we reproduce the details of some iterations of the computation of a particular solution using JPL ephemeris DE403.

The algorithm is started using as initial nodes, Q_i, that is, the components of $Q^{(0)}$, points on a quasi-halo orbit of the Sun–Earth+Moon system around the L_1 point with $\beta = 0.20$ and $\gamma = 0.08$. The initial epoch is fixed to be January 1 of the year 2000, and 40 nodes are used with a time step, Δt, between them of 180 days. This covers a total time span of 19.7 years. So, the total number of revolutions "around" the equilibrium point L_1 is approximately 39 and one point (approximately) has been taken on each revolution to perform the multiple shooting. In Figure 3.13 we show the (x, y) projection of the orbit after different iterations of the procedure. All the figures are represented in normalised coordinates centred at the L_1 point. The first plot corresponds to the orbit, computed with the analytical expansions, from where the points Q_i were taken. It is an approximate solution (due to the truncation and asymptotic character of the series) of the RTBP equations of motion. The next two, showing large discontinuities at some points, are the results obtained after the first two iterations. The different pieces that constitute the orbit do not match at the nodes in these first steps because the initial conditions were taken from a solution of the RTBP and now we are integrating these initial conditions in a model including all the bodies of the solar system with its real motion. These discontinuities are so large because of the highly unstable character of the solution and because the few number of nodes per revolution that have been taken. The last plot corresponds to the orbit computed after

8 iterations. The discontinuities that appear in the first iterations are reduced to "zero" by the method. In the first step, adding the corrections applied at all the nodes, the total correction in position ($|\Delta Q^{(0)}_{1,2,3}|_2 + |\Delta Q^{(0)}_{7,8,9}|_2 + ...$) is of 319600.6 km and of 9360.6 km/day in velocity, which means an average value for the corrections at each point of 8000 km and 1044,1 235 km/day. After eight iterations the total amount of the corrections has been reduced to 37 mm and less than 1 mm/day, for positions and velocities, respectively. Taking shorter time intervals between consecutive nodes, the norm of the function F is much smaller at the first steps and the number of Newton iterations decreases. For the Sun–Earth+Moon system, a value of Δt equal to 7 days requires no more than 4 or 5 iterations to get a final solution with discontinuities at the nodes smaller than tracking errors. For the Earth–Moon system, computations must be done more carefully and a time step of half a day usually gives good results.

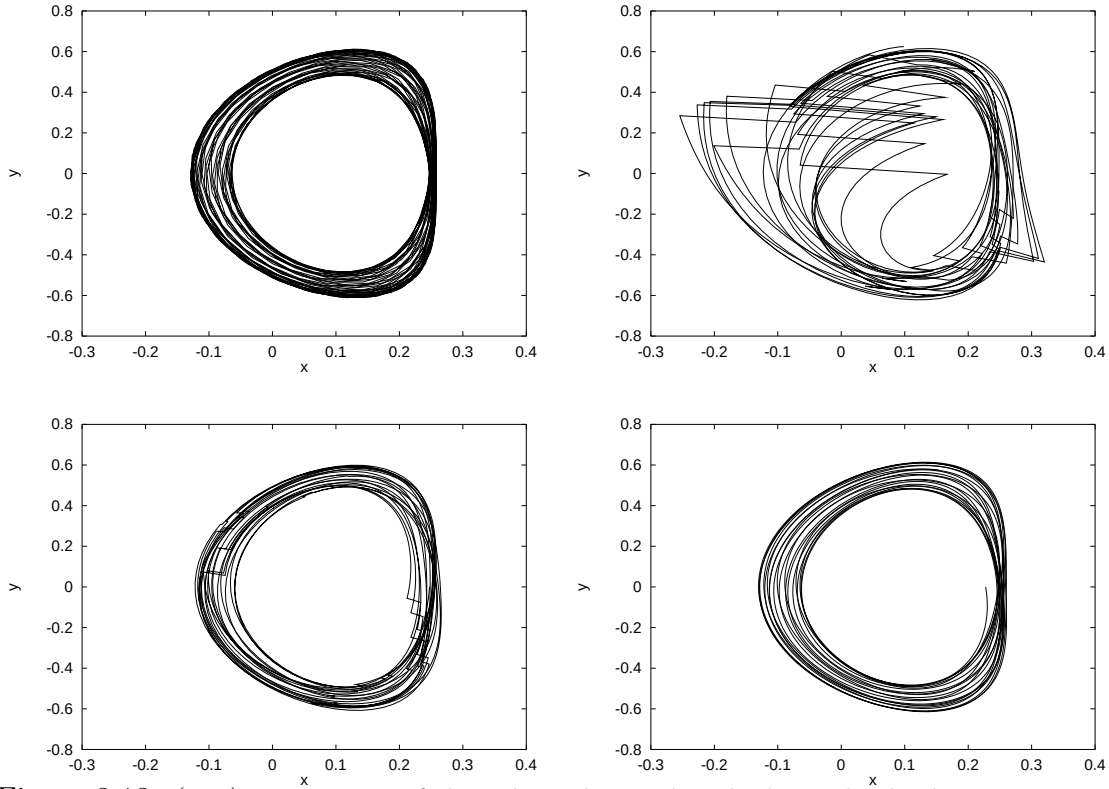

Figure 3.13: (x, y) projections of the orbits obtained with the multiple shooting procedure at different steps. The figure on the left upper corner is the orbit of the RTBP, computed with the expansions, from which the initial points Q_i are taken. The orbits with large jumps discontinuities are the ones obtained after the first two iterations. The figure on the right lower corner is the orbit computed after 8 iterations. The initial orbit is a quasi-halo orbit with $\beta = 0.2$ and $\gamma = 0.08$.

Resonances

The L_2 point in the Earth–Moon system is quite close to a resonance with the solar effects which in some sense, results in the "distance" between the RTBP model and the real one being too large so as to easily extend the solutions of the RTBP to the real problem.

In order to deal with this situation Andreu, in [1] and [2], has introduced a time-dependent restricted four body model that, within a certain degree of simplicity, captures some of the most basic dynamical properties of the true motion around the libration points. The model is time periodic since it depends in just one frequency: the difference between the mean synodical frequencies of the Sun and the Moon. This makes the computation of the most relevant invariant objects of the dynamics simpler.

The main success of the model is that it has allowed the computation of halo-type orbits around L_2 for very large time spans, covering at least a Saros period. When the analytical techniques are applied to get the centre manifold around the dynamical substitutes of the libration points, the results allow only for the exploration of energy levels very close to the one of he dynamical substitute, so the information obtained is poor.

3.4 Transfers to LPO and the Use of Invariant Manifolds

In this and in the next sections the role of the invariant manifolds as natural channels of motion for spacecraft missions will be explained. Here we would like to mention that these manifolds, which play an important role in the evolution of the solar system and that when used for the design of spacecraft missions enhance the set of opportunities and can save precious fuel, are often seen as celestial mechanics "tricks" with no theory supporting them.

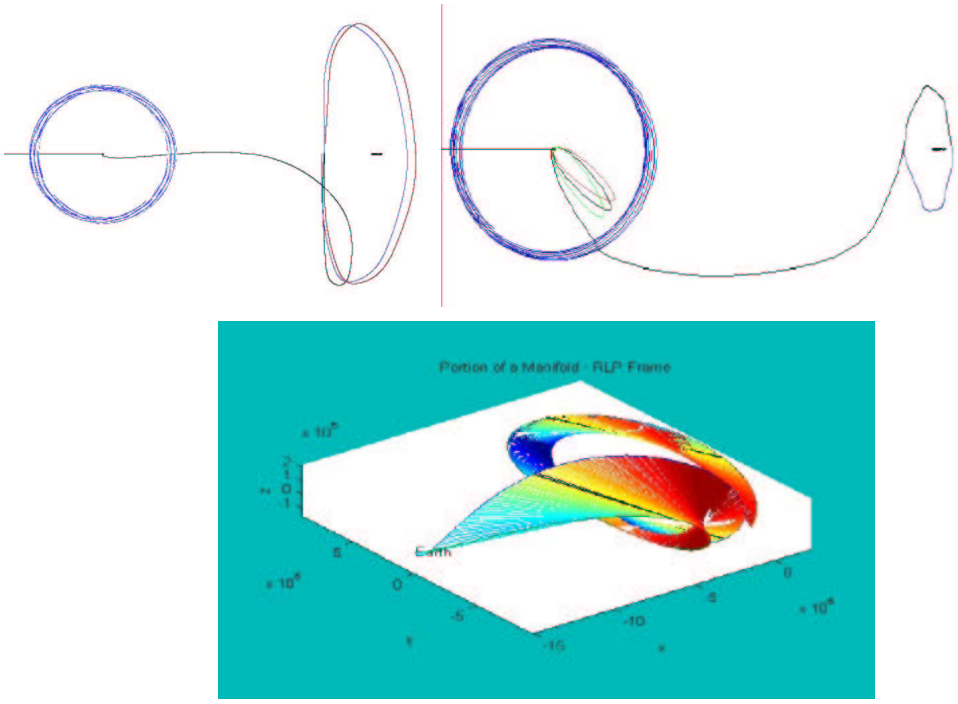

Figure 3.14: Three different kinds of transfer to a libration point orbit: direct transfer, gravitational assisted transfer and transfer using invariant manifolds ([147]).

More recently, the heteroclinic connections in the region of space near L_1 and L_2 have also been

successfully exploited for mission design. As scientific goals become increasingly ambitious and, therefore, mission trajectory requirements become more complex, innovative solutions become necessary. Thus, new directions emerge, such as the studies of dynamical channels and transport in and through this region of space that offers options for transit-type orbits and low energy captures. When coupled with numerical techniques, frequently based on a differential correction process, the results of all these investigations are powerful and effective techniques for generating accurate and varied libration point trajectory options that may serve as a basis for many types of future mission opportunities. It is important to note that these various investigations are all ongoing and far from completion. Yet, even at this juncture, early insights and preliminary observations have yield useful results with immediate and significant impact.

3.4.1 Transfer Using Invariant Manifolds

There are two different approaches in the computation of transfer trajectories to a libration point orbit. One uses direct shooting methods (forward or backward) together with a differential corrector, for targeting and meeting mission goals. Proceeding in this way one can get direct or gravitational assisted transfers, such as the ones shown in Figure 3.14.

Since the libration point orbits, for values of the energy not too far from the ones corresponding to the libration point, have a strong hyperbolic character, its is also possible to use their stable manifold for the transfer. This is what is known in the literature as the dynamical systems approach to the transfer problem. Other ways to obtain transfer trajectories from the Earth to a libration point orbit use optimisation procedures. These methods look for orbits between the Earth and the libration orbit maintaining some boundary conditions, subject to some technical constraints, and minimising the total fuel to be spent in manoeuvres during the transfer (see [167]). According to Masdemont, see [175] and [163], in the dynamical systems approach one can proceed as follows:

1. Take a local approximation of the stable manifold at a certain point of the nominal orbit. This determines a line in the phase space based on a point of the nominal orbit.

2. Propagate, backwards in time, the points in the line of the local approximation of the stable manifold until one or several close approaches to the Earth are found (or up to a maximum time span is reached). In this way some globalisation of the stable manifold is obtained.

3. Look at the possible intersections (in the configuration space) between the parking orbit of the spacecraft and the stable manifold. At each one of these intersections the velocities in the stable manifold and in the parking orbit have different values, v_s and v_p. A perfect manoeuvre with $\Delta v = v_s - v_p$ will move the spacecraft from the parking orbit to an orbit that will reach the nominal orbit without any additional manoeuvre.

4. Then $|\Delta v|$ can be minimised by changing the base point of the nominal orbit at which the stable manifold has been computed (or any equivalent parameter).

Note that, depending on the nominal orbit and on the parking orbit, the intersection described in the third item can be empty, or the optimal solution found in this way can be too expensive. To overcome these difficulties several strategies can be adopted. One possibility is to perform a

transfer to an orbit different from the nominal one and then, with some additional manoeuvres, move to the desired orbits. In a next section we will show how these last kind of transfers can be performed. Another possibility is to allow for some intermediate manoeuvres in the path from the vicinity of the Earth to the final orbit.

In the case the nominal orbit is a quasi-halo or Lissajous orbit and any phase can be accepted for the additional angular variable, the stable manifold has dimension 3. This produces, from one side, a heavier computational task than in the case of halo orbits, but from the other side it gives additional possibilities for the transfer. One should think that the stable manifolds of the full centre manifold (for a fixed value of t) have dimension 5 which offers a lot of possibilities.

3.4.2 The TCM Problem

The Trajectory Correction Manoeuvres (TCM) problem, deals with the manoeuvres to be done by a spacecraft in the transfer segment between the parking orbit and the target nominal one. The purpose of the TCMs is to correct the error introduced by the inaccuracies of the injection manoeuvre.

In connection with the Genesis mission (see [128]), the TCM problem has been studied in [183] and [185]. For this mission a halo type orbit, around the L_1 point of the Earth–Sun system, is used as nominal orbit. The insertion manoeuvre, from the parking orbit around the Earth to the transfer trajectory, is a large one, with a Δv of the order of 3000 m/s; for the Genesis mission, the error in its execution was expected to be about a 0.2 % of Δv (1 sigma value) and a key point to be studied is how large the cost of the correction of this error is when the execution of the first correction manoeuvre is delayed.

In the paper by Serban et al. [185], two different strategies are considered in order to solve the problem, both using an optimisation procedure and producing very similar results. It is numerically shown that, in practice, the optimal solution can be obtained with just two TCMs and that the cost behaves almost linearly with respect to both TCM1 epoch and the launch velocity error.

The same results can be obtained without using any optimal control procedure. This is what is done in [158] and [182]. The quantitative results, concerning the optimal cost of the transfer and its behaviour as a function of the different free parameters, turn out to be the same as in [185]. Additionally, we provide information on the cost of the transfer when the correction manoeuvres cannot be done at the optimal epochs. These results are qualitatively very close to those obtained by Wilson et al. in [179] for the cost of the transfer to a Lissajous orbit around L_2, when the time of flight between the departure and the injection in the stable manifold is fixed but the target state (position and velocity) on the manifold is varied. For this problem it is found that the cost of the transfer can rise dramatically.

In our approach, the transfer path is divided in three different legs:

- The first leg goes from the fixed departure point to the point where the TCM1 is performed. Usually, this correction manoeuvre takes place few days after the departure.

- The second leg, between the two trajectory correction manoeuvres TCM1 and TCM2, is used to perform the injection in the stable manifold of the nominal orbit.

- The last path corresponds to a piece of trajectory on the stable manifold. Since both TCM1 and TCM2 are assumed to be done without errors, the spacecraft will reach the nominal halo orbit without any additional impulse.

Let t_1, t_2 and t_3 be the TCM1, TCM2 and arrival epochs, respectively, and Δv_1, Δv_2 the values of the correction manoeuvres at t_1 and t_2. In this way, given the departure state, X_{dep}, and the time t_1, we define $X_1 = \varphi_{t_1}(X_{dep})$, where $\varphi_t(X)$ denotes the image under the flow of the point X after t. Then, the transfer condition is stated as

$$\varphi_{t_2-t_1}(X_1 + \Delta v_1) + \Delta v_2 = \varphi_{t_2-t_3}(X_a), \tag{3.12}$$

where X_a represents the arrival state to the target orbit, which is chosen as $X_a = X_a^h + d \cdot V^s(X_a^h)$ in the linear approximation of the stable manifold based at the point X_a^h. In (3.12), a term like $X_1 + \Delta v_1$ has to be understood as: to the state X_1 (position and velocity) we add Δv_1 to the velocity. Note that for a given insertion error ϵ (which determines X_{dep}) we have six equality constraints, corresponding to the position and velocity equations (3.12), and ten parameters: t_1, t_2, t_3, Δv_1, Δv_2 and X_a (given by the parameter along the orbit) which should be chosen in an optimal way within mission constraints.

The sketch of the exploration procedure is the following. To start with, we consider the error of the injection manoeuvre and t_1 fixed. Two types of explorations appear in a natural way: the fixed time of flight transfers for which t_3 is fixed, and the free time of flight transfers, where t_3 is allowed to vary. In both cases, we start the exploration by fixing an initial value for the parameter along the orbit, X_a. In the case of fixed time of flight, the problem then reduces to seven parameters (t_2, Δv_1, Δv_2) and the six constraints (3.12). Using Δv_1 and Δv_2 to match the constraints (3.12), the cost of the transfer, $\|\Delta v\| = \|\Delta v_1\| + \|\Delta v_2\|$, is seen as a function of t_2. In the case of free time of flight, $\|\Delta v\|$ is seen as a function of t_2 and t_3, or equivalently, as a function of t_2 and the parameter along the flow, $t_{ws} = t_3 - t_2$.

Once we have explored the dependence of the transfer cost on t_2 and t_3, we study the behaviour when moving the parameter along the orbit, X_a. Finally, the dependence with respect to the magnitude of the error (which is determined by the launch vehicle) and t_1 is studied (which, due to mission constraints, is enough to vary in a narrow and coarse range).

As an example, Figure 3.15 shows the results obtained when: the magnitude of the error in the injection manoeuvre is $-3m/s$, the first manoeuvre is delayed 4 days after the departure ($t_1 = 4$), the total time of flight and t_3, is taken equal to 173.25 days.

Several remarks should be done concerning the figure:

- The solutions of equation (3.12) are grouped along three curves at least. For $t_2 = 99.5$ days there is a double point in the cost function, corresponding to two different possibilities.

- For $t_2 = 113$ days we get the optimum solution in terms of fuel consumption: $\|\Delta v_1\| + \|\Delta v_2\| = 49.31$ m/s. This value is very close to the one given in [185] for the MOI approach, which is 49.1817 m/s. The discrepancies can be attributed to slight differences between the two nominal orbits and the corresponding target points.

- When t_2 is small or very close to the final time, t_3, the total cost of the TCMs increases, as it should be expected.

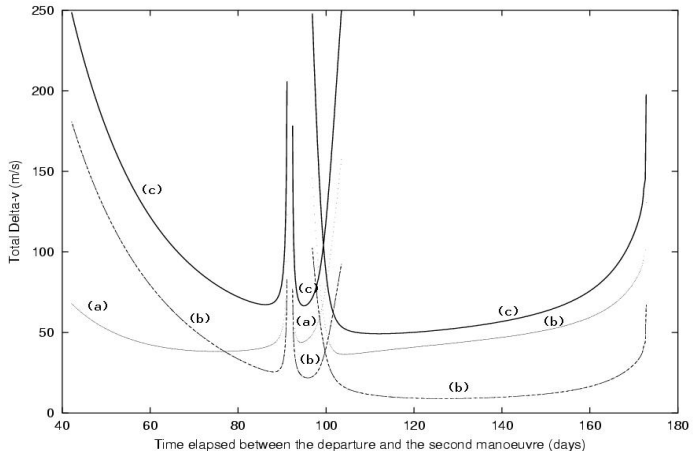

Figure 3.15: Cost of the trajectory correction manoeuvres when TCM1 is delayed 4 days after departure and the total time of flight is fixed to 173.25 days. The curves labelled with (a) correspond to $\|\Delta v_1\|$, those with (b) to $\|\Delta v_2\|$ and those with (c) to the total cost: $\|\Delta v_1\| + \|\Delta v_2\|$.

- Around the values $t_2 = 92$, 97 and 102 days, the total cost increases abruptly. This sudden growth is analogous to the one described in [183] in connection with the TCM problem for the Genesis mission. It is also similar to the behaviour found in [179] for the cost of the transfer to a Lissajous orbit around L_2, when the time of flight between the departure and the injection in the stable manifold is fixed. This fact can be explained in terms of the angle between the two velocity vectors at $t = t_2$. This is, when changing from the second to the third leg of the transfer path. This angle also increases sharply at the corresponding epochs.

3.5 Transfers Between Libration Point Orbits

In this section we will describe a method to perform transfers between libration point orbits around the same equilibrium point.

The interest on this problem was initially motivated by the study of the transfer from the vicinity of the Earth to a halo orbit around the equilibrium point L_1 of the Earth-Sun system ([46], [236], [175]). There, it was shown that the invariant stable manifolds of halo orbits can be used efficiently for the transfer from the Earth, if we are able to inject the spacecraft into these manifolds. This can be easily achieved when the orbits of the manifold come close to the Earth. But this is true only when the halo orbit is large enough, or when the effect of the Moon, bending some orbits of the manifold, is big enough to bring these orbits to the vicinity of the Earth. For small halo orbits, if a swingby with the Moon is used, there are launch possibilities only during two or three days per month (see [157], [236], [163], [175]). These launching possibilities can be longer for halo orbits with larger z-amplitude. This is because they have a stable manifold coming closer to the Earth. After the transfer from the Earth to a large halo orbit has been done, we must be able to go from it to a smaller one in a not very expensive way, in terms of the Δv consumption and time. Although this rule also applies for the transfer to Lissajous orbits, the study of the transfer

between Lissajous orbits was first motivated by the missions HERSCHEL, Plank and GAIA of the European Space Agency Scientific Program (see section 2). HERSCHEL is the cornerstone project in the ESA Science Program dedicated to far infrared Astronomy. Planck, renamed from COBRAS/SAMBA, is expected to map the microwave background over the whole sky and is now combined with HERSCHEL for a common launch in 2007. Several options were considered during the orbit analysis work. The one finally adopted was the so-called "Carrier", where both spacecraft are launched by the same Ariane 5, but will separate after launch. For this option, the optimum solution is a free transfer to a large amplitude Lissajous orbit. HERSCHEL will remain in this orbit whereas Planck, of much less mass, will perform a size reduction manoeuvres.

In what follows we will consider the problem of the transfer between halo type orbits and between Lissajous orbits, always around the same libration point.

3.5.1 Transfers Between Halo Orbits

The method that we present is based on the local study of the motion around the halo orbits and uses the geometry of the problem in the neighbourhood of an orbit of this kind (see [175], [164]). The approach is different from the procedure developed by Hiday and Howell (see [170], [171]) for the same problem. In the Hiday & Howell approach, a departure and arrival states on two arbitrary halo orbits are selected, and a portion of a Lissajous orbit is taken as a path connecting these states. At the patch points there are discontinuities in the velocity which must be minimised. The primer vector theory (developed by Lawden [202] for the two body problem) is extended to the RTBP and applied to establish the optimal transfers.

In a first step of our approach we study the transfer between two halo orbits which are assumed to be very close in the family of halo orbits. With this hypothesis, the linear approximation of the flow in the neighbourhood of the halo orbits, given by the variational equations, is good enough to have a better understanding of the transfer.

Assume that at a given epoch, t_1, we are on a halo orbit, H_1, and that at this point a manoeuvre, $\Delta v^{(1)}$, is performed to go away from the actual orbit. At $t = t_2 > t_1$, a second manoeuvre, $\Delta v^{(2)}$, is executed in order to get into the stable manifold of a nearby halo orbit H_2. Denoting by $\Delta\beta$ the difference between the z-amplitudes of these two orbits, the purpose of an optimal transfer is to perform both manoeuvres in such a way that the performance function

$$\frac{\Delta\beta}{\|\Delta v^{(1)}\|_2 + \|\Delta v^{(2)}\|_2},$$

is maximum.

Let φ be, as usual, the flow associated to the differential equations of the RTBP and $\varphi_\tau(y)$ the image of a point $y \in \mathbb{R}^6$ at $t = \tau$, so we can write

$$\varphi_\tau(y+h) = \varphi_\tau(y) + D\varphi_\tau(y)H + O(\mid h \mid^2) = \varphi_\tau(y) + A(\tau)h + O(\mid h \mid^2).$$

Let $\beta(0)$ be the initial point on a halo orbit, H_1, with z-amplitude β. The corresponding points in the phase space at $t = t_1, t_2$, and assuming that the time required to execute the manoeuvre can be neglected, will be, respectively,

$$\varphi_{t_1}(\beta(0)) + \begin{pmatrix} 0 \\ \Delta v^{(1)} \end{pmatrix}, \quad \text{and} \quad \varphi_{t_2}(\beta(0)) + A(t_2)A(t_1)^{-1} \begin{pmatrix} 0 \\ \Delta v^{(1)} \end{pmatrix}.$$

At $t = t_2$, the insertion manoeuvre, $\Delta v^{(2)}$, into the stable manifold of the halo orbit of z-amplitude $\beta + \Delta\beta$ is done. So, denoting by $A_{t_1,t_2} = A(t_2)A(t_1)^{-1}$, we must have

$$\varphi_{t_2}(\beta(0)) + A_{t_1,t_2}\begin{pmatrix} 0 \\ \Delta v^{(1)} \end{pmatrix} + \begin{pmatrix} 0 \\ \Delta v^{(2)} \end{pmatrix} = \varphi_{t_2}(\beta(0) + \Delta\beta) + \gamma_2 e_{2,\beta+\Delta\beta}(t_2) + \gamma_3 e_{3,\beta+\Delta\beta}(t_2),$$

where $e_{2,\beta+\Delta\beta}(t_2)$ and $e_{3,\beta+\Delta\beta}(t_2)$ are the eigenvectors related to the stable direction and to the tangent to the orbit direction, respectively, of the orbit of amplitude $\beta + \Delta\beta$ at $t = t_2$. The first term in the right hand side of the above equation can be written as

$$\varphi_{t_2}(\beta(0) + \Delta\beta) = \varphi_{t_2}(\beta(0)) + \frac{\partial\varphi_{t_2}(\beta(0))}{\partial\beta}\Delta\beta + O((\Delta\beta)^2).$$

We normalise taking $\Delta\beta = 1$, so the equation to be solved is

$$A_{t_1,t_2}\begin{pmatrix} 0 \\ \Delta v^{(1)} \end{pmatrix} + \begin{pmatrix} 0 \\ \Delta v^{(2)} \end{pmatrix} = \frac{\partial\phi_{t_2}(\beta(0))}{\partial\beta} + \gamma_2 e_{2,\beta}(t_2) + \gamma_3 e_{3,\beta}(t_2),$$

from which we can isolate $\Delta v^{(1)}$, $\Delta v^{(2)}$, getting

$$\Delta v^{(1)} = u_{10} + \gamma_2 u_{12} + \gamma_3 u_{13},$$

$$\Delta v^{(2)} = u_{20} + \gamma_2 u_{22} + \gamma_3 u_{23}.$$

All the magnitudes that appear in these two equations, except the scalars γ_2 and γ_3, are three-dimensional vectors. As $\Delta\beta = 1$ has been fixed, the maxima of the performance function corresponds to the minima of $\|\Delta v^{(1)}\|_2 + \|\Delta v^{(2)}\|_2$. Computing the derivatives of this function with respect to γ_2 and γ_3 and equating them to zero, we get a system of two polynomial equations of degree four in the two variables γ_2 and γ_3, that must be solved for each couple of values t_1, t_2 (which are the only free parameters).

The results of the numerical computations show that for a fixed value of t_1, there are, usually, two values of t_2 at which the performance function has a local maximum (for values of t_1 close to 90º and 240º there are three and four maxima). The difference between these two values of t_2 is almost constant and equal to 180º. That is, after the first manoeuvre has been done, the two optimal possibilities appear separated by a difference of 1/2 of revolution.

The cost of the transfer using the optimal t_2 is almost constant and the variation around the mean value does not exceed the 4%. As an example, if the z-amplitude of the departure orbit is β =0.1, the optimum value is reached using the first maximum for $t_1 = 102^o$ and $t_2 = 197^o$. For these particular values, the cost of the transfer, per unit of $\Delta\beta$, is of 696 m/s. The cost increases with β: for β =0.15, the optimal value is Δv = 742 m/s ($t_1 = 102^o$, $t_2 = 193^o$) and for β =0.2 Δv = 785 m/s ($t_1 = 101^o$, $t_2 = 187^o$). It has been found that the variation with respect to β of the optimal value of the cost is almost linear. The value of t_1 for the first manoeuvre is almost constant and equal to 100º, the corresponding point in the physical space being always very close to the $z = 0$ plane. For very small values of β, the second manoeuvre must be done after $t_2 = 270^o$, but this value decreases quickly and for $\beta \in (0.1, 0.3)$ it is of the order of $t_2 = 190^o$, approximately. That is, one has to wait, typically, 1/4 of revolution after the first manoeuvre, to do the second one.

The transfer computed with the above procedure is not optimal if the initial and final orbits are not close to eachother. This is because the solution given by the linear analysis is not good enough when the orbits have very different z-amplitudes. Several possibilities are discussed in [164]. As a final conclusion we can say that the cost of a unitary transfer is of 756 m/s and the behaviour with the z–amplitude β is almost linear. In this way, the cost of the transfer between two halo orbits of amplitudes β =0.25 and 0.08 is $(0.25-0.08)\times$ 756 m/s = 128.5 m/s. In Figure 3.16 we show the three projections of a transfer trajectory that goes form $\beta = 0.25$ to $\beta = 0.08$

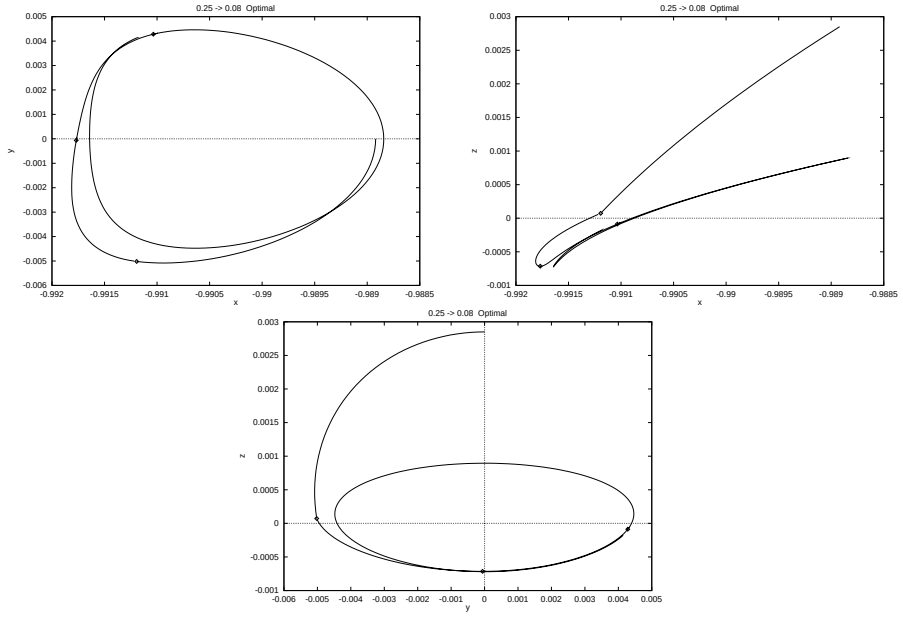

Figure 3.16: Projections of the transfer trajectory starting at a departure orbit of z-amplitude $\beta = 0.25$ and arriving at a final one with z-amplitude $\beta = 0.08$. The dotted points correspond to the epochs at which the manoeuvres have been done.

3.5.2 Transfers Between Lissajous Orbits

The method of this section is based in the dynamical study of the linearised RTBP equations of motion about a collinear equilibrium point. The development was initiated during preliminary studies of the HERSCHEL/Plank mission (see [111]) and is fully developed in [12] and [154].

Let us start with the solution of the linear part of the equations of motion (3.7) which can be written as,

$$\left.\begin{aligned} x(t) &= A_1 e^{\lambda t} + A_2 e^{-\lambda t} + A_3 \cos\omega t + A_4 \sin\omega t \\ y(t) &= cA_1 e^{\lambda t} - cA_2 e^{-\lambda t} - \bar{k}A_4 \cos\omega t + \bar{k}A_3 \sin\omega t \\ z(t) &= A_5 \cos\nu t + A_6 \sin\nu t \end{aligned}\right\} \tag{3.13}$$

where A_i are arbitrary constants and c, $\bar{k}$, ω, λ and ν are constants depending only on c_2.

Introducing amplitudes and phases (3.13) can also be written as

$$\left.\begin{array}{l} x(t) = A_1 e^{\lambda t} + A_2 e^{-\lambda t} + A_x \cos(\omega t + \phi) \\ y(t) = cA_1 e^{\lambda t} - cA_2 e^{-\lambda t} + \bar{k} A_x \sin(\omega t + \phi) \\ z(t) = A_z \cos(\nu t + \psi) \end{array}\right\} \tag{3.14}$$

where the relations are $A_3 = A_x \cos\phi$, $A_4 = -A_x \sin\phi$, $A_5 = A_z \cos\psi$ and $A_6 = -A_z \sin\psi$.

The key point is that choosing, $A_1 = A_2 = 0$, we obtain periodic motions in the xy components with a periodic motion in the z component of a different period. These are the Lissajous orbits in the linearised restricted circular three-body problem, A_x, A_z being the maximum in plane and out of plane amplitudes respectively. The first integrals A_1 and A_2 are directly related to the unstable and stable manifold of the linear Lissajous orbit. For instance, the relation $A_1 = 0, A_2 \neq 0$, defines a stable manifold . Any orbit verifying this condition will tend forward in time to the Lissajous (or periodic) orbit defined by A_x, A_z since the A_2-component in (3.13) will die out. A similar fact happens when $A_1 \neq 0, A_2 = 0$, but now backwards in time. Then, this later condition defines a unstable manifold.

The analysis consits of computing the manoeuvres that keep the A_1 component equal to zero in order to prevent escape from the libration zone, and studiing how the amplitudes change when a manoeuvre is applied. We note that for the linear problem the motion in the z-component is uncoupled from the motion in the xy component and z-manoeuvres only change the A_z amplitude but do not introduce instability. Assuming that the motion takes place in a Lissajous orbit with $A_z^{(i)}$ amplitude and phase ψ_i and the desired final z-amplitude is $A_z^{(f)}$. The possible z-manoeuvres $\Delta\dot{z}$ which performs the transfer at time t_m are given by,

$$\frac{\Delta\dot{z}}{\nu} = A_z^{(i)} \sin(\nu t_m + \psi_i) \pm \sqrt{{A_z^{(f)}}^2 - {A_z^{(i)}}^2 \cos^2(\nu t_m + \psi_i)} \tag{3.15}$$

We note that if,

- $A_z^{(f)} \geq A_z^{(i)}$ the transfer manoeuvre is possible at any time.
- $A_z^{(f)} < A_z^{(i)}$ the transfer manoeuvre is possible only if the expression inside the square root is positive; more precisely, when $t \in \left[\varepsilon, \frac{\pi}{\nu} - \varepsilon\right] \cup \left[\frac{\pi}{\nu} + \varepsilon, \frac{2\pi}{\nu} - \varepsilon\right]$, where $\varepsilon = \frac{1}{\nu}(\arccos(\frac{A_z^{(f)}}{A_z^{(i)}}) - \psi_i)$. This condition essentially says that it is not possible to reduce the amplitude with an impulsive manoeuvre in case that the actual position at time t_m has a z component bigger than $A_z^{(f)}$.

The change in the in-plane amplitude is a little more tricky since one must keep the unstable component equal to zero. Assuming that the motion takes place in a Lissajous orbit with $A_x^{(i)}$ amplitude and phase ϕ_i and the desired final in-plane amplitude is $A_x^{(f)}$, the possible manoeuvres at time t_m are given by,

$$(\Delta\dot{x}, \Delta\dot{y}) = \alpha \frac{1}{\sqrt{c^2 + \bar{k}^2}} (d_2, -\bar{k} d_1), \quad \alpha \in \mathbb{R} \tag{3.16}$$

where, α, indicating the size of the manoeuvre can be,

$$\alpha = A_x^{(i)} \sin(\omega t_m + \phi_i - \beta) \pm \sqrt{{A_x^{(f)}}^2 - {A_x^{(i)}}^2 \cos^2(\omega t_m + \phi_i - \beta)}.$$

Where β is a fixed angle given by the direction of the vector $(c, \bar{k})$. Again we observe that if,

- $A_x^{(f)} \geq A_x^{(i)}$, the transfer manoeuvre is possible at any time.
- $A_x^{(f)} < A_x^{(i)}$, the transfer manoeuvre is possible only when the expression inside the square root is positive; more precisely, when $t \in \left[\delta, \frac{\pi}{\omega} - \delta\right] \cup \left[\frac{\pi}{\omega} + \delta, \frac{2\pi}{\omega} - \delta\right]$, where $\delta = \frac{1}{\omega}(\arccos(\frac{A_x^{(f)}}{A_x^{(i)}}) - \phi_i + \beta)$.

We also note that the manoeuvre (3.16) always ahs the same direction. This direction plays a similar role to the direction orthogonal to the z-plane in the case of the previous commented z-manoeuvres.

Once the target amplitudes are selected, the epochs of the manoeuvres essentially can be chosen according to the following possibilities,

- Select t_m in such a way that the Δv expended in changing the amplitude be a minimum.
- Select t_m in such a way that you arrive at the target orbit with a selected phase.

Assuming that the amplitudes prior and after the manoeuvres are different, in the first case the optimal t_m for changing the in-plane amplitude is when the angle $\omega t_m + \phi_i$ verifies $\omega t_m + \phi_i = \beta + \frac{\pi}{2} + k\pi$, $k \in \mathbb{Z}$. In this case the minimum fuel expenditure for the manoeuvre is $|A_x^{(f)} - A_x^{(i)}|$. In a similar way the optimal t_m for a change in the out of plane amplitude is when $\nu t_m + \psi_i$ verifies $\nu t_m + \psi_i = \frac{\pi}{2} + k\pi$, $k \in \mathbb{Z}$ and the manoeuvre is given by $\Delta \dot{z} = \nu(A_z^{(f)} - A_z^{(i)})$.

In case that we decide to arrive at the selected Lissajous orbit with a certain phase the analysis proceeds considering the in-plane and out-of-plane amplitudes A_x and A_z written in term of its respective components A_3, A_4 and A_5, A_6 and studying the angle which they define. A particular interesting case are the manoeuvres which maintain the amplitudes (the non trivial possibilities of (3.15) and (3.16)). In this case an in-plane manoeuvre (3.16) at time t_m produces an in-plane change of phase given by,

$$\phi_f - \phi_i = -2(\omega t_m - \beta + \phi_i) \qquad (\text{mod } 2\pi), \tag{3.17}$$

and an out-of-plane manoeuvre (3.15) produces an out-of-plane change of phase given by,

$$\psi_f - \psi_i = -2(\nu t_m + \psi_i) \qquad (\text{mod } 2\pi). \tag{3.18}$$

These manoeuvres give two strategies for the avoidance of the exclusion zone needed in many missions (see, for instance, [80]), besides the well known z-strategy given by (3.18), we have another xy one given by (3.17) which for the HERSCHEL/Plank mission implies only a delta-v expenditure of 15 m/s every six years (see [111] and [154]).

3.6 Homoclinic and Heteroclinic Connections

In the preceding sections we have shown how to use the local dynamics around a halo orbit for "local" purposes. In this one we will study the global behaviour of the invariant stable/unstable manifolds, of the central manifolds of L_1 and L_2, to perform some acrobatic motions connecting libration orbits around those equilibrium points.

In order to obtain heteroclinic trajectories between libration orbits around L_1 and L_2, we have to match an orbit of the unstable manifold of a libration orbit around one point, with another orbit, in the stable manifold of a libration orbit around the other point. This is, both orbits have to be the same one. Since these orbits, when looked in the X coordinate of the RTBP system, have to go from one side of the Earth to the other one, the place where we look for the connection is the plane $X = \mu - 1$, this is, the plane orthogonal to the X axis that cuts it at the point where the centre of the Earth is located.

Although the technical details are much more complex, the main idea is similar to the computations introduced in [193] for $L_{4,5}$ connections. Once a Jacobi constant is fixed, we take initial conditions in the linear approximation of the unstable manifold of all the libration orbits inside the level of energy. Since the energy is fixed, we have three free variables (usually q_1, q_2 and p_2). A scanning procedure in these variables is done. Since the selected orbits will leave the neighbourhood of the libration point, each initial condition in the variables (q, p) is changed into RTBP coordinates and then propagated forward in time until it crosses the plane $X = \mu - 1$. We apply the same procesure to the orbits in the stable manifold, where all the propagation is done backward in time.

We have to remark that as usual, the unstable and stable manifolds have two branches. In the process we select only the branches that, at the initial steps of the propagations approach the $X = \mu - 1$ plane.

Since the Jacobi constant is fixed, the set of all RTBP values $\mathcal{C} = \{(Y, \dot{Y}, Z, \dot{Z})\}$ obtained, characterise the branch of the manifold of all the libration orbits around the selected equilibrium point for the particular section. Let us denote these sets by $\mathcal{C}_i^{+sj}$, where $+$ or $-$ denote the branch of the s (stable) or u (unstable) manifold of the L_j, $j = 1, 2$ libration orbits at the i-th intersection with the $X = \mu - 1$ plane.

Looking at the above mentioned branches of the manifolds, the simplest heteroclinic orbits will be obtained from $\mathcal{I}_{1^-} = \mathcal{C}_1^{-s1} \cap \mathcal{C}_1^{-u2}$ and $\mathcal{I}_{1^+} = \mathcal{C}_1^{-u1} \cap \mathcal{C}_1^{-s2}$. Both sets give transfer orbits that cross the plane $X = \mu - 1$ once. We will denote by $\mathcal{I}_{k^-}$ (respectively $\mathcal{I}_{k^+}$) the set of heteroclinic trajectories from L_2 to L_1 (resp. from L_1 to L_2) that cross the plane $X = \mu - 1$ k times, following the above mentioned branches of the manifold. We note that, due to the symmetries of the RTBP equations, for any heteroclinic orbit from L_1 to L_2 we have a symmetrical one from L_2 to L_1 and so just one exploration must be done.

Unhopefully, it has been found (see [123]) that $\mathcal{I}_{1^+}$ is empty and so one must look for connections crossing at least twice the plane $X = \mu - 1$. In this case many possibilities of connections appear. As an example, in Figure 3.17 a connection between a Lissajous orbits around L_2 and quasi-halo orbit around L_2 is displayed. Both the 3-D representation of the homoclinic orbits and the intersections with the surface of section $Z = 0$, around both equilibrium points, are given.

As another kind of connection, the homoclinic transition inside the central manifold, that differences the central Lissajous orbits from the quasi-halo ones, is computed in [123]. These kind of solutions are interesting because they perform a transition from a planar motion (close to a Lyapunov orbit) to an inclined orbit (close to the quasi-halo orbits) without any Δv. Figure 3.18 shows one of these orbits in central manifold (q, p) variables. Unfortunately, the transition is very slow but probably, with very small Δv, it could be possible to accelerate the transition from planar to inclined motion.

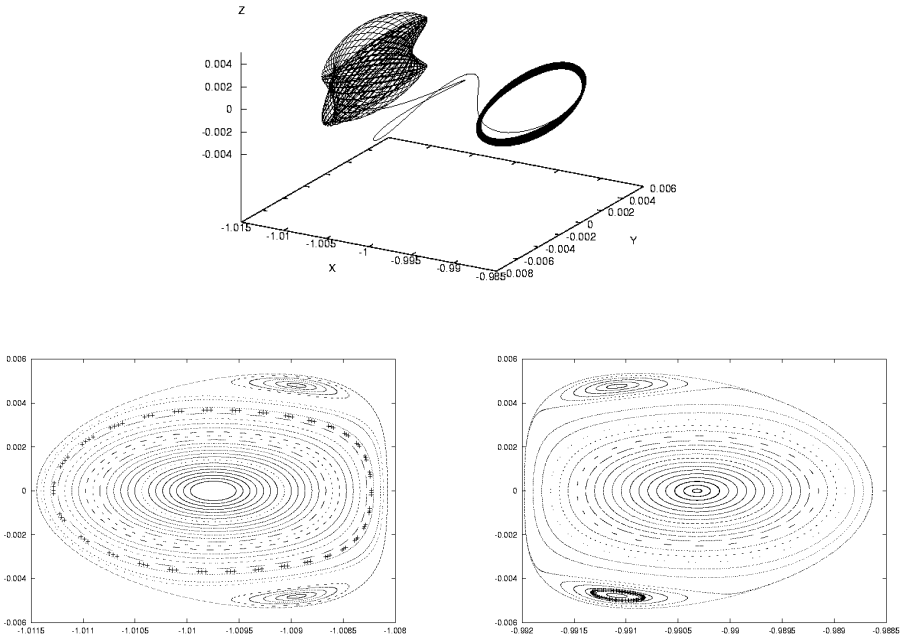

Figure 3.17: L_1-L_2 heteroclinic connection between a Lissajous orbit around L_2 and a quasi-halo orbit around L_1. In the lower pictures the intersections of the orbits with the surface of section ($Z = 0$) for L_2 (left) and for L_1 (right) are displayed with crosses.

3.7 Weak Stability Boundaries and Low Energy Transfers

According to Simó [210]: "It seams feasible to produce accurate and enough complete descriptions of the dynamics on the centre manifolds of the collinear libration points as well as large parts of the corresponding stable and unstable manifolds. Having these concepts in hand, the design of space missions *à la carte*, involving the vicinities of these points, could be done in an automatic way". Although not all the theoretical and practical questions underlying the above idea and required for its implementation have been solved, some progress has been done and will be summarised in this section.

The invariant manifold structures associated to the collinear libration points, provide not only the framework for the computation of complex spacecraft mission trajectories, but also can be used to understand the geometrical mechanisms of the material transport in the solar system. This approach has been used recently for the design of low energy transfers from the Earth to the Moon [159] and for a "Petit Grand Tour" of the Moons of Jupiter [20], [148]. It has also been used to explain the behaviour of some captured Jupiter comets, see [186], [187].

The weak stability boundary, although it is not a clearly defined concept, provides also some kind of low energy transfers, as will be explained in what follows.

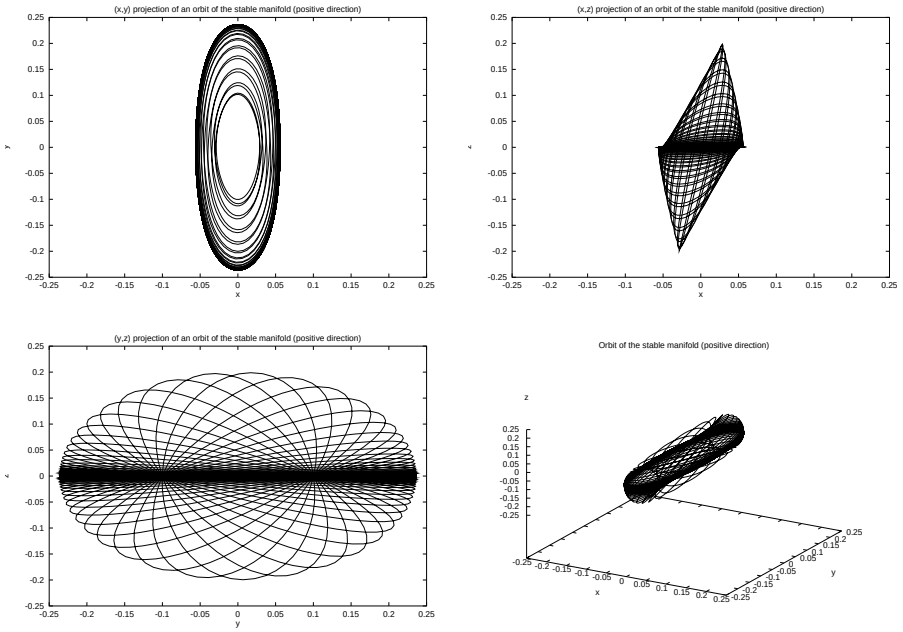

Figure 3.18: Homoclinic transition between Lyapunov orbits inside the central manifold (in central manifold coordinates).

3.7.1 The Weak Stability Boundary

The weak stability boundary (WSB) is a concept mainly developed after [61] and the rescue of the Hiten spacecraft [62]. The transfer trajectory of this spacecraft from the Earth to the Moon first visited a neighbourhood of the collinear libration point L_1 of the Earth-Sun system. Afterwards, it went to the vicinity of the L_2 point of the Earth-Moon system and finally reached the Moon. This kind of transfer trajectories require a large transfer time (between 60 to 100 days) but a small Δv (they can save up to 150 m/s with respect to a Hohmann transfer) since they eliminate the hyperbolic excess velocity at lunar periapsis upon arrival and use the dynamics of the problem in a more natural. For this reason, they are also called low energy transfers.

The WSB (also named fuzzy boundary) has not got a precise definition (at least in the mathematical sense of the word). Some definitions that can be found in the literature are: "a generalisation of the Lagrange points and a complicated region surrounding the Moon", "a region in phase space supporting a special type of chaotic motion for special choices of elliptic initial conditions with respect m_2",.... According to Belbruno [68], the WSB can also be defined algorithmically in the following way:

In the framework of the RTBP, consider a radial segment, l, departing from the small primary m_2. Take trajectories for the infinitesimal body, m, starting on l which satisfy

1. The particle m starts its motion at the periapsis of the oscullating ellipse.
2. The initial velocity vector of the trajectory is perpendicular to the line l.
3. The initial two-body Kepler energy of m with respect to m_2 is negative.

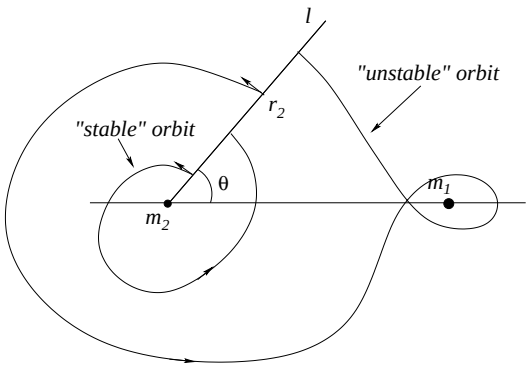

Figure 3.19: Qualitative representation of stable and unstable orbits about m_2.

4. The eccentricity of the initial two-body Keplerian motion is held fixed along l.

According to [67], the motion of a particle with the above initial conditions is *stable* about m_2 if: after leaving l it makes a full cycle about m_2 without going around m_1 and returns to l at a point with negative Kepler energy with respect to m_2. Of course, the motion will be *unstable* if the above condition is not fulfilled.

Belbruno claims (without giving any proof or numerical evidence) that as the initial conditions vary along l, there is a finite distance $r^*(\theta, e)$, depending on the polar angle θ (which l makes with the x-axis) and the eccentricity e of the initial oscullating ellipse, such that

- If $r_2 < r^*$, the motion is stable.
- If $r_2 > r^*$, the motion is unstable.

Furthermore, $r^*(\theta, e)$ is a smooth function of θ and e which defines the WSB

$$\mathcal{W} = \{r^*(\theta, e) \mid \theta \in [0, 2\pi], e \in [0, 1]\}$$

The above definition has several weak points:

1. The requirements 1. and 2. on the initial conditions fix the modulus of the velocity and its direction, but not the sense. So, there are two different orbits with the initial conditions specified in Belbruno's definition, which can have different stability behaviour.

2. It is not true that for fixed values of θ and e there is a finite distance $r^*(\theta, e)$ defining the boundary of the stable and unstable orbits. Figure 3.20 shows this fact clearly. In this Figure we have represented for a fixed value of $e = 0.70$ and for $\theta \in [0, 2\pi]$, the points associated to initial conditions producing an stable orbit, using the two possible senses of the velocity at the perigee. As it has been said, the two plots do not agree since two orbits with the same initial position and opposite velocities may have different stability properties. If we draw any line through the origin (which is the point where we have set m_2), there are several transitions from stability to instability. In fact, for a fixed value of θ, the set of stable points recalls a Cantor set.

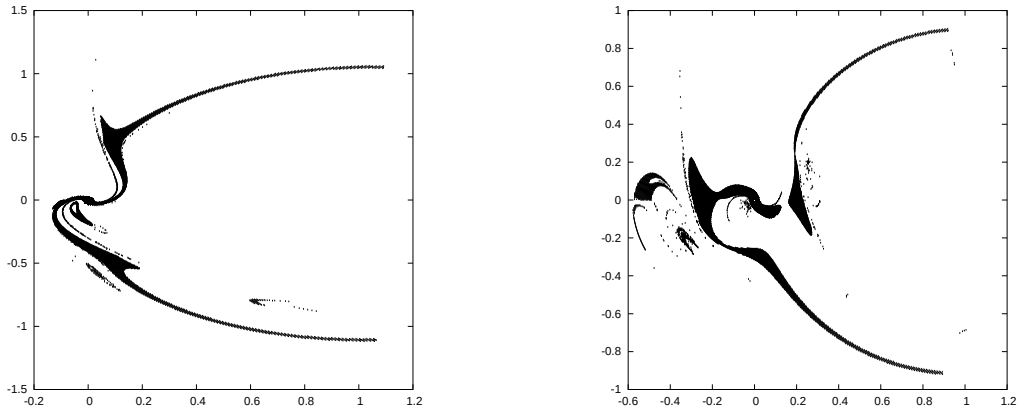

Figure 3.20: Stable initial positions $(x,\ y)$ about m_2 (at the origin) for $\theta \in [0, 2\pi]$ according to Belbruno's definition. $\mu = 0.012$ (Earth-Moon mass ratio) and $e = 0.70$. The two plots correspond to the two possible senses of the velocity at the perigee of the oscullating ellipse.

The suitable setting for the WSB is the restricted four body problem, as follows from the kind of trajectories associated to the low energy transfers and as it is also established in [64]. This paper has an heuristic explanation, using invariant manifolds and Hill's regions, about how a ballistic capture by the Moon can take place but it has not any numerical computation supporting the claims.

3.7.2 Numerical Determination of WSB and Low Energy Transfers

There is only a few number of papers dealing with the numerical computation of WSB, now with a different definition from the algorithmic one given in the preceding section. They are, in fact, procedures to determine transfer trajectories with low Δv requirements of two different kinds:

1. Direct numerical search (see [60], [66], [65] and [69]).

2. Computations using invariant manifolds (see [70]).

The direct numerical search is usually done directly in accurate models of motion. The method developed in [66] is a forward targeting algorithm that uses as initial orbit a Keplerian ellipse with an Earth apoapsis of 1.5 million kilometres. The one developed in [65], [60] and [69] is backward/forward integration with three steps:

1. First a backward integration from the final injection conditions up to the vicinity of the L_1 libration point of the Earth-Sun system (at 1.5 million kilometres from the Earth). This vicinity is what is defined, in an ambiguous way, as the WSB.

2. Second, a forward propagation from the Earth departure to the WSB region. An optimal intermediate lunar gravity assist may be incorporated in this trajectory.

3. A matching of the forward/backward trajectories using a constrained parameter optimisation algorithm.

Using this methodology, a large number of trajectories can be obtained for certain Sun-Earth-Moon configurations, as is shown in the above mentioned papers.

The computations using invariant manifolds, which uses the natural dynamics of the problem, proceeds along the following steps:

1. The first step is to decouple the restricted four body problem (spacecraft-Moon-Earth-Sun) in two coupled three body systems: spacecraft-Moon-Earth and spacecraft-Earth-Sun.

2. Within each three body system they transfer from the vicinity of the Earth into the region where the invariant manifold structure of the Earth-Sun libration points interacts with the invariant manifold structure of the Moon-Earth libration points. The region of intersection is computed using a Poincaré section (along a line of constant x-position passing through the Earth) which helps to glue the Sun-Earth Lagrange point portion of the trajectory with the lunar ballistic capture portion.

3. The Earth to Moon trajectory is integrated in the bi-circular four body model where both the Moon and the Earth are assumed to move in circular orbits about the Earth and the Sun respectively. Finally, the bicircular solution is differentially corrected to a fully integrated trajectory with the JPL ephemerides.

The second item of this procedure must be done as follows: first a suitable Sun–Earth L_2 periodic orbit is computed as well as their stable and unstable manifolds. Some orbits on the stable manifold come close to the Earth and, at the same time, points close to the unstable manifold propagated backwards in time come close to the stable manifold. So, with an small Δv, is possible to go from the Earth to the unstable manifold of this periodic orbit. At the same time, when we consider the L_2 point of the Earth–Moon system, is has periodic orbits whose stable manifold "intersect" the unstable manifold that we have reached departing from the Earth and are temporary captured by the Moon. With a second small Δv we can force the intersection to behave as a true one.

This second procedure, which is also known as the Shoot the Moon method, gives the good approach for the computation, in a systematic way, of all the possible low energy transfer orbits. The term "low energy" applied to these trajectories is due to the small manoeuvres that must be done.

Using the same ideas of the Shoot the Moon procedure, the "Petit Grand Tour" of the moons of Jupiter can be designed. In a first step, the Jovian–moons n-body system is decoupled into several three–body systems. The tour starts close to the L_2 point of an outer moon (for instance Ganymede). Thanks to an heteroclinic connection between periodic orbits around L_1 and L_2, we can go from the vicinity of L_2 to the vicinity of L_1 and, in between, perform one o several loops around Ganymede. Now, we can look for "intersections" between the unstable manifold of the periodic orbit around the L_1 point and the stable manifold of some p.o. around the L_2 point of some inner moon (for instance Europa). By the same considerations, we can turn around Europa and leave its influence through the L_1 point. Once the orbits have been obtained, they are refined to a more realistic model easily.

3.7.3 Solar System Low Energy Transfers and Astronomical Applications

As Lo and Ross [188] suggested, the exploration of the phase space structure as revealed by the homoclinic/heteroclinic structures and their association with mean motion resonances, may provide deeper conceptual insight into the evolution and structure of the asteroid belt (interior to Jupiter) and the Kuiper belt (exterior to Neptune), plus the transport between these two belts and the terrestrial planet region.

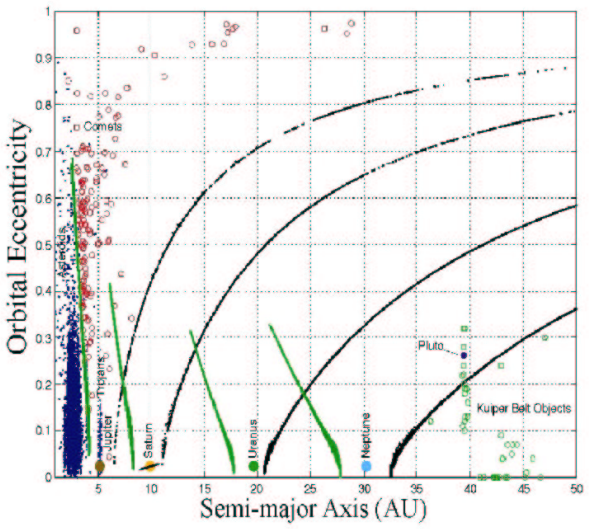

Figure 3.21: Dynamical channels in the solar system. Local semi-major axis versus orbital eccentricity. The L_1 (grey) and L_2 (black) manifolds for each of the giant outer planets is displayed. Notice the intersections between manifolds of adjacent planets, which leads to chaotic transport. Also shown are the asteroids (dots), comets (circles) and Kuiper Belt objects (lighter circles). (see [188]).

Potential Earth–impacting asteroids may use the dynamical channels as a pathway to Earth from nearby heliocentric orbits in resonance with the Earth. This phenomena has been observed recently in the impact of comet Shoemaker–Levy 9 with Jupiter, which was in 2:3 resonance with Jupiter just before impact. Also, the behaviour of comet Oterma that switches from a complicated trajectory outside the orbit of Jupiter to one lying within, can be explained with this kind of ideas. To make the transition, the comet passed through a bottleneck near two of Jupiter's libration points–where objects maintain a fixed distance relative to the planet and the Sun.

Numerical simulations of the orbital evolution of asteroidal dust particles show that the earth is embedded in a circumsolar ring of asteroidal dust known as the zodiacal dust cloud. Both simulations and observations reveal that the zodiacal dust cloud has structure. When viewed in the Sun–Earth rotating frame, there are several high density clumps which are mostly evenly distributed throughout the Earth's orbit. The dust particles are believed to spiral towards the Sun from the asteroid belt, becoming trapped temporarily in exterior mean motion resonances with the Earth. it is suspected that the gross morphology of the ring is given by a simpler RTBP

model involving the homoclinic and heteroclinic structures associated with the libration points.

A complete exploration of all the possible connections between the manifolds related to the libration points of the Solar System bodies should be of interest, not only for spacecraft mission design, but also to understand better the dynamics of the solar system.

3.8 Station Keeping

3.8.1 The Target Mode Approach and the Floquet Mode Approach

The problem of controlling a spacecraft moving near an inherently unstable libration point orbit is of current interest. In the late 1960's, Farquhar [113] suggested several station–keeping strategies for nearly–periodic solutions near the collinear points. Later, in 1974, a station–keeping method for spacecraft moving on halo orbits in the vicinity of the Earth–Moon translunar libration point (L_2) was, published by Breakwell, Kamel, and Ratner [72]. These studies assumed that the control could be modelled as continuous. In contrast, specific mission requirements influenced the station–keeping strategy for the first libration point mission. Launched in 1978, the International Sun–Earth Explorer–3 (ISEE–3) spacecraft remained in a near–halo orbit associated with the interior libration point (L_1,) of the Sun–Earth/Moon barycentre system for approximately three and one half years [145]. Impulsive manoeuvres at discrete time intervals (up to 90 days) were successfully implemented as a means of trajectory control. Since that time, more detailed investigations have resulted in various station–keeping strategies, including the two identified here as the Target Point and Floquet Mode approaches.

The Target Point method (as presented by Howell and Pernicka [92], Howell and Gordon [90], and Keeter [94], which is based in Breackwell's ideas) computes correction manoeuvres by minimising a weighted cost function. The cost function is defined in terms of a corrective manoeuvre as well as position and velocity deviations from a nominal orbit at a number of specified future times t_i. The non–final state vectors at each time t_i are denoted as "target points." The target points are selected along the trajectory at discrete time intervals that are downstream of the manoeuvre. In contrast, the Floquet Mode approach, as developed by Simó et al. [107], [108], incorporates invariant manifold theory and Floquet modes to compute the manoeuvres. Floquet modes associated with the monodromy matrix are used to determine the unstable component corresponding to the local error vector. The manoeuvre is then computed in such a way that the dominant unstable component of the error is erradicated. It is noted that both approaches have been demonstrated in a complex model such as the Earth–Moon system.

Target Point Approach

The goal of the Target Point station–keeping algorithm is to compute and implement manoeuvres to maintain a spacecraft "close" to the nominal orbit, i.e., within a region that is locally approximated in terms of some specified radius centred about the reference path. To accomplish this task, a control procedure is derived from minimisation of a cost function. The cost function, J, is defined by weighting both the control energy required to implement a station–keeping manoeuvre, Δv, and a series of predicted deviations of the six–dimensional state from the nominal orbit at specified future times. The cost function includes several sub-matrices from the state

transition matrix. For notational ease, the state transition matrix is partitioned into four 3×3 sub-matrices as

$$\Phi(t_k, t_0) = \begin{bmatrix} A_{k0} & B_{k0} \\ C_{k0} & D_{k0} \end{bmatrix}. \tag{3.19}$$

The controller, in this formulation, computes a Δv in order to change the deviation of the spacecraft from the nominal path at some set of future times. The cost function to be minimised is written in general as

$$J = \Delta v^T Q \Delta v + p_1^T R p_1 + v_1^T R_\nu v_1 + p_2^T S p_2 + v_2^T S_\nu v_2 + p_3^T T p_3 + v_3^T T_\nu v_3, \tag{3.20}$$

where superscript T denotes transpose. The variables in the cost function include the corrective manoeuvre, Δv at some time t_c, and p_1, p_2 and p_3 that are defined as 3×1 column vectors representing linear approximations of the expected deviations of the actual spacecraft trajectory from the nominal path (if no corrective action is taken) at specified future times t_1, t_2 and t_3, respectively. Likewise, the 3×1 vectors v_1, v_2 and v_3 represent deviations of the spacecraft velocity at the corresponding t_i. The future times at which predictions of the position and velocity state of the vehicle are compared to the nominal path are denoted as target points. They are represented as Δt_i such that $t_i = t_0 + \Delta t_i$. The choice of identifying *three* future target points is arbitrary.

In equation. (3.20), Q, R, S, T, R_ν, S_ν, and T_ν, are 3×3 weighting matrices. The weighting matrix Q is symmetric positive definite; the other weighting matrices are positive semi–definite. The weighting matrices are generally treated as constants that must be specified as inputs. Selection of the appropriate weighting matrix elements is a trial and error process that has proven to be time–consuming. A methodology has been developed that automatically selects and updates the weighting matrices for each manoeuvre. This "time-varying" weighting matrix algorithm is based solely on empirical observations.

Determination of the Δv corresponding to the relative minimum of this cost function allows a linear equation for the optimal control input, i.e.,

$$\begin{aligned} \Delta v^* \;=\; & -\left[Q + B_{10}^T R B_{10} + B_{20}^T S B_{20} + B_{30}^T T B_{30} + D_{10}^T R_\nu D_{10} + D_{20}^T S_\nu D_{20} + D_{30}^T T_\nu D_{30}\right]^{-1} \\ & \times \left[\left(B_{10}^T R B_{10} + B_{20}^T S B_{20} + B_{30}^T T B_{30} + D_{10}^T R_\nu D_{10} + D_{20}^T S_\nu D_{20} + D_{30}^T T_\nu D_{30}\right) v_0 \right. \\ & \left. + \left(B_{10}^T R A_{10} + B_{20}^T S A_{20} + B_{30}^T T A_{30} + D_{10}^T R_\nu C_{10} + D_{20}^T S_\nu C_{20} + D_{30}^T T_\nu C_{30}\right) p_0\right], \end{aligned} \tag{3.21}$$

where v_0, is the residual velocity (3×1 vector) and p_0 is the residual position (3×1 vector) relative to the nominal path at the time t_0. The performance of the modified Target Point algorithm is not yet truly "optimal," though it has been proved to successfully control the spacecraft at reasonable costs. This accomplishment alone provides the user with a quick and efficient way to obtain reasonable station–keeping results. Given some procedure to select the weighting matrices, the manoeuvre is computed from equation. (3.21). The corrective manoeuvre (Δv^*) is a function of spacecraft drift (in both position and velocity with respect to the nominal orbit), the state transition matrix elements associated with the nominal orbit, and the weighting matrices. It is assumed here that there is no delay in implementation of the manoeuvre; the corrective manoeuvre occurs at the time t_0, defined as the current time. Note that this general method could certainly accommodate inclusion of additional target points. Although the nominal orbit that is under consideration here is quasi-periodic, the methodology does not rely on periodicity; it should be applicable to any type of motion in this regime.

In this application, three additional constraints are specified in the station–keeping procedure to restrict manoeuvre implementation. First, the time elapsed between successive manoeuvres must be greater than or equal to a specified minimum time interval, t_{min}. This constraint may be regulated by the orbit determination process, scientific payload requirements, and/or mission operations. Time intervals of one to three days are considered in the Earth-Moon system. The second constraint is a scalar distance (p_{min}) and specifies a minimum deviation from the nominal path (an isochronous correspondence) that must be exceeded prior to manoeuvre execution. For distances less than p_{min} manoeuvre computations do not occur. Third, in the station–keeping simulation, the magnitude of position deviations are compared between successive tracking intervals. If the magnitude is decreasing, a manoeuvre is not calculated. For a corrective manoeuvre to be computed, all three criteria must be satisfied simultaneously.

After a manoeuvre is calculated by the algorithm, an additional constraint is specified on the minimum allowable manoeuvre magnitude, Δv_{min}. If the magnitude of the calculated — Δv is less than Δv_{min} then the recommended manoeuvre is cancelled. This constraint is useful in avoiding "small" manoeuvres that are approximately the same order of magnitude as the manoeuvre errors. It also serves to model actual hardware limitations.

Floquet Mode Approach

An alternative strategy for station–keeping is the Floquet Mode approach, a method that is significantly different from the Target Point approach. It can be easily formulated in the circular restricted three–body problem. In this context, the nominal halo orbit is periodic. The variational equations for motion in the vicinity of the nominal trajectory are linear with periodic coefficients. Thus, in general, both qualitative and quantitative information can be obtained about the behaviour of the nonlinear system from the monodromy matrix, M, which is defined as the state transition matrix (STM) after one revolution along the full halo orbit.

The knowledge of the dynamics of the flow around a halo orbit, or any solution close to it, allows possibilities other than the station–keeping procedure described here, such as the computation of transfer orbits both between halo orbits and from the Earth to a halo orbit [163], [164]. The behaviour of the solutions in a neighbourhood of the halo orbits is determined by the eigenvalues, λ_i, $i = 1, ..., 6$ and eigenvectors e_i, $i = 1, ..., 6$ of M. Gathering the eigenvalues by pairs, their geometrical meaning is the following:

a) The first pair (λ_1, λ_2) with $\lambda_1 \cdot \lambda_2 = 1$ and $\lambda_1 \approx 1500$, is associated with the unstable character of the small and medium size halo orbits. The eigenvector, $e_1(t_0)$, associated with the largest eigenvalue, λ_1, defines the most expanding direction, related to the unstable nature of the halo orbit. The image under the variational flow of the initial vector $e_1(t_0)$, together with the vector which is tangent to the orbit, defines the linear approximation of the unstable manifold of the orbit. In a similar way, $e_2(t_0)$ can be used to compute the linear approximation of the stable manifold.

b) The second pair (λ_3, λ_4) = (1, 1) is associated with neutral variables (i.e., unstable modes). However, there is only one eigenvector with eigenvalue equal to one. This vector, $e_3(t_0)$ is the tangent vector to the orbit. The other eigenvalue, $\lambda_4 = 1$, is associated with variations of the energy (or the period) of the orbit through the family of halo orbits. Along the orbit, the vectors e_3 and e_4 span an invariant plane under the flow.

c) The third couple, (λ_5, λ_6), is formed by two complex conjugated eigenvectors of modulus one. The restriction of the flow to the corresponding two–dimensional invariant subspace, is essentially a rotation. This behaviour is related to the existence of quasi-periodic halo orbits around the halo orbit (see [235]).

When considering dynamical models of motion different from the restricted three–body problem, halo orbits are no longer periodic, and the monodromy matrix is not defined. Nevertheless, for quasi-periodic motions close to the halo orbit (and also for the Lissajous orbits around the equilibrium point) the unstable and stable manifolds subsist. The neutral behaviour can be slightly modified including some instability which, from a practical point of view, is negligible when compared with the one associated with λ_1.

Instead of the vectors $e_i(t)$ it is convenient to use the Floquet modes $\overline{e}_i(t)$ which, for the periodic case, are defined as six periodic vectors from which the $e_i(t)$ can be easily recovered (see [109]). For instance $\overline{e}_1(t)$ is defined as $e_1(t) \cdot \exp[-(t/T)\log\lambda_1]$, where T is the period of the halo orbit. The control algorithm is developed to use this information for station–keeping purposes. The emphasis is placed on formulating a controller that will effectively eliminate the unstable component of the error vector, $\delta(t) = (\delta x, \delta y, \delta z, \delta\dot{x}, \delta\dot{y}, \delta\dot{z})$ defined as the difference between the actual coordinates obtained by tracking and the nominal ones computed isochronously on the reference orbit. At any epoch, t, δ can be expressed in terms of the Floquet modes

$$\delta(t) = \sum_{i=1}^{6} \alpha_i \overline{e}_i(t). \tag{3.22}$$

The objective of the controller is to add a manoeuvre such that the magnitude of the component of the error vector in the unstable direction, α_1, is reduced to zero. The five remaining components do not produce large departures from the reference orbit. In contrast, the component of the error vector along the unstable mode increases by a factor of λ_1 in each revolution.

Denoting the impulsive manoeuvre as $\Delta = (0, 0, 0, \Delta_x, \Delta_y, \Delta_z)^T$, cancelling the unitary unstable Floquet mode requires

$$\frac{\overline{e}_1}{\|\overline{e}_1\|} + (0, 0, 0, \Delta_x, \Delta_y, \Delta_z)^T = \sum_{i=2}^{6} c_i \overline{e}_i(t). \tag{3.23}$$

From these equations Δ_x, Δ_y, Δ_z can be obtained as a function of c_5 and c_6. These free parameters are determined by either imposing a constraint on the available directions of the control or minimising a suitable norm of Δ.

For practical implementation it is useful to compute the so–called projection factor along the unstable direction. It is defined as the vector π such that $\delta \cdot \pi = \alpha_1$. Note that for the computation of π only the Floquet modes are required, so it can be computed and stored together with the nominal orbit. To annihilate the unstable projection, α_1, with a manoeuvre, $\Delta v = (0, 0, 0, \Delta_x, \Delta_y, \Delta_z)^T$, we ask $(\delta + \Delta v) \cdot \pi = 0$. In this way,

$$\Delta_x \pi_4 + \Delta_y \pi_5 + \Delta_z \pi_6 + \alpha_1 = 0, \tag{3.24}$$

is obtained, where π_4, π_5 and π_6 are the last three components of π. Choosing a two axis controller, with $\Delta_z = 0$, and minimising the Euclidean norm of Δv, the following expressions for Δ_x and Δ_y are obtained,

$$\Delta_x = -\frac{\alpha_1 \pi_4}{\pi_4^2 + \pi_5^2}, \quad \Delta_y = -\frac{\alpha_1 \pi_5}{\pi_4^2 + \pi_5^2}. \tag{3.25}$$

In a similar way, a one or three axis controller can be formulated.

Once the magnitude of the manoeuvre is known, the determination of the epoch at which it must be applied is an important issue to be addressed. The study of this question requires the introduction of the gain function, $g(t) = \|\Delta\|^{-1}$, where Δ is the unitary impulsive manoeuvre. It measures the efficiency of the control manoeuvre along the orbit to cancel the unitary unstable component. This component is obtained using the projection factors and the error vector. As the projection factor changes along the orbit, the same error vector has different unstable components. Then, it is natural to consider a delay in the manoeuvre until reaching a better epoch with less cost. So, the function to be studied is

$$R(t) = \frac{\exp\left(t \log\left(\frac{\lambda_1}{T}\right)\right)}{g(t)}. \tag{3.26}$$

However, as shown in [107], this function is always increasing. Therefore, it is never good to wait for a manoeuvre except for operational reasons.

As it has been said, when the station keeping has to span for a long time, the satellite can tend to deviate far away from the nominal orbit. This could happen since the cancellation of the unstable component does not take care of the neutral components which might grow up to the limit of loosing controllability. In order to prevent large deviations of the satellite from the nominal orbit, it is advisable to perform manoeuvres of insertion into the stable manifold. The main idea of the strategy is to put the satellite in a such state that approaches the nominal orbit asymptotically in the future. This strategy is, in principle, much cheaper than to target to the nominal orbit itself since the latter case can be considered, from an implementation point of view, as a sub-case of targeting to the stable manifold. Moreover, even when the controllability using only unstable component cancellation manoeuvres (UCCM) is assured, it can be advantageous to perform an insertion into the stable manifold since the control effect of this manoeuvres usually persist for a longer time span than UCCM. Moreover, subsequent UCCM would be cheaper due to the fact that the satellite is closer to the nominal orbit, and consequently the projection of the deviation in the unstable component is smaller.

Although the idea is simple, the implementation is not so easy since, in the first place, the target state in the stable manifold can not be accomplished with a single manoeuvre as it happens with UCCM and secondly, the actual state of the satellite is known but affected by tracking errors. Moreover the manoeuvres to be done will be noised by some errors too. We refer to [86] for the details of the implementation.

As a final remark, several constraints that impact the manoeuvres must be specified in the procedure. The most relevant are the time interval between two consecutive tracking epochs (tracking interval), the minimum time interval between manoeuvres, and the minimum value of α_1, that can not be considered due solely to tracking errors.

Special emphasis must be placed on the evolution of α_1. With no tracking errors, the evolution of this parameter is exponential in time (see Figures 3.22 and 3.23). When adding tracking errors,

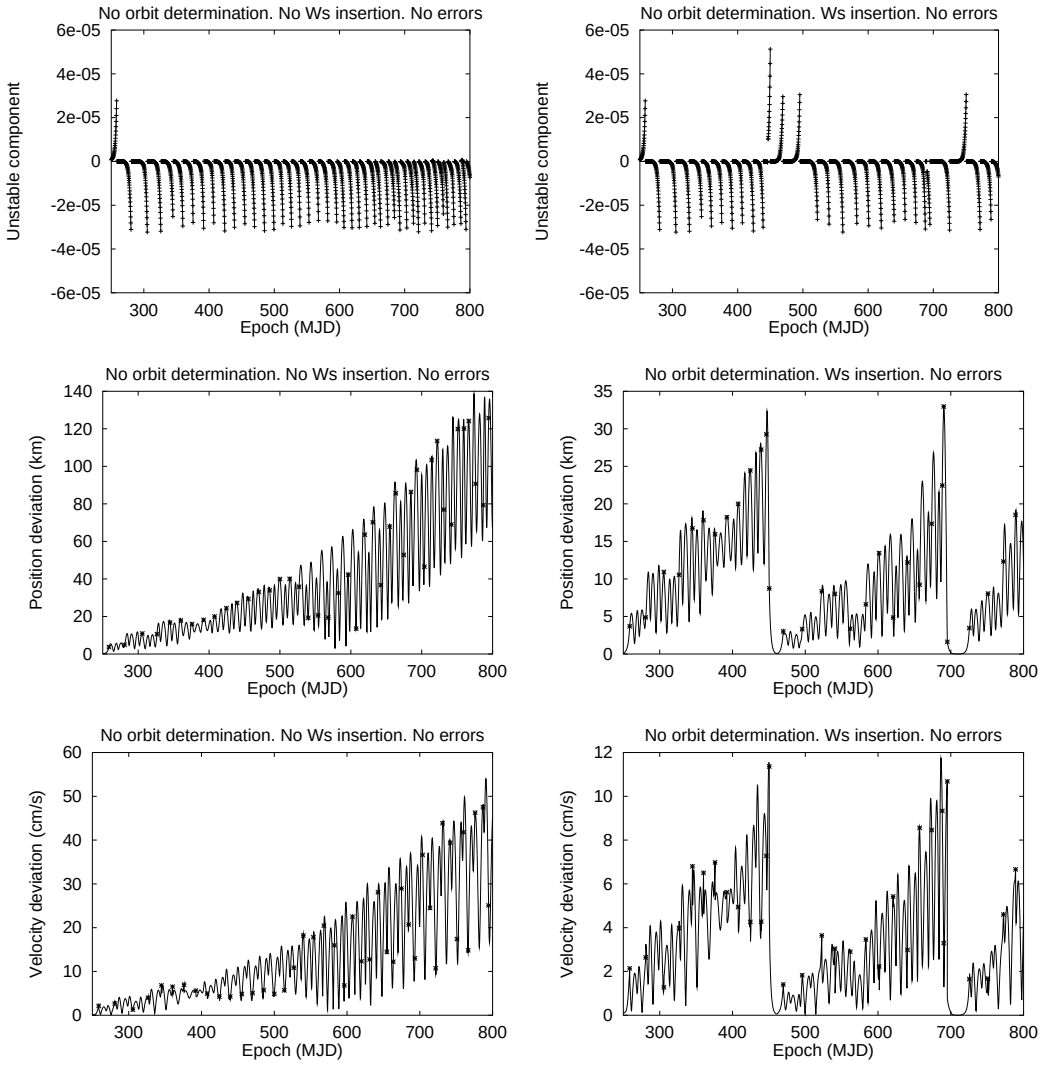

Figure 3.22: From top to bottom evolution with time of the unstable component, position deviations with respect to the nominal trajectory and velocity deviations. In the all figures no orbit determination has been performed because the simulations have been done with no errors for the tracking and the execution of the manoeuvres. There is only an error at the initial insertion epoch. In the left hand side figures there are no manoeuvres for the insertion in the stable manifold while in the right hand side yes. These manoeuvres can be clearly seen because after its execution the distance to the nominal orbit goes to zero both in position and in velocity. The discontinuities that appear in these two figures are associated to the execution of the manoeuvres. The points marked with a cross are those at which the tracking has been performed and then ones marked with a star are those at which a manoeuvre has been executed.

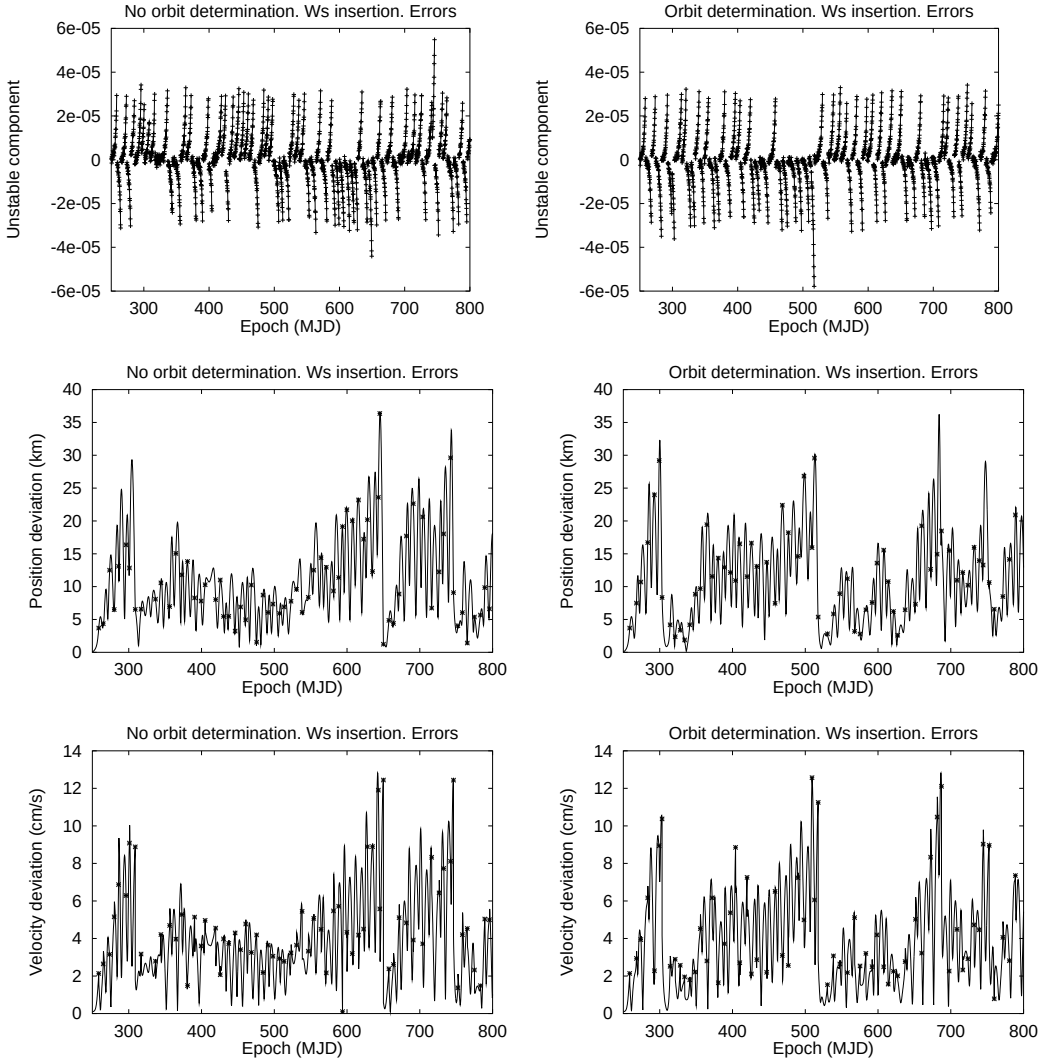

Figure 3.23: From top to bottom evolution with time of the unstable component, position deviations with respect to the nominal trajectory and velocity deviations. In the left figures no orbit determination if performed while in the right hand side ones yes. In all the figures the manoeuvres and the tracking are performed with errors. There is also an error at the initial insertion epoch. There are manoeuvres for the insertion in the stable manifold that can be clearly seen at the moments at which the distance to the nominal orbit decreases to very small values (which is not equal to zero because there is an error added to the manoeuvres). The points marked with a cross are those at which the tracking has been performed and then ones marked with a star are those at which a manoeuvre has been executed.

and in order to prevent a useless manoeuvre, this value must be greater than the minimum. So, the minimum value must be selected as a function of the orbit determination accuracy. On the other hand, the value of α_1 should not be too large because this increases the value of the manoeuvre in an exponential way. Thus, a maximum value is chosen such that if α_1, is greater than the maximum, a control manoeuvre will be executed to cancel the unstable component. When α_1, is between minimum and maximum values, the error can be due to small oscillations around the nominal orbit. In this case, a manoeuvre is executed only if the error has been growing at an exponential rate in the previous time steps and the time span since the last manoeuvre agrees with the selected one. Also, if the magnitude of the calculated Δv is less than Δv_{min}, then the recommended manoeuvre is cancelled. Once these parameters have been fixed, there are no more free variables allowing any further minimisation.

3.8.2 Numerical Results

In Figures 3.22 and 3.23 we show some results of simulations done for a halo orbit around L_2 in the Earth-Moon system. We display the evolution of the unstable component and the deviations from the nominal trajectory, in position and velocity in different situations. In Figure 3.22 the manoeuvres are done without any error, while in Figure 3.23 they are performed with errors. In each Figure we show the results of the station keeping strategy with and without stable manifold insertion manoeuvres. From them, the exponential grow of α_1 as well as the role of the insertion manifold manoeuvres, become clear.

Finally, in Figure 3.24 the averaged Δv used for the station keeping is displayed. As in the previous case, the simulations correspond to a halo orbit around L_2 in the Earth-Moon system. If no insertion manifold manoeuvres are done, there appears an exponential grow of the Δv. On the contrary, if these manoeuvres are executed the station keeping cost per year remains constant. From this Figure it is also clear that a good orbit determination procedure can be useful to reduce the total Δv.

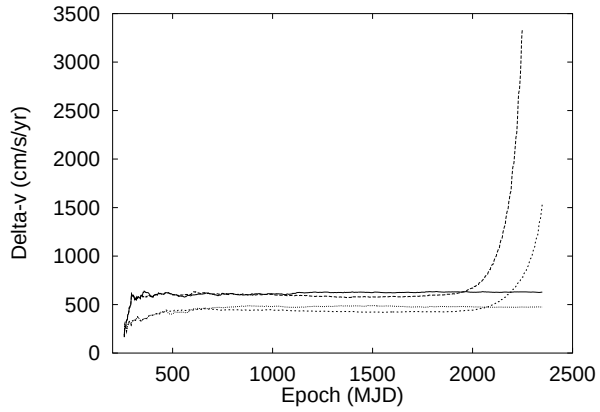

Figure 3.24: Averaged Δv used for the station keeping in cm/s/year in different situations. The two curves with an exponential grow of the Δv correspond to simulations with no insertions in the stable manifold. For the upper curve there was no orbit determination. The other two curves, for which there seems to be a finite limit for the Δv, we have used insertion manoeuvres in the stable manifold. The one with lower cost uses orbit determination and the other no.

Chapter 4

New Trends in the Assessment of Mission Design

The invariant manifold structures of the collinear libration points for the restricted three-body problem give the framework for understanding transport phenomena from a geometric point of view. In particular, the stable and unstable invariant manifold tubes associated to libration point orbits are the phase space conduits transporting material between primary bodies for separate three-body systems. These tubes can be used to construct new spacecraft trajectories, such as a "Petit Grand Tour" of the moons of Jupiter. The new trends in the assessment of mission design should include these methodologies, and others, mainly derived from the application of results coming from Dynamical Systems Theory. The capabilities of modern computers make possible new tools that just some years ago could only be considered in a theoretical base.

Certainly, many of these tools are of too high degree of complexity to be used in a raw form. In any case, as the goal of this section, we aim not at the theoretical part of tools by themselves which are already described in the literature and up to some extent in the previous sections, but to the practical applications that could be derived. In certain aspects a parallel example would be the final user of a modern car or electronic device. The actual degree of complexity of the mechanical and electronic parts make it impossible for the final user to construct a product like this, anyway the final user has an overall control of the machines and its capabilities in a very simplified and ergonomic way.

Up to now, the mission analysis of even simple libration point trajectories need to be done by highly trained people in astrodynamics, and even some re-computations of trajectories to accommodate a new demand or constraint could need of the order of few days the get the final one. New space missions are increasingly more complex, requiring new and unusual kinds of orbits to meet their scientific goals, orbits which are not easily found by the traditional conic approach. The delicate heteroclinic dynamics employed by the Genesis Discovery Mission illustrates the need for a new paradigm: study of the three-body problem using dynamical systems theory as laid out by Poincaré (see [163, 150, 126]). This significant increase of libration point missions with high degree of complexity and the navigation in the Solar System using low energy transfers, claim for a design tool of easy use. The human presence in a space gateway station located at L_1 Earth-Moon system to service missions to the Moon and to the libration points of the Sun-Earth system, among other applications, will benefit from a design tool that, in an interactive way,

could provide estimations and real trajectories to fullfill a mission on demand.

Of course the complete design and construction of a such a complex tool is a major task. At this point, our objective is to present some interfaces that could be of interest mainly from the point of view of graphical interaction with the final user and the link with its dynamical systems base.

4.1 Current Software Tools

Libration point mission design capabilities have significantly improved over the last two decades. To our knowledge, three different space centres have developed their own software tools for mission analysis at libration points: GSFC, JPL and ESOC. Here we will describe just their main features since we have not had the possibility to compare their actual capabilities.

4.1.1 Tools at the European Space Agency

The Interplanetary Navigation Software Tool (INTNAV), developed by GMV under ESOC contract, performs trajectory determination and trajectory trim manoeuvres analysis. The package has some extensions which allow the mission analysis of libration point orbits, including the triangular libration points.

The capabilities of INTNAV include the design and generation of the Launch and Early Orbit Phase, of the Transfer Phase using multiple lunar swing-bys and of the operational quasi-periodic orbits. The tracking of the spacecraft in the different mission phases is assumed by range, range-rate, VLBI from ground-based facilities and on-board optical navigation. The tool has a graphical user interface for the relevant mission parameters and case definition. The results are presented in graphical form and/or in detailed tabular and log files.

INTNAV was finished in 1996 and, to our knowledge, no further extensions have been done, in particular it lacks the ones related to the use of invariant manifolds for mission analysis purposes.

4.1.2 Tools at Goddard Space Flight Center

Before 1990, the software of choice at GSFC was the Goddard Mission Analysis System (GMAS). This software had complete optimisation functionality as well as the capability to model any kind of perturbing force. The software allowed user created object modules to be linked into the run sequence as a way to allow the user access to data for trajectory analysis. During the early 1990's, the GSFC operational PC program called SWINGBY was developed. SWINGBY had a graphical user interface (GUI) to provide instantaneous feedback of the trajectory design in multiple coordinate systems. It was designed to be a high fidelity numerical targeting tool to support libration missions, providing also support to lunar, planetary, and deep space missions, including gravity assist. SWINGBY still provides complete mission analysis and operations for the WIND, SOHO, and ACE missions as well as lunar Prospector and Clementine. From this NASA development beginning, commercial applications, such as Analytical Graphics Inc's (AGI) Astrogator, were advanced and are now in operational use. These tools support a direct method, typically using shooting methods, of attaining a desired trajectory.

As mission concepts become more ambitious, increasing innovation is necessary in the design of trajectories. Design capabilities for libration point missions have significantly improved in recent years and should continue the progress. A recent change in the mission design is the use of a dynamical systems approach to allow more of the optimisation burden to be performed autonomously. These efforts include Generator. The success of SWINGBY for construction of trajectories in this regime is an evidence of the improvement in computational capabilities. Nevertheless, conventional tools, including commercial applications like STK/Astrogator, do not currently incorporate any theoretical understanding of the multi-body problem and do not exploit dynamical relationships.

Nonlinear dynamical systems theory offers new insights into multi-body regimes, where qualitative information is necessary concerning sets of solutions and their evolution. For application to spacecraft trajectory design, it is helpful to first consider special solutions and invariant manifolds, since this aspect of dynamical systems offers immediate insight. An example of development in this area is called Generator. GSFC in collaboration with Purdue University, is developing various dynamical systems methodologies combined in a software tool (see [147]).

4.1.3 Tools at the Jet Propulsion Laboratory

LTool is JPL's mission analysis tool with specialisation in libration orbits. It has been used by the Genesis Mission for its pre-launch mission design as well as in current post-launch operations. It is also being used by the Terrestrial Planet Mission to study formation flight both in halo orbits and in SIRTF-like heliocentric orbits. It can also be used to design conventional conic-based interplanetary missions. LTool is not a program, but what is known as a Problem Solving Environment which has a Command Line User Interface, Graphical User Interface and 3D visualisation capabilities, all integrated into a common software environment. Matlab, Mathematica, and JPL's Quick are other examples of Problem Solving Environments. The user can use LTool interactively, or run LTool in batch mode for larger and longer computations. Various modules enable the users to compute conic orbits, halo orbits, invariant manifolds associated to halo orbits. Using a user-programmable differential corrector (multiple shooting) the various trajectory segments may be glued together to produce an end-to-end trajectory.

Some of the features of LTool are: Ability to produce end-to-end trajectories, starting from first guess solutions to fully integrated trajectories with JPL ephemeris models. LTool tracks coordinates and units. Trajectories are handled as abstract continuous functions of time. An algebraic function permits users to manipulate trajectory functions algebraically. In addition to trajectory design, LTool also provides coverage analysis using a technique called multi-resolution visual calculus. Currently, low thrust trajectory integration module is being added.

The LTool environment is created using the object oriented Python CLUI, with Qt GUI, and OpenGL graphics. The integrated environment is called PyShell. Fortran, C, and C++ modules are pulled into the PyShell environment using UDL (Unified Description Language), a tool developed by the LTool Team. Currently LTool runs under LINUX, but a Windows version is expected. This modular architecture allows the users to program at a high level, using a high-level language (Python), while providing speed and flexibility with the Fortran, C, and C++ modules. The various LTool modules provide a high level astrodynamic programming language . This approach greatly increases the user's ability to prototype and to solve problems interactively.

The modules of LTool dealing with the analytical computation of libration point orbits have been done by the authors of the present report.

4.2 A New Implementation of the Mathematical Tools

The inherent complexity of the problem, with intriguing properties, that at some point lead to the appearance of the ambiguous term "fuzzy boundary", which turns out later in the WSB, has its roots in the six dimensional saddle $\times$ center $\times$ center that we find in the neighbourhood of the collinear libration points.

The dynamical structures of the three-body problem (such as stable and unstable manifolds, and bounding surfaces), reveal much about the morphology and transport of particles within the solar system, be they asteroids, dust grains, or spacecraft. The cross-fertilisation between the study of the natural dynamics in the solar system and engineering applications has produced a number of new techniques for constructing spacecraft trajectories with desired behaviours, such as rapid transition between the interior and exterior Hill's regions, resonance hopping, and temporary capture (see [20]).

The invariant manifold structures associated to the collinear libration points for the restricted three-body problem, which exist for a range of energies, provide a framework for understanding the aforementioned dynamical phenomena from a geometric point of view. In particular, the stable and unstable invariant manifold tubes associated to periodic and quasi-periodic orbits around the libration points L_1 and L_2 are phase space structures that conduct particles to and from the smaller primary body (e.g., Jupiter in the Sun-Jupiter-comet three-body system), and between primary bodies for separate three-body systems (e.g., Saturn and Jupiter in the Sun-Saturn-comet and the Sun-Jupiter-comet three-body systems)(see [187]).

These invariant manifold tubes can be used to produce new systematic techniques for constructing spacecraft trajectories with interesting characteristics. These may include mission concepts such as a low energy transfer from the Earth to the Moon ([70]) and a "Petit Grand Tour" of the moons of Jupiter.

As we already described in the section 3.2, one of the technical problems is that we have to face with objects inside a high dimensional space, and so very difficult to be represented, wherein a four dimensional set of libration point orbits act as saddle points. The mathematical tools developed up to present, and essentially based in normal forms or in Lindstedt-Poincaré procedures, pretend, in some way, to decrease the degrees of freedom as well as to decouple the hyperbolic parts from the elliptical ones in order to simplify and study the problem from a mathematical point of view. They should be the base for the construction of new devices that permit the mission analysis in a systematic way and avoiding trial and error as much as possible. Let us enumerate briefly strong and weak points of these methodologies.

- **Normal Form Methods**
  - Provide a full description of the orbits in any selected energy level of interest.
  - Provide the uncoupling between central, stable and unstable manifolds.
  - The change of variables between the usual position and velocity and the normal form variables can be explicitly obtained in both ways.

  - The variables in the central part have not an special meaning. This is, in general they do not provide explicitly to which type of libration orbit refer.
  - The change of variables is implemented as a long series expansion and is relatively time consuming to evaluate.

- **Lindstedt-Poincaré Methods**
  - They provide full descriptions of levels of energy close to the one of the libration point.
  - The variables, amplitudes and phase have a very concrete and dynamical meaning. In fact they are the well known action-angle variables of the Hamiltonian systems.
  - Because they are invariant tori, libration point orbits are selected fixing the amplitudes and varying the phases in a linear way. This is libration point orbits are seen as straight lines moving uniformly in time in suitable coordinates.
  - The usual coordinates of position and velocity are obtained by a straightforward evaluation of the series.
  - They provide only a partial description of levels of energy containing both Lissajous and halo orbits.
  - The change of variables from the usual position and velocity to the amplitudes and phases is not direct and must be implemented through iterative numerical procedures.

The combination of the best properties of each methodology with an effective implementation of the numerical procedures, is the basis for the obtention of very efficient gadgets for the mission design in the Solar System using the libration points. Let us comment some directions that we think could be of major interest.

4.2.1 Gadgets Derived from Normal Form Computations

One of the best properties of the Poincaré sections of the normal forms about libration points is that they provide a full description of the orbits in a neighbourhood of them. Moreover, for levels of energy close to the libration point the invariant curves pointing to Lissajous trajectories distribute in a neat way about the fixed points corresponding to periodic orbits (see section 3.2), using interpolation techniques and the normal form computations, it is not difficult to construct a database for any libration point in the solar system. The database can be used to generate, to display and to interact with trajectories in an immediate way. Our group in Barcelona has developed a very simple prototype (see Figures 4.1 and 4.2). The user selects an energy level or chooses a certain orbit inside an energy level just moving the mouse. The characteristics of the orbits are presented in an instantaneous way, and the generation of the trajectory and the initial conditions in the stable or unstable manifold (also in the database) are immediate. Using efficient and fast numerical integration desired trajectories are generated and chosen at once.

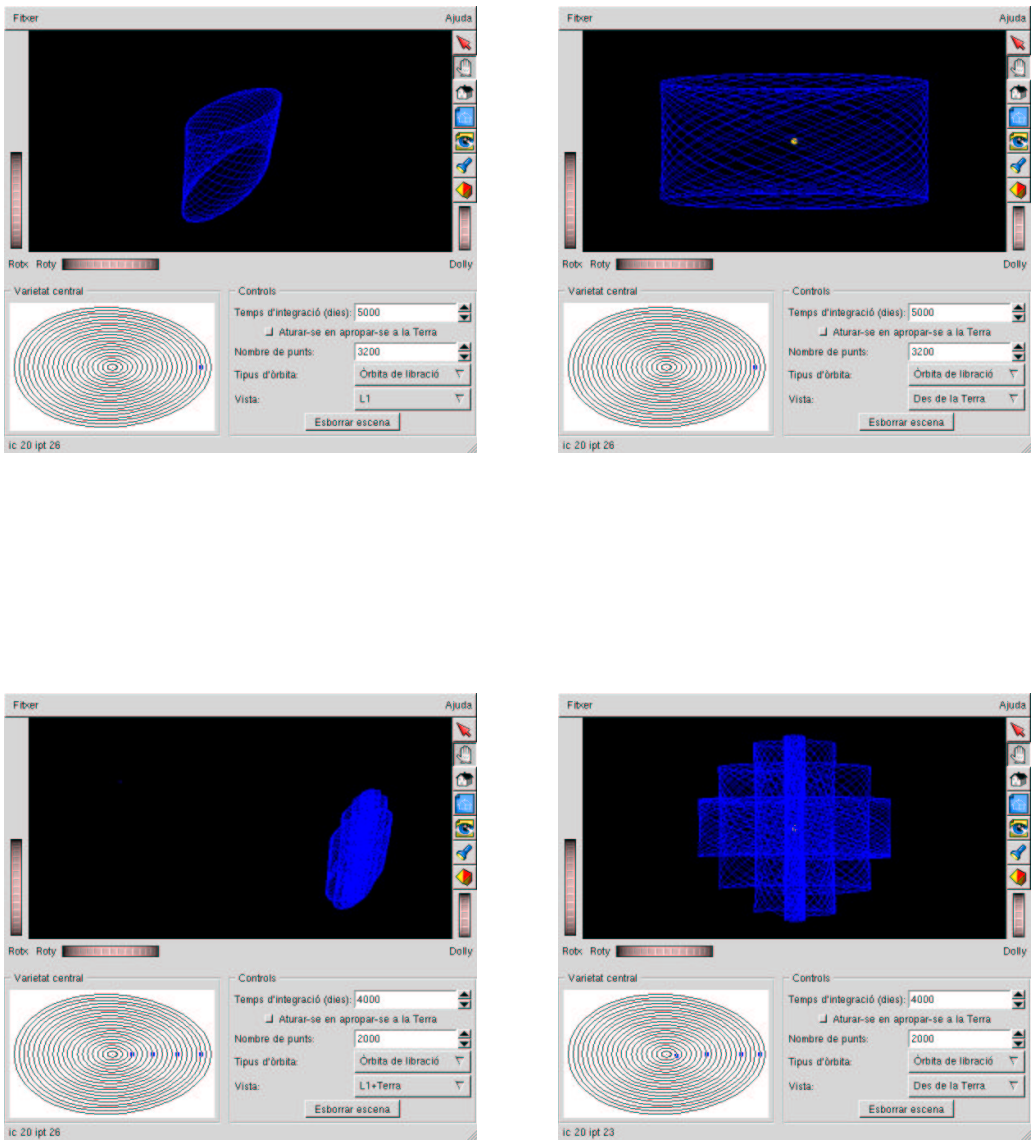

Figure 4.1: Screen-shots of a possible gadget using the Poincaré sections of the normal form. The basic capability includes a Poincaré section (down and left of each plot) where one selects the appropriate orbit by clicking. The user interacts with standard graphical interfaces. Here we present some Lissajous orbits seen from different viewpoints. In the right hand side figures, the orbits are seen from the Earth and the central yellow point represents the Sun.

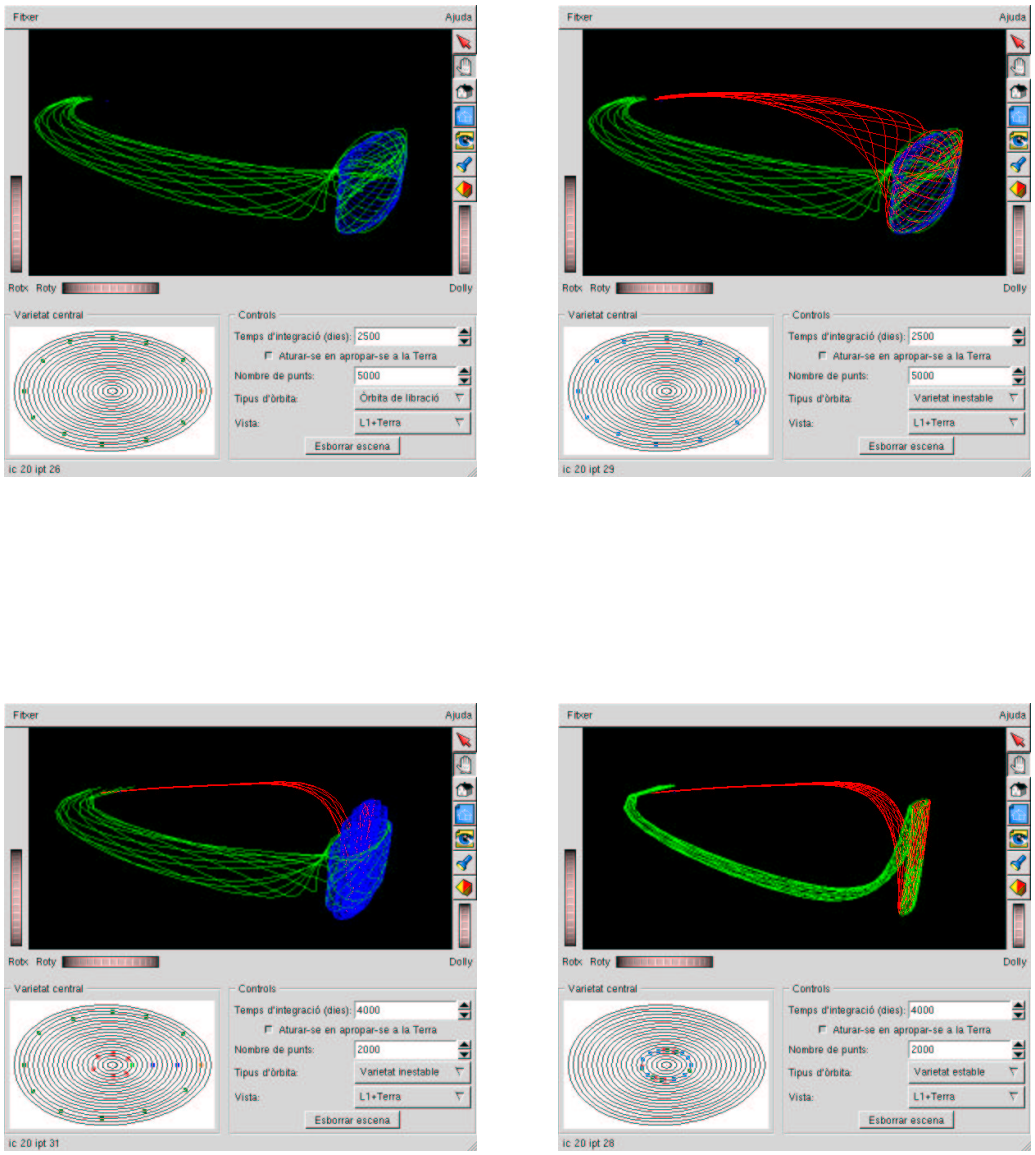

Figure 4.2: In the gadgets, libration point orbits (blue) can be computed and represented together with some trajectories of their stable manifold (green) and/or of the unstable manifold (red). The computation and display is immediate due to the design of the internal database.

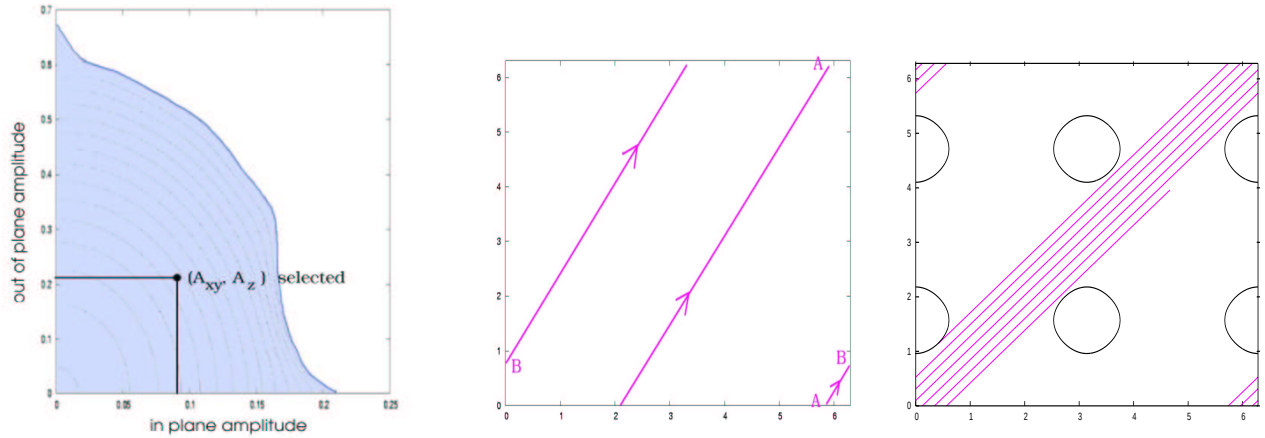

Figure 4.3: Lissajous orbits are determined by two amplitudes and two phases. In the left-hand side plot we represent a qualitative picture that lets the user select an appropriate orbit. Once selected, the points of the trajectory are characterised by two phases in $[0, 2\pi] \times [0, 2\pi]$. These are the angular variables in what we refer as the Effective Phases Plane (EPP). In the EPP the Lissajous trajectory is seen as an straight line in the EPP moving with constant velocity and fixed slope (central plot). The EPP can also contain information about restrictions or requirements of the trajectory. In the right-hand side figure we present an example which includes the exclusion zone that must be avoided (see [154] for more details).

4.2.2 Gadgets Derived from Lindstedt-Poincaré Methods

Again a database, or even direct evaluation of the series expansions can be used to generate trajectories and their manifolds. The selection of a given Lissajous orbit is immediate from the in-plane and out-of-plane amplitudes. Once these amplitudes are selected, the trajectory is easily displayed in the plane of effective phases (EPP), which in fact, from a dynamical systems point of view is the representation of the angular variables of the torus (see Figure 4.3). In the EPP, the trajectory is seen as a straight line moving with a constant velocity. It is also possible to represent special zones in the EPP such as the exclusion zone about the solar disc for missions about L_1 in the Sun–Earth system (see Figure 4.4). In the EPP, manoeuvres in the in-plane component, or in the out of plane component, which maintain the amplitudes of the tori can be seen as symmetrical jumps of the straight line. These manoeuvres can be instantaneously computed and could be represented in the same EPP as possible choices for the mission designer (see again Figure 4.4).

Once in a libration regime, a change of libration orbit, this is a change of amplitudes, can be easily tracked using the EPP. The best places for the manoeuvres including the required restrictions can be displayed and the choice for the mission analyst is clear as we represent in the example of Figure 4.5.

The Lindstedt expansions have also the possibility of adding the amplitudes related to the unstable and stable component of the Lissajous orbits. This fact provides the capability of considering the unstable and stable invariant manifolds of the Lissajous orbits and again the

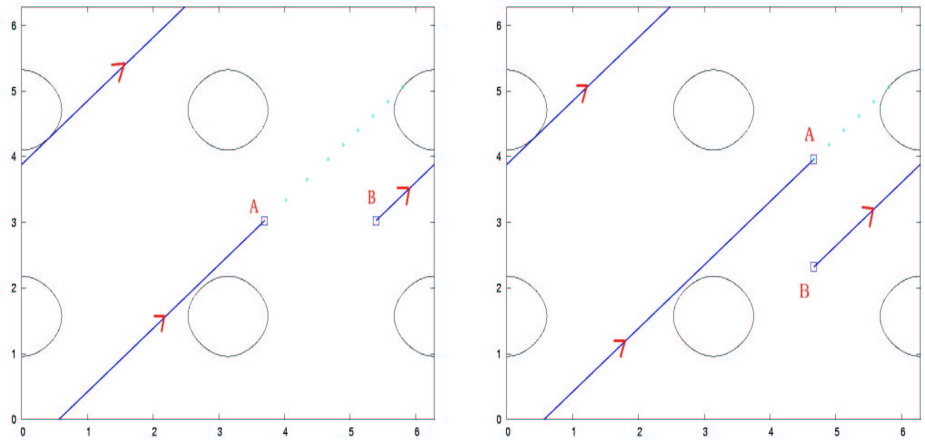

Figure 4.4: Essentially, manoeuvres are seen as jumps of the straight trajectory in the EPP (jointly with a possible jump in the amplitudes). For certain types of manoeuvres, such as the exclusion avoidance maintaining the amplitudes, they look as horizontal or vertical displacements, depending on whether in-plane or out-of-plane manoeuvres are applied. These type of manoeuvres have symmetrical properties too and this makes their planning very easy. In the plots we represent exclusion zone avoidance manoeuvres in the in-plane and out-of-plane components sometime before the satellite is going to hit an exclusion zone. A delta-v makes the satellite jump from point A to point B in the EPP.

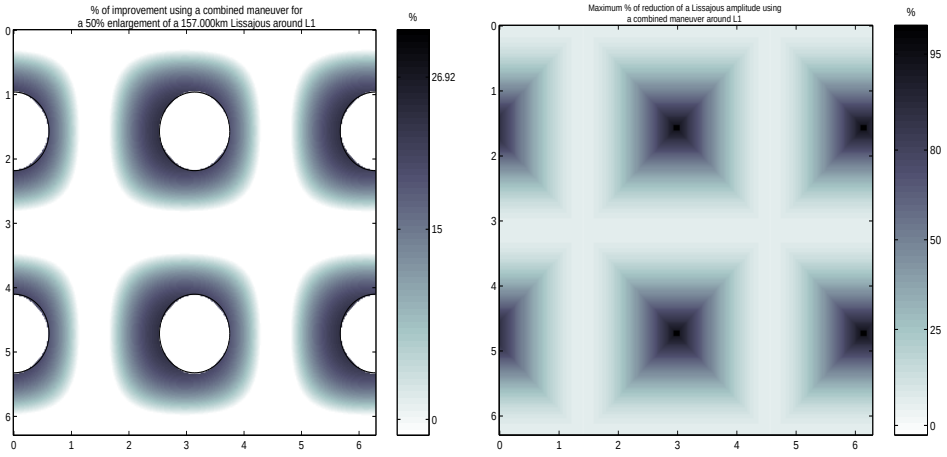

Figure 4.5: The EPP can also be used to represent the most convenient places for manoeuvres such as a change of amplitudes. In this example, in the left-hand side plot we represent the suitable places where a manoeuvre of enlargement of the libration point orbit improves the cost of a certain strategy using two manoeuvres. In the right-hand side plot we display the maximum percentage of reduction possible at each given point od the EPP.

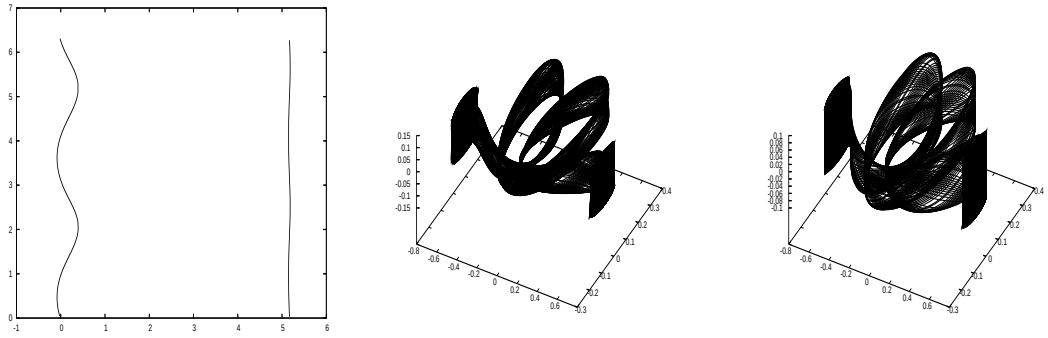

Figure 4.6: Example of a case where the EPP is used to display information about the manifolds of the libration point orbit. The two curves represented in the EPP correspond to the orbits having an heteroclinic connection with a certain libration point orbit. The corresponding heteroclinic connections of each curve are respectively displayed in the 3D plots. The different regions in the EPP can be used to control the transfer trajectories between the distinct libration regimes as well as transit and non transit orbits in a similar way that the Poincaré sections commented in 4.2.3.

EPP parametrising all the possible choices of the initial state. In this case, for instance, one can easily represent the different regions to transfer to distinct libration regimes or to the Earth or to any other body in the EPP. See Figure 4.6 for an example.

Finally it is also very convenient to consider the EPP for the transfer orbit to libration point orbits linked with the launch window in the Earth departure. In this way the mission designer can take into account just with a sight both the required launch conditions and the final state in the libration regime.

4.2.3 Poincaré Sections Far from the Libration Regimes

For the solar system navigation (this includes transfer trajectories between planets or transfer trajectories between the moons of the planets as well as transfers from or to stations in libration point regimes) it is very important to have a map of the main roads. This concept is represented in Figure 4.7 where an artist conception of the road-map, also known by the interplanetary superhihgway, is pictured by Cici Koenig from Caltech.

Nevertheless, this is one of the parts that still needs more theoretical study. The building blocks (these are the orbits of the libration point regimes) are well known but, up to now, few effort has been put on the knowledge of their interconnections. Apart from some examples, the computation of transfer orbits relating libration point regimes of different primaries in a systematic way is still missing. Although the numerical tools to analyse them are already developed.

An important idea in this new mission design concept is to place ad hoc Poincaré sections where the manifolds coming from different systems meet. This is displayed in Figure 4.8, where S represents the Sun and P_1, P_2 two planets, but the example works as well for a planet and two moons. The manifolds of two libration point orbits, one coming from the S–P_1 system and the other one from the S–P_2 one meet at a Poincaré section located in different places. The appropriate location of the Poincaré section will depend on the type of problem to be solved and

Figure 4.7: Artist conception of the low energy transfer channels in the solar system (Cici Koenig, JPL-Caltech).

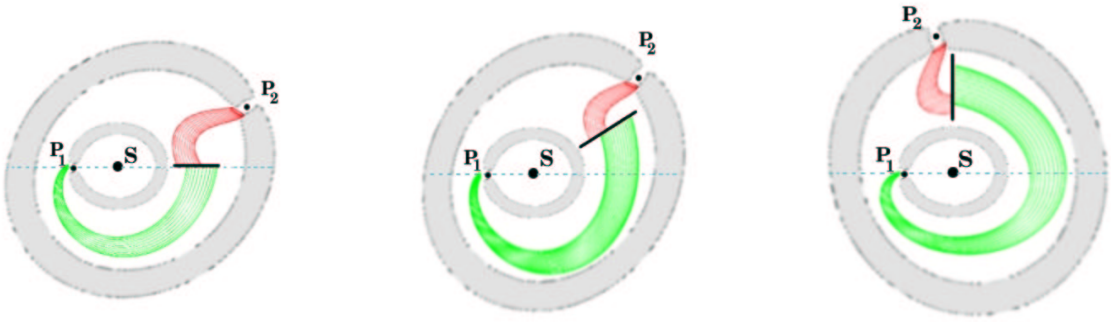

Figure 4.8: The natural way to study the transfer orbits between different planets or libration point regimes is via the Poincaré section located at suitable places. In this figure we represent three possible Poincaré sections located at different angles with respect to the S–P_1 line. The gray regions represent the well known Hill regions which are forbidden for the satellite due to its associated energy.

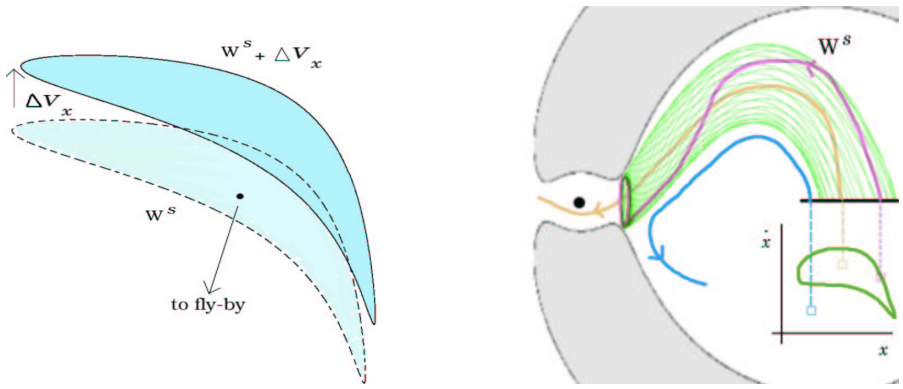

Figure 4.9: Example of a Poincaré section at $y = 0$ of the planar RTBP. The plot of the stable manifold is displayed in the $x\dot{x}$ coordinates. We note that a delta-v in the x component moves the plot up or down (left-hand side plot). In the right hand side we display the different qualitative roles of the points in the $x\dot{x}$ plane with respect to the plot of the manifold. We remark that the points inside the region produce low energy fly-bys.

in general more theoretical work must be done in order to fill in a database with the most suitable ones. But in any case, let us describe the important role of this tool with some examples of planar orbits in a RTBP framework. For the examples, we assume that the Poincaré section is located in the $y = 0$ axis of the synodical S–P_1 system, this is, as it is represented on the left-hand side plot of Figure 4.8, on the blue line which represents the x-axis. If we consider the variables x and $\dot{x}$ for the Poincaré map, we note that selecting a point on it, since $y = 0$ is already fixed, three of the four coordinates of the planar problem are determined. For the remaining one, $\dot{y}$, we note that it is equivalent to choose the energy of the trajectory when considering the Jacobi constant of the S–P_1 restricted three body problem. If we are dealing with the manifold of a libration point orbit, both the orbit and its manifolds have the same energy and so $\dot{y}$ is also determined. This is, a point in the Poincaré map and a given level of energy determine a trajectory.

The second important thing to remark is that these Poincaré maps can be used as gateways in the Solar System exploration. Continuing with the former example with the section located at $y = 0$, the ordinary plot of the manifold in the $x\dot{x}$ coordinates of the Poincaré section is a curve homeomorphic to a circle (see Figure 4.9). Assuming that the plot corresponds to the stable manifold (W^s) of a libration point orbit, the points on the curve give the x and $\dot{x}$ values at $y = 0$ that with $\dot{y}$ matching the same energy as the libration orbit, tend to the libration orbit as the time increases. But, at the same level of energy, the x, $\dot{x}$ conditions chosen inside the curve produce transit orbits towards the small primary, these are *low energy flyby orbits*, whilst the conditions taken outside the curve produce non transit orbits. A similar thing happens when the curve on the Poincaré map corresponds to the unstable manifold of the libration orbit (W^u) considering trajectories backwards in time.

When the plots of the manifolds are at the same level of energy the intersection of an W^u curve with an W^s curve produce homoclinic or heteroclinic orbits. These are the asymptotic trajectories that connect the same or distinct libration point orbits with zero cost in the models. These properties about transitions and asymptotic trajectories are also explained in Figure 4.10

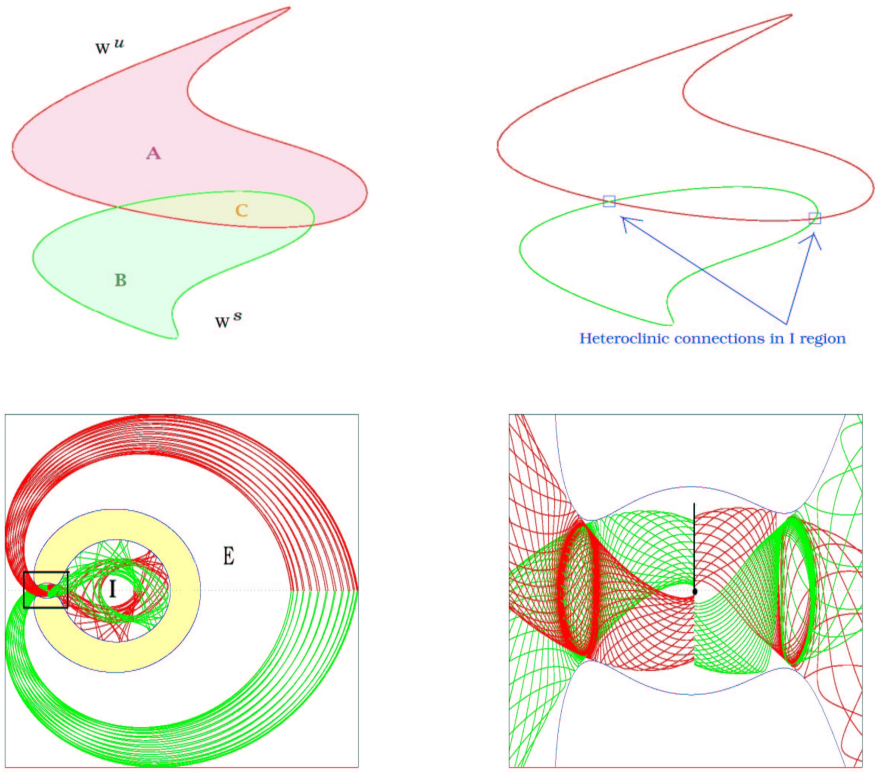

Figure 4.10: Using a Poincaré section containing the small primary and perpendicular to the line of both primaries, the plots of the manifolds of the libration point orbits control the gateways between distinct regimes as we represent in this example. Let us denote the regimes by, E (exterior to the zero velocity curve), I (interior to the zero velocity curve) and P (the bottleneck between E and I and where the small primary is). Let us assume that we plot respectively the stable and unstable manifolds of Liapunov orbits about L_1 and L_2 in the same level of energy. For this energy level, orbits in the A part of the Poincaré plot correspond to the orbits which go from E to P. Orbits in the B part go from P to I and, as a consequence, orbits in C transit from E to I. The crossings of the plots correspond to heteroclinic connections from the Liapunov orbit about L_1 to the one about L_2 in the example.

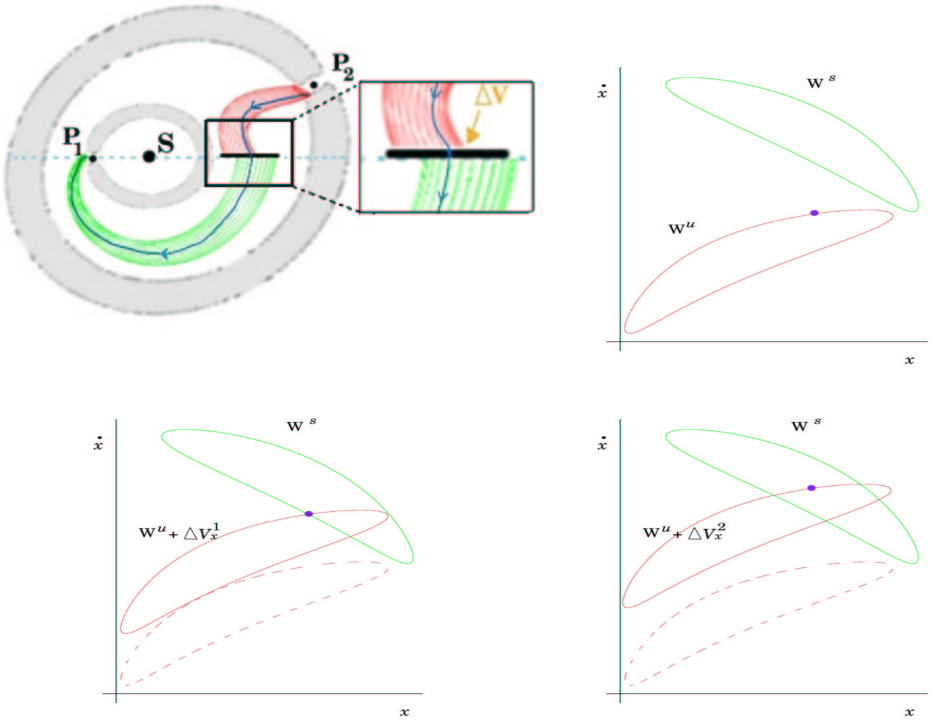

Figure 4.11: Example of a simple procedure that a mission designer may use to transfer between libration point orbits associated with P_1 and P_2. Having placed a Poincaré section at $y = 0$, we display the $x\dot{x}$ coordinates corresponding to the unstable manifold coming from P_1 (in red) and the stable one going towards P_2 (in green) in the upper plots. The bold point indicates the selected orbit of the W^u. Applying a manoeuvre at $y = 0$ the satellite can either be injected in the stable manifold or transfered to the P_2 interior region for a low energy flyby as we see in the bottom plots. See more explanations in the text.

and it is the main key for the Solar System exploration using low energy transfers.

As a final remark let us illustrate with an example the possible role of the Poincaré sections in a facility for the mission design. Let us assume that we want to transfer a satellite from a planar libration point orbit in the S–P_1 system to another one in the S–P_2 of Figure 4.8. Choosing the Poincaré section at $y = 0$ we obtain the left-hand side plot of Figure 4.11. The unstable manifold comes from the libration point orbit associated with P_1 and the stable one from the libration point orbit associated with P_2. For the sake of simplicity, both manifolds have been computed using uncoupled systems. This is, in the computations of the unstable manifold, P_2 has not been taken into account, as well as P_1 has not been taken into account in the computations of the stable manifold. We also assume that the departure orbit chosen in the unstable manifold corresponds to the bold point we see in the section plot.

As we see, the curves do not intersect. Besides they correspond to different levels of energy. But the mission designer has an easy way to find a possible delta-v at the surface of section,

and to obtain a transfer trajectory suitable as initial guess in any classical optimisation method. Increasing the x component of the velocity, the W^u curve moves upwards. So we can easily locate the bold point on the W^s curve as it is represented in the plot of Figure 4.11. In this way we match the x, $\dot{x}$ and y components of an W^s point in the section. Finally $\dot{y}$ is selected in order that the final condition be in the same level of energy as the target orbit, this gives us the y component of the delta-v we need.

If we had wanted to transfer to the interior region about P_2, this is to obtain an orbit approaching P_2 in a low energy flyby, we would have chosen the x component of the delta-v in such a way that the bold point were located inside the W^s curve (see the right-hand side plot of Figure 4.11) and then, choosing again the $\dot{y}$ to match the energy of the W^s manifold.

4.2.4 Maps of Asymptotic Orbits

As we already presented in the section 3.6, the homoclinic and heteroclinic orbits are the ones that depart asymptotically from a libration point orbit and tend also asymptotically to the same one, or to other one, inside the same level of energy. This is they belong to both unstable and stable manifolds of libration point orbits, and provide natural transfers between orbits in the same level of energy at zero cost.

Asymptotic orbits can be considered in the same system (i.e. joining for instance libration point orbits from L_1 and L_2 in the Sun-Earth system or in the Earth-Moon system) or in different systems (i.e joining a libration point orbit in one system and with another libration point orbit of another system). The knowledge of these orbits can be very useful in the design of missions and may provide the backbone for other interesting orbits in the future. Up to now, and at least using coherent models, research has been focused on the computation of this type of orbits joining libration point orbits of the same system, and the tools to compute them, using either normal forms or Lindstedt methods (which are developed up to a big extent, see [166], [14], [5] and [22]). So it would be possible to have a database of these type of trajectories in a RTBP framework and considering libration point orbits about L_1 and L_2.

The potential use of these orbits is very clear since they provide transfer trajectories between libration point regimes at zero cost. For instance, a database could include information in the following directions

- characteristics of the initial and final orbit.
- crossings at different Poincaré sections.

For example, when the mission designer needs to transfer from a libration point orbit about L_1 to a libration point orbit about L_2, could consult the database and to choose the heteroclinic connection that best suits his purposes. This orbit could then be used as starting point in an iterative procedure including all the required restrictions.

The information of crossings at different Poincaré sections can be used as further information that could be included in the devices presented in the previous sections.

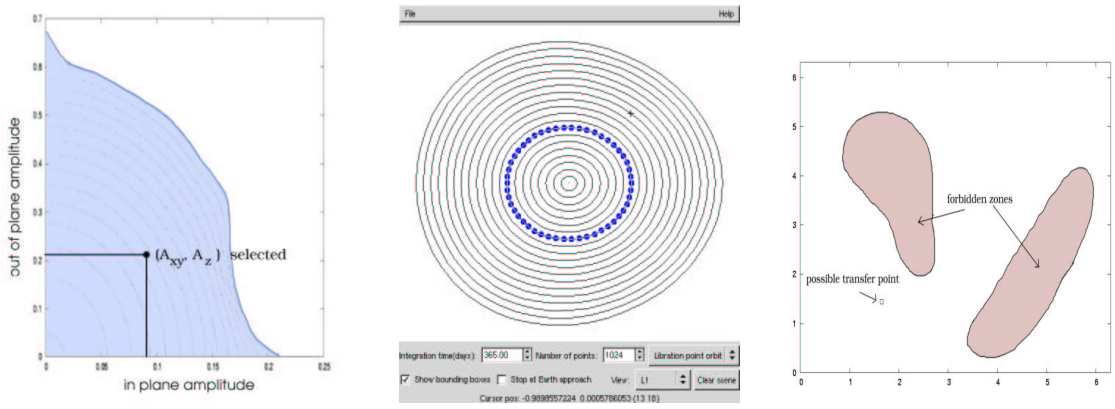

Figure 4.12: Example of basic tools to study the transfer to a Lissajous libration point orbit. The user selects a target orbit with suitable amplitudes (left). Then he uses the Poincaré map with the EPP to select a transfer trajectory with the required restrictions (centre and right).

4.2.5 The Coordination of the Gadgets

We have commented some of the main building blocks that could be used in the generation and choice of basic trajectories. All these tools should be implemented in a final device which permits the study of a particular mission from the different points all-together as well as the implementation of automatic duties: to match the trajectory at certain point, to minimise the delta-v consumption restricted to certain constraints... These ones go from the usual iterative procedures for the implementation of differential corrector using parallel shooting to optimisers of a certain objective function subjected to constraints. Any of them need good initial seeds that the former tools, due to the their specific design, are able to provide and thus far avoiding a blind search.

4.3 Some Examples of Applicability

Let us discuss briefly how different situations could be tackled using the above tools.

4.3.1 Direct Transfer to a Lissajous Orbit

In the simplest example we consider a transfer to a libration point orbit about any of L_1 or L_2 in the Sun-Earth or Earth-Moon system such as many examples in section 2. The mission designer chooses a suitable target orbit as a point in the amplitudes plane (see Figure 4.12) and the curve is highlighted in the Poincaré section. Of course the selected amplitudes can be changed at any time later at will. Then, the point of the stable manifold producing close encounters with Earth is selected in the EPP just by scrolling the mouse, or clicking in the invariant curve of the Poincaré map, or even in an automatic way. Also in the EPP we can include restrictions such as the eclipse avoidance zones in order to maximise the time in the libration area without this type of manoeuvres. Departure conditions about the Earth could also be checked in a similar

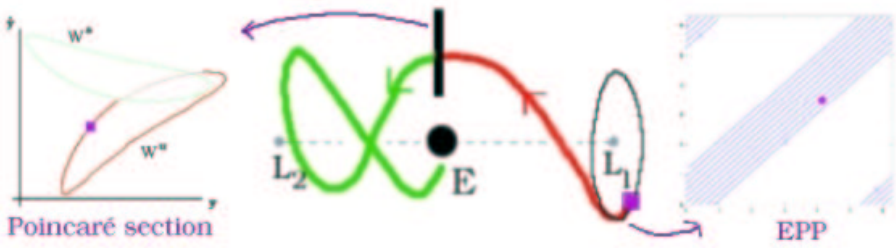

Figure 4.13: Example of the process of mission design in the final part of a a Genesis like trajectory. After completing the L_1 phase, the spacecraft is returned to Earth after a passage in the L_2 region. For this purpose the mission designer could use the EPP to control the suitable places for departure from the station orbit about L_1 using the stable manifold. A Poincaré section placed in the $x = x_{\text{Earth}}$ and containing the W^u coming from L_1 and the W^s of the L_2 area with the same level of energy is used for the design. The mission designer chooses a departure point in the EPP which produces a point in the Poincaré section bouncing towards Earth. This is, outside the W^s plot.

way. The orbit obtained in this way is then used as a seed for an optimiser which includes all the restrictions.

4.3.2 Tours in the Sun-Earth Libration Regime

These type of missions include as examples the GENESIS trajectory (see section 2.1.6) or some parts of the extended mission ISEE-3 (see section 2.1.1). The main characteristics are acrobacies of the spacecraft in a region about the Earth visiting the Sun-Earth L_1 and L_2 area. Of course the same rules apply for tours in the L_1, L_2 regime of any other system like Earth-Moon. Let us consider as an example the Genesis mission design, where the spacecraft is transfered to L_1, remains there for two years, and then it comes back to Earth after having a short pass in the L_2 region. In a first step, the mission designer should compute the transfer trajectory as in the previous example. During the phase of station maintenance at L_1, the EPP and the control of the unstable components (which also could be provided by the Lindstedt methods), can be used to control possible requirements and restrictions in the trajectory such as the exclusion zone avoidance and for performing station keeping manoeuvres. After completing the L_1 phase, the spacecraft is transfered back to Earth via a short visit to the L_2 region. For this purpose, the mission designer uses both the EPP to control the phase departure at L_1, and a Poincaré section placed at $x = x_{\text{Earth}}$ in the Sun-Earth rotating coordinates. In this Poincaré section he plots both the unstable manifold coming from the actual orbit at L_1 and the stable manifold of the orbits about L_2 with the same energy as the unstable one coming from L_1. He needs to pick up a departure phase in the EPP that maps "outside" the W^s plot in the Poincaré section (this is bounces inside after visiting the L_2 region) having an approach to Earth. This procedure gives the initial seed of this particular mission design.

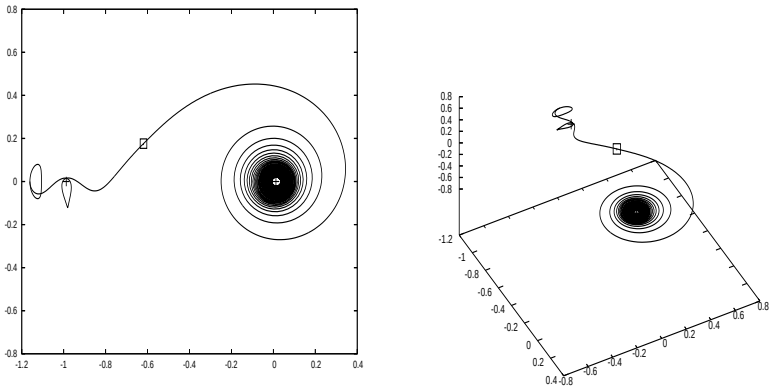

Figure 4.14: Example of a transfer to a halo orbit about L_2 in the Earth-Moon system using low thrust and invariant manifolds. In this example the low thrust propulsion stops once the satellite is on the stable manifold of the target orbit. We also note that the spacecraft goes through the L_1 region, and in fact, the part of the transfer from L_1 to L_2 can be designed using the tools of the previous point.

4.3.3 Missions Related to the Space Gateway Station

During the last decades the efficiency of the Shuttle to service spacecraft about the Earth such as the Hubble Space Telescope has been proved many times. Human crews have recovered and repaired spacecraft providing enhancements to the Hubble Space Telescope and replacing failed control gyros. The new plans of putting expensive telescopes at L_1 or L_2 in the Sun-Earth system would benefit from a human presence too. Nevertheless, the trip to L_1 and L_2 takes about three months in a radiation environment. In this sense, the solution is a Space Gateway Station located at L_1 in the Earth-Moon system. The transfer form the Earth to the Station takes about 3 or 5 days, and the transfer from the Sun-Earth L_1 or L_2 to the Station may take three months but it is cheap. Low energy transfers from L_1 to L_2 in the Earth-Moon system could also be used to service satellites at L_2 or even to service the link with a Lunar base in the far side of the Moon. Low thrust transfer trajectories to L_1 and L_2 can be used to transfer big cargos to assemble the Station at L_1 (see Figure 4.14). In fact, the notion of human missions to libration points has been proposed for more than a generation. Human mission concepts have examined the viability and utility of human mission support for scientific missions in the vicinity of libration points in the Sun-Earth, Earth-Moon and possibly Sun-Mars systems. Science fiction writers and futurists have proposed concepts for permanent colonies at certain (linearly) stable libration points (e.g., Gerard K. O'neil, founder of the L_5 Society, who promoted the idea of putting a colony at the Earth-Moon L_5 libration point). Here we will concentrate in the collinear libration points L_1 and L_2. Moreover, the libration points provide a number of other potential human mission architecture such as,

- Earth–Moon libration point L_1: a gateway station for Lunar surface missions.

- Sun–Earth and Earth–Moon libration points as staging points for interplanetary missions.

Human missions to the Earth-Moon libration point L_1 have been proposed as a gateway to support routine missions to the lunar surface. The libration point acts as a transfer point, allowing human missions from the Earth to the libration point to be decoupled from the follow-on leg leaving from the libration point to the lunar surface. In this manner, it is possible to then land at almost any lunar location desired, at any time, and then return to the station located at the libration point. An attractive feature of this mission concept is that only elements supporting lunar landing/ascent from the surface actually go to the lunar surface. Earth return elements remain at the libration point. Earth return from a libration point provides greater flexibility in transfer opportunities than for a departure from a fixed higher latitude lunar parking orbit for either a direct return to Earth's surface or to a rendezvous with an orbiting space station.

For the case of departure and return to a particular parking orbit, such as the International Space Station orbit, the L_1 lunar libration point mission has certain advantages over an Apollo style lunar orbit rendezvous approach, especially for multiple landing sites at higher latitudes. Let us comment these advantages briefly.

- It provides a minimal orbit plane alignment issue for non-equatorial lunar landing sites.
- A free Earth return trajectory from L_1 is afforded for missions to almost all lunar latitudes.
- Assuming a lunar orbit insertion prior to final descent to surface, it provides anytime access to/from the lunar surface. The lunar orbit rendezvous approach provides access only to sites in proximity to the lunar orbit plane.
- It allows the reuse of the lunar landing vehicle and avoids problems associated with reusing a lunar orbit rendezvous vehicle.
- Vehicles sized for lunar orbit rendezvous missions can, in some instances, be used for lunar libration point missions.
- Station-keeping cost at the lunar libration point is very small. The lunar libration point approach avoids parking orbit stability problems associated with a complex selenopotiential which, over the time, can produce peak-to-peak altitude variations for some low lunar orbits so large that they result in surface impact. Depending on the inclination, low lunar orbits altitudes in the range of 60 to 100 km can result in surface impact in 10 to 100 days.

On the other hand, the main disatvantatge of the lunar orbit rendezvous over the lunar libration point is that the mission time, and sometimes the Δv cost, can be smaller for near equatorial sites.

The benefit and utility of the libration point gateway concept reveals itself in an evolutionary, rather than an expeditionary mission. Future evolutionary concepts could also incorporate replenishing propellant oxidiser on the Moon by mining lunar rock or soil for its relatively high oxygen content. The lack of atmosphere permits a surface launch via an electro-magnetic launch device. In addition, unmanned satellites in halo orbits about the collinear libration points L_1 and L_2 can support fully accessible, uninterrupted robotic or human communication links.

Also, human missions to the Sun-Earth and Earth-Moon libration points have been suggested as staging/departure points for future human interplanetary trajectories. The libration points

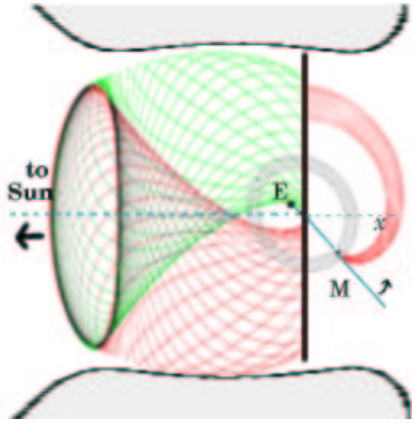

Figure 4.15: The natural way to transfer from the Space Gateway Station to a libration point orbit in the Sun-Earth system, is to look at the cross of the manifolds at a certain Poincaré section and then to use the methodology similar as the one in Figure 4.11. In this plot Sun and Earth-Moon barycentre are aligned in the x axis. The relative position Sun-Earth-Moon repeats approximately each month and the Poincaré section mostly depends on the angle between the Earth-Moon line and the x axis.

offer a location from which to conduct long term construction of massive interplanetary spacecraft that has low orbit maintenance cost and is essentially free of man-made hypervelocity orbital debris. With the aid of a powered Earth gravity assist, interplanetary injection manoeuvres, beginning at the libration point, can be effected for a lower performance cost than for departure from low Earth orbit.

Human presence at L_2 in the Sun-Earth system has been proposed too. In 1998 Wes Huntress, then Associate Administrator for Space Science at NASA Headquarters, suggested the use of astronauts for the deployment of the NGST in deep space.

As an example of a part of the mission design associated with a Space Gateway located at L_1 Earth-Moon system, let us consider the major problem of servicing satellites located at L_1 and L_2. This can be easily tackled using the Poincaré sections that we previously presented (see Figure 4.15). Essentially, to transfer the satellite to be serviced from the Sun-Earth libration point to the Space Gateway Station, we depart from the first orbit using its unstable manifold and then, at some place, we insert the satellite on the stable manifold of the libration point orbit where the Station is located. As we showed, this type of manoeuvres can be easily computed once a Poincaré section is selected, and the relative position of the possible Poincaré sections with respect to Sun, Earth and Moon repeats approximately every month. The transfer of the spacecraft back to the Sun-Earth libration regime can be resolved in a similar way. Of course, the transfer of the astronauts from Earth to the Space Gateway Station follows the discussion of the previous point on direct transfers to libration point orbits as well as possible transfers form the libration Earth-Moon regimes to the Moon. Finally, the transfer between L_1 and L_2 regimes in the Earth-Moon system can be implemented either by Poincaré sections or using the maps of asymtotic orbits discussed in section 4.2.4.

4.3.4 Interplanetary Missions and Satellite Tours

At this point, there is some evidence that invariant manifolds associated with libration point orbits of different planets intersect in position (see Figure 3.21 in page 106). In this case, the techniques of mission design associated with libration point orbits of different planets, and presented in section 4.2.3 could be used. Missions like the ones in section 2.2 and others would be potential candidates to this type of mission design. The drawback is that, at least for the exterior planets, the time to obtain the encounter could be of the order of hundreds of years. In this case, small manoeuvres to obtain big deviations of the trajectory in hyperbolic regimes, and outside of the scope of this report, could be used to asses the mission design. Other possibilities should be the use of low trust propulsion, or the traditional transfer approach (conic orbits) in combination with the libration point regimes.

Nevertheless there exist situations where the techniques presented in this section might work without further assistance. This includes missions towards Mars and Venus and specially missions related to the moons of planets. In this later case, JIMO and the *Petit Grand Tour* of the moons of Jupiter are examples where the techniques associated with the Poincaré sections can be used as mission design tools to obtain cheap transfers between the moons.

As an example and complement, let us comment the procedure that in [127] led to the construction of a given itinerary to the moons of Jupiter. Using the above mentioned database of Poincaré sections one should be able to systematise and automatise the computations.

The first step is to approximate a spacecraft motion in the $n+1$ body gravitational field of Jupiter and n of its planet-sized moons into several segments of purely three body motion involving Jupiter, the ith moon, and the spacecraft. Koon et al. studied a transfer from Ganymede to Europa and found that the fuel consumption for impulsive burns, as measured by the total norm of velocity displacements, Δv, to be less than half the Hohmann transfer value which is about 1500 m/s. Further studies using the same approach down-load this value to 20 m/s. The line of the tour is as follows: starting beyond Ganymede's orbit, the spacecraft is ballistically captured by Ganymede, orbits it once, escapes in the direction of Europa, and ends in a ballistic capture at Europa.

One advantage of this Petit Grand Tour as compared with the Voyager-type fly-bys is the "leap-frogging" strategy. In this new approach to mission design, the spacecraft can orbit a moon in a loose temporary capture orbit for a desired number of circuits, escape the moon, and then perform a transfer delta-v to become ballistically captured by a nearby moon for some number of revolutions about that moon, etc. Instead of fly-bys lasting only seconds, a scientific spacecraft can orbit several different moons for any desired duration. Furthermore, the total delta-v necessary is much less than that necessary using purely two-body motion segments. The design of the Petit Grand Tour in the planar case is guided by two main ideas (see [127]) that can be implemented using the previous gadgets.

1. The motion of the spacecraft in the gravitational field of the three bodies Jupiter, Ganymede, and Europa is approximated by two segments of purely three body motion in the planar, circular, restricted three-body model. The trajectory segment in the first three body system, Jupiter-Ganymede-spacecraft, is appropriately patched to the segment in the Jupiter-Europa-spacecraft three-body system.

2. For each segment of purely three body motion, the invariant manifolds tubes of L_1 and L_2 periodic orbits leading toward or away from temporary capture around a moon, as in Figure 4.16, are used to construct an orbit with the desired behaviours. This initial solution is then refined to obtain a trajectory in a more accurate four-body model.

The patched three-body model considers the motion of a particle (or spacecraft) in the field of n bodies, considered two at a time, for instance, Jupiter and its ith moon, M_i. When the trajectory of a spacecraft comes close to the orbit of M_i, the perturbation of the spacecraft's motion away from purely Keplerian motion about Jupiter is dominated by M_i. In this situation, we say that the spacecraft's motion is well modeled by the Jupiter-M_i-spacecraft restricted three-

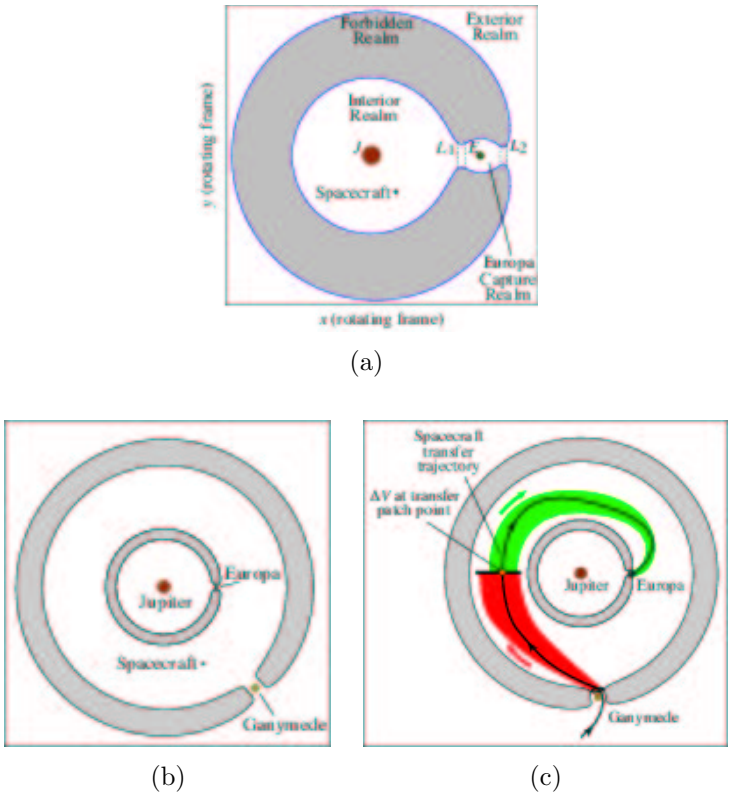

Figure 4.16: The patched three-body model. (a) The co-orbiting frame with Europa is shown, otherwise known as the *rotating frame*. The spacecraft's motion in each Jupiter-moon-spacecraft rotating frame is limited to the region in white due to constant energy in that system (constant Jacobi integral). We work with three-body energy regimes where the region surrounding the Moon's orbit (shaded) is energetically forbidden to spacecraft motion. Note small opening near moon, permitting capture and escape. (b) The four-body system approximated as two nested three-body systems. This picture is only a schematic, as the spacecraft's motion conserves the Jacobi integral in only one system at a time. (c) We seek an intersection between dynamical channel enclosed by Ganymede's L_1 periodic orbit unstable manifold and dynamical channel enclosed by Europa's L_2 periodic orbit stable manifold (shown in schematic). Integrate forward and backward from patch point (with Δv to take into account velocity discontinuity) to generate desired transfer trajectory between the moons (see [14]).

body problem.

There comes a point along the spacecraft's trajectory at which a rocket burn manoeuvre, effecting a change in velocity of magnitude Δv, will make the spacecraft's perturbation switch from being dominated by M_i to being dominated by another moon, M_k. The set of possible "switching orbits," which we will refer to as the *switching region* is the analogue to the "sphere of influence" concept used in the patched-conic approach to trajectory design, which guides a mission designer regarding when to switch the central body for the model of the spacecraft's Keplerian motion. The goal is to find piecewise continuous trajectories in the phase space (continuous in position, but allowing for discontinuities in the velocity, for which impulsive rocket burns will be necessary) which lead a spacecraft from a loose orbit about M_i to a loose orbit about M_k. We refer to the phase space of these loose orbits as the "capture realm." In the procedure we outline, we seek intersections between invariant manifold "tubes" which connect the capture realm of one moon with that of another moon.

In the planar case, as we already explained, these solid tubes are bounded by stable and unstable invariant manifold tubes of periodic orbits about L_1 and L_2, which act as separatrices separating *transit orbits* from *non-transit orbits* (see Figures 4.9 and 4.10). Transit orbits lead toward or away from a capture realm, whereas non-transit orbits do not. The stable and unstable manifolds of the periodic orbits about L_1 and L_2 are the phase space structures that provide a conduit for orbits between realms within each three-body systems as well as between capture realms surrounding primary bodies for separate three-body systems (see [20]).

The study of the planar circular restricted three-body problem (see [20, 187, 70, 127]) revealed the basic structures controlling the dynamics. But current and future missions will require three-dimensional capabilities, such as control of the latitude and longitude of a spacecraft's escape from and entry into a planetary or moon orbit. For example, a future mission to send a probe to orbit Europa may desire a capture into a high inclination polar orbit around Europa ([136, 129, 134, 216]). Three-dimensional capability is also required when decomposing a multi-body system into three-body subsystems which are not co-planar, such as the Earth-Sun-spacecraft and Earth-moon-spacecraft systems. (The tilt in the orbital planes of the Earth around the sun and the moon around the Earth is about 5 degrees.) These demands may imply dropping the restriction of planar motion, and extension of results to the spatial model. In our current work on the spatial three-body problem (see also [148]), we have shown that the invariant manifold structures of the collinear libration points still act as the separatrices between two types of motion: (i) inside the invariant manifold tubes, the motion consists of transit through a neck, a set of paths called transit orbits; (ii) outside the tubes, no such transit motion is possible. We have designed an algorithm for constructing orbits with any prescribed itinerary and obtain some initial results for a basic itinerary (see [14]) which can be applied to the construction of a three-dimensional Petit Grand Tour of the Jovian moon system. By approximating the dynamics of the Jupiter-Europa-Ganymede-spacecraft four-body problem as two three-body subproblems, we seek intersections (in position space only) between the tubes of transit orbits enclosed by the stable and unstable manifold tubes. As shown in Figure 4.17, we have been able to design an example low energy transfer trajectory from an initial Jovian insertion trajectory, leading to Ganymede and finally to Europa, ending in a high inclination orbit around Europa.

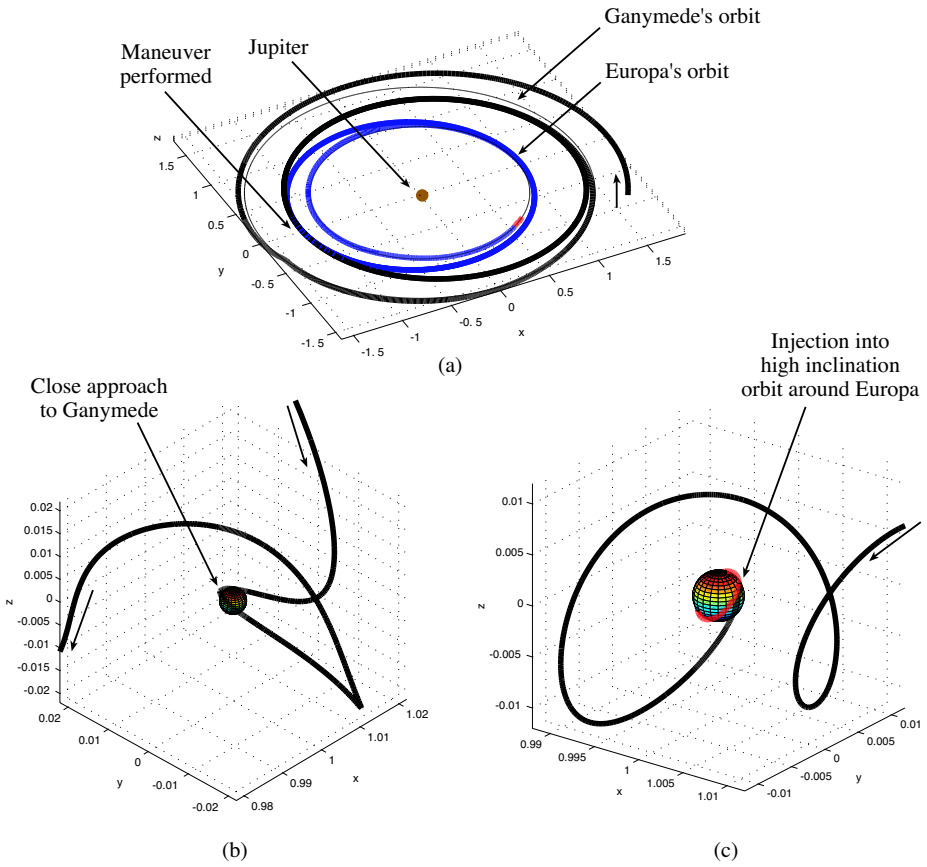

Figure 4.17: The three dimensional Petit Grand Tour space mission concept for the Jovian moons. (a) We show a spacecraft trajectory coming into the Jupiter system and transferring from Ganymede to Europa using a single impulsive manoeuvre, shown in a Jupiter-centred inertial frame. (b) The spacecraft performs one loop around Ganymede, using no propulsion at all, as shown here in the Jupiter-Ganymede rotating frame. (c) The spacecraft arrives in Europa's vicinity at the end of its journey and performs a final propulsion manoeuvre to get into a high inclination circular orbit around Europa, as shown here in the Jupiter-Europa rotating frame (see [14]).

4.3.5 Shoot the Moon

The general idea to obtain low energy transfers to the Moon is similar to the one of the Petit Grand Tour. The goal is to produce transfer orbits from the Earth ending at a lunar capture orbit, using less fuel than in a Hohmann transfer. This problem was first considered by Belbruno and Miller (see [153]) and applied to the Hiten mission in 1991 (see section 2.2.1). The procedure using invariant manifolds and developed by Koon et al. in [20], is based in the construction of trajectories with prescribed itineraries and has the following three key steps:

1. Decouple the Sun–Earth–Moon-Spacecraft system (which is a restricted 4–body problem) in two restricted 3–body problems: the Sun–Earth–Spacecraft and the Earth–Moon-Spacecraft systems.

2. Use the stable/unstable manifolds of the periodic orbits about the Sun–Earth system L_2 libration points to provide a low energy transfer from the Earth to the unstable/stable manifolds of periodic orbits around the Earth–Moon L_2 libration point. The "low energy" required is needed because some manoeuvres must be done in order to depart slightly from the manifolds and also because the manifold intersection is not a true one, since they are related to different restricted problems.

3. Finally, use the stable manifolds of periodic orbits around the Earth–Moon libration points to provide a ballistic capture about the Moon.

In fact, the procedure works as follows: first a suitable Sun–Earth L_2 periodic orbit is computed as well as their stable and unstable manifolds. Some orbits on the stable manifold come close to the Earth and, at the same time, points close to the unstable manifold propagated backwards in time come close to the stable manifold. So, with an small Δv is possible to go from the Earth to the unstable manifold of this periodic orbit. At the same time, when we consider the L_2 point of the Earth–Moon system, is has periodic orbits whose stable manifold "intersect" the unstable manifold that we have reached departing from the Earth and are temporary captured by the Moon. With a second small Δv we can force the intersection to behave as a true one (see Figure 4.18).

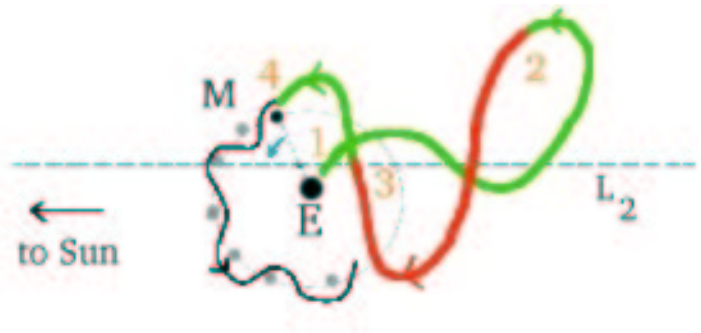

Figure 4.18: Example of a low energy transfer to the Moon. The satellite departs from Earth (1) near the stable manifold of a L_2 orbit in the Sun-Earth sytem and bouncing back near the unstable manifold (2) of the same libration point orbit. Arriving at the L_2 region in the Eart-Moon system, it is inserted at the interior region of the Poincaré section corresponding to the stable manifold and approaching the Moon (3). Finally a small manoeuvre produces the capture by the Moon (4).

In the same framework of cheap missions related to the Moon, an example of a suitable way for a lander to the Moon could be done launching from Earth towards L_1 in the Sun-Earth system and bouncing back to an L_2 libration point orbit in the Earth-Moon system from where using its stable manifold we arrive to the Moon. The mission could extend in the way back to Earth, launching from the Moon towards L_2 in the Sun-Earth system and returning to Earth in a Genesis like trajectory (see Figure 4.19).

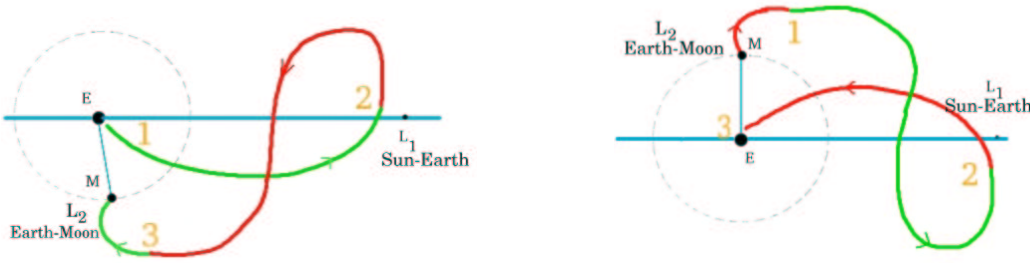

Figure 4.19: Examples of low energy transfers from Earth to Moon (left) and from Moon to Earth. The approach is similar to the described in Figure 4.18.

4.3.6 Asteroid Hazard and Mining

As it has already been commented in section 3.7.3, the exploration of the phase space structure as revealed by the homoclinic/heteroclinic structures and their association with mean motion resonances, may provide deeper conceptual insight into the evolution and structure of the asteroid belt (interior to Jupiter) and the Kuiper belt (exterior to Neptune), plus the transport between these two belts and the terrestrial planet region.

It is estimated that about 1% of the asteroids are in a regime with potential close encounters with the Earth. Potential Earth–impacting asteroids may use the dynamical channels as a pathway to Earth from nearby heliocentric orbits in resonance with the Earth. This phenomena has been observed recently in the impact of comet Shoemaker–Levy 9 with Jupiter, which was in 2:3 resonance with Jupiter just before impact. Of course at some time, many of these asteroids or comets driven by the invariant manifolds of the Sun-Earth libration points will transit the bottleneck that the zero velocity curves draw about the Earth. This fact constitutes a serious hazard, and in fact, there is some evidence that the collision that caused the extinction of the dinosaurs might have been produced by an object in these energy levels.

Sky-watchers located at selected places, such as L_2 in the Sun-Earth libration point, could prevent from possible hazards. In case of detection, only small manoeuvres would be needed to deflect the dangerous body. At the same time, small deviations of the trajectories of some asteroids could be used to station them in selected orbits with the purpose of mining.

4.4 Extensions and Complementary Open Problems

4.4.1 Applications of Libration Point Orbits to Formation Flight

The idea of flying multiple spacecraft with a mutual scientific goal is not new. However, attacking this problem in such a demanding dynamical regime as it is posed by the unique behaviour in the vicinity of the libration points has recently become apparent. Only through a combination of the mathematical tools that have essentially affected a paradigm shift in three-body mission design (e.g., dynamical systems theory), creativity, and confidence in the existing tools has such a mission scenario been realized. One of the most exciting determinations in studies of this type

is that many more valuable mission options are available.

The excellent observational properties of the L_2 point of the Earth–Sun system have lead to consider this location for missions requiring a multiple spacecraft in a controlled formation flying. Darwing, LISA and TPF are three of the more challenging examples of such missions.

Two basic orbital strategies have been analysed for a formation flying mission at the libration points: a *nominal orbit strategy* and a *base orbit strategy*. In the nominal orbit strategy each spacecraft follows its own predefined orbit, while in the base orbit strategy each spacecraft follows an orbit relative to a predefined one, known as the base orbit. The base orbit may have no spacecraft on it. In the next two sections we will briefly discuss the results that have been obtained in both approaches.

The Nominal Orbit Strategy

Barden and Howell [217], [218] and [221] have considered the possibility of using quasi–periodic solutions around the halo orbits and the libration points, as natural locations for a constellation. In their studies, a certain number of spacecraft are initially placed along a planar curve close to any of the two kinds of the above mentioned tori and, in a first step, they analyse their natural motion (see Figure 4.20).

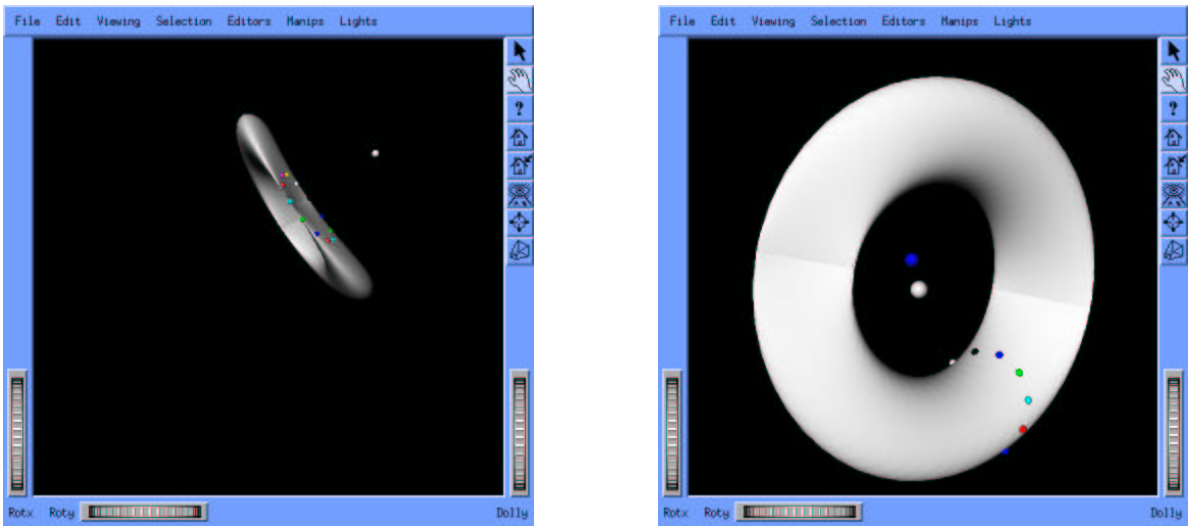

Figure 4.20: Simulation of formation flight in a quasi-halo orbit. The white torus represents the quasi-halo and the small coloured spheres on it, the spacecraft. The remaining two spheres (white and blue) represent the Earth and the Sun.

In the quasi-halo case, the torus itself is related to an underlying periodic halo orbit. As the initial planar curve evolves in time along the torus, in the direction of motion of the underlying halo orbit, there are certain aspects of the evolution of the curve that are of particular interest. The curve appears simply closed and nearly circular in configuration space. When the amplitude of the curve is small, i.e., less than 1000 km, the curve is considered to be planar. However, as the curve evolves, it changes size and shape. By identifying the plane containing the curve, one

can view the constellation from a point along the normal to the plane. Although the plane will not persist, the deviations from the reference one are small: less than 1% of the distance between spacecraft when they are on opposite sides of the constellation. In addition to the variations in size and shape, there is a winding aspect of the motion due to the change of the relative locations of the points of the curve. This is because the torus is self–intersecting in the configuration space at the two xz-plane crossings.

This type of natural motion, as an option for formation flying, is very appealing from a dynamical perspective. From a practical standpoint, however, this formation will likely not meet the constraints and scientific requirements of a generic mission. The likely scenario is that some pre-specified formation will be mandated.

Barden and Howell consider six spacecraft evenly distributed on a circle of radius 100 km in a plane coincident with the rotating libration point coordinates y and z (parallel to the yz plane) and around a Lissajous type orbit as an example of non-natural formation. At each manoeuvre, the formation is forced to be on the plane, but there will be out-of-plane excursions for each of the spacecraft between the manoeuvres; the amplitude of the excursions will vary for each vehicle. In a first simulation, four manoeuvres per revolution in the xy plane (nearly equally spaced in time) are executed, where all six spacecraft implement their respective manoeuvres simultaneously. The size of the manoeuvres ranges from 0.043 m/s to 0.12 m/s achieving a total cost of 2.93 m/s for a duration of 355 days (which is equivalent to two revolutions along the baseline Lissajous trajectory in the xy plane. These manoeuvres are necessary to define a nominal path for each of the spacecraft; additional station-keeping manoeuvres will also be required to accommodate errors and uncertainties. Even for the baseline motion, however, out-of-plane excursions between the manoeuvres reach a maximum value at any time of approximately 20 km in this example. The only means of reducing this deviation is to increase the frequency of the manoeuvres. With manoeuvres every 11 days, instead of 44 days, the out-of-plane deviations never exceed 1.8 km. The total cost is of 2.77 m/s which is smaller than the 2.93 m/s required. However, fixed planes can be specified where the total cost increases with the increased number of manoeuvres.

Formation Flight in the Vicinity of a Libration Point: The TPF Case

The TPF Mission (Terrestrial Planet Finder) is one of the pieces of the NASA Origins Program. The goal of TPF is to identify terrestrial planets around stars nearby the Solar System (see [219]). For this purpose, a space-based infrared interferometer with a baseline of approximately 100 m is required. To achieve such a large baseline, a distributed system of five spacecraft flying in formation is an efficient approach. Since the TPF instruments need a cold and stable environment, near Earth orbits are not suitable. Two potential orbits have been identified: a SIRTF-like heliocentric orbit and a libration orbit near the L_2 Lagrange point of the Earth-Sun system.

There are several advantages of using a libration orbit near L_2. Such orbits are easy and inexpensive to get to from Earth. Moreover, for missions with heat sensitive instruments (e.g. IR detectors), libration orbits provide a constant geometry for observation with half of the entire celestial sphere available at all times. The spacecraft geometry is nearly constant with the Sun, Earth, Moon always behind the spacecraft thereby providing a stable observation environment, making observation planning much simpler. In this section we present some of the results of [220]

which contain preliminary computations of the TPF mission.

From the dynamical point of view, the TPF Mission can be broken into four phases:

1. **Launch and Transfer Phase.** For the simulation, it is assumed that the spacecraft starts in a typical 200 km altitude parking orbit at 28.5 deg inclination and a halo orbit is used as a target Baseline Orbit. At the appropriate time, the spacecraft performs a major manoeuvre of about 3200 m/s. This injects the spacecraft onto the stable manifold of the halo orbit to begin the Transfer Phase. The transfer trajectory is designed by using an orbit of the stable manifold with a suitable close approach to the Earth.

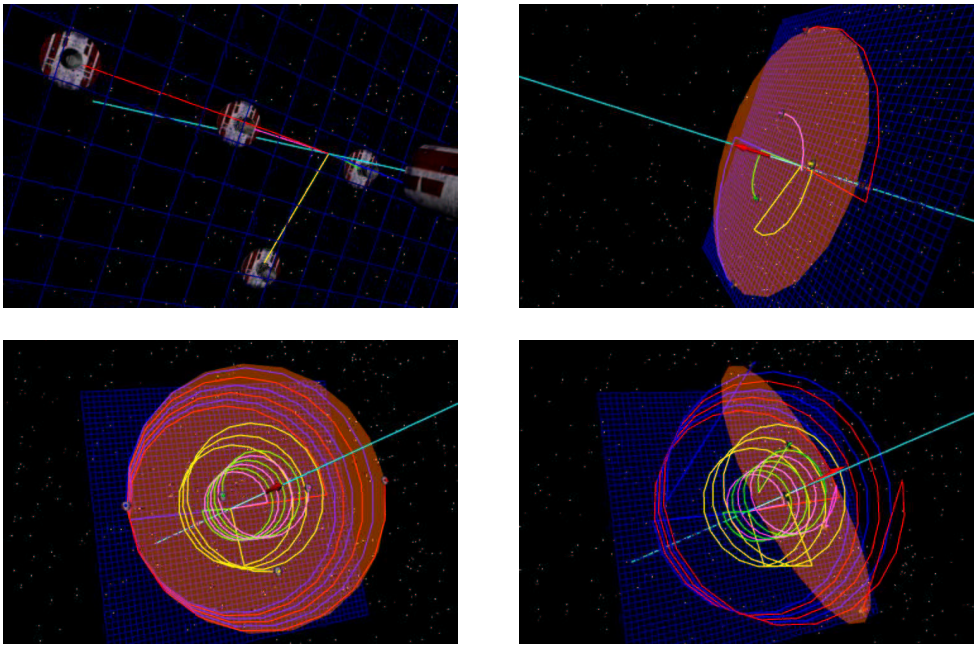

Figure 4.21: Simulation of some basic manoeuvres for TPF.

Deployment Time	$R = 1$	$R = 3$
1 h	$5.5 \times 10^{-2}\, D$	$5.6 \times 10^{-2}\, D$
3 h	$1.9 \times 10^{-2}\, D$	$2.7 \times 10^{-2}\, D$
5 h	$1.3 \times 10^{-2}\, D$	$2.2 \times 10^{-2}\, D$
10 h	$0.9 \times 10^{-2}\, D$	$1.8 \times 10^{-2}\, D$
100 h	$0.5 \times 10^{-2}\, D$	$1.5 \times 10^{-2}\, D$

Table 4.1: Estimation of the deployment cost in cm/s as a function of the deployment time.

2. **Deployment Phase.** It is assumed that all the spacecraft of the formation reach the Baseline Orbit in a single spacecraft. This trigger out the Deployment Phase. The five satellites are manoeuvred to reach their initial positions on the different points of a 20-gon of 100m diameter at the same time. The Deployment Phase can last for several hours,

and simulations between 1 and 10 hours have been done. Assuming that deployment is performed using two impulsive manoeuvres and that a selected satellite has to be put in the edge of an 20-gon of diameter D meters and it will be doing R revolutions per day, the Table 4.1 summarises the estimation of the deployment cost in cm/s as a function of the deployment time.

3. **Pattern Maintenance Phase.** Once the initial configuration has been established, the spacecraft will manoeuvre to follow the edge of the 20-gon to provide a suitable spin rate for the formation. The nominal spin rate used for this simulation is 360 deg every 8 hours. The period where the pattern is maintained is called the Pattern Maintenance Phase. Assuming that a spacecraft is spinning in a 20-gon of diameter D meters and doing R revolutions per day, is obtained that: *Formation maintenance cost per satellite in cm/s per day* $= 0.0023\ D\ R^2$.

4. **Reconfiguration Phase:** Once sufficient data has been acquired for one star system, the formation will be pointed to another star for observation. Repointings occur during the Reconfiguration Phase. The computations for the Reconfiguration Phase cost is similar to the Deployment Phase except for the fact that the spacecraft do not depart from the same location (i.e. the Mother Ship).

Estimation of TPF Budget for a Ten Year's Mission

Table 4.2 presents an estimation of the Δv cost associated to satellites located in an N-gon of 50 and 100 m around a L_2 base halo orbit spinning at the rate of 3 revolutions per day and for a 10 year's mission is also given.

Manoeuvre cost per S/C	50 m Diameter Case	100 m Diameter Case
Halo Insertion	5 m/s	5 m/s
Initial Deployment (10h)	0.009 m/s	0.018 m/s
Formation Maintenance	0.1 m/s/day	0.2 m/s/day
Station Keeping (z-Axis)	3 m/s/year	3 m/s/year
Reconfiguration (estimate)	0.05 m/s/day	0.1 m/s/day
10 Year Δv Budget	583 m/s	1130 m/s

Table 4.2: Estimation of the Δv cost associated to satellites located in an N-gon around a L_2 base halo orbit.

Halo insertion cost due to transfer from the Earth and station keeping, including avoidance of the exclusion zone that could be required in case of using an L_2 Lissajous orbit, is also included. The usual station keeping can be assumed to be absorbed in the so often performed pattern maintenance manoeuvres. Manoeuvres are also considered to be done with no error, so control correction manoeuvres are not included.

Some Issues that Should Be Studied in Formation Flight

Definition of the basic trajectory

The definition of the nominal trajectory of a single spacecraft is a concept that has been widely used. The problem arises for a constellation of several satellites around the libration points. In this case we have to face with magnitudes with very different orders. For instance, in the TPF case

- Distance from Earth to spacecraft $\sim 1.5 \sim 10^6$ km.
- Distance between spacecraft ~ 100 m or less.
- Maximum deviation between two spacecraft ~ 20 cm. These maximum deviations allowed are smaller than the usual tracking errors for libration point satellites. This means that the navigation formation must be done autonomously.

The definition of the basic trajectory, suitable for working purposes, requires the specification of two different things:

- The path followed by some distinguished point of the constellation: the basic nominal orbit.
- The relative motions of all the spacecraft with respect to the basic nominal orbit.

From the practical point of view, this implies that two separate station keeping procedures must be developed:

- One for preventing deviations of the spacecraft form the basic trajectory. This requires some synchronism in the execution of the manoeuvres, in order to prevent possible large deviations between satellites due to the high instability of the libration point orbits.
- One for the acquisition and maintenance of precise formation.

Note that these two different kind of manoeuvres are also of different orders of magnitude.

Estimation of station keeping costs

It is known that for the maintenance of a single satellite around a libration point orbit, a few cm/s per year of Δv are needed. It remains to be analysed the cost for a set of linked (highly correlated orbits) satellites, which is clearly not equal to the sum of the individual costs at all, because of the instability. This station keeping can not be performed with some of the standard strategies which just keep the spacecraft in a neighbourhood of a given nominal orbit.

Once an specific configuration has been fixed (for instance a collinear one around an equilibrium point, with two spacecraft with a separation of 100 m rotating on a fixed (sidereal) plane with an angular velocity of 3 revs/day) a first estimation of the Δv required for keeping the formation can be done computing the residual accelerations. These are the differences between the accelerations given by the vector-field equations and the true acceleration due to the proper motions of the spacecraft. For the above example, some first estimations give a value of 20 cm/s

per day, for each satellite. The same configuration, but rotating with an angular velocity of 1 rev/day, requires 2.5 cm/s per day.

We note that continuous thrust must be used to keep the formation. If the continuous thrust is turned off, it is important to know the time that the formation will still be within constraints.

Configuration changes

The problem of changing a given configuration into another one, can be studied in a first approximation as a "Lambert like" problem connecting two different states in the nonlinear RTBP regime. The basic idea consists of following the natural dynamics for the orbits around the libration points. For this purpose, we also suggest to set a good parametrisation of the space of solutions allowing an easy identification of the states of a spacecraft. The solution of this problem will give impulsive manoeuvres at the initial and final states, which can be used as initial guesses in a more refined and realistic procedure.

Transfer from the Earth to the basic trajectory and deployment of the constellation

For a constellation of few and not very large satellites, in a formation of a few hundred meters of diameter, it seems reasonable to study the transfer as a single body that has to be deployed after reaching the basic nominal orbit. The study of the transfer is rather well known, since it is easy to get good approximations of the invariant manifolds of the nominal solutions (at least in the (Earth+Moon)-Sun situation). Once the final nominal orbit is reached, the problem could be formulated in two steps:

- In the first step, the linked cluster of satellites must change its orientation, using suitable attitude manoeuvres (one for the acquisition and maintenance of precise formation).
- In the second step the spacecraft should reach their final states using the acquisition formation like manoeuvres. Since the manoeuvres must avoid collisions, the design of the deployment becomes more complicated.

Formation Maintenance

Linear stabilising control techniques may be sufficient for formation maintenance, since only small changes about a known nominal trajectory are presumably needed. Such techniques are well developed for single vehicles in the context of flight control of aircraft, but the challenge of coordinated control of multiple vehicles remains difficult. However, some tools of this sort are available and some more are being developed in the context of Earth-bound satellites, aircraft formations, and flocks of underwater vehicles.

Formation Reconfiguration

For large dynamic motions beyond the linear regime, such as formation reconfiguration, nonlinear tools such as optimal control that can handle low thrust trajectory design are most likely needed. The design of low-thrust trajectories in nonlinear regimes still requires further development. Primer vector theory, even for the impulsive case, is not immediately extensible from the two-body to the three-body problem. Existing numerical algorithms suffer from the numerical sensitivity of the underlying nonlinear problem. Tools such as modern software for optimal reconfiguration of a satellite group and which make use of the mechanical structure of the problem seem to be appropriate in some cases.

4.4.2 Obtaining Better Models of Motion

For any mission design, the first approach has to be the study of the problem in the simplest but meaningful situation. This means that simple idealistic models should be used to get a first idea of the different magnitudes involved. Some of these models are:

- For the motion, of either a single spacecraft or a constellations, around the equilibrium points of the (Earth+Moon)-Sun system, the RTBP is a good starting model. The effect of the remaining bodies of the solar system is small. This problem is rather well known and the dynamics around the equilibrium points is well understood.

- For motions around the triangular equilibrium points of the Earth–Moon system the RTBP is not a good model of motion. The effect of the Sun is large and the real dynamics around the equilibrium points seems to be, in some cases, far from the one corresponding to the RTBP model. More accurate four body problems should be introduced and studied including the Sun, the Earth and the Moon as primaries.

These four body models should be used to reinforce the study problems like

- The ones associated with "Le Petit Grand Tour".

- Low energy transfers to a ballistic capture at the Moon.

- Low energy transfers to mild unstable orbits around the triangular equilibrium points of the Earth-Moon system.

The better understanding of these problems should clarify the weak stability boundary concept, as defined by Belbruno. Some of the magnitudes that should be estimated with these simple models are:

- The nominal orbit to be used as a first guess for more refined models.

- The requirements for the station keeping within the desired accuracy.

- Simple transfer trajectories to change formation configurations.

Aside from the gravitational models, some effort should be done in the development of models including the solar radiation pressure. This can be useful for the station keeping strategies since, if the station keeping manoeuvres can be executed using solar radiation pressure, the contamination of the spacecraft due to the execution of an impulsive manoeuvre is avoided, and this enlarges the observation intervals of the spacecraft. In addition, the solar radiation pressure can play an important role in the formation flight problem, when the requirements for the mutual distances are very severe.

4.4.3 Issues that Should Be Studied Concerning the Space Gateway

- Precise determination of libration point orbits in the Earth-Moon system for long time spans.
- Determination of the regions on the surface on the Moon that guarantee a return to the libration point, for different values of the Δv to be used in the departure.
- For fixed values of Δv (for the departure from the Moon) and an upper bound Δt for the transfer time, determination of the regions on the surface of the Moon that guarantee a return to the libration point orbit.
- Parametric study of the Δv and transfer time required for the transfer to and from the Earth to the libration point orbit, for a large set of libration point orbits.
- Contingency plans for different kinds of errors in the execution of manoeuvres.

Moreover, in the case of human support the space mission designers must balance the benefits versus payoffs taking into account the following items,

- Crew de-conditioning due to long-term weightlessness.
- Crew exposure to galactic cosmic radiation and solar particle events.
- Limitations on mission opportunities and stay times at the libration points, for missions to/from an Earth based parking orbit facility (i.e., International Space Station).
- Additional mass associated with crew habitat and consumables.
- Additional propellant mass associated with faster transfers to/from the libration points and associated transfer abort considerations.

Bibliography

Models of Motion Near the Equilibrium Points

[1] M.A. Andreu. *The Quasi-bicircular Problem.* PhD thesis, Dept. Matemàtica Aplicada i Anàlisi, Universitat de Barcelona, Barcelona, Spain, 1999.

[2] M.A. Andreu. Dynamics in the Center Manifold Around L_2 in the Quasi-Bicircular Problem. *Celestial Mechanics and Dynamical Astronomy*, 84(2):105–133, 2002.

[3] F. Gabern and À. Jorba. A Restricted Four-Body Model for the Dynamics near the Lagrangian Points of the Sun-Jupier System. *Discrete and Continuous Dynamical Systems. Series B*, 1(2):143–182, 2001.

[4] G. Gómez, J. Masdemont, and J.M. Mondelo. Solar System Models with a Selected Set of Frequencies. *Astronomy & Astrophysics*, 390:733–749, 2002.

[5] G. Gómez, M. Marcote, and J.M. Mondelo. The Invariant Manifold Structure of the Spatial Hill's Problem. Preprint, 2004.

[6] K.C. Howell and J.J. Guzman. Spacecraft Trajectory Design in the Context of a Coherent Restricted Four–Body problem with Application to the MAP Mission. In *Congress of the International Astronautical Federation*, volume IAF Paper 00–A.5.06, 2000.

[7] L. Mohn and J. Kevorkian. Some Limiting Cases of the Restricted Four Body Problem. *The Astronomical Journal*, 72:959–963, 1967.

[8] D.J. Scheeres and N.X. Ving. The Restricted Hill Four–Body Problem. In *43rd Congress of the International Astronautical Federation,* IAF Paper 92–0006, 1992.

[9] D.J. Scheeres. The Restricted Hill Four–Body Problem with Applications to the Earth–Moon–Sun System. *Celestial Mechanics and Dynamical Astronomy*, 70(2):75–98, 1998.

[10] C. Simó and T.J. Stuchi. Central Stable/Unstable Manifolds and the Destruction of KAM Tori in the Planar Hill Problem. *Physica D*, 140(1–2):1–32, 2000.

[11] W. Wiesel. The Restricted Earth–Moon–Sun Problem I: Dynamics and Libration Point Orbits. Technical report, Air Force Institute of Technology Wright-Patterson AFB, Ohio, 45433, 1984.

The Phase Space Around the Collinear Points

[12] J. Cobos and J.J. Masdemont. Astrodynamical Applications of Invariant Manifolds Associated with Collinear Lissajous Libration Orbits. In *Libration Point Orbits and Applications*, 2003.

[13] C. Díez, À. Jorba, and C. Simó. A Dynamical Equivalent to the Equilateral Libration Points of the Earth-Moon System. *Celestial Mechanics*, 50(1):13–30, 1991.

[14] G. Gómez, W.S. Koon, M.W. Lo, J.E. Marsden J.J. Masdemont and S.D. Ross. Connecting Orbits and Invariant Manifolds in the Spatial Restricted Three-Body Problem. *Nonlinearity*, 17:1571–1606, 2004.

[15] G. Gómez and J.M. Mondelo. The Phase Space Around the Lagrange Points of the RTBP. *Physica D*, 157(4):283–321, 2001.

[16] J. Györgyey. On the Non–Linear Stability of Motion Around L_3 in the Elliptic Restricted Problem of the Three Bodies. *Celestial Mechanics*, 36(3):281–285, 1985.

[17] À. Jorba and J.J. Masdemont. Dynamics in the Center Manifold of the Restricted Three–Body Problem. *Physica D*, 132:189–213, 1999.

[18] À. Jorba and J.J. Masdemont. Nonlinear Dynamics in an Extended Neighbourhood of the Translunar Equilibrium Point. In C. Simó, editor, *Hamiltonian Systems with Three or More Degrees of Freedom*, 1999.

[19] À. Jorba and J. Villanueva. Numerical Computation of Normal Forms Around Some Periodic Orbits of the Restricted Three Body Problem. *Physica D*, 114:197–229, 1998.

[20] W.S. Koon, M.W. Lo, J.E. Marsden, and S.D. Ross. Heteroclinic Connections Between Periodic Orbits and Resonance Transitions in Celestial Mechanics. *Chaos*, 10(2):427–469, 2000.

[21] J. Llibre, R. Martínez, and C. Simó. Transversality of the Invariant Manifolds Associated to the Lyapunov Family of Periodic Orbits Near L_2 in the Restricted Three–Body Problem. *Journal of Differential Equations*, 58:104–156, 1985.

[22] J.J. Masdemont. High Order Expansions of Invariant Manifolds of Libration Point Orbits with Applications to Mission Design. *Preprint*, 2004.

[23] J.M. Mondelo. *Contribution to the Study of Fourier Methods for Quasi–Periodic Functions and the Vicinity of the Collinear Libration Points*. PhD thesis, Dept. Matemàtica Aplicada i Anàlisi, Universitat de Barcelona, Barcelona, Spain, 2001.

Determination of Periodic Orbits Around the Collinear Equilibrium Points

[24] M.A. Andreu and C. Simó. Translunar Halo Orbits in the Quasibicircular Model. In A. Roy, editor, *The Dynamics of Small Bodies in The Solar System*. NATO, ASI (Maratea, Italy), 1998.

[25] T.A. Bray and C.L. Goudas. Three Dimensional Periodic Oscillations About L_1, L_2, L_3. *Advances in Astronomy and Astrophysics*, 5:71–130, 1967.

[26] J.V. Breakwell and J. Brown. The Halo Family of Three Dimensional Periodic Orbits in the Earth–Moon Restricted Three Body Problem. *Celestial Mechanics*, 20(4):389–404, 1979.

[27] E.J. Doedel, R.P. Paffenroth, H.B. Keller, D.J. Dichmann, J. Galán-Vioque, and A. Vanderbauwhede. Computation of Periodic Orbits of Conservative Systems with Applications to the 3–body Problem. *Int. J. Bifurcation and Chaos*, 2002.

[28] R.W. Farquhar and A.A. Kamel. Quasi-Periodic Orbits About the Translunar Libration Point. *Celestial Mechanics*, 7(4):458–473, 1973.

[29] C.L. Goudas. Three Dimensional Periodic Orbits and their Stability. *Icarus*, 2:1–18, 1963.

[30] P. Guillaume. New Periodic Solutions of the Three Dimensional Restricted Problem. *Celestial Mechanics*, 10(4):475–495, 1974.

[31] M. Hénon. Vertical Stability of Periodic Orbits in the Restricted Problem I. Equal Masses. *Astronomy & Astrophysics*, 28:415–426, 1973.

[32] T.A. Heppenheimer. Out–of–Plane Motion About Libration Points: Nonlinearity and Eccentricity Effects. *Celestial Mechanics*, 7:177–194, 1973.

[33] K.C. Howell. Three Dimensional Periodic Halo Orbits. *Celestial Mechanics*, 32(1):53–72, 1984.

[34] K.C. Howell and H.J. Pernicka. Numerical Determination of Lissajous Trajectories in the Restricted Three-Body Problem. *Celestial Mechanics*, 41(1–4):107–124, 1988.

[35] S. Icthiaroglou, K. Katopodis, and M. Michalodimitrakis. Restricted Problem: Families of Vertical Critical Periodic Orbits. *Astronomy & Astrophysics*, 90:324–326, 1980.

[36] M. Michalodimitrakis. A New Type of Connection Between the Families of Periodic Orbits of the Restricted Problem. *Astronomy & Astrophysics*, 64(1):83–86, 1978.

[37] F.T. Nicholson. Effect of Solar Perturbation on Motion Near the Collinear Earth–Moon Libration Points. *AIAA Journal*, 5(12):2237–2241, 1967.

[38] C.A. Ocampo and G.W. Rosborough. Solar Sail Trajectories Near the Sun–Earth L_1 Libration Point. *Advances in the Astronautical Sciences*, 76:1253–1272, 1991.

[39] H.J. Pernicka and K.C. Howell. Sun–Earth Libration Point Trajectories that Avoid the Solar Exclusion Zone. *Journal of the Astronautical Sciences*, 38(3):269–288, 1990.

[40] J.D. Porter. Final Report for Lunar Libration Point Flight Dynamics Study. NASA-GSFC Contract NAS-5-11551, General Electric Co. April 1969.

[41] F. C. Vandenbussche, P. Temporelli. The Trip to the L1 Halo Orbit. *ESA Bulletin* 88, 1996.

[42] C.G. Zagouras and P.G. Kazantzis. Three-Dimensional Periodic Oscillations Generating From Plane Periodic Ones Around the Collinear Lagrangian Points. *Astrophysics Space Science*, 61(4):389–409, 1979.

Analytical Computations

[43] M.L. Lidov et al. Semi–Analytical Method for Calculationg the Motion of a Space Vehicle in the Vicinity of a Collinear Libration Point. *Cosmic Research*, 14(6):775–785, 1976.

[44] M.L. Lidov et al. Analytical Method of Calculating Motion in a Halo Orbit and the Problem of Screening the Spacecraft from Solar Radiation in Project Relict–2. *Cosmic Research*, 32(1):1–28, 1994.

[45] R.W. Farquhar. The Moon's Influence in the Location of the Sun–Earth Exterior Libration Point. *Celestial Mechanics*, 2(2):131–133, 1970.

[46] G. Gómez, À. Jorba, J.J. Masdemont, and C. Simó. *Dynamics and Mission Design Near Libration Point Orbits – Volume 3: Advanced Methods for Collinear Points*. World Scientific, 2000.

[47] G. Gómez, J. Llibre, R. Martínez, and C. Simó. *Dynamics and Mission Design Near Libration Point Orbits – Volume 1: Fundamentals: The Case of Collinear Libration Points*. World Scientific, 2000.

[48] G. Gómez, J.J. Masdemont, and C. Simó. Lissajous Orbits Around Halo Orbits. *Advances in the Astronautical Sciences*, 95:117–134, 1997.

[49] G. Gómez, J.J. Masdemont, and C. Simó. Quasihalo Orbits Associated with Libration Points. *Journal of The Astronautical Sciences*, 46(2):1–42, 1999.

[50] K.C. Howell and J.V. Breakwell. Almost Rectilinear Halo Orbits. *Celestial Mechanics*, 32(1):29–52, 1984.

[51] J.M. Jensen. Hamiltonian Bifurcation Theory Applied to the Halo Periodic Orbits in the Restricted Three Body Problem. Master's thesis, The University of Texas at Austin, Austin, Texas, USA, 1996.

[52] M.L. Lidov and V.Y. Rabinovich. Investigation of Families of Three–Dimensional Periodic Orbits of the Three–Body Problem. *Cosmic Research*, 17(3), 1979.

[53] A.P. Markeev. Two–Dimensional Periodic Motion of a Satellite Relative to the Center of Mass Near a Collinear Libration Point. *Cosmic Research*, 17(3), 1979.

[54] D.L. Richardson. Analytical Construction of Periodic Orbits About the Collinear Points. *Celestial Mechanics*, 22(3):241–253, 1980.

[55] D.L. Richardson. Halo Orbit Formulation for the ISEE-3 Mission. *Journal of Guidance and Control*, 3(6):543–548, 1980.

[56] D.L. Richardson. A note on the Lagrangian Formulation for Motion About the Collinear Points. *Celestial Mechanics*, 22(3):231–235, 1980.

[57] D.L. Richardson and N.D. Cary. A Uniformly Valid Solution for Motion About the Interior Libration Point of the Perturbed Elliptic-Restricted Problem. In *AAS/AIAA Astrodynamics Specialist Conference, AAS Paper 75-021.*, July 1975.

[58] L. Steg and J.P: De Vries. Earth–Moon Libration Points: Theory, Existente and Applications. *Space Science Reviews*, 5(3):210–233, 1966.

[59] W. Wiesel. Floquet Reference Solutions for the Lunar Theory and the Jovian Moon System. *Journal of Guidance and Control*, 4(6):586–590, 1981.

Weak Stability Boundaries

[60] M. Belló-Mora, F. Graziani, P. Teofilato C. Circi, M. Porfilio and M. Hechler: 'A Systematic Analysis on Weak Stability Boundary Transfers to the Moon'. *International Astronautical Federation*, 2000.

[61] E. Belbruno: 'Lunar Capture Orbits, a Method for constructing Earth-Moon Trajectories and the Lunar GAS Mission'. *AIAA paper No. 87-1054*, 1987.

[62] E. Belbruno and J.K. Miler: 'A Ballistic Lunar Capture Trajectory for the Japanese Spacecraft Hiten'. *JPL, IOM 312/90.4–1371*, 1990.

[63] E. Belbruno and J. Miller: 'Sun-Perturbed Earth to Moon Transfers with Ballistic Capture'. *Journal of Guidance, Control and Dynamics.* **16**, 770–775, 1993.

[64] E. Belbruno: 'The Dynamical Mechanism of Ballistic Lunar Capture Transfers in the Four Body Problem from the Perspective of Invariant Manifolds and Hill's Regions'. *CRM, Preprint n. 270*, Barcelona, 1994.

[65] E. Belbruno R. Humble and J. Coil: 'Ballistic Capture Lunar Transfer Determination for the US Air Force Academy Blue Moon Mission'. *AIAA/AAS Astrodynamics Specialist Conference.* Paper No. 97-171, 1997.

[66] E. Belbruno: 'Calculation of Weak Stability Boundary Ballistic Lunar Transfer Trajectories'. *AIAA/AAS Astrodynamics Specialist Conference.* Paper No. 2000-4142, 2000.

[67] E. Belbruno: 'Analytic Estimation of Weak Stability Boundaries and Low Energy Transfers'. *Contemporary Mathematics.* **292**,17–45, 2002.

[68] E. Belbruno: *Capture Dynamics and Chaotic Motions in Celestial Mechanics.* Princeton University Press, 2004.

[69] C. Circi and P. Teofilato: 'On the Dynamics of Weak Stability Boundary Lunar Transfers'. *Celestial Mechanics and Dynamical Astronomy.* **79**,41–72, 2001.

[70] W.S. Koon, M.W. Lo, J.E. Marsden and S.D. Ross: 'Low Energy Transfer to the Moon'. *Celestial Mechanics and Dynamical Astronomy.* **81**,63–73, 2001.

Station Keeping and Control

[71] J.V. Breakwell. Investigation of Halo Satellite Orbit Control. Technical Report CR–132858, NASA, 1973.

[72] J.V. Breakwell, A.A. Kamel, and M.J. Ratner. Station-Keeping for a Translunar Communications Station. *Celestial Mechanics*, 10(3):357–373, 1974.

[73] D. Cielaszyk and B. Wie. New Approach to Halo Orbit Determination and Control. *Journal of Guidance, Control and Dynamics*, 19(2):266–273, 1996.

[74] G. Colombo. The Stabilization of an Artificial Satellite at the Inferior Conjunction Point of the Earth–Moon System. Technical Report 80, Smithsonian Astrophysical Observatory Special Report, 1961.

[75] H.M. Dusek. Optimal Station Keeping at Collinear Points. *Progress in Astronautics and Aeronautics*, 17, 1966.

[76] P.E. Elyasberg, T.A. Timokhova, and M.N. Boyarski. The Flight Maintenance in the Vicinity of a Libration Centre and the One–Impulse Transfer Trajectory to the Limited Orbit in this Region. In *First International Symposium on Spacecraft Flight Dynamics, ESA SP–255*, pages 55–64. European Space Agency (Darmstadt, Germany), 1986.

[77] J.A. Erickson and A.B. Glass. Implementation of ISEE–3 Trajectory Control. In *AAS/AIAA Astrodynamics Specialist Conference*, 1979.

[78] E.A. Euler and E.Y. Yu. Optimal Station Keeping at Collinear Points. *Journal Spacecraft and Rockets*, 8:513–517, 1971.

[79] R.W. Farquhar. Station–Keeping in the Vicinity of Collinear Libration Points with an Application to a Lunar Communications Problem. In *Space Flight Mechanics, Science and Technology Series*, volume 11, pages 519–535. American Astronautical Society, New York, 1967.

[80] R.W. Farquhar. The Control and Use of Libration Point Satellites. Technical Report TR R346, Stanford University Report SUDAAR–350 (1968). Reprinted as NASA, 1970.

[81] R.W. Farquhar. Limit Cycle Analysis of a Controlled Libration Point Satellite. *Journal of the Astronautical Sciences*, 17:267–291, 1970.

[82] R.W. Farquhar. Comments on Optimal Controls for Out of Plane Motion About the Translunar Libration Point. *Journal Spacecraft and Rockets*, 8(7):815–816, 1971.

[83] P. Di Giamberardino and S. Monaco. On Halo Orbits Spacecraft Stabilization. *Acta Astronautica*, 38:903–925, 1996.

[84] G. Gómez, K.C. Howell, J. Masdemont, and C. Simó. Station-Keeping Strategies for Translunar Libration Point Orbits. *Advances in the Astronautical Sciences*, 99:949–967, 1998.

[85] G. Gómez, J. Llibre, R. Martínez, and C. Simó. Station Keeping of Libration Point Orbits. Technical Report ESOC Contract 5648/83/D/JS(SC), Final Report, ESA, 1985.

[86] G. Gómez and J.J. Masdemont. Refinements of a Station–Keeping Strategy for Libration Point Orbits. Preprint, 2003.

[87] T.A. Heppenheimer. Optimal Controls for Out of Plane Motion About the Translunar Libration Point. *Journal of Spacecraft and Rockets*, 7:1088–1092, 1970.

[88] H. Heuberger. Halo Orbit Station Keeping for ISEE–C. In *AAS/AIAA Spaceflight Mechanics Conference*, 1977.

[89] K.C. Howell and S.C. Gordon. Station–Keeping Strategies for Libration Point Orbits. School of Aeronautics and Astronautics. Purdue University.

[90] K.C. Howell and S.C. Gordon. Orbit Determination Error Analysis and a Station–Keeping Strategy for Sun–Earth L_1 Libration Point Orbits. *Journal of the Astronautical Sciences*, 42(2):207–228, April–June 1994.

[91] K.C. Howell and T.M. Keeter. Station–Keeping Strategies for Libration Point Orbits: Target Point and Floquet Mode Approaches. In *AAS/AIAA Spaceflight Mechanics Meeting, AAS Paper 95-195*, 1995.

[92] K.C. Howell and H.J. Pernicka. Stationkeeping Method for Libration Point Trajectories. *Journal of Guidance, Control and Dynamics*, 16(1):151–159, 1993.

[93] T.R. Kane and E.L. Marsh. Attitude Stability of a Symmetric Satellite at the Equilibrium Points in the Restricted Three Body Problem. *Celestial Mechanics*, 4(4):468–489, 1971.

[94] T.M. Keeter. Station–Keeping Strategies for Libration Point Orbits: Target Point and Floquet Mode Approaches. Master's thesis, School of Aeronautics and Astronautics, Purdue University, West Lafayette, Indiana, 1994.

[95] P.S. Krasilnikov and A.L. Kunitsyn. On the Stabilization of the Collinear Libration Points of the Restricted Circular Three–Body Problem. *Celestial Mechanics*, 15:41–51, 1977.

[96] M.L. Lidov and S.S. Lukyanov. Statistical Estimates in the Control Problem for Motion of a Space Vehicle in the Vicinity of a Collinear Libration Point. *Cosmic Research*, 14(6):785–797, 1976.

[97] S.S. Lukyanov. Control of a Spacecraft's Motion in the Vicinity of a Collinear Libration Point of the Circular Three–Body Problem by Means of Light Pressure. *Cosmic Research*, 19(4):348–357, 1981.

[98] D.P. Muhonen. Accelerometer Enhanced Orbit Control Near the Sun Earth L_1 Libration Point. In *Space Flight Mechanics, Science and Technology Series, AIAA Paper 83-0018*, 1983.

[99] T. Prieto-Llanos and M.A. Gómez-Tierno. Station Keeping at Libration Points of Natural Elongated Bodies. *Journal of Guidance, Control and Dynamics*, 17(4):787–794, 1994.

[100] C.L. Pu and T.N. Edelbaum. Four–Body Trajectory Optimization. *AIAA Journal*, 13(3):333–336, 1975.

[101] M.J. Ratner. *Station Keeping for a Translunar Communication Station*. PhD thesis, Stanford University, Stanford, USA, 1973.

[102] J. Rodríguez-Canabal. Operational Halo Orbit Maintenance Technique for SOHO. European Space Agency, (Darmstadt, Germany, editor) *Second International Symposium on Spacecraft Flight Dynamics, ESA SP–255*, pages 71–78, 1986.

[103] J. Rodriguez-Canabal and M. Hechler. Orbital Aspects of the SOHO Mission Design. *Advances in the Astronautical Sciences*, 69:347–357, 1989.

[104] D.J. Scheeres, D. Han, and Y. Hou. The Influence of Unstable Manifolds on Orbit Ucertainty. In *AAS/AIAA Astrodynamics Specialist Conference, AIAA Paper 98–4559*, 1998.

[105] D.J. Scheeres and N.X. Ving. Dynamics and Control of Relative Motion in an Unstable Orbit. In AIAA Paper 2000–4135, 2000.

[106] R. Servan, W.S. Koon, M.W. Lo, J.E. Marsden, L.R. Petzold, S.D. Ross, and R.S. Wilson. Optimal Control for Halo Orbit Missions. 2000.

[107] C. Simó, G. Gómez, J. Llibre, and R. Martínez. Station Keeping of a Quasiperiodic Halo Orbit Using Invariant Manifolds. In *Second International Symposium on Spacecraft Flight Dynamics*, pages 65–70. European Space Agency, Darmstadt, Germany, October 1986.

[108] C. Simó, G. Gómez, J. Llibre, R. Martínez, and R. Rodríquez. On the Optimal Station Keeping Control of Halo Orbits. *Acta Astronautica*, 15(6):391–397, 1987.

[109] W. Wiesel and W. Shelton. Modal Control of an Unstable Periodic Orbit. *Journal of the Astronautical Sciences*, 31(1):63–76, 1983.

Missions to the Collinear Libration Points

[110] M. Beckman and J.J. Guzman. Triana Mission Design. *Advances in the Astronautical Sciences*, 103:1549–1568, 2000.

[111] J. Cobos and M. Hechler. FIRST Mission Analysis: Transfer to Small Lissajous Orbits around L_2. Technical Report MAS Working Paper No. 398, ESOC, 1997.

[112] D.W. Dunham. Utilization of Libration–Point Orbits. In *Problemi di Astronautica e di Meccanica Celeste a Ricordo del Prof. G. Colombo.*, pages 239–274. Atti della Accademia delle Science di Torino, Suppl. al Vol 122, 1988.

[113] R.W. Farquhar. Far Libration Point of Mercury. *Astronautics & Aeronautics*, 5(8):4, 1967.

[114] R.W. Farquhar. Lunar Communications with Libration–Point Satellites. *Journal of Spacecraft and Rockets*, 4(10):1383–1384, 1967.

[115] R.W. Farquhar. Future Missions for Libration–Point Satellites. *Astronautics & Aeronautics*, 7(5):52–56, 1969.

[116] R.W. Farquhar. The Utilization of Halo Orbits in Advanced Lunar Operations. Technical Report TN D–6365, NASA, 1971.

[117] R.W. Farquhar. A Halo–Orbit Lunar Station. *Astronautics and Aeronautics*, 10(6):59–63, 1972.

[118] R.W. Farquhar. Halo-Orbit and Lunar-Swingby Missions of the 1990's. *Acta Astronautica*, 24:227–234, 1991.

[119] R.W. Farquhar. The Flight of ISEE–3/ICE: Origins, Mission History and a Legacy. In *AAS/AIAA Astrodynamics Specialist Conference*, 1998.

[120] R.W. Farquhar. The Role of the Sun–Earth Collinear Libration Points in Future Space Explorations. *Space Times*, 39(6):9–12, 2000.

[121] R.W. Farquhar and D.W. Dunham. Use of Libration–Point Orbits for Space Observatories. In *Observatories in Earth Orbits and Beyond, Ed by Y. Kondo, Kluwer Academic Publishers*, pages 391–395, 1990.

[122] R.W. Farquhar, D.P. Muhonen, C. Newman, and H. Heuberger. The First Libration Point Satellite. Mission Overview and Flight History. In *AAS/AIAA Astrodynamics Specialist Conference*, 1979.

[123] G. Gómez, À. Jorba, J.J. Masdemont, and C. Simó. A Dynamical Systems Approach for the Analysis of the SOHO Mission. In *Third International Symposium on Spacecraft Flight Dynamics*, pages 449–454. European Space Agency, Darmstadt, Germany, October 1991.

[124] H. Hornby and W.H. Allen. Mission to the Libration Centers. *Astronautics & Aeronautics*, 4(7):78–82, 1966.

[125] M.C. Huber et al. The History of the SOHO Mission. *ESA Bulletin*, 86:25–35, 1996.

[126] W.S. Koon, M.W. Lo, J.E. Marsden and S.D. Ross. The Genesis Trajectory and Heteroclinic Connections, *AAS Paper 99-451, AAS/AIAA Astrodynamics Specialist Conference*, Girdwood, Alaska, 1999.

[127] W.S. Koon, M.W. Lo, J.E. Marsden and S.D. Ross. Constructing a Low Energy Transfer between Jovian Moons. *Contemporary Mathematics, American Mathematical Society* **292**, 129–145, 2002.

[128] M.W. Lo, B.G. Williams, W.E. Bollman, D. Han, Y. Hahn, J.L. Bell, E.A. Hirst, R.A. Corwin, P.E. Hong, K.C. Howell, B.T. Barden, and R.S. Wilson. Genesis Mission Design. In *AIAA Space Flight Mechanics, Paper No. AIAA 98–4468*, 1998.

[129] J. Ludwinski, M. Guman, J. Johannesen, R. Mitchell and R. Staehle. The Europa Orbiter Mission Design, *Paper No. 98-4.2.02*, presented at the *49th International Astronautic al Congress*, Melbourne, Australia, Sep. 28 - Oct. 2, 1998.

[130] M. Nagatomo and H. Matsuo. Concept of a Helio–Stationary Spacecraft. In *Proceedings of the Eight International Symposium on Space Technology and Science, Tokyo*, pages 533–538, 1969.

[131] H.J. Pernicka, D. Henry, and M. Chan. Use of Halo Orbits to Provide a Communication Link Between Earth and Mars. In *AAS/AIAA Astrodynamics Conference, Paper 92-4585*, 1992.

[132] W. Raithel. The Role of Cis-Lunar Libration Point in Lunar Operations. In *Proceedings of the 3rd Space Congress, Cocoa Beach, Florida*, 1966.

[133] P. Sharer and T. Harrington. Trajectory Optimization for the ACE Halo Orbit Mission. In *AAS/AIAA Astrodynamics Specialist Conference*, volume AIAA Paper 96–3601–CP, 1996.

[134] D.J. Scheeres, M.D. Guman and B. Villac. Stability Analysis of Planetary Satellite Orbiters: Application to the Europa Orbiter. *J. of Guidance, Control, and Dynamics* **24**(4), 778–787, 2001.

[135] L. Steg. Libration–Point Satellites. In *XVII International Astronautical Congress Proceedings: Astrodynamics, Guidance and Control, Madrid*, pages 59–64, 1966.

[136] T. Sweetser, R. Maddock, J. Johannesen, J. Bell, P. Penzo, A. Wolf, S. Williams, S. Matousek and S. Weinstein. Trajectory Design for a Europa Orbiter Mission: A Plethora of Astrodynamic Challenges, *Paper No. AAS 97-174*, presented at *AAS/AIAA Space Flight Mechanics Meeting, Huntsville, AL, Feb. 1997.*

Trajectory Design

[137] J.L. Bell et al. Genesis Trajectory Design. *Advances in the Astronautical Sciences*, 103:1525–1537, 2000.

[138] A. C. Clarke. Stationary Orbits. *Journal of the British Astronomical Association*, 57:232–237, 1947.

[139] G. Colombo. Sui Satelliti del Sistema Terra–Luna. *Rediconti Accademia Nazionale Dei Lincei, Series 8*, 28:169–172, 1960.

[140] C.A. Cross. Orbits for an Extra-Terrestrial Observatory. *Jounal of the British Interplanetary Society*, 13(4):204–207, 1954.

[141] R.W. Farquhar. Utilization of Multi-Body Trajectories in the Sun–Earth–Moon System. Technical Report 80740, NASA Technical Memorandum, 1980.

[142] R.W. Farquhar. ISEE–3 A Late Entry in the Great Comet Chase. *Astronautics and Aeronautics*, 21(9):50–55, 1983.

[143] R.W. Farquhar and D.W. Dunham. A New Trajectory Concept for Exploring the Earth's Geomagnetic Tail. In *AIAA Aerospace Sciences Meeting*, 1980.

[144] R.W. Farquhar and D.W. Dunham. Libration–Point Staging Concepts for Earth–Mars Transportation. Technical Report M002, NASA, 1986.

[145] R.W. Farquhar, D.P. Muhonen, C.R. Newman, and H.S. Heuberger. Trajectories and Orbital Maneuvers for the First Libration–Point Satellite. *Journal of Guidance and Control*, 3(6):549–554, 1980.

[146] R.W. Farquhar, D.P. Muhonen, and D.L. Richardson. Mission Design for a Halo Orbiter of the Earth. *Journal Spacecraft and Rockets*, 14(3):170–177, 1977.

[147] D. Folta and M. Beckman. Libration Orbit Mission Design: Applications of Numerical and Dynamical Methods. In *Libration Point Orbits and Applications*, World Scientific, 2003.

[148] G. Gómez, W.S. Koon, M.W. Lo, J.E. Marsden, J.J. Masdemont, and S.D. Ross. Invariant Manifolds, the Spatial Three-Body Problem and Space Mission Design. *Advances in The Astronautical Sciences*, 109, 1:3–22, 2001.

[149] K.C. Howell, B.T. Barden, R.S. Wilson, and M.W. Lo. Trajectory Design Using a Dynamical Systems Approach with Application to Genesis. In *AAS/AIAA Astrodynamics Specialist Conference, AAS Paper 97-709.*, 1997.

[150] K.C. Howell, B.T. Barden, and M.W. Lo. Application of Dynamical Systems Theory to Trajectory Design for a Libration Point Mission. *J. of the Astronautical Sciences* **45**(2), 161–178, 1997.

[151] D.L. Richardson. Halo orbit formulation for the ISEE-3 mission. *J. of Guidance and Control* **3**, 543–548, 1980.

[152] A.A. Sukhanov, N.A. Eismont, and A.V. Prudloglyad. Trajectory Design for Experimental Mission to Sun–Earth L_1 and L_2 Points Using SEP. *J. of the Braz. Soc. Mechanical Sciences*, 21:313–321, 1999.

Transfer Trajectories

[153] E. Belbruno and J. Miller. Sun-Perturbed Earth to Moon Transfers with Ballistic Capture. *Journal of Guidance, Control and Dynamics*, 16:770–775, 1993.

[154] E. Canalias, J. Cobos, J.J. Masdemont. Impulsive Transfers Between Lissajous Libration Point Orbits. Preprint 2003.

[155] L.A. D'Amario and T.N. Edelbaum. Minimum Impulse Three–Body Trajectories. *AIAA Journal*, 12(4):455–462, 1974.

[156] D.W. Dunham, S.J. Jen, C.E. Roberts, A.W. Seacord, P.J. Sharer, D.C. Folta, and D.P. Muhonen. Transfer Trajectory Design for the SOHO Libration-Point Mission. In *43rd Congress of the International Astronautical Federation,* IAF Paper 92–0066, 1992.

[157] N. Eismont, D. Dunham, J. Sho-Chiang, and R.W. Farquhar. Lunar Swingby as a Tool for Halo–Orbit Optimization in Relict–2 Project. In *Third International Symposium on Spacecraft Flight Dynamics, ESA SP–326*. European Space Agency (Darmstadt, Germany), 1991.

[158] G. Gómez, M. Marcote, and J.J. Masdemont. Trajectory Correction Manoeuvres in the Transfer to Libration Point Orbits. In *Proceedings of the Conference Libration Point Orbits and Applications*. World Scientific, G. Gómez et al. Eds. pages 287–310, 2003.

[159] W.S. Koon, M.W. Lo, J.E. Marsden, and S.D. Ross. Low Energy Transfer to the Moon. *Celestial Mechanics and Dynamical Astronomy*, 81(1):63–73, 2001.

[160] H. Matsuo et al. Optimization of Low Thrust Trajectories for Collinear Lagrange Point Mission. In *Proceedings of the Symposium on Mechanics for Space Flight, Tokyo*, pages 87–102, 1983.

[161] M.L. Lidov et al. Earth–Moon Halo Orbit Flight Paths in the Vicinity of the Earth–Sun Libration Point L_2. *Cosmic Research*, 30(4):353–369, 1992.

[162] S.J. Sponaugle et al. Optimal Cycling Between Cislunar and Cismartian Libration Points with Reussable Nuclear Electric Transfer Vehicles. *Advances in the Astronautical Sciences*, 75:141–161, 1991.

[163] G. Gómez, A. Jorba, J. Masdemont, and C. Simó. Study of the Transfer from the Earth to a Halo Orbit Around the Equilibrium Point L_1. *Celestial Mechanics*, 56(4):541–562, 1993.

[164] G. Gómez, A. Jorba, J. Masdemont, and C. Simó. Study of the Transfer Between Halo Orbits. *Acta Astronautica*, 43(9–10):493–520, 1998.

[165] G. Gómez, À. Jorba, J.J. Masdemont, and C. Simó. Moon's Influence on the Transfer from the Earth to a Halo Orbit. In A. E. Roy, editor, *Predictability, Stability and Chaos in N-Body Dynamical Systems*, pages 283–290. Plenum Press, 1991.

[166] G. Gómez and J.J. Masdemont. Some Zero Cost Transfers Between Halo Orbits. *Advances in the Astronautical Sciences*, 105(2):1199–1216, 2000.

[167] M. Hechler. SOHO Mission Analysis L_1 Transfer Trajectory. Technical Report MAO Working Paper No. 202, ESA, 1984.

[168] T.A. Heppenheimer. Steps Toward Space Colonization: Colony Location and Transfer Trajectories. *Journal of Sapcecraft and Rockets*, 15(5):305–312, 1978.

[169] L.A. Hiday and K.C. Howell. Impulsive Time–Free transfers Between Halo Orbits. School of Aeronautics and Astronautics. Purdue University, 1992.

[170] L.A. Hiday and K.C. Howell. Transfers Between Libration–Point Orbits in the Elliptic Restricted Problem. In *AAS/AIAA Spaceflight Mechanics Conference, Paper AAS 92-126.*, 1992.

[171] K.C. Howell and L.A. Hiday-Johnston. Time-Free Transfers Between Libration-Point Orbits in the Elliptic Restricted Problem. *Acta Astronautica*, 32:245–254, 1994.

[172] K.C. Howell, D.L. Mains, and B.T. Barden. Transfer Trajectories from Earth Parking Orbits to Sun–Earth Halo Orbits. In *AAS/AIAA Spaceflight Mechanics Meeting, AAS Paper 94-160*, 1994.

[173] B.L. Jones and R.H. Bishop. Rendezvous Targeting and Navigation for a Translunar Halo Orbit. *Journal of Guidance, Control and Dynamics*, 17(5):1109–1114, 1994.

[174] W.S. Koon, M.W. Lo, J.E. Marsden, and S.D. Ross. Shoot the Moon. In *AAS/AIAA Space Flight Mechanics Meeting, Paper AAS 00-166*, 2000.

[175] J.J. Masdemont. *Estudi i Utilització de Varietats Invariants en Problemes de Mecànica Celeste*. PhD thesis, Universitat Politècnica de Catalunya, Barcelona, Spain, 1991.

[176] P. Sharer, J. Zsoldos, and D. Folta. Control of Libration Point Orbits Using Lunar Gravity–Assisted Transfer. *Advances in the Astronautical Sciences*, 64:651–663, 1993.

[177] S. Stalos, D. Folta, B. Short, J. Jen, and A. Seacord. Optimum Transfer to a Large–Amplitude Halo Orbit for the Solar and Heliospheric Observatory (SOHO) Spacecraft. *Advances in the Astronautical Sciences*, 84:639–650, 1993.

[178] T.F. Starchville and R.G. Melton. Optimal Low–Thrust Transfers to Halo Orbits About the L_2 Libration Point in the Earth–Moon System (Elliptical Problem). *Advances in the Astronautical Sciences*, 99:1489–1505, 1998.

[179] R.S. Wilson, K.C. Howell and M.W. Lo. Optimization of Insertion Cost Transfer Trajectories to Libration Point Orbits. *Advances in the Astronautical Sciences*, 103:1569–1586, 2000.

Contingency Plans

[180] D.W. Dunham. Contingency Plans for the ISEE–3 Libration Point Mission. In *AAS Astrodynamics Specialist Conference*, AAS Paper 79–129, 1979.

[181] D.W. Dunham. Contingency Study for the Third International Sun–Earth Explorer (ISEE–3) Satellite. Technical report, Computer Sciences Corporation, 1979.

[182] G. Gómez, M. Marcote, and J.J. Masdemont. Trajectory Correction Manoeuvres in the Transfer to Libration Point Orbits. To appear in Acta Astronautica.

[183] K.C. Howell and B.T. Barden. Brief Summary of Alternative Targeting Strategies for TCM1, TCM2 and TCM3. Private communication, 1999.

[184] C.E. Roberts and R. Short. Injection Contingency Recovery Strategies for Halo Orbit Transfer Trajectories. In *AAS/AIAA Astrodynamics Specialist Conference*, volume AIAA Paper 96–3600–CP, 1996.

[185] R. Servan, W.S. Koon, M.W. Lo, J.E. Marsden, L.R. Petzold, S.D. Ross, and R.S. Wilson. Halo Orbit Mission Correction Maneuvers Using Optimal Control. 2000.

Astronomical Applications

[186] K.C. Howell, B.G. Marchand, and M.W. Lo. Temporary Satellite Capture of Short–Period Jupiter Family Comets from the Perspective of Dynamical Systems. In *AAS/AIAA Space Flight Mechanics Meeting, AAS Paper 00-155*, 2000.

[187] W.S. Koon, M.W. Lo, J.E. Marsden, and S.D. Ross. Resonance and capture of jupiter comets. *Celestial Mechanics and Dynamical Astronomy*, 81(1):27–38, 2001.

[188] M.W. Lo and S. Ross. SURFing the Solar Sytem: Invariant Manifolds and the Dynamics of the Solar System. Technical Report 312/97, 2-4, JPL IOM, 1997.

Methodological References

[189] L. Carpenter. Periodic Orbits in Trigonometric Series. In G.E.O. Giacaglia, editor, *Periodic Orbits, Stability and Resonances*, pages 192–209, 1970.

[190] A. Deprit. Canonical Transformations Depending on a Small Parameter. *Celestial Mechanics*, 1(1):12–30, 1969.

[191] A. Deprit, J. Henrard, and A.R.M. Rom. Trojan Orbits II. Birkhoff's Normalization. *Icarus*, 6(3):381–406, 1967.

[192] G.E.O. Giacaglia. *Perturbation Methods in Non–Linear Systems*. Springer–Verlag, 1972.

[193] G. Gómez, J. Llibre, and J. Masdemont. Homoclinic and Heteroclinic Solutions in the Restricted Three-Body Problem. *Celestial Mechanics*, 44:239–259, 1988.

[194] G. Gómez and J. Masdemont. Libration Point Orbits: The State of the Art from the Dynamical Systems Approach. In A. B. Bertachini de A. Prado, editor, *Advances in Space Dynamics (ISBN 85-901487-1-8)*, pages 1–49. IMPE Brasil, 2000.

[195] G. Gómez, J.M. Mondelo, and C. Simó. Refined Fourier Analysis Procedures. Preprint.

[196] À. Jorba. *Quasiperiodic Perturbations of Ordinary Differential Equations*. PhD thesis, Universitat de Barcelona, Barcelona, Spain, 1991.

[197] À. Jorba and C. Simó. On Quasiperiodic Perturbations of Elliptic Equilibrium Points. *SIAM J. of Math. Analysis*, 27:1704–1737, 1996.

[198] À. Jorba and J. Villanueva. On the Normal Behaviour of Partially Elliptic Lower Dimensional Tori of Hamiltonian Systems. *Nonlinearity*, 10:783–822, 1997.

[199] À. Jorba and J. Villanueva. On the Persistence of Lower Dimensional Invariant Tori Under Quasiperiodic Perturbations. *J. Nonlinear Science*, 7:427–473, 1997.

[200] A.A. Kamel. *Perturbation Theory Based on Lie Transforms and its Application to the Stability of Motion Near Sun Perturbed Earth–Moon Triangular Libration Points*. PhD thesis, Stanford University, Stanford, USA, 1962.

[201] A.A. Kamel. Expansion Formulae in Canonical Transformations Depending on a Small Parameter. *Celestial Mechanics*, 1(2):190–199, 1969.

[202] D.F. Lawden. *Optimal Trajectories for Space Navigation*. Butterworths & Co. Publishers, London, 1963.

[203] F.R. Moulton. *Periodic Orbits*. The Carnegie Institution of Washington, 1920.

[204] J.R. Pacha. *On the Quasi–Periodc Hamiltonian Andronov–Hopf Bifurcation*. PhD thesis, Dept. de Matemàtica Aplicada I, Universitat Politècnica de Catalunya, Barcelona, Spain, 2002.

[205] H. Poincaré. *Les Méthodes Nouvelles de la Mécanique Céleste*. Gauthier–Villars, 1892, 1893, 1899.

[206] H. Rüssmann. On the Stability of an Equilibrium Solution in Hamiltonian Systems of Two Degrees of Freedom. In V. Szebehely, editor, *Instabilities in Dynamical systems*, pages 303–305. NATO, ASI (Cortina d'Ampezzo, Italy), 1979.

[207] C.L. Siegel and J.K. Moser. *Lectures on Celestial Mechanics*. Springer–Verlag, 1971.

[208] C. Simó. Analytical and Numerical Computation of Invariant Manifolds. In D. Benest and C. Froeschlé, editors, *Modern Methods in Celestial Mechanics*, pages 285–330. Editions Frontières, 1990.

[209] C. Simó. Effective Computations in Hamiltonian Dynamics. In Société Mathématique de France, editor, *Cent ans après les Méthodes Nouvelles de H. Poincaré*, pages 1–23, 1996.

[210] C. Simó. Dynamical Systems Methods for Space Missions on a Vicinity of Collinear Libration Points. In C. Simó, editor, *Hamiltonian Systems with Three or More Degrees of Freedom*, pages 223–241. Kluwer Academic Publishers, 1999.

[211] E.M. Standish. User's Guide to the JPL Lunar and Planetary Ephemeris Export Package. Technical report, NASA–Jet Propulsion Laboratory, 1985.

[212] E.M. Standish. JPL Planetary and Lunar Ephemerides, DE405/LE405. Technical Report JPL IOM 314.10–127, NASA–Jet Propulsion Laboratory, 1998.

[213] J. Stoer and R. Bulirsch. *Introduction to Numerical Analysis*. Springer Verlag, 1983.

[214] E. Stromgren. Connaissance Actuelle des Orbites dans le Probleme des Trois Corps. Publikationer og Mindre Meddelelser fra Köbenhauns Observatorium No. 100, 1925.

[215] V. Szebehely. *Theory of Orbits*. Academic Press, 1967.

[216] B.F. Villac and D.J. Scheeres. Escaping Trajectories in the Hill Three-Body Problem and Applications. *J. of Guidance, Control, and Dynamics* **26**(2), 224-232, 2003.

Formation Flight

[217] B.T. Barden and K.C. Howell. Formation Flying in the Vicinity of Libration Point Orbits. In *AAS Paper 98-169, Monterey, CA.*, 1998.

[218] B.T. Barden and K.C. Howell. Dynamical Issues Associated with Relative Configurations of Multiple Spacecraft near the Sun–Earth/Moon l_1 Point. In *AAS Paper 99-450, Girdwood, Alaska.*, 1999.

[219] C.A. Beichman, N.J. Wolf, and C.A. Lindensmith (Eds.). *The Terrestrial Planet Finder (TPF)*. JPL Publications 99–003, 1999. (http://tpf.jpl.nasa.gov).

[220] G. Gómez, M.W. Lo, J.J. Masdemont, and K. Museth. Simulation of formation flight near L_2 for the tpf mission. In *ASS/AIAA Space Flight Mechanics Conference. Paper AAS 01-305*, 2001.

[221] K.C. Howell and B.T. Barden. Trajectory Design and Station Keeping for Multiple Spacecraft in Formation Near de Sun-Earth L_1 Point. In *General Conference of the International Astronautical Federation. Paper IAF-99-A.7.07*, 1999.

[222] K.C. Howell and B.G. Marchand. Control Strategies for Formation Flight in the Vicinity of the Libration Points. In *AAS Paper 03-113, Ponce, Puerto Rico*, 2003.

[223] B.G. Marchand and K.C. Howell. Formation Flight Near L_1 and L_2 in the Sun-Earth/Moon Ephemeris System Including Solar Radiation Pressure. In *AAS Paper 03-596, Ponce, Puerto Rico*, 2003.

[224] B.G. Marchand and K.C. Howell. Aspherical Formations Near the Libration Points in the Sun-Earth/Moon Ephemeris System. In *AAS Paper 04-157, Maui, Hawai*, 2003.

Triangular Libration Points

[225] K.B. Bhatnagar and P.P. Hallan. Effect of Perturbed Potentials on the Stability of Libration Points in the Restricted Problem. *Celestial Mechanics*, 20(1):95–103, 1979.

[226] J.V. Breakwell and R. Pringle. Resonances Affecting Motion Near the Earth–Moon Equilateral Libration Points. *Progress Astronautics and Aeronautics*, 17, 1966.

[227] R. Broucke. Traveling Between the Lagrange Points and the Moon. *Journal of Guidance and Control*, 2(4):257–263, 1979.

[228] E. Castellà and À. Jorba. On the Vertical Families of Two-Dimensional Tori Near the Triangular Points of the Bicircular Problem. *Celestial Mechanics and Dynamical Astronomy*, 76:35–54, 2000.

[229] B. K. Cheng. Motion Near the Triangular Points in the Elliptic Restricted Problem of Three Bodies. *Celestial Mechanics*, 19(1):31–41, 1979.

[230] A. Deprit and A. Deprit-Bartholomé. Stability of the Triangular Lagrangian Points. *The Astronomical Journal*, 72(2):173–179, 1967.

[231] A. Deprit, J. Henrard, J. Palmore, and J.F. Price. The Trojan Manifold in the System Earth–Moon. *Monthly Notices of the Royal Astronomical Society*, 137(3):311–335, 1967.

[232] W.T. Feldt and Y. Schulman. More Results on Solar Influenced Libration Point Motion. *AIAA Journal*, 4(4):1501–1502, 1966.

[233] G. De Fillipi. Station Keeping at the L_4 Libration Point: A Three Dimensional Study. Master's thesis, Dept. Aeronautics and Astronautics, Air Force Institute of Technology Wright-Patterson AFB, Ohio, USA, 1978.

[234] R. Freitas and F. Valdes. A Search for Natural or Artificial Objects Located at the Earth–Moon Libration Points. *Icarus*, 42:442–447, 1980.

[235] G. Gómez, À. Jorba, J.J. Masdemont, and C. Simó. *Dynamics and Mission Design Near Libration Point Orbits – Volume 4: Advanced Methods for Triangular Points*. World Scientific, 2000.

[236] G. Gómez, J. Llibre, R. Martínez, and C. Simó. *Dynamics and Mission Design Near Libration Point Orbits – Volume 2: Fundamentals: The Case of Triangular Libration Points*. World Scientific, 2000.

[237] D. Jamison. Uses of the Trojan Libration Points of the Earth–Sun System. *Journal of Spacecraft and Rockets*, 3(4):595–596, 1966.

[238] A.A. Kamel and J.V. Breakwell. Stability of Motion Near Sun–Perturbed Earth–Moon Triangular Points. In G.E.O. Giacaglia, editor, *Periodic Orbits, Stability and Resonances*, pages 82–90, 1970.

[239] R. Kolenkiewicz and L. Carpenter. Periodic Motion Around the Triangular Libration Points in the Restricted Problem of Four Bodies. *The Astronomical Journal*, 72(2):180–183, 1967.

[240] R. Kolenkiewicz and L. Carpenter. Stable Periodic Orbits About the Sun Perturbed Earth–Moon Triangular Points. *AIAA Journal*, 6(7):1301–1304, 1968.

[241] A.L. Kunitsyn and A.A. Perezhogin. On the Stability of Triangular Libration Points of the Photogravitational Restricted Circular Three–Body Problem. *Celestial Mechanics*, 18(4):395–408, 1978.

[242] A.M. Leontovic. On the Stability of the Lagrange Periodic Solutions of the Restricted Problem of Three Bodies. *Soviet Math. Dokl.*, 143(3):425–428, 1962.

[243] A.P. Markeev. On the Stability of the Triangular Libration Points in the Circular Bounded Three–Body Problem. *Applied Mathematics and Mechanics*, 33:105–110, 1969.

[244] A.P. Markeev. Stability of the Triangular Lagrangian Solutions of the Restricted Three–body Problem in the Three–Dimensional Circular Case. *Soviet Astronomy*, 15:682–686, 1972.

[245] A.P. Markeev. *Libration Points in Celestial Mechanics and Astrodynamics (in Russian).* Moscou (Available on microfiche A79–15867), 1978.

[246] R. Mckenzie and V. Szebehely. Non–Linear Stability Motion Around the Triangular Libration Points. *Celestial Mechanics*, 23(3):223–229, 1981.

[247] F. Mignard. Stability of L_4 and L_5 Against Radiation Pressure. *Celestial Mechanics*, 34(1–4):275–287, 1984.

[248] J. Olszewski. On the Practical Stability of the Triangular Points in the Restricted Three–Body Problem. *Celestial Mechanics*, 4(1):3–14, 1971.

[249] E.W. Paul and G. Shapiro. Stabilization of the Lagrangian Solutions of the Three Body Problem. *Astronautica Acta*, 11:410–417, 1965.

[250] R. Roosen. A Photographic Investigation of the Gegenschein and the Earth–Moon Libration Point L_5. *Icarus*, 9:429–439, 1968.

[251] H. Schechter. Three Dimensional Nonlinear Stability Analysis of the Sun–Perturbed Earth–Moon Equilateral Points. *AIAA Journal*, 6(6):1223–1228, 1968.

[252] B.E. Schutz. Orbital Mechanics of Space Colonies at L_4 and L_5 of the Earth–Moon System. In *AIAA Astrodynamics Specialist Conference*, volume AIAA Paper No. 77–33, 1977.

[253] C. Simó, G. Gómez, À. Jorba, and J. Masdemont. The Bicircular Model Near the Triangular Libration Points of the RTBP. In A. Roy and B. Steves, editors, *From Newton to Chaos*, pages 343–370. Plenum Press, 1995.

[254] B.D. Tapley and J.M. Lewallen. Solar Influence on Satellite Motion Near the Stable Earth–Moon Libration Points. *AIAA Journal*, 2(4):728–732, 1964.

[255] B.D. Tapley and B.E. Schultz. Further Results on Solar Influenced Libration Point Motion. *AIAA Journal*, 3(10):1954–1956, 1965.

[256] B.D. Tapley and B.E. Schultz. Persistent Solar Influenced Libration Point Motion. *AIAA Journal*, 6(7):1405–1406, 1968.

[257] B.D. Tapley and B.E. Schultz. Numerical Studies of Solar Influenced Particle Motion Near Triangular Earth–Moon Libration Points. In G.E.O. Giacaglia, editor, *Periodic Orbits, Stability and Resonances*, pages 128–142, 1970.

[258] J.F.C. Van Velsen. Isoenergetic Families of Quasiperiodic Solutions Near the Equilateral Solution of the Three–Body Problem. *Celestial Mechanics*, 23(4):383–395, 1981.

[259] J.P. De Vries. The Sun's Perturbing Effect on Motion Near the Triangular Lagrange Point. In *Proceedings XIII–th IAC*, pages 432–450, 1964.

[260] A.L. Whipple. Three–Dimensional Regions of Stability About the Triangular Equilibrium Points. *Celestial Mechanics*, 30(4):385–394, 1983.

[261] L.E. Wolaver. Effect of Initial Configurations in Libration Point Motion. *Progress Astronautics and Aeronautics*, 17: 1966.